The role of WT1 in nephron endowment and glomerulosclerosis (GS) / Chronic Kidney Disease (CKD)

Ahzad Ahmad

99076418

Doctor of Philosophy

Institute of Genetic Medicine (IGM)

November 2016

ABSTRACT

The DDS/+ mouse is a model for glomerulosclerosis in Denys Drash Syndrome (DDS). The mutation results in a 20% reduction in nephron number that triggers a compensatory cascade of events leading to glomerulosclerosis. However, the mechanisms controlling the rate of maturation of nephrons and determining final nephron number within a kidney are not fully known. Stereological examinations on newborn kidneys were performed for glomerular count. Microarray analysis of foetal kidneys was carried out to reveal differentially expressed genes. 1136 differentially expressed genes were identified by microarray, of which the top 5 genes encoded mitochondrial tRNAs. Ingenuity Pathway Analysis indicated the involvement of renal developmental and tRNA splicing in the underlying mechanisms. Cross-database analyses revealed at least 216 genes that contain intragenic WT1 target sequence therefor represent potential direct targets of WT1 that are mis expressed due to the mutation. Given the expression changes of apoptosis related genes, TUNEL staining to identify apoptosis was carried out to reveal insignificant differences between genotypes. Given abnormal expression of mitochondrial tRNAs, immunofluorescence and western blotting were carried out and confirmed the presence of WT1 protein in mitochondrial isolates. Furthermore, metabolic profiling revealed abnormalities in the oxidative phosphorylation system in WT1 mutant cells compared with wild type.

This study identified a list of genes that are associated with WT1 induced nephron underdosing, many of which have not previously been linked with nephrogenesis. The data suggests a role for apoptosis in nephron underdosing, however, more strikingly, the differentially expressed genes point to more complex molecular interactions involving mitochondria and WT1. To date, there are no reports of WT1 involvement in any aspect of mitochondrial biology. Molecular analyses verified WT1 protein is found in mitochondria indicating the potential for direct involvement of WT1 in mitochondria and, therefore, a potential for mitochondrial involvement in nephron development and endowment. These data suggest a previously unrecognised component of nephrogenesis that should be considered in future investigations to further uncover the various pathways involved in final nephron endowment.

DEDICATION

To my parents, thank you.

ACKNOWLEDGEMENTS

I would like to thank my supervisor Colin Miles for inspiration, encouragement and many cups of chocolate and coffee. Many thanks also to various master and undergraduate students that I co-supervised and help with lab works.

Thank you to the entire lab group for their support, help in basic lab skills and in general.

I would like to thank mitochondrial group in helping with mitochondrial experiment.

Table of Contents

Abstract *i*
Dedication *ii*
Acknowledgements *iii*
Table of contents *1*
List of Figures and Tables *5*
List of Acronyms and Abbreviations *9*

CHAPTER 1 INTRODUCTION ***10***
1.1 - Wilms Tumor 1 gene: *9*
1.2 – Kidney: Normal structure and function *12*
1.3 – Normal Kidney Development *15*
1.4 - Chronic Kidney Disease *21*
1.4.1 – Background *21*
1.4.2 – Glomerulosclerosis *24*
1.5 – Denys Drash Syndrome (DDS) *25*
1.5.1 – Background *25*
1.5.2 – Animal Model - Wt1$^{tmT396/+}$ mice (a.k.a DDS/+) *26*
1.6 – Mitochondria *29*
1.7 – WT1, apoptosis and cell viability *31*
1.8. - WT1 and disease *33*
1.8.1 - WT1 mutation, kidney development and disease *33*
1.8.2 - WT1 mutant mouse models of glomerulosclerosis – this subheading discusses mostly the previous data and findings of Caroline Wroe (PhD, 2009) and Colin Miles that lead to my work in this thesis. *34*
1.6 - Project strategy *39*
1.7 - Experimental plan *40*
1.8 - Overview of main objectives *41*
1.8.1. Project Aims *41*

CHAPTER 2. MATERIALS AND METHODS ***42***
2.2 Wt1$^{loxP/loxP}$ mice (DDS20) *42*
2.3 Collection, preparation and analysis of Microarray data *44*
2.3. Mouse Embryonic Fibroblast (MEF) - preparation from Embryos, MEF cell culture and preservation *46*
2.4.2 Tamoxifen preparation *48*
2.5.1. Tamoxifen on MEF (primary cell culture) *48*
2.5.2 Tamoxifen preparation for in vivo experiment *49*
2.5. Histology *50*
2.5.1. Tissue fixation and sectioning *50*
2.5.1.1. Wax fixation and sectioning *50*
2.5.1.2. Cryofixation *50*

2.5.2. Haematoxylin and Eosin (H&E) staining 51
2.6. Molecular Biology 51
2.6.1. DNA preparation for genotyping: 51
2.6.2. PCR genotyping mix: 52
2.6.2.1. PCR conditions: 53
2.6.2.1.1. loxP and Cre genotyping: 53
2.6.2.1.2. DDS/+ genotyping: 53
2.6.3. DNA extraction using QIAGEN Tissue DNA Extraction Kit 54
2.6.4. RNA extraction 54
2.6.5. Reverse Transcription – Polymerase Chain Reaction (RT-PCR) of RNA 55
2.6.6. Quantitative PCR (qPCR): 56
2.6.6. Gel electrophoresis 56
2.7. Immunostaining 57
2.7.1. Apoptosis Kit 57
2.7.2. TUNEL Staining: 57
2.8 Cell Counts: 58
2.8.1 Apoptotic cell count: 58
2.8.2 Nephron count: 59
2.8.3 Analysis 59
2.9 PNA Staining: 60
2.10 Western blot 61
2.11 Alamar Blue Assay 62
2.12 Cytochrome C Oxidase / Succinate Dehydrogenase (COX/SDH) Double-labeling Histochemistry 63
2.13 Copy number analysis 63
2.14 Mitochondrial isolation 64
2.14.1 Isolation of Mitochondria using Reagent-based Method for Cultured Cells 64
2.14.2 Isolation of Mitochondria using Dounce Homogenization for Tissues 64
2.14. Preparation of fresh MEF for FACS with MitoTracker® 65
2.15 Seahorse mitochondrial analysis (XFe) 65
2.16 Statistical analysis 66

CHAPTER 3. DISRUPTED NEPHROGENESIS IN MURINE DENYS DRASH SYNDROME. **67**
3.1 Introduction 67
3.2 Results 69
3.3 Summary of key findings: 83
3.4 Discussion 83

CHAPTER 4. ALTERED GENE EXPRESSION PATTERNS DURING KIDNEY DEVELOPMENT IN MURINE DENYS DRASH SYNDROME ***89***

Introduction *89*

4.1 Microarray data and analysis of DDS/+ mice e17.5 kidneys versus wild type *90*

4.2 Reduction in tRNA expression levels, but not ND5, confirmed in independent DDS/+ mutant kidney samples. *98*

4.3 Nuclear genes with the largest fold-change *102*

4.4 Selected genes within the top 150 ranked by fold change *103*

4.5 Ingenuity Pathway Analysis (IPA) *105*

4.6 Comparative Database Analysis *108*

4.7 Summary of key findings *122*

4.8 Discussion *122*

CHAPTER 5. APOPTOSIS IN DEVELOPING KIDNEYS OF MURINE DENYS DRASH SYNDROME MICE **AND DISRUPTION OF MOUSE EMBRYONIC FIBROBLAST CELLULAR METABOLISM** ***129***

Introduction *129*

5.1 Apoptosis gene list *130*

5.2 Apoptosis staining *131*

5.2.1 Localizing apoptotic segment of developing nephron of P0 kidney *131*

5.2.2 Quantifying the TUNEL signals on cortex region of P0 kidney section *135*

5.3 Mouse Embryonic Fibroblast impairment of cellular metabolism *139*

5.3.1 Tamoxifen-induced MEF versus normal MEF *139*

5.3.2 Oxygen deprived MEF (Tamoxifen) *141*

5.4 Summary of key findings: *143*

5.5 Chapter Discussion *143*

CHAPTER 6. A MITOCHONDRIAL ROLE FOR WT1 ***146***

Introduction *146*

6.1 Mitochondrial related functional analysis, Public and Published Cross-Databases Analysis *148*

6.1.1 ToppGene® *148*

6.1.2 MitoCarta 2.0 *149*

6.1.3 STRING database *153*

6.2 Mitochondrial function: Succinic dehydrogenase (SDH) and Cytochrome oxidase (COX) staining *155*

6.3 ex-vivo system for WT1 *158*

6.3.1: DDS20 is a null allele. *159*

6.3.2 DDS20 Mouse Embryonic Fibroblast *160*

6.3.3: MitoTracker® staining *162*
6.3.4: Flow cytometry analysis *165*
6.4 – WT1 localisation within mitochondria *166*
6.4.1 – WT1 localisation in e17.5 kidney fraction *166*
6.4.2 – Mouse Embryonic Fibroblast fraction comparison *170*
6.5 Comprehensive mitochondrial analysis using metabolic profiling *172*
6.6. Conditionally immortalised human podocyte cells *181*
6.7 Summary of key findings *183*
6.7. Chapter discussions *184*
6.9. Conclusion *188*

CHAPTER 7. GENERAL DISCUSSION ***189***

Summary *195*

APPENDICES ***197***

REFERENCES ***224***

LIST OF FIGURES AND TABLES

Figure 1.1.1. Figures show the exons of WT1 gene and the protein with 4 zinc

Figure 1.2.1: Figures showing the location and the surrounding tissues of

Figure 1.2.2: Figures showing the A) cross-sectioned kidney and zoomed-in at

Figure 1.3.1: Stages of normal for kidney development in mouse.

Figure 1.3.2: Significant turn points of lineage relationship of cells in developing

Figure 1.4.2.1. Representative figure of H&E-stained kidney sections

Figure 1.5.2.1: DDS/+ (Wt1^{tmT396}/+) mouse strain production

Figure: 1.6.1: Figure depicting the cross-section and internal structure

Figure 1.7.1: Representative diagram of possibility that disrupted within

Figure 1.8.2.1: WT1 mutant DDS/+ (Wt1$^{tmT396/+}$), Denys Drash Syndrome

Figure 1.8.2.2: Mesangial volume fraction of a 3-month-old DDS/+

Figure 1.8.3: 1 month of age DDS/+ mice showing negative correlation between

Figure 1.8.2.4: Increased of Renin granulation in juxtaglomerular apparatus

Figure 1.8.2.5: Percentage of endothelial cell fenestration in newborn DDS/+

Figure 1.8.2.6: (A) Survival graph of wild type, Wt1^{insGFP}/+ and DDS/+ mice

Figure 2.1.1: Figure illustrate inducible knockout utilizing the Cre^{ERT2} system

Figure 2.1.2: Representative diagram of mutant Wt1 allele with loxP sites

Figure 2.1.3: Representative PCR genotyping using exon 8 primers of wild

Figure 3.2.1: Representative figure depicting the P0 (new born) mice kidney

Figure 3.2.2: A. Representative section of P0 kidney stained with PNA/methyl

Figure 3.2.3: Representative diagram of P0 kidney section stained with

Table 3.2.1: Summary of measurements/counts carried out on P0 female kidneys

Figure 3.2.4: Summary of measurements/counts carried out on P0 female kidneys

Table 3.2.2 Results of the Kolmogorov-Smirnov Test and the Shapiro-Wilk Test

Figure 3.2.5: Q-Q plots for data normalisation. Everything is within

Table 3.2.3: Results of the Levene Test indicating the

Table 3.2.4: Results of ANOVA and the P-value of each measurements are

Figure 3.2.6: Box-whisker plots of data showing nephron number and nephron

Table 3.2.5: Pearson correlation (r) matrix of all factors calculated against each

Table 3.2.6: ANOVA of statistically significance of the model for prediction indicating

Table 3.2.7: Result of stepwise method for significant predictor for nephron number
Table 3.2.8: ANOVA of statistically significance of the model for prediction
*Figure 3.4.1: Projection of nephron number (current counts at 15.9% and *Miles*
Figure 4.1.1: A chip-to-chip comparison before and after normalization. The
Figure 4.1.2: Boxplots of log2 transformed expression values before and
Figure 4.1.3: PCA of expression values for normalized and filtered genes
Figure 4.1.4: The heatmap shows a two-dimensional clustering of the top 50
Table 4.1.1: List of significant differentially expressed genes (p < 0.05) with
Figure 4.2.1: Whisker-Box plot of qRT-PCR analysis of independent samples
Figure 4.2.2: Representative gel electrophoresis of qRT-PCR analysis
Table 4.2.3: Table: Show the non-normalized data obtained from qRT-PCR
Table 4.2.4: ND5 sample group is not different to control group.
Figure 4.2.5: Gel electrophoresis of qRT-PCR products from cDNA
Figure 4.3.1: Whisker-Box plot of qRT-PCR showing nuclear genes
Table 4.4.1: qRT-PCR of selected genes in the microarray list for
Figure 4.4.2: A) A selection of reference genes used in qRT-PCR, GAPDH
Figure 4.5.1: Ingenuity Pathway Analysis showing networks of interacting molecules
Figure 4.5.2: Table show IPA analysis of genes list from our microarray
Figure 4.6.1: A Venn diagram showing overlap of comparison database of 3
Figure 4.6.2: Comparison of WT1 ChIPseq datasets in embryonic kidneys and
Figure 4.6.3: A model representation of nephrogenic area of developing kidney
Figure 4.6.4: Comparison database Venn diagrams showing overlap of the two
Figure 4.6.5: A Venn diagram showing overlap of comparison database
Figure 4.6.6: (Continuation as not enough space to list all) A Venn diagram
Figure 4.6.7: (Continuation as not enough space to list all) A Venn diagram showing
Figure 4.6.8: IPA functional analysis in relation to nephron and glomerular
Figure 4.6.9: Adaptation of KEGG pathway (combination of multiple KEGG pathway
Figure 4.6.10: IPA functional analysis for genes associated with post-translational
Figure 4.6.11: STRING diagram showing olfactory related genes differentially
Figure 4.8.1: TBLASTN output from ENSEMBL for (A), tRNA-his Affymetrix
Figure 4.8.2: A diagram of expression analysis from GenitoUrinary Development

Figure 4.8.3: A diagram of expression analysis from GenitoUrinary Development
Table 5.1.1: Listed are the genes related to apoptosis that were
Figure 5.2.1: Representative figure wild type kidney showing the
Figure 5.2.2: Immunofluorescence of TUNEL staining (Life Technologies) to detect
Figure 5.2.3: Immunofluorescence of TUNEL staining (Life Technologies) to detect
Figure 5.2.4: Representative figures of TUNEL staining of P0 kidneys. All
Figure 5.2.5: Counts (normalized by log10) of TUNEL signals (events) from sections
Table 5.2: SPSS calculation using one-way ANOVA of the TUNEL signal counts
Figure 5.3.1: Bar chart depicting the absorbance value of Alamar Blue according
Figure 5.3.2: Box-plot chart depicting the absorbance value of Alamar Blue
Figure 6.1.1.1: Cellular component and disease list categories annotated from
Figure 6.1.2.1: Venn diagram of E17.5 array gene list and mitochondria MitoCarta
Table 6.1.2.1: List of genes with description of nuclear gene encoding mitochondrial
Figure 6.1.2.2: ChIP data visualised using UCSC Genome Browser: Downstream
Figure 6.1.3.1: STRING analysis of mitochondrial related genes. 26 cross-database
Figure 6.2.1: Representative figures of Succinic dehydrogenase (SDH) and
Figure 6.2.2: Representative figures of COX-SDH staining of foetal kidney for every
Figure 6.3.1.1: qRT-PCR of day one newborn mice kidney after injection of
Figure 6.3.2.1: qRT-PCR of mouse embryonic fibroblast (MEF) after cultured,
Table 6.3.2.1: Gene expression profiles of Sulf1 and CD55 from MEF cells available
Figure 6.3.3.1: Immunofluorescence of mouse embryonic fibroblasts (MEFs)
Figure 6.3.3.2: Representative figure showing disruption of mitochondrial network
Figure 6.11: Figure showing MFI (Mean florescence intensity) of flow cytometry
Figure 6.4.1.1: Western blots of wild type e17.5 foetal kidneys, isolated
Figure 6.4.1.2: Western blots of wild type e17.5 foetal kidneys, isolated foetal
Figure 6.4.1.3: Western blots of wild type e17.5 foetal kidneys, isolated foetal
Figure 6.4.2.1: Western-blot (with florescence secondary antibody) of MEF (no
Figure 6.5.1: XF Cell Mito Stress Test time points and compartments for
Figure 6.5.2: Figures of XF Cell Mito Stress Test. Multiple time points readings
Figure 6.5.3: Box-Plot charts showing the important time points/sections of XF
Figure 6.6.1: Double immunofluorescence staining of MitoTracker® and WT1

Figure 7.1.1: A) and B) depicting the summation of role of WT1 in formation of

Figure 7.1.2: A model depicting the proposed mechanism of nephron endowment in

Figure 7.1.3: Potential mechanisms of factors related to low nephron number

LIST OF ABBREVIATIONS

DDS	Denys Drash Syndrome
DGS	Diffuse glomerulosclerosis
DNA	Deoxyribonucleic acid
2-D	2- dimensional
3-D	3- dimensional
E17.5	Embryonic day 17
EMT	Epithelial-mesenchymal transition
FSGS	Focal segmental glomerulosclerosis
H&E	Haematoxylin and Eosin
IHC	Immunohistochemistry
MET	Mesenchyme epithelium transition
MGV	Mean glomerular volume
MGW	Mean glomerular width
P0	Newborn mice
PCR	Polymerase chain reaction
PEC	Parietal epithelial cell
RNA	ribonucleic acid
TGFβ	Transforming growth factor β
VEGF	Vascular endothelial growth factor
WT1	Wilms tumour suppressor gene 1
Zn	Zinc

CHAPTER 1. INTRODUCTION

1.1 - Wilms Tumor 1 gene:

Located at chromosome 11p13, the WT1 gene spans across 10 exons (Hammes *et. al.,* 2001). Exons 5 and exon 9 provide the location of the main alternative splice donor sites. Exon 7-10 encodes four zinc finger (ZF) domains. It is postulated that WT1 plays a role in RNA processing by binding to both GC-rich and TC repeat elements, in addition to the well-established role as a transcriptional regulator (Morrison *et. al.,* 2008). Consistent with these functional differences, WT1 antibody staining shows localization within the nucleus that appears as diffuse, typical of transcription factors, or speckles, typical of splicing factors (Discenza *et. al.,* 2004). In normal kidney development, WT1 is important for metanephric mesenchyme survival and ureteric-bud induction (Miguel *et al.* 2005). WT1 gene plays a crucial role in urogenital system normal development and in some tumours such as Wilms tumour when mutated or misregulated. It exhibits a complex interaction in different tissues, with monoallelic and biallelic expression of both parents, tissue-specific and can be polymorphic imprinting pattern. There are multiple WT1 transcript reported of WT1 with evidence suggesting a non-AUG (CUG) translation initiation codon in some cases. Example of diseases related to mutation of WT1 is Denys-Drash Syndrome (DDS). In the kidney, when the WT1 related pathway is dysregulated, is can contribute to development of glomerulosclerosis, and specifically related to a specific type Primary Focal Segmental Glomerulosclerosis (FSGS). As a transcriptional factor, WT1 is important for cell survival and cellular development. (Hamilton et al., 1995), and recognize the sequence 5-GCG(T/G)GGGCG-3 (Stoll et al., 2007, Hashimoto et al., 2014) for DNA binding. Among the genes that were found to be the target for WT1 are Bmp7 that is essential for kidney development and Sulf1 which important in glomerular filtration.

WT1 is crucial for the urogenital development, and it also been shown to have tumour suppressor role. This is thought to be isoform specific. WT1 is a zinc finger DNA binding protein. WT1 isoforms without KTS (-KTS) motif are seen to have transcription factors functions (Smolen et al., 2004). WT1 isoforms having KTS (+KTS) motif have the ability to bind to mRNA and involve in mRNA metabolism and spicing (Markus et al., 2006). Intron 9 of WT1 provides the most important splice site, the +KTS and -KTS are different

due to the insertion of 3 amino acids difference, lysine, threonine, and serine, located between zinc fingers 3 and 4, in +KTS which is crucial for kidney and gonad development (Hammes et. al., 2001). Exon 5 of WT1 provide site for insertion of an alternatively spliced 17-amino acid segment (Hossain and Saunders, 2001). These 4 isoforms were the main form of WT1 proteins, and interaction of these 4 isoforms are thought to control the differentiation and cellular proliferation with their own target (Haber et al., 1991).

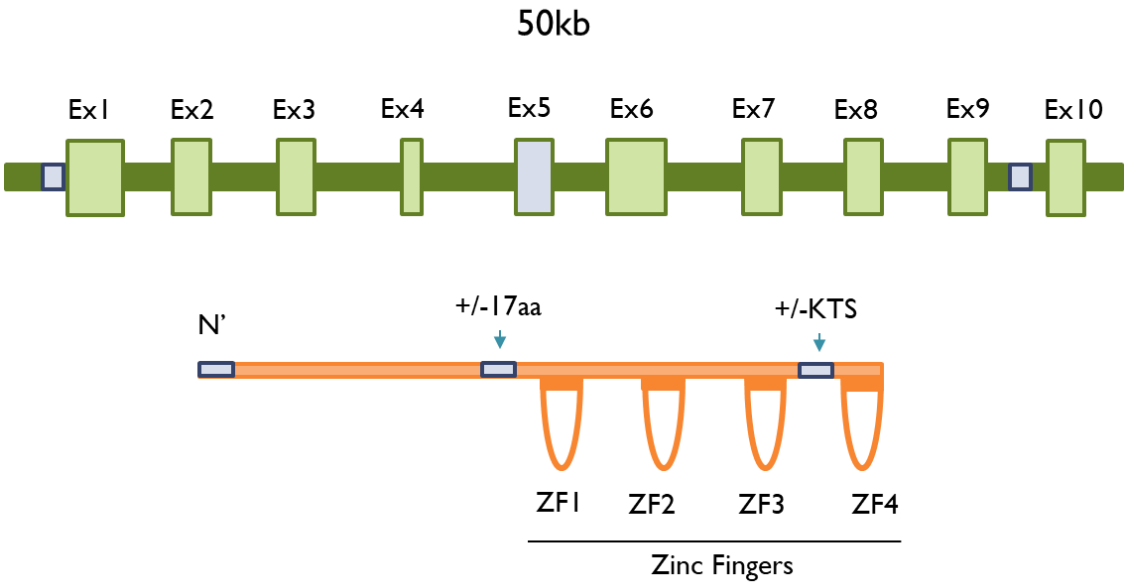

Figure 1.1.1. Figures show the exons of WT1 gene and the protein with 4 zinc finger (ZF) motifs at the C-terminus and a proline/glutamine-rich DNA-binding domain at the N-terminus.

Call et al. (1990) and Gessler et al. (1990) were the first to isolate WT1 protein when postulating the causative factors in Wilms tumour. Disruption of the DNA binding motif of WT1 either by somatic or constitutional mutation will result in a dominant negative phenotype. The WT1 (-KTS) isoforms was seen to be localised inside the nucleus in diffuse pattern, whereas WT1(+KTS) shows speckled pattern within the nucleus. Although different isoforms and mutations may show distinct patterns of subnuclear localisation, WT1 dominant negative protein interacting with other WT1 wild type

associated proteins may result in protein complex formation that concentrated within nucleus. Since then, Scharnhorst et al. (1999) described further 32 WT1 isoforms, further the complexity of WT1 activity and expression.

Davies et al. (2000) showed in a site-directed mutational experiment that only the disruption of the zinc fingers was sufficient to generate proteins with different properties in vitro. +/- KTS isoforms of WT1 retain their balance of expression when not interacting with targeted DNA. Introducing DNA of its target would disrupt the interactions of linkers and zinc fingers, and would bind to specific sites, with -KTS involved in a C-terminal helix-capping. Following this, Laity et al. (2000) generated different WT1 isoforms interacting with different locations allowing it to act at both the transcriptional and posttranscriptional levels. Mitsuya et al. (1997) study on fibroblast and lymphocyte shows biallelic expression nature of WT1, complementing the findings by Jinno et al. (1994) biallelic WT1 in more than half of the cells of preterm placental villus and foetal brain, suggesting tissue specific and individual-specific modifier.

In a study by Niksic et al. (2004), up to half of Wt1 protein was shown to localized in cytoplasm. Wt1 proteins were continuously shuttled between cytoplasm and nucleus, including WT1 (+/-KTS) isoforms. Cytoplasmic WT1 proteins are mostly associated with ribonucleoprotein particles (RNPs) and are involved in regulation of translation.

1.2 – Kidney: Normal structure and function

In a normal developed adult, grossly kidneys are paired organs, have a general shape of a bean measuring about 6cm wide, 11cm long and 3cm thick. Each kidney weighs approximately 150grams, positioned at the level of T12-L3, with the right kidney positioned slightly lower than the left kidney due to the surrounding organs. Blood is supplied to the kidney via a pair of renal arteries and exit via a renal vein from each kidney. From the renal pelvis, urine is drained through the ureter to the urinary bladder. Each of the kidneys are enclosed by renal capsule that made of thin fibrous connective tissues as a protective against injuries and infections. The renal capsule is surrounded by a layer of adipose tissue, which in turn enclosed by renal fascia.

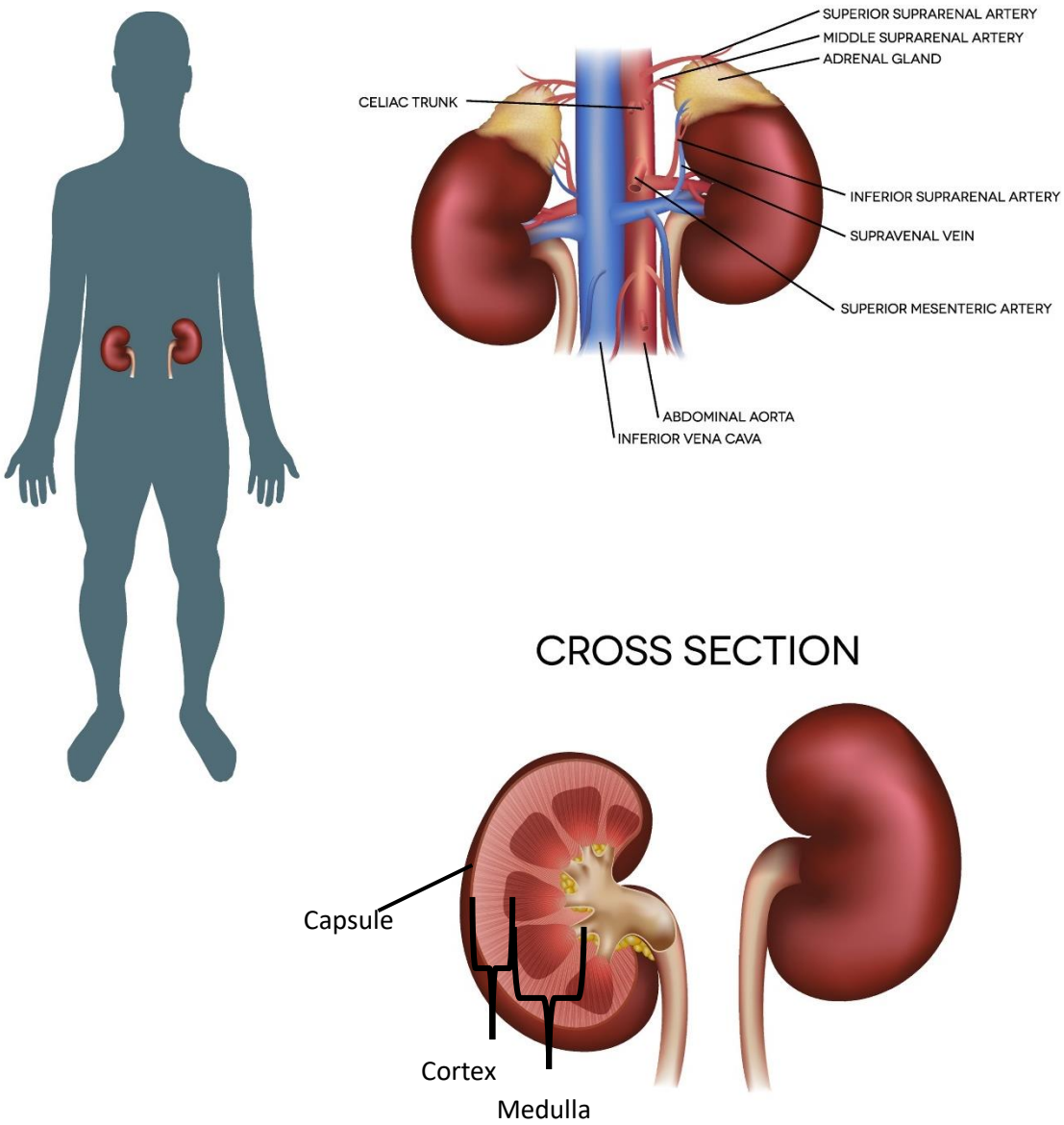

Figure 1.2.1: Figures showing the general location and the cross section of the kidney. The cross-section showing the capsule, cortex, and medulla. The Cortex consists of renal corpuscles (glomerulus) and convoluted tubules. Medulla is the innermost layer, consisting loops of tubules and collecting ducts, and clustered into renal pyramids (pyramid-like appearance) separated by renal columns, that concentrate to become calyces that formed funnel, called renal pelvis that funnel out urine to the ureter. Image, guniita©123RF.com.

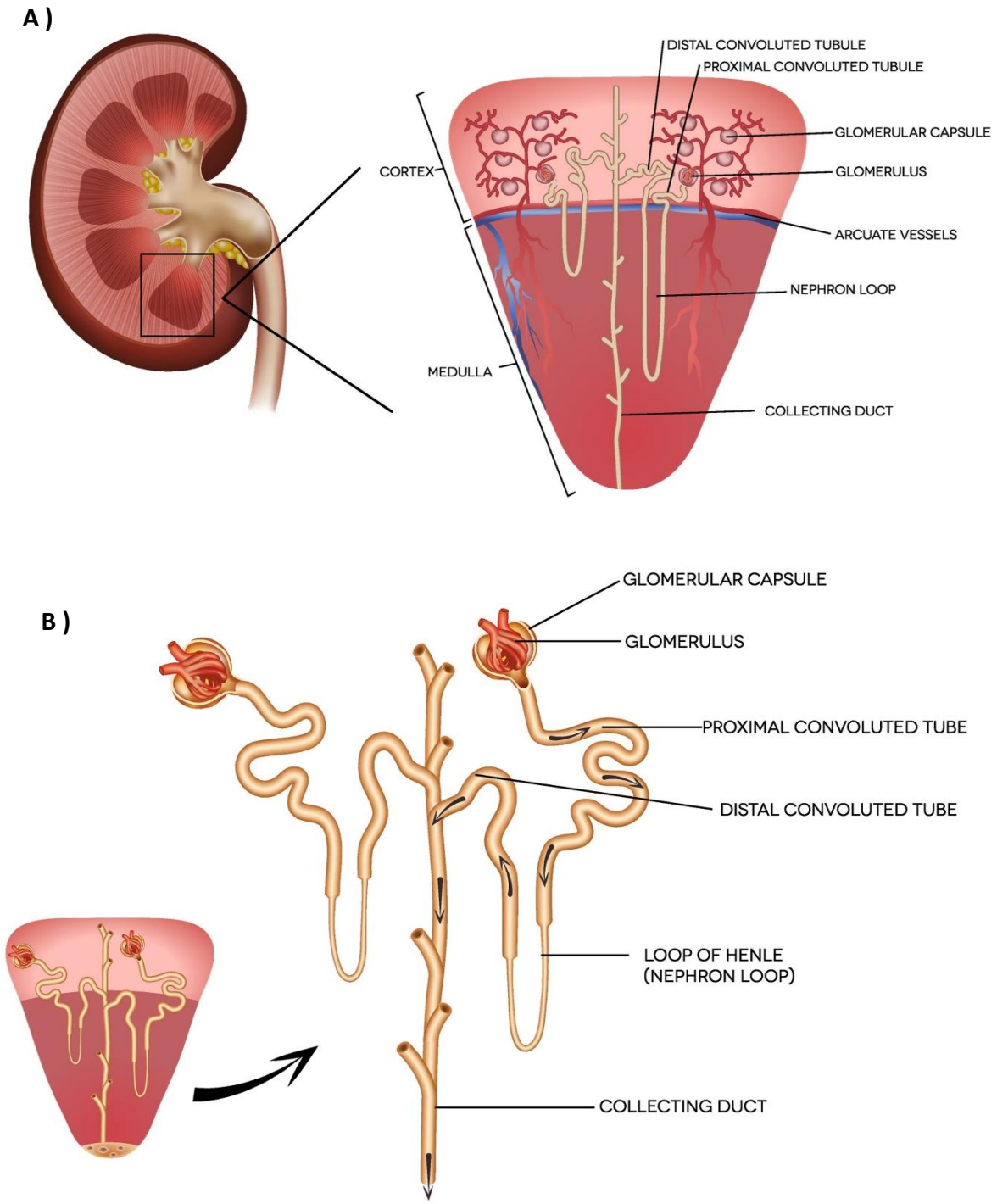

Figure 1.2.2: Figures showing the A) cross-sectioned kidney and zoomed-in at the border between cortex and medulla and B) the structure of the functional unit of the

kidney, the nephron. Cortex is the area of the kidney where most glomerulus are located. Glomerulus is the part which filters the plasma. Image, guniita©123RF.com.

The kidneys as a paired organ serve the human body with multiple important functions. Inside the kidney, the most important structural and functional unit is the nephron. On average, each adult kidney has about 1 million nephrons and this can vary between individuals. The nephron regulates the contents of the plasma that flows through the kidney via the processes of filtration, reabsorption, secretion, and excretion. The most obvious function of the kidneys is the excretion of waste metabolites from the body, including but not limited to, urea, creatinine, uric acid and others such as drugs and toxins in the urine. The kidneys also selectively reabsorb the required elements back such as required electrolytes, water, amino acids and glucose in the renal tubules, and regulates pH balance. By regulating the fluid and electrolyte balance, kidneys regulate the body osmotic pressure, termed osmoregulation. They also serve as an endocrine organ, in which an enzyme, renin, is secreted which is involved in regulating blood pressure, production of erythropoietin, which is essential for normal red blood cell formation, and in converting vitamin D precursor to its active form, 1, 25-dihydroxycholecalciferol (calcitriol).

1.3 – Normal Kidney Development

During normal embryogenesis, at e8-e9.5 of mice foetal development, the first hint of kidney formation is the appearance of a pair of nephric ducts (ND) (a.k.a Wolffian duct) which dorsally grows from the intermediate mesoderm (IM) just under the 5th somite. This duct grows reaching the cloaca, sequentially forming pronephric than mesonephric tubules. The anterior end of pronephric duct consists of a transient rudimentary structure called pronephros that is non-functional in mammals, that rapidly degenerates. As the ND grows, the middle part, made up of mesenchymal cells (a.k.a. mesonephric duct), condenses to give rise to mesonephric tubules. These tubules having the mesonephros anteriorly are transient and degenerate as the duct develop

caudally, until the metanephric kidneys develop from induction with metanephric mesenchyme (MM) (Saxén and Sariola, 1987, Dressler G, 2006).

At e10.5-11, at the hind limb of the nephric duct just under the 25th somite, outgrows an epithelial tissue budding, the ureteric bud (UB). The initiation of kidney development requires reciprocal and sequential interaction of intermediate mesoderm (IM) derived tissue, an outgrowth of epithelial tissue from the nephric duct, when the ureteric bud (UB) emerge and invading the adjacent metanephric mesenchyme (MM) (Figure 1.3.1) (Saxén, 1987). After the initial budding, signals from the metanephric mesenchyme (MM) direct the subsequent branching of the ureteric bud tips, forming a polarized renal vesicle (RV) (Costantini and Kopan., 2010) further generating an arborized network of collecting duck system, that concentrates and transports urine out from glomeruli to the ureter and bladder.

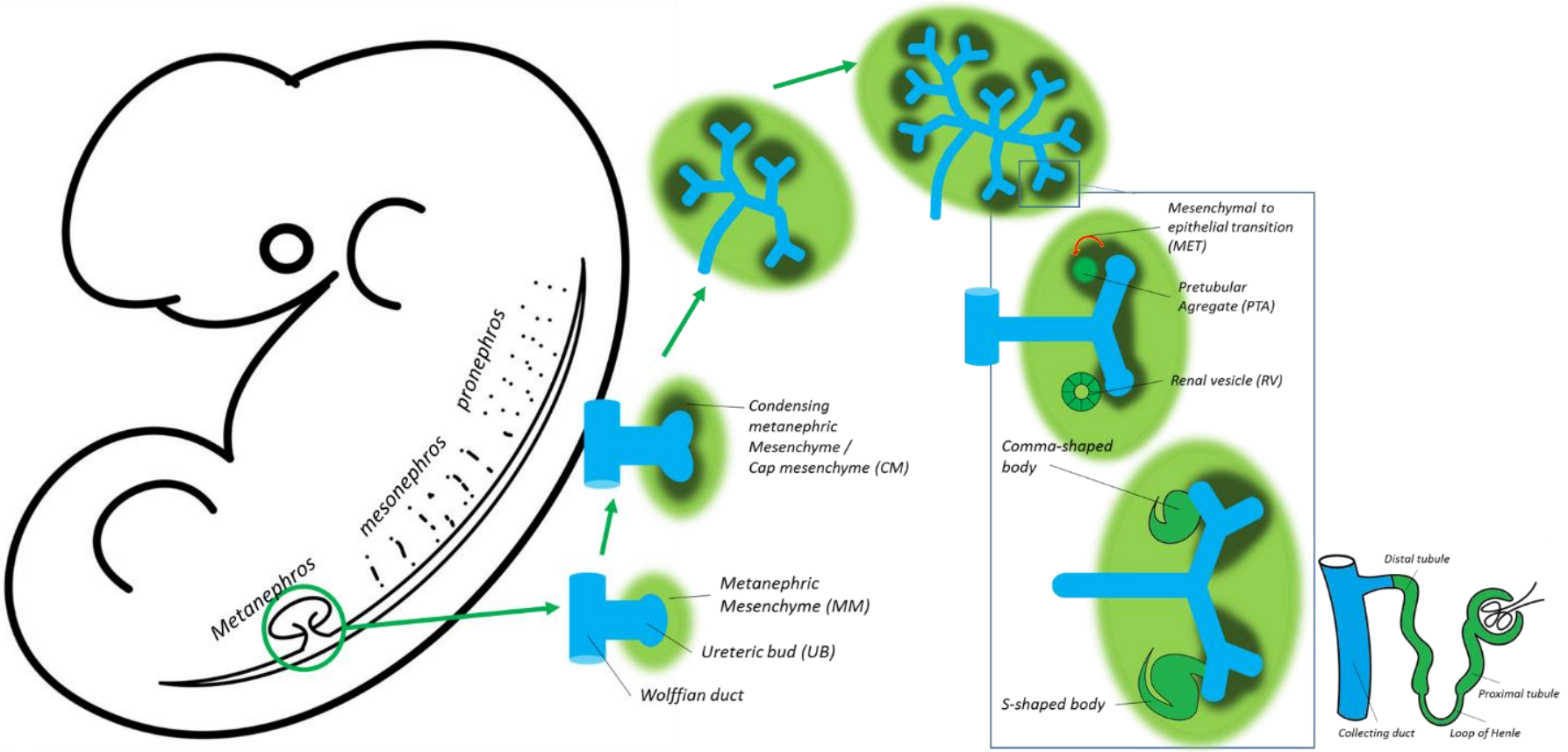

E11	E11	E12	E12.5	E13.5	Start at E15 to P12

Low concentration but generalized WT1 expression → High concentration but more cell specific WT1 expression

Figure 1.3.1: Stages of normal for kidney development in mouse. Schematic representation of kidney development showing maturation from condensed mesenchyme to comma shaped body, then S-shaped body, then mature glomerulus. WT1 expression levels are represented by the lowest bar. WT1 is expressed at low levels throughout the metanephric mesenchyme, in the adult WT1 expression is restricted to podocytes but is expressed at high levels.

As the polarized RV grows, the distal part grows, attaches and links to the bordering UB forming a connected structure. The connected RV quickly grow and advance to form comma-shaped bodies (CSB) and grow further to be S-shaped bodies (SSB). SSB is retain the polarized attribute, having proximal, intermediate and distal segments that connects to the UB. The most proximal segment subsequently expands into two layers of epithelial of visceral and parietal, respectively later known as Bowman's capsule and podocytes. The segmentation of SSB further evolves to become the mature nephron composed of glomerulus (proximally), proximal tubule, loop of Henle and distal tubule (distally) that connected to the collecting duct. The mature nephron is seen as early as E16.5 however various stages of nephron development can still be seen until postnatal. All the nephron development stages coexist at the same time (Hartman et al., 2007). This actually one of the reasons why with presence of non-fatal factors that affect kidney development, the range of reduction of nephron number is not very profoundly different from wildtype, nonetheless important long term.

WT1 gene plays central role in initiating nephrogenesis as shown in a gene knockout experiment in transgenic mice (Kreidberg et al., 1993). WT1 was shown to be expressed in the condensing mesenchyme (cap mesenchyme, CM) and also specializing cells in glomerular formation (visceral epithelial/podocytes) (Pritchard-Jone et al., 1990, Rackley et al., 1993, Yeger et al., 1992), with the expression was documented to be lowest in metanephric mesenchyme with generalized expression throughout developing kidney, becoming more concentrated as specialization continues with the highest in the S-tubular forms, then the expression gradually lowers as maturation of glomerular progresses, which WT1 expression absent from tubules and concentrated in specialized cells of the mature glomeruli uniformly express WT1, the

podocytes cells which only can be seen to actively express WT1 in mature glomerulus (Yeger et al., 1996).

The expression pattern of WT1 is restricted in general embryogenesis and the intracellular expression pattern in renal development contribute to the possibility of WT1 having specific and dedicated roles in specific tissues and cell specific differentiation. It is also likely that it serves as main regulator of glomerular and nephron differentiation and to some extent functional maturation (Yeger et al., 1996). The expression of WT1 persists into the postnatal period at relatively high levels with concurrent continuation of growth and maturation processes of mouse kidney (Armstrong et al., 1993, Buckler et al., 1991, Rackley et al., 1993., Saxen et al., 1987) which is later followed by a steady decrease to low level adult expression 2 weeks after birth (Yeger et al., 1996) once the kidney tissues are differentiated to functional specialization and the glomeruli mature and losses it's proliferative ability.

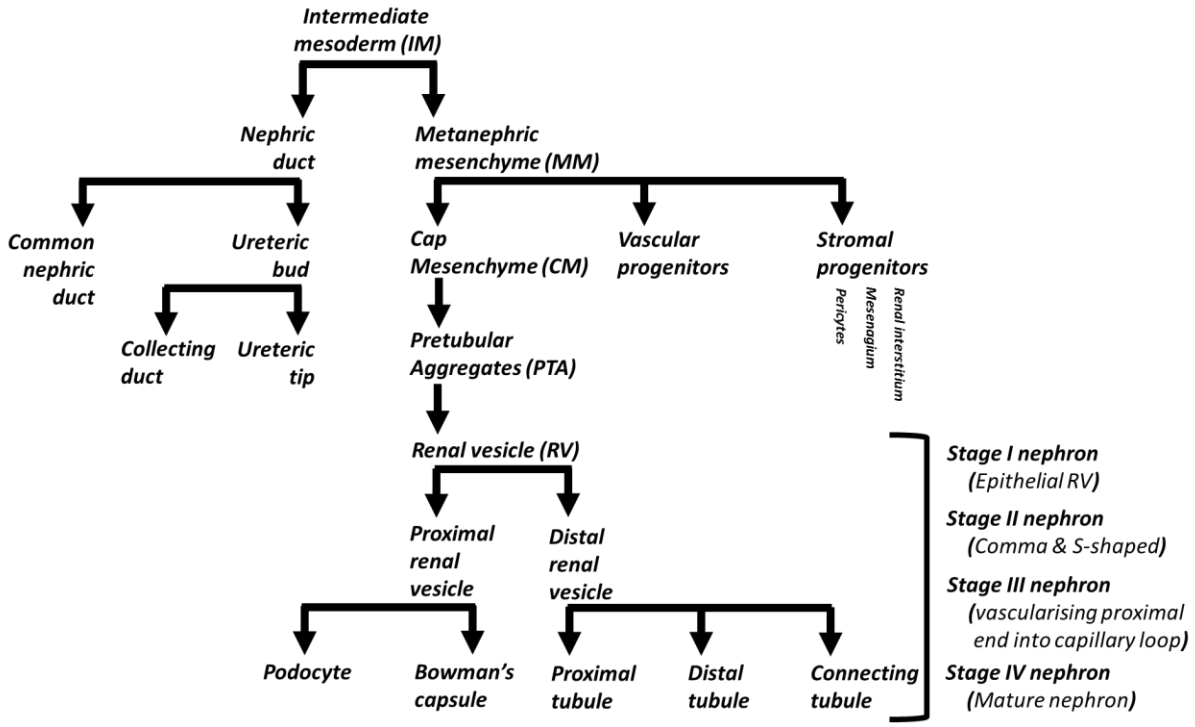

Figure 1.3.2: Significant turn points of lineage relationship of cells in developing kidney (adapted from Little and McMahon, 2012)

During kidney developmental processes, three main progenitor populations have been proposed from cell-fate studies (reviewed by Little and McMahon 2012), those are the cap mesenchyme (CM), vascular progenitors and stromal progenitors.

It is thought that notwithstanding the slightly different of starting time of each individual nephron, the local expression of nephron development is the same. Embryonic nephron shows patterns of origin underneath the ureteric tip while final nephron push post birth resulting in multiple direct connecting nephron per ureteric tip (Rumballe et al., 2011).

1.4 - Chronic Kidney Disease (CKD)

1.4.1 – Background

Chronic renal disease is a reduction of renal function attributed to structural abnormalities as evidenced by changes in glomerular filtration rate (GFR) or pathological examinations (National Kidney Foundation, 2002).

Chronic kidney disease (CKD) is an irreversible loss of renal function for at least three months. It is a major public health issues and is a significant burden on health care funding. The prevalence of CKD and end-stage renal disease (ESRD) is high in advanced countries and is increasing worldwide. It is estimated that the prevalence of CKD in the US was 16.8% while in Asia the prevalence ranged from 12.1% to 17.5%, data were collected in 2007-2008 and 2006-2007 respectively (Ingsathit et al., 2010, Chen et al., 2009). In Malaysia, the incidence and prevalence of patients with ESRD on dialysis had increased from 88 and 325 per million population (pmp) respectively in 2001 to 170 and 762 pmp respectively in 2009. The increase in ESRD was largely driven by the increasing incidence of diabetic kidney disease (DKD) accounting for 58% of new patients accepted for dialysis (Lim et al., 2011). The increasing incidence is attributed to the increasing population of ageing people and chronic non-communicable disease

(non-infectious in origin) such as hypertension and diabetes mellitus as the main cause, with the projection of exceeding 2 million people will be on dialysis for CKD by 2030 (Szczech and Lazar 2004).

However, for paediatric cases, the causes of CKD are a bit different. The North American Paediatric Renal Trials and Collaborative Studies (NAPRTCS) registry collected data on paediatric CKD patient, including below 21 years old since 1994, providing a number of causes of CKD in children (Fivush et al., 1998, NAPRTCS 2008). In the NAPRTCS report, it is documented that the most common causes included congenital anomalies of the kidney and urinary tract (CAKUT) (48%) followed by hereditary nephropathies (10%), followed by others such as glomerulonephritis, haemolytic uremic syndrome, congenital nephrotic syndrome and others (Harambat et al., 2011). The cases and incidence of individual diseases varies with age accordingly. All these diseases contribute to development of CKD in children, which in most cases contributes to glomerulosclerosis and varies across races. For example, in African American children the incidence of glomerulosclerosis is 3 times higher (19% versus 6%) than Caucasian children (NAPRTCS 2008). These causes of CKD were found to be similar in registries in Belgium and Italy (Ardissino et al., 2003, Mong et al., 2010).

The growing number of cases of ESRD places an enormous burden in both economic and social terms and on the healthcare system. In an economic evaluation among the Ministry of Health dialysis centres in Malaysia, the cost of dialysis and erythropoietin was RM2,500 per month for a patient (Hooi et al., 2005). In the US, the cost of medical care was 1.7 times higher in patients with CKD stage 3 and 2.6 times higher in those with stage 4 CKD compared with controls (Smith et al., 2004). Early kidney disease is largely asymptomatic and patients often present late with complications of CKD. As such, targeted screening and early intervention will be necessary to reduce the burden of the disease. Primary care providers play a key role in the early identification, treatment and improving the outcome of patients with CKD. Awareness of CKD among primary care providers should be increased and they should be equipped to treat these patients. As the prevalence of diabetes is increasing and DKD remains the most common cause of CKD, optimal control of diabetes will be necessary to prevent CKD.

Chronic kidney disease is increasing worldwide (Arora, 2012). Glomerulosclerosis, resulting in reduced renal filtration and leading to renal failure is the common aetiology of a range of conditions leading to CKD – most notably diabetic nephropathy. Once triggered, glomerulosclerosis spreads throughout the kidney and the stress of reduced renal filtration causes death of podocyte cells, thus exacerbating the condition. It is known that the stress of reduced renal filtration induced by nephron underdosing, for example, as a result of poor maternal nutrition or preterm birth, is a key risk factor for susceptibility to glomerulosclerosis in adult (Bertram et al., 2011).

The evaluation of kidney function is done through equations estimating the glomerular filtration rate (eGFR), replacing the traditional serum creatinine in 1999. Due to the more reliable evaluation system, more people have been identified and labelled as CKD. In a population of ageing people at 70 years old and over, about half would have eGFR of <60 mL/min/1.73 m^2 (Ebert et al., 2017) which is actually the advocated threshold for diagnosing CKD (National Kidney Foundation 2002). The higher prevalence of detectable CKD with ageing also would increase the burden of manging CKD (KDIGO 2012).

It is suggested that CKD shares a common pathway of progressive injury. This is shown by the common appearance of glomerulosclerosis, vascular sclerosis and tubulointerstitial fibrosis (Olson and Heptinstall 1988) (basically a progressive scarring of renal tissues). The adaptation capabilities of the nephron are reduced as the changes occur with time and injury, eventually scarring occurs, and further reduces the capabilities of nephron and kidney as a whole, perpetuating a vicious circle, that ends up in end stage renal failure. The possible mechanisms underlying sclerosis may be different in relation to different kind of disease, but they may involve some factors such as; possible underlying predispositions for CKD, genetic factors and low nephron number, podocyte loss, hemodynamic factors, proteinuria, various cytokines and growth factors, renin–angiotensin–aldosterone system (RAAS) and specific mechanisms of tubulointerstitial fibrosis (Fogo 2007).

1.4.2 – Glomerulosclerosis

Glomerular sclerosis also known as glomerulosclerosis is the condition where the glomerulus and its blood vessel in the kidney are scarred and hardened. Focal segmental glomerulosclerosis is where only some part of the glomeruli is damage or sclerosed. Both global and focal glomerulosclerosis have been shown to occur in various populations, age groups and kidney donors (Rule et al., 2010, Kubo et al., 2003, Hoy et al., 2003). In older people where there is reduction in podocyte number, a crucial functional cell in the glomerulus for filtration, this causes the glomerular tuft collapse and influences the development of glomerulosclerosis (Hodgin et al., 2015).

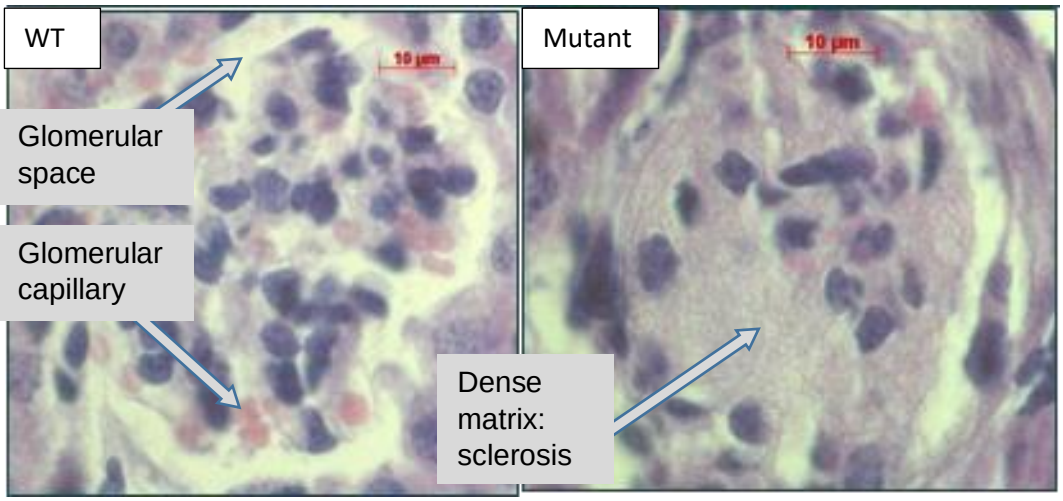

Figure 1.4.2.1. Representative figure of H&E-stained kidney sections from wild type (wt) mice and mice revealing glomerular sclerosis (dense matrix of sclerosis), obliteration of the glomerular space and glomerular capillary. Image curtesy of Ahzad MSc (2010).

Normal adults have some degree of a sclerosed glomerulus, but the upper reference (95th percentile) limit was determined from 1847 kidney donors for normotensive living kidney donors according to age (Kremers et al., 2015). For example, in a biopsy of a kidney showing 20 glomeruli, one of them is expected to be sclerosed in a 25-year-old, whereas 6 glomeruli are expected to be sclerosed in a 75-year-old. In patients with kidney diseases, risk estimation for CKD progression would be better with this age-specific glomerulosclerosis estimation (Srivastava et al., 2018, Hommos et al.,

2018). FSGS, when seen in a biopsy of human kidney, is usually considered pathological. FSGS can be caused by a number of factors, one of those is the genetics. Genetic mutations that encode for protein functions in podocytes, slit diaphragm, glomerular basement membrane and fenestrated endothelial layer of the filtration barrier would contribute to FSGS formation. In children, FSGS usually follows an autosomal recessive pattern, in which the most common genes involved are nephrin (*NPHS1*), podocin (*NPHS2*), and phospholipase C epsilon 1 (*PLCE1*). For autosomal dominant FSGS, it usually manifested in older children, adolescents and adults.The most common genes involves are; inverted formin, FH2, and WH2 domain containing (*INF2*), actinin alpha 4 (*ACTN4*), *TRPC6*, *WT1*, and *LMX1B* (Barua et al., 2013, Hinkes et al., 2007, Santín et al., 2011). FSGS in these cases might presented as familial disease or sporadic, autosomal dominant or recessive, X-linked or matrilineal, in which case are thought to be related to mitochondria (An et al., 2018).

1.5 – Denys Drash Syndrome (DDS)

1.5.1 – Background

Denys-Drash syndrome (DDS) is featured by a triad of male pseudohermaphroditism, Wilms tumour and progressive renal disease. In the kidneys of these patients, there will be diffuse mesangial sclerosis, scarring of the kidney that is seen from infancy, marked by proteinuria that later progress to nephrotic syndrome and renal failure. Pelletier et al. (1991) managed to identify a genetic mutation in the WT1 gene in 10 of his DDS patients (out of 17 patients). Later on, Baird et al. (1992) showed 6 out of 8 of his DDS patients had a similar genetic defect of heterozygous germline mutations. DDS patients were shown to have a germline point mutation in WT1 gene in the eighth or ninth exons, which resulted in the substitution of single amino acid, and almost all of these patients developed Wilms tumour in the kidney. By investigating these patients, Hastie (1992) demonstrated that the WT1 gene is important in development of the genitourinary system, with evidence of the WT1 mutation having a dominant negative effect in these cases. In the process of sexual differentiation, the WT1 gene interacts with SF1 (steroidogenic factor 1), and this is crucial for gonadogenesis in mammals. It acts via the regulation of MIS (Mullerian inhibiting

substance). In normal physiological development, Müllerian duct will form later female reproductive organs later on (these include oviducts, uterus, cervix, upper vagina), however in males, Müllerian duct regression (self-apoptosis) will occur, and WT1(-KTS) isoforms was shown before to be related to this switching of Müllerian duct continuous development or regression (Nachtigal et al., 1998). The WT1(-KTS) isoform was shown in vivo to be able to transactivate a gene that can determine sex in humans; the SRY gene, by promotor region binding and at least four mutations of WT1 were seen in DDS causing SRY gene failure for promotor activation (Hossain and Saunders 2001). In DDS glomerulopathies, it is thought that the loss of WT1 functions impairs the podocyte development and maintenance, and WT1 knockout mice showed podocyte differentiation defects, leading to kidney failure and early death (Dong et al., 2015). However, the exact molecular mechanism of how WT1 mutation cause the changes at cellular level is still undetermined.

1.5.2 – Animal Model - *Wt1*$^{tmT396/+}$ mice (a.k.a DDS/+)

Heterozygous *Wt1*^{tmT396}/+ a.k.a DDS/+ mouse in this thesis, were first produced in Patek laboratory at the Sir Alastair Currie Cancer Research UK Laboratories, University of Edinburgh. Mice were then transported to Newcastle Medical School, Newcastle University in accord with our Home Office licence. In both settings mice been given similar feed pellets with extra of sunflower seed given in Newcastle. All animal sources used in the study listed were taken from Newcastle animal breeding centre. In the beginning, *WtV1* gene targeting vector when introduced, inserting a Leu2/neo cassette in the middle of *Wt1* exon 9 (Figure 1.5.2.1-a). This brings about an amino acid substitution (S395R) which subsequently causes a premature termination within zinc finger 3 as a result of translational stop at codon 396 (*Wt1*^{tmT396}) inclusions. In general, it resulted in truncated protein of 7.3kDa with loss of the next 52 amino acids, together with the KTS insert (main isoform forming point) and the last zinc finger 4. The production and identification of these ES cells (*DDS*/+) by multiple analysis has been illustrated in detail in Patek et. al., 1999. Accurately targeted, 129/Ola-derived ES cells were then injected into host blastocysts of C57BL/6JLac. The product chimeric mice identified by their coat colour were then backcrossed to the original 129/Ola background

mice to get it close to the original wildtype as possible. Southern blot analysis identified the targeted ES cells (*DDS*/+) as distinct from the demonstrated bands of a wild-type (19kb) and mutant (13kb) (Patek et. al., 1999, Patek et. al., 2008), this was confirmed by PCR (Figure 1.5.2.1-c). In order to advocate the line of pure 129/Ola genetic background, continuous breeding of heterozygous 129/Ola males with wild-type 129/Ola females as described by Patek *et. al.,* 2008. This would maintain *Wt1*^{tmT396}/+ mice as female *DDS*/+ mice are not fertile (Patek *et. al.,* 2008) and unsuited for breeding. Heterozygous (*DDS*/+) mice were detected normally using PCR analysis of mice DNA utilising 3 primers in the same PCR reaction: Ex9F2 (5'-AGACCTTCTCTGTCCGTTTAG-3') positioned in exon 9, neo52 (5'-GATGCC TGCTTGCCGAATATCATGG-3') positioned in the neo cassette, and Cre1R (5'-TGTTCTGAATCTCCTGGACA-3') positioned in intron 10. Amplification of the wild-type allele is by the primers Ex9F2 and Cre1R, producing a 345bp band product in wild-type and heterozygous mice (however not for *Wt1*^{tmT396} allele because of intervening 3.4kb Leu2/neo cassette). As for the primer pair neo52 and Cre1R, amplification of *Wt1*^{tmT396} allele produce a 600bp band product in heterozygous and homozygous mice. For the rest of the thesis, this heterozygous *Wt1*^{tmT396} mice will be recorded as DDS/+ mice.

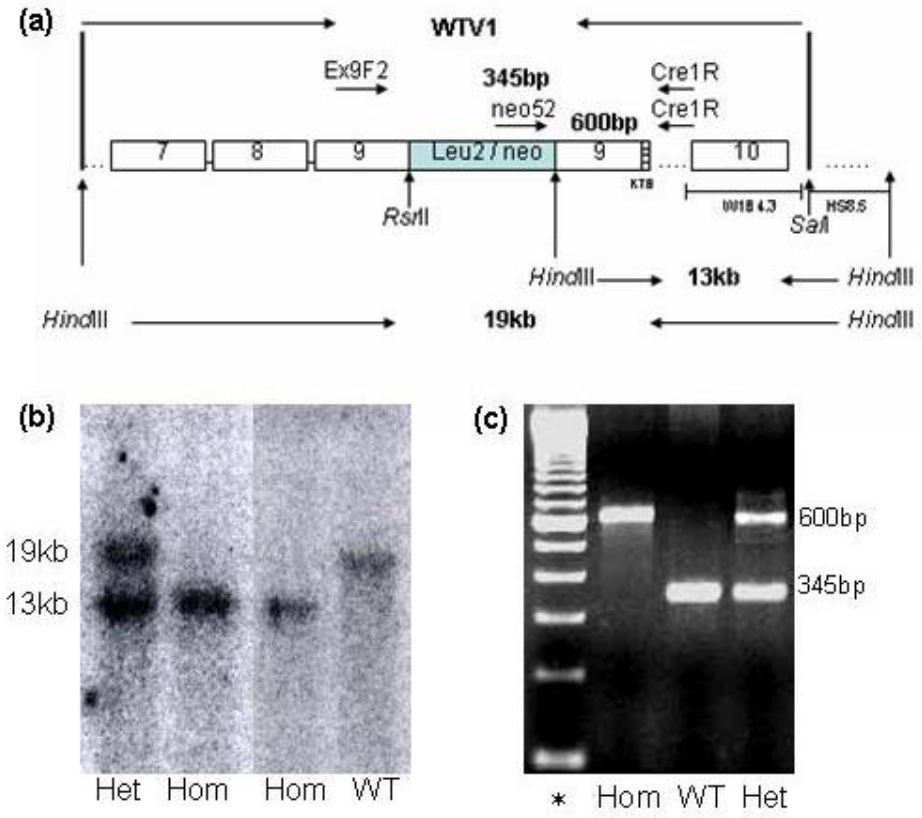

Figure 1.5.2.1: DDS/+ mouse strain production

(a) WtV1 inserts of the Leu2/neo cassette into Wt1 exon 9 (blue coloured). This instigates an amino acid substitution (S395R) and premature termination within zinc finger 3 by inclusion of a translational stop at codon 396. Figure 1.6 (b) Southern blot probing and generating bands of 19kb for the wild type allele and 13kb for the Wt1^{tmT396} allele (heterozygous (het), homozygous mutants (hom) and wild type (WT)). Figure 1(c) PCR bands of wild type (WT), DDS+/- (het, heterozygous) and Wt1^{tmT396}+/+ (hom, homozygous) (wild type - 345 bp, Wt1^{tmT396} - 600bp). Image reproduced with permission from Patek et. al., 2008.

1.6 – Mitochondria

Mitochondria are important energy production organelles of eukaryotic cells. They have a double membrane and one of their major functions is to produce ATPs by oxidative phosphorylation (OXPHOS), as well as other cellular processes such as iron-sulphur cluster biogenesis and calcium homeostasis (Duchen 2000, Stehling and Lill 2013). In an individual cell, there will be numerous mitochondria, the number of which varies between cells and between individuals.

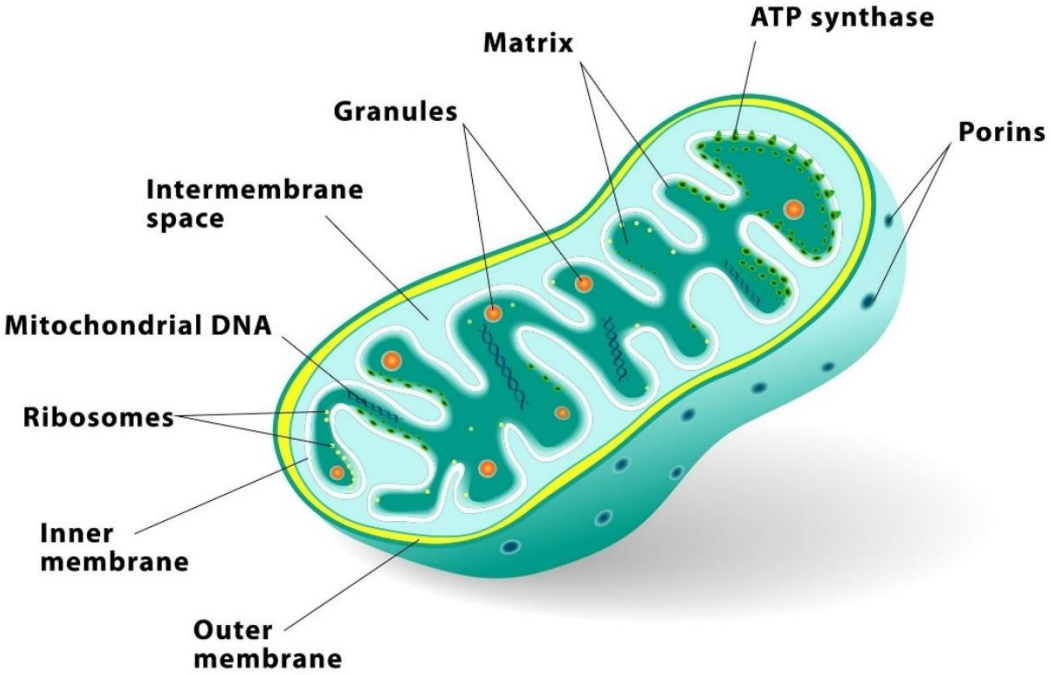

Figure: 1.6.1: Figure depicting the cross-section and internal structure of mitochondria. Image, designua©123RF.com

Mitochondria has its own DNA, mtDNA, that is circular, at 16.6kb that encodes 22 mitochondrial tRNAs, 13 proteins of OXPHOS subunits and two mitochondrial ribosomal RNAs (mt-rRNAs) (Anderson et al., 1981). MtDNAl is exclusively inherited from the maternal ovum (Giles et al., 1980). For a mitochondrial to function properly, the mtDNA is not enough. There are about 1300 known nuclear-encoded mitochondrial proteins that will be transported into mitochondrial to support various functions and OXPHOS system (Calvo et al., 2016). So as the mitochondrial system depends on both mtDNA and

nuclear DNA, it is understandable that mitochondrial diseases would be caused by both nuclear and, mtDNA defects with their inheritance pattern, matrilineal (maternal) inheritance, or it can also be secondary from ageing associated somatic mutations (Greaves et al., 2014).

Mitochondrial dysfunction would result in abnormalities in mitochondrial function, predominantly affecting tissues and organs which have high energy requirement. Clinically it can arise either in infancy or adulthood and can either affect various body systems or can also be isolated to certain organs only (Lightowlers et al., 2015). The recorded prevalence of mitochondrial diseases is around 4.7 for every 100000 children (Skladal et al., 2003) and about 12.5 for every adult population (Gorman et al., 2015). Mitochondrial diseases are very difficult to detect as correlation between the genotype and phenotype is somewhat lacking, which means diagnosis tends to be missed and complicated.

With mtDNA having multiple copies of mitochondria within a single cell, this give rise to a unique aspect of mtDNA in which if all of mtDNA is of similar copies, this is called homoplasmy; there can also be a mixed population of mutant and wild type mtDNA, this is called heteroplasmy. mtDNA mutations are predominantly functionally recessive; a specific proportion of mutated mtDNA has to be present before a biochemical defect becomes apparent. (Stewart and Chinnery 2015). When the threshold is exceeded, the most common biochemical defect is a reduction in the activity of the associated OXPHOS enzyme complex(s).. The most common mutational event for primary mtDNA disease is point mutations which are usually maternally inherited and also large-scale mtDNA deletions which usually occur *de novo* at the embryonic stage.

Until to date, no study has proven any connection between the WT1 gene and mitochondrial genes and how they might relate each other.

1.7 – WT1, apoptosis and cell viability

Apoptosis is a controlled active mode of cell death that is part of a normal physiological process which minimizes disruption to adjacent cells and structures (Taylor et al., 2008) and uses energy to proceed (Green and Kroemer, 2005).It plays an important role in tissue remodelling, regeneration and the establishment of tissue architecture in developmental processes (Meier et al., 2000). A dysfunction in apoptosis will contribute to an imbalance between mitosis and apoptosis, which manifests as developmental abnormalities, cancer or degenerative disease.

During kidney development, the rate of apoptosis is highest during development (Koseki et al., 1992), and is involved in nephron number and pattern determination. A normally functioning kidney is critically dependent on intricate multicellular arrangement and nephron patterning. Loss of normal apoptosis regulation and balance can contribute to an exaggerated proliferative response. which can manifest as acute and chronic kidney diseases such as chronic tubular atrophy, podocytopenia and acute kidney injury (AKI) (Lorz et al., 2006, Olsen et al., 1985, Shankland SJ, 2006, Hughes and Savil, 2005).

At the cellular level, apoptotic cells show a distinct pattern of loss of specialised structures such as microvilli and also the loss of cell junctions, followed by cytoplasmic shrinkage, coalescent of nucleus in condensed mass, that later on breaks into fragments. The cells become convoluted after losing intracellular fluid and ions, and later breaks down into multiple membrane-enclosed apoptotic bodies that will be phagocytosed by mononuclear-phagocyte cells or sometimes the adjacent surrounding cells (Haanen and Vermes 1995) without activation of unnecessary inflammatory cells (Kroemer et al., 2005).

Cell viability is maintained by an intricate interplay of various survival factors that actuate intracellular survival pathways and lethal factors that mediate the dormant lethal pathways to apoptosis system (Sanz et al., 2008) (Figure 1.7.1). Typically, cell death is an outcome of the cell microenvironment (Green and Kroemer, 2005, Riedl and Salvesan, 2007, Lorz et. al., 2006) in which surrounding the cells can be regulators of cell survival (e.g. soluble mediators, nutritional factors, and the extracellular matrix) or lethal factors (e.g. cytokines and cell stress). When triggered, cells may undergo

apoptosis through two main pathways: the intrinsic (intracellular homeostasis) and/or extrinsic pathways (ligation of plasma membrane death receptors).

Extrinsic apoptotic pathway commenced when a death receptor is bound and ligated (Fas, tumor necrosis factor receptors) (reviewed in Tait and Green 2010) leading to the recruitment and assembly of multimolecular complexes (e.g. FADD (Fas associated death domain), caspase 8 and 10) (Ashkenazi and Dixit, 1999, Thorburn 2004) which are then activated upon oligomerization and in turn activate downstream effector caspases (caspase 3 and 7). The intrinsic pathway implicates intracellular organelles complex interactions and the centre of it is mitochondria (Riedl and Salvesan, 2007, Green and Kroemer, 2005, Ferri and Kroemer, 2001, Ravagnan et. al., 2002).

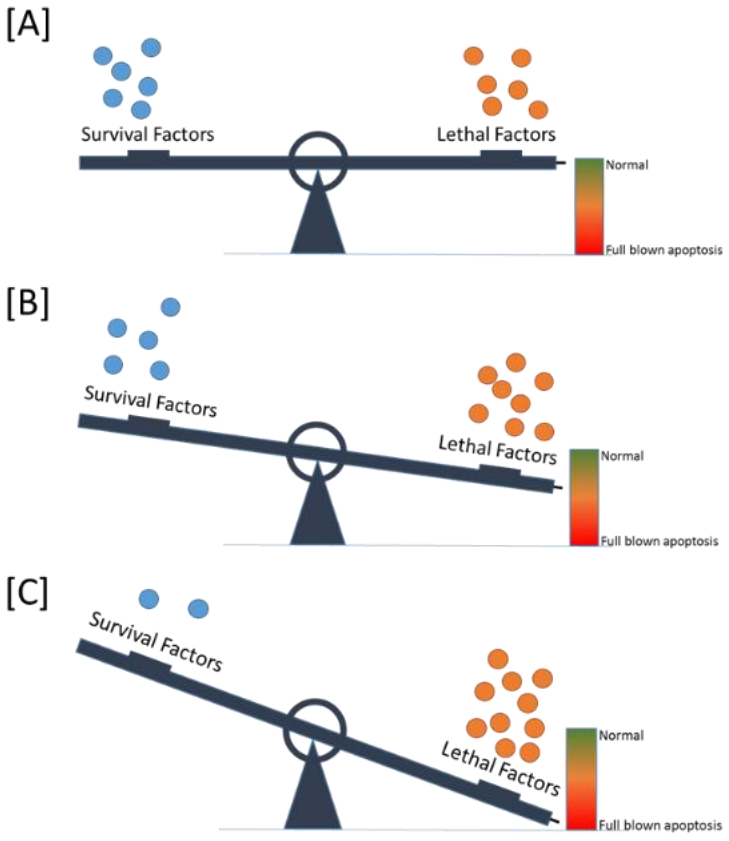

Figure 1.7.1: Representative diagram of possibility that disrupted within the mutant kidney.

A complex interaction of proapoptotic and antiapoptotic members of Bcl2 family is integral for intrinsic pathways regulation. Among the most important, the proapoptotic Bak and/or Bax is triggered by the sentinel activator BH3-only proteins. (Tait and Green, 2010), which will induce permeabilization of outer membrane of mitochondria, releasing more downstream proapoptotic factors, including cytochrome c, SMAC/DIABLO and AIF (apoptosis-inducing factor). These later then further promote apoptosis, either through caspase-dependent or caspase-independent pathways.

1.8. - WT1 and disease

1.8.1 - WT1 mutation, kidney development and disease

Mammalian kidneys develop from the metanephric mesenchyme and ureteric epithelium interaction, consisting of three major stages. The intermediate mesoderm develops into the metanephric blastema, followed by ureteric bud outgrowth and branching, and subsequently the metanephric blastema condenses and forms renal epithelial cells (Kreidberg *et al.,* 1993).

In 1993, Kreidberg et al. developed a knockout mouse model for the WT1 gene. Mice lacking WT1 present with complete kidney agenesis and display the earliest renal deficiency of any knockout mouse (Sainio, et al. 1997, Ahzad Msc Project 2010). Knockout of the WT1 gene generated mice with multiple defects that died mid-gestation of abnormal heart development and completely lacked kidneys (Kreidberg et al., 1993, Patek et al., 2008). In adults, Wt1 is found to normally be expressed in podocyte cells of the kidney, gonad, spleen, the mesothelial lining of various organs, and granulosa and Sertoli cells (Lahiri et al., 2007). However, during kidney development, Wt1 is expressed in the metanephric mesenchyme at low levels and increases in the condensing mesenchyme of the developing nephron (known as comma- and s-shaped bodies) before becoming restricted to posterior part of the nephron and ultimately the podocyte cells of the mature glomerulus (Mundlos *et. al*., 1993).

Wilms' tumour suppressor gene (*WT1*) mutations in Denys Drash Syndrome (DDS) highlight the important developmental role of *WT1* and link *WT1* mutation with

glomerulosclerotic kidney disease (GS) (Pelletier *et. al*., 1991). However, recently WT1 gene mutations have been implicated in non-syndromic kidney disease. 66% of cases of infant chronic renal disease carry mutations in either WT1, NPHS or LAMB2 genes (Hinkes *et. al*., 2007). Furthermore, WT1 mutations have been shown to contribute more widely to kidney disease, with mutations identified in numerous studies of nephritic syndrome (Ruf *et. al*., 2004, Gbadegesin *et. al*., 2007).

1.8.2 - WT1 mutant mouse models of glomerulosclerosis – this subheading discusses mostly the previous data and findings of Caroline Wroe (PhD, 2009) and Colin Miles that lead to my work in this thesis.

The failure to develop a full complement of nephrons is a significant risk factor for kidney disease later in life. However, the molecular mechanisms by which nephron number is determined are not fully known. The Miles laboratory has experimental evidence from mouse models carrying WT1 mutations (Patek et. al., 1999, 2003, 2007, Wroe PhD thesis] that both nephron underdosing and a failure to develop a full complement of podocyte cells contributes to the development of glomerulosclerosis in murine DDS.

Miles Lab with the work of Caroline Wroe (PhD, 2009) has bred and characterized a genetically modified mouse strain that expresses a dominant negative mutant form of Wt1 (DDS/+ mice). The $Wt1^{tmT396}$ mutation is analogous to a severe mutation causing aggressive form of Denys Drash Syndrome (Patek 199). DDS/+ mice show a 22% reduction in nephron number (Figure 1.8.2.1-A) and a failure to develop a full number of podocytes (Figure 1.8.2.1-B).

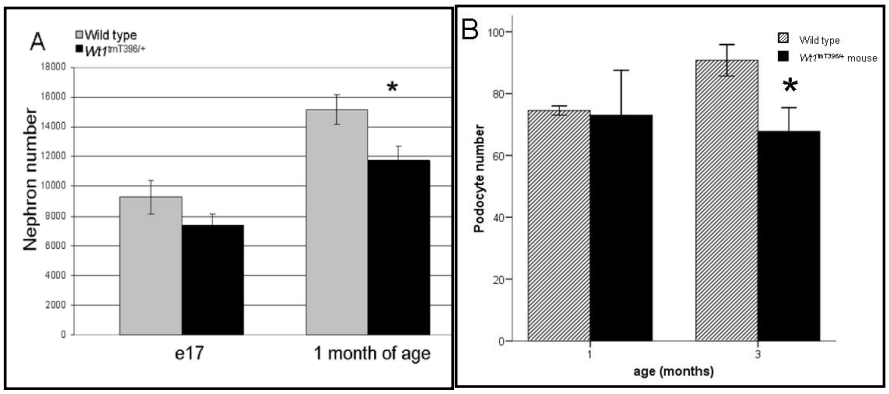

Figure 1.8.2.1: *WT1 mutant DDS/+ (Wt1$^{tmT396/+}$), Denys Drash Syndrome (DDS) mice present with a 22% reduction in nephron number (A) at 1 month of age (*p=0.034, n=6 per genotype). (B) Failure to develop a full complement of podocyte cells between 1 and 3 months of age. 25% fewer podocytes were observed in 3 months old DDS/+ glomeruli compared to wild type (*p=0.045, n=6). (Wroe, PhD thesis, 2009).*

In order to investigate the progression of GS, kidneys from *DDS*/+ mice were compared with those of wild type littermates before proteinuria and overt GS pathology sets in (Patek *et. al*., 2008). An increase of 20% in mesangial volume fraction was seen using Transmission Electron microscopy (TEM) and stereology in 3-month-old *DDS*/+ kidneys consistent with the typical features of early glomerulosclerosis (Figure 1.8.2.2).

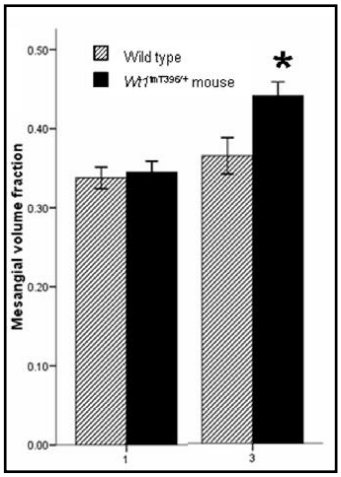

Figure 1.8.2.2: *Mesangial volume fraction of a 3 month old DDS/+ glomeruli showing increases by 20% (*p=0.023, n=6). (Wroe, PhD thesis, 2009).*

In order to determine the consequences of reduced nephron number, the mean glomerular volume was measured in kidneys of one-month old mice. An increased mean glomerular volume with a strong negative correlation with nephron number (Figure 1.8.3) was observed in *DDS*/+ kidneys, indicative of compensatory hypertrophy. All other parameters were normal at this timepoint indicating that the first insult leading to GS is a reduction in nephron number sufficient to induce compensatory hypertrophy in the presence of normal numbers of podocytes (Figure 1.8.3 and Figure 1.8.2.1). Thus, the kidney is already responding to stress.

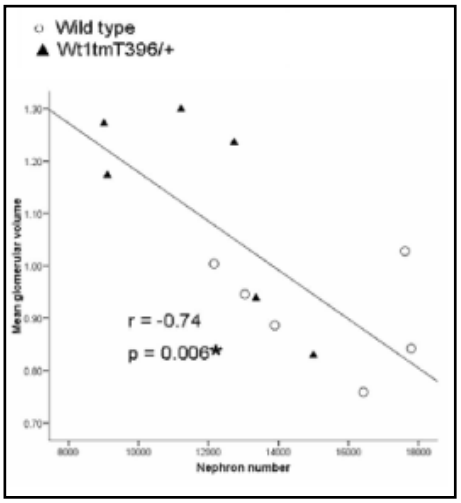

Figure 1.8.3*: 1 month of age DDS/+ mice showing negative correlation between nephron number and mean glomerular volume (MGV) compared to wild type. DDS/+ kidneys show reduced nephron number and compensatory hypertrophy prior to glomerular abnormalities. (r = -0.74, *p=0.006). (Wroe, PhD thesis, 2009).*

DDS/+ mice were also previously reported to show renin hyperplasia within the juxtaglomerular apparatus (JGA) of chimeric (*DDS*/+↔+/+) glomeruli (Patek *et. al*., 2003). At the time this was suggested to be due to the reduction in filtration due to glomerulosclerosis, however, analysis of the JGA *DDS*/+ mice at 3 months of age showed that renin hypergranulation was also seen within the JGA of *DDS*/+ heterozygotes prior to extensive glomerulosclerosis (Figure 1.8.2.4).

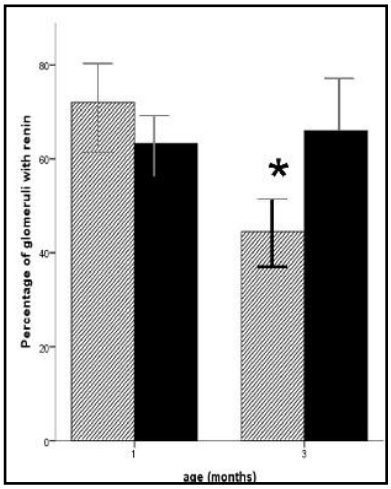

Figure 1.8.2.4: *Increased of Renin granulation in juxtaglomerular apparatus from 45% (+/-7%) in wild type to 66% (+/-11) in DDS/+, (*p=0.015, n=6). (Wroe, PhD thesis, 2009).*

Just before the onset of overt glomerulosclerosis, a normal glomerulus will attempt to compensate for renal stress by activation of the renin-angiotensin system (RAS). Some abnormalities within the podocyte were seen within *DDS*/+ glomeruli and also some localised abnormality of the glomerular basement membrane (GBM), though statistically not of significance. The most obvious change was the overall number of podocytes per glomerulus which was 25% lower in *DDS*/+ kidneys of 3-month-old mice when compared to wild type (Figure 1.8.2.1). Although the percentage was not substantial, this may reflect a role for Wt1 in the second wave of podocyte recruitment during adults that has been recently described (Appel *et. al*., 2009).

In addition, newborn *DDS*/+ mice show evidence of increases in glomerular maturation. The maturing glomerulus shows open and well-defined capillary loops, fenestrated endothelial cells and well-defined podocytes and parietal epithelial cells. Under EM it was noted that *DDS*/+ glomeruli appeared to have more open capillary loops. The maturation of the glomerulus can be measured by measuring the fenestration of endothelial cells and this dramatic morphology can be quantified under EM by measuring the percentage of fenestration. The amount of fenestration was measured in newborn *DDS*/+ mice and shown to be double the percentage compared to wild type (Figure 1.8.2.5).

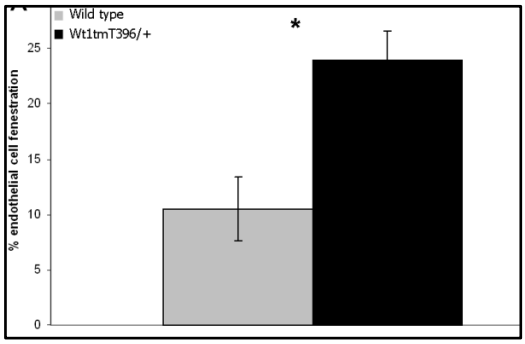

Figure 1.8.2.5: *Percentage of endothelial cell fenestration in newborn DDS/+ showing doubling compared to wild type (p=0.027,* t-test, *n=3 each group). (Wroe PhD thesis, 2009)*

These data show that *DDS*/+ mice might have an accelerated development and maturation during the process of nephrogenesis. Fascinatingly, the mechanisms controlling the rate of maturation of nephrons and the signals triggering nephrogenesis to stop remain unknown. The disruption of these processes in the DDS/+ mice suggest they may provide a way to understand this process. We postulated that there exists the possibility of negative feedback loop expressed from these maturing glomeruli inhibiting further increase of nephron number in nephrogenesis. This also raised the questions of the molecular pathways and functions of the mutant *Wt1* molecules within the kidney.

DDS mutations, like *DDS*/+, typically produce an abnormal protein product and are considered dominant, whereas there is a related syndrome (WAGR syndrome) that is caused by haploinsufficiency for *WT1* resulting in a condition with a reduced risk of developing Wilms' tumour. In order to compare the effects of dominant DDS-like mutations with haploinsufficiency, a wholly inbred (129/Ola) haploinsufficient *Wt1* mouse strain was created. The *Wt1*^{insGFP}/+ strain have one copy of Wt1 inactivated by insertion of green fluorescent proteins (GFP). *Wt1*^{insGFP}/+ mice remain healthy beyond one year of age (Figure 1.8.2.6-A) with less than 10% presenting with proteinuria and GS detectable by light microscopy at 11 months of age, in contrast to *DDS*/+ mice. This finding is consistent with the more severe clinical presentation of DDS compared to WAGR syndrome.

Comparison of nephron and podocyte numbers revealed that *Wt1*^{insGFP}/+ mice show reduced nephron number without podocyte underdosing Figure 1.8.2.6-B, C).

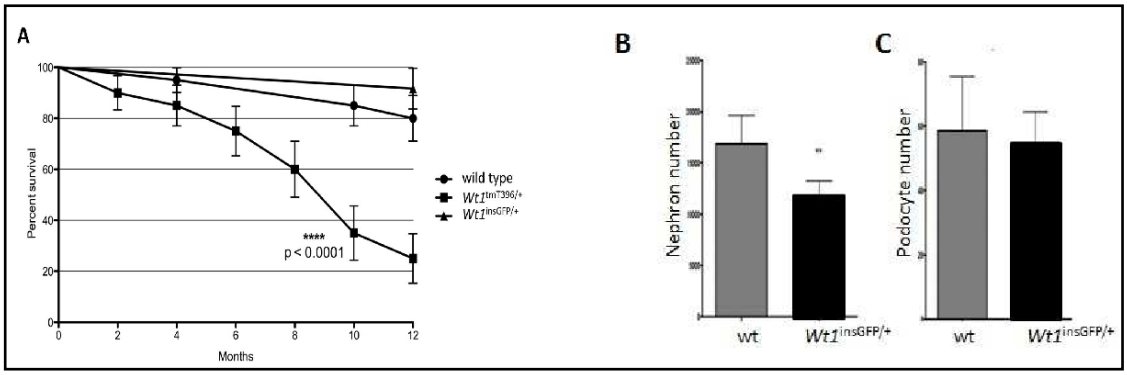

Figure 1.8.2.6: (A) *Survival graph of wild type, Wt1^{insGFP}/+ and DDS/+ mice* ***(B)*** *Reduced nephron number in Wt1insGFP/+ mice at 1 month of age (**p=0.0071, n=5 per genotype).* ***(C)*** *Normal podocyte endowment Wt1insGFP/+ at 3 months of age (p=0.741, n=6 per genotype). [Miles unpublish data]*

Despite both strains showing a reduction in nephron number, the severity of glomerulosclerosis is associated with podocyte endowment, implying that the *DDS*/+ mutation affects the glomerular response to the stress of nephron underdosing, whereas haploinsufficiency does not.

This project aims to exploit these refined genetic models of Wt1 mutation to investigate the mechanisms underlying both nephron and podocyte endowment.

1.9 - Project strategy

For the first part, we are going to compare gene expression profiles of isolated unilateral whole kidney from DDS/+ and wild type mice to identify the molecular pathways involved in changes leading to glomerulosclerosis and end stage renal failure. Such pathways will increase our understanding of this stage of glomerulosclerosis and may suggest potential therapeutic targets.

Secondly, given the recent demonstration that podocytes can develop from parietal epithelial cells in adults and, the failure in adult podocyte generation in DDS/+ mice, podocytes and parietal epithelial cells will be analysed in this DDS model using immunohistochemistry and microarray analysis of purified glomeruli.

Subsequently we will develop ex vivo experimental systems with which to validate our findings in a physiologically relevant situation, using primary kidney cells freshly isolated from mice.

1.10 - Experimental plan

In order to highlight gene expression changes more likely to be causative, whole fetal kidney (e17.5) mRNA will be analysed by Affymetrix expression microarray. Previous histology results indicate that nephron number is normal at e17 but that nephrogenesis begins to cease prematurely in DDS/+ mice at the time of birth, as shown by the presence of mature glomeruli in newborn mutant kidneys.

Whilst whole kidney analysis may “dilute” gene expression differences, ie, the cells affected may represent a small proportion of the whole kidney, we chose not to introduce potential sources of error by attempting to enrich subsets of cells for analysis but, instead, have designed the experiment such that small differences can be identified with confidence and, as far as possible, the samples will only differ with respect to genotype.

The gene lists derived from this analysis will provide a unique insight into the molecular pathways controlling the cessation of nephrogenesis and nephron endowment. These experiments should create valuable, unique datasets that will shed light on two critical, yet poorly understood aspects of kidney development. Furthermore, an understanding of the processes of late nephrogenesis and post-natal podocyte production could potentially be exploited to increase podocyte/nephron numbers for therapeutic purposes.

This *DDS*/+ mutation might have accelerated development and maturation during the process of nephrogenesis. Fascinatingly, the mechanisms controlling the rate of maturation of nephrons and the signals triggering nephrogenesis to stop remain unknown. The disruption of these processes in the DDS/+ mice suggest they may provide a way to understand this process. We postulated that there exists the possibility of feedback loop expressed from these maturing glomeruli inhibiting further increase of

nephron number in nephrogenesis. This also raised the questions of the molecular pathways and functions of the mutant *Wt1* molecules within the kidney.

However, the molecular mechanisms by which nephron number is determined are not fully known. The disruption of these processes in the DDS/+ mice suggest they may provide a way to understand this process.

1.11 Overview of main objectives

The overall aim is to investigate potential gene targets for future augmenting kidney function.

Given the established causal link between nephron underdosing, podocyte loss and chronic kidney disease, this project will consist of fundamental research into the mechanisms underlying both of these aspects of kidney development. Using mouse models of WT1 that develop glomerulosclerosis with age, mimicking human CKD, the molecular pathways regulating final nephron number will be investigated by conducting microarray analysis to identify gene expression changes in late-gestation foetal kidneys. Similarly, the molecular pathways that are disrupted during podocyte development later in neonatal life will be identified by microarray analysis. The identification of factors/pathways regulating nephron and podocyte endowment will provide potential therapeutic targets.

1.11.1. Project Aims

Specific Objectives:

1. To use WT1 mutant mice to understand the fundamental mechanisms regulating nephron and podocyte number. These basic aspects of development are currently poorly understood.
2. To investigate the WT1 pathway or molecular involvement in the mouse models that would lead to glomerulosclerosis / diseased kidneys.

CHAPTER 2. MATERIALS AND METHODS

2.1 *Wt1*$^{loxP/loxP}$ mice (DDS20)

Transgenic mouse model

In view of the fact that the progress of the Nobel first gene knockout technique in mice in 1989 by Mario R. Capecchi, Martin Evans and Oliver Smithies, numerous study have been made to model human diseases in mice. Owing to the embryonic mortality of *WT1* null mice, the function of WT1 in later phase of kidney growth, Wilms' tumorigenesis and the function in mature podocyte are not known (Patek *et al.,* 2008). Even though the likelihood of Wilms tumour develop in human DDS cases is 90%, merely a single case of tumour had been discovered in the mouse model (Patek *et al.,* 1999). Examination of the mice discovered the tumour cell had an exon 9 skip event in WT1 transcript. The *Wt1*^{tmT396} mutation model show truncated zinc finger (ZF) 3 at codon 396. Subsequently, to broaden the understanding of the effect of skipping exon 9 in WT1 gene and the function of ZF3, an inducible conditional WT1 gene knockout (Cre-*LoxP* system) mouse has been developed in the Miles laboratory. This mouse model carries *WT1* alleles flanked by loxP sites before and after exon 9 (zinc finger 3) with the function to knockout exon 9 when Cre recombinase is expressed.

The Cre-*loxP* technique is a system to overcome early embryonic lethality when compared to conventional knockout systems. It can be tissue-specific knockout of specific genes and can be time-specific when needed for more refined experiment. The method is very practical in elimination of a transgene or precise genetic sequence to imitate deletions, for example in a time course-dependant experiment. Cre is a 38 kDa recombinase protein derived from bacteriophage P1 that intercede site specific recombination between matching *loxP* sites. by means of fusing Cre to a mutated oestrogen receptor ligand-binding domain, the Cre recombinase is able to be expressed when introduced to synthetic oestrogen homologue, Tamoxifen (Indra *et al.,* 1999).

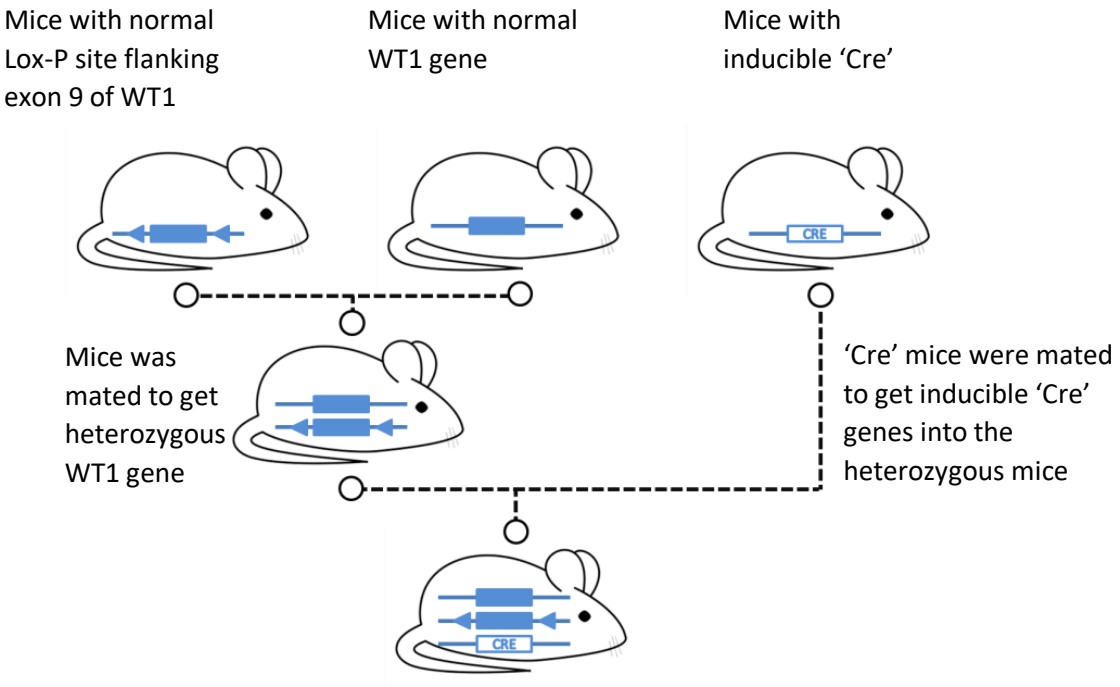

Figure 2.1.1: Figure illustrate inducible knockout utilizing the Cre^{ERT2} system. Cre^{ERT2} transgene mice are crossbred to mice carrying the floxed gene. In the absence of tamoxifen, Cre is not active. When tamoxifen is administered, recombination of loxP sites (floxed) resulted in deletion of the intervening sequence.

In order to facilitate temporal manipulation over Cre mediated recombination in experiments, the mice having the loxP modified WT1 alleles were crossed breed with ROSA-CreERT2 mice having ubiquitous expression of Cre recombinase that is fused to an oestrogen receptor, consequently placing it under control of Tamoxifen (Vooijs et al. 2001).

By means of conditional knock-out or knock-in technique, premature mortality of mouse model can be evaded. Utilizing this null *WT1* gene conditional mouse knockout model cultivated in Miles Laboratory, the scope of experiment can be extended.

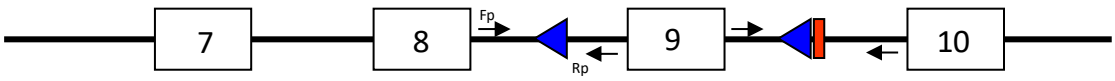

Fp = forward primer, Rp = reverse primer

Figure 2.1.2: Representative diagram of mutant Wt1 allele with loxP sites (blue) flanking exon 9 (Zn finger 3). FRT sites (red).

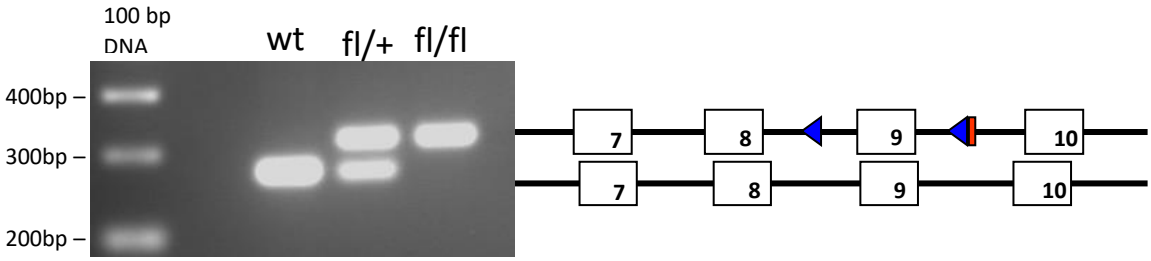

Figure 2.1.3: Representative PCR genotyping using exon 8 primers of wild type type (wt) (¬320bp) and mutant (¬270bp), heterozygous (fl/+) and homozygous (fl/fl) mutant mice.

2.2 Collection, preparation and analysis of Microarray data

In order to expand our knowledge of stages involved in development of glomerulosclerosis and to find a potential therapeutic target, evaluating the gene expression profile of isolated unilateral whole kidney from DDS/+ and wild type mice would lead to discovering the altered molecular pathways involved that leads to glomerulosclerosis and end stage renal failure.

In order to emphasize on gene expression that more likely to be contributory, whole foetal kidney (e17.5) mRNA was analysed by Affymetrix expression microarray. Prior histological study of this strain indicate that nephron number is normal at e17 and seems subjectively to have the nephrogenesis cease too early in DDS/+ mice, as shown

by the presence of more mature glomeruli in newborn mutant kidney compared to wild type at the time of birth (Wroe, 2009).

Although whole kidney analysis may “dilute” gene expression discrepancy, i.e., the fraction of cells affected possibly will be represented by a small section from the whole kidney, I opted not to institute potential sources of inaccuracy by endeavouring to enrich any subsets of cells for analysis with artificial ex vivo set up, but as an alternative have deliberately design the experiment so that such small variation can be identified with conviction and, as far achievable, the samples would only differ in revere to their genotype:

1. Both mice was of the same strain and are wholly inbred, eradicating any potential strain-specific discrepancy.

2. Embryos were sexed and sex-matched for analysis (only one sex group for expression microarray).

3. Embryos were age-matched (e17.5)

4. The foetal kidney were selected unilaterally (avoiding any unknown variables due to left-right asymmetry).

5. Foetal kidneys were peeled of renal capsule.

17 days pregnant mice were culled according to Home Office recommendation. Foetuses were decapitated, and kidneys were extracted and were instantly placed in liquid nitrogen and stored at -80^{0}C. Foetal tails tips were cut and used for genotyping and sexed genotyped. RNA was isolated from whole kidney samples using the RNA extraction kit (Qiagen RNeasy micro kit (Cat No./ID 74004)).

RNA pellet was resuspended in RNase free H_20 according to kit protocol. The quality and RNA concentration were verified by Nanodrop (UV spectrometry) and sent to Source Bioscience for quality control and microarray.

Microarray was performed using Affymetrix Mouse 1.0 ST V1 chips and analysed using the Genespring 12.5 computer program (Agilent technology). Samples were normalized per chip to internal control and non-expressed intron control.

In technical terms, before applying any of the statistical analysis methods, the data must be normalized. Normalization is used to reduce unwanted variation across chips and may use information from multiple chips. It would rectify for general chip brightness and other issues that may affect the numerical value of expression strength, facilitating the user to more confidently compare gene expression assessment between samples. For microarray, quantile normalization is routinely done to make the data distributions identical in statistical properties for further analysis. After performing normalization all gene expression values lower than 0% quantile were set to the value of this 0% quantile (5.74557625 for this experiment) to eliminate low level signals being too much scattered to be used in a reproducible analysis.

Genes were quality controlled and check and recheck for expression with qRT-PCR on multiple primers (full list of 238 primers were used). Pathway analysis was performed with Ingenuity Pathway Analysis (IPA), STRING and KEGG pathways.

2.3. Mouse Embryonic Fibroblast (MEF) - preparation from Embryos, MEF cell culture and preservation

Before proceeding to the embryos, D-PBS (Invitrogen cat number 14287-072), Trypsin/EDTA (cat number R-001-100) and MEF medium were prewarm at 37°C. MEF medium was prepared by combination of: 450ml DMEM (Dulbecco's Modified Eagle Medium) (high glucose without sodium pyruvate) 1x (Invitrogen cat number 41965-039), 50ml FBS (Foetal Bovine Serum) (Invitrogen cat number 16000-036), 5ml NEAA (MEM Non-essential amino acids 100x) (Invitrogen cat number 11140-035), and 5ml Penicillin/Streptomycin containing 5000 units of penicillin and 5000ug of streptomycin in 0.85% saline.

E13-14.5 embryos were used in this MEF culture. The abdomen of the pregnant mice was washed and swab clean with 70% ethanol. The uterus was removes in bulk

and washed with PBS. The individual sac and placenta were separated from rest, and then washed with warm sterile PBS 3x. The individual embryo is transferred to clean dish and separated from the placenta and wash clean with PBS. The individual embryo was transferred to 6 well culture plate and washed with warm PBS 3x using Pasteur pipette. Small part of the tail of each embryo were cut and transferred to 1.5ml tube for genotyping and labelled properly. The embryos were dissected and all the visceral, heart, liver (which looks reddish) were removed and discarded. The embryos then were clean and washed with warm PBS. The dissection was done under dissecting microscope for easy viewing.

Afterwards, the dissected embryos were transferred to tissue culture hood (clean/sterile). Individual dissected embryo was placed in petri dishes and 2ml trypsin/EDTA were added. Embryo was minced with scissors and scalpels as finely as possible. This is repeated to all embryos using new/clean utensils. Additional 5ml of trypsin/EDTA was added to the minced tissue. The petri dishes were incubated for 15 minutes at 37ºC or until individual cells were visible under microscope. Next the content was transferred to a 50ml tube using sterile pipette. 13ml of prewarmed MEF medium was added to the tube and mix up and down. Letting the tube on a rack, after allowing the bigger pieces to settle down at the bottom of the tube, the top 12ml was transferred to one or two T25 culture flask. The remaining 8ml from the tube was transferred to another T25 flask. All flask was incubated at 37ºC at fix CO2 and O2 for best result. and were observe for cell adherence. Cells were split when confluency was seen. Of note, MEF do not need feeding with new media every day. Only when the media turn yellowish in about 2-3 days and split to new flask if overgrown.

To split the cells, for best practice, a complete medium was prewarmed and feed to the cells for few hours prior to splitting. From the T25 flask, the medium was aspirated and discarded. The cells were washed first with prewarmed PBS (5ml for T25) and discarded after few gentle swirls. 1ml of prewarmed trypsin/EDTA was added to the cells and swirl to overall cell surface gently and then incubate at 37ºC. for every 5 to 10 minutes, the detachment of cells was monitored under microscope and the T25 was gently shaken. The last step was repeated until all cells were detached from the flask surface. After cells was seen to be detached, the trysin/EDTA was inactivated by adding prewarmed MEF medium (amounting to 10 volume totals, 10% FBS). The cell solution

was gently pipetted up and down using a 10ml pipette to homogenize the cells. To split to 3 T25 flask, additional MEF medium was added to total of 15ml, and then divided into 3 (5ml each) into a new T25 flask. The cells were monitored for adherence and confluence as before, split when needed and used for intended experiments.

To preserve a cell line, cells were preserved and frozen at -80ºC and in nitrogen cryogenic tank for long term. To freeze the cells from T25 flask, the medium was aspirated, and cells were washed with 5ml of prewarmed PBS. Cells were detached using trypsin/EDTA using similar technique as cell splitting. After the cells were seen to be detached under the microscope, the trysin/EDTA was inactivated by adding prewarmed MEF medium (amounting to 10 volume totals, 10% FBS). The medium containing the cells were transferred to 10ml tube and centrifuged at 1200rpm. Medium were aspirated and discarded. Cell palette was resuspended with 2ml Gibco™ Recovery™ Cell Culture Freezing Medium (cat number 12648010) and mix thoroughly. The media then were aliquot 1ml into each cryotube. The cryotube was then put into freezing container containing isopropanol and put into -80ºC and in nitrogen cryogenic tank for long term.

2.4 Tamoxifen preparation

2.4.1. Tamoxifen on MEF (primary cell culture)

Exon 9 of WT1 in MEF (with presence of Cre-ER) was deleted by addition of 1uM Tamoxifen (Sigma H7904-5MG, (Z)-4-Hydroxytamoxyfen, Lot #094M4049V). Tamoxifen was prepared in 1M stock (1000x) dissolved in cell culture grade dimethyl sulfoxide (DMSO) and stored at -20 C. Molecular weight: 371.51 1 molar = 371.5 g/l 1 molar = 371.5 mg/ml 1mM = 371.5 ug/ml.

Tamoxifen were prepared at 10mM stock in ethanol (EtoH). To add to cells (MEF), following protocol was followed:

1) 5 ml medium (DMEM) + 5 ul of 10 mM stock (= 10 uM)

2) Filter the solution through 0.2 um filter.

3) Add to culture medium at ratio of 1:10 (i.e. 0.5 ml + 4.5 ml full culture media) to get final concentration of 1 uM Tamoxifen.

Cell at passage 1 (one) were allowed to grow in the Tamoxifen containing medium for 48 hours, then a small portion was genotype using PCR for deleted exon 9 at the end of 48 hours. If by any chance there are still not fully deleted, the cells were allowed to grow for another 24 hours in a new Tamoxifen containing medium. Usually all the cells would have exon 9 deleted after 72 hours when PCR were repeated.

Cells were then allowed to continue growing in normal medium without Tamoxifen after above protocol and were passaged until passage 5 (five) to dilute any remaining Tamoxifen from the cells before being used for any experiments.

2.4.2 Tamoxifen preparation for in vivo experiment

The solution comprises of 20mg Tamoxifen (Sigma), dissolved in 200µl 100% EtOH (42° C shaking) then later then mix this 200µl with 1800µl of peanut oil. Intraperitoneal injection of 2.5mg Tamoxifen was administered to pregnant female mice from a heterozygous (flox/+ Cre^{ERT2}) X heterozygous (flox/+) mating to inactivate WT1 prior to birth. For newborn mice, Tamoxifen 2.5mg was administered subcutaneously to newborn mice from heterozygous (flox/+ Cre^{ERT2}) X heterozygous (flox/+) mating. Mice of all possible genotypes were injected with Tamoxifen (prior to genotyping).

2.5. Histology

2.5.1. Tissue preparation

2.5.1.1. Wax fixation and sectioning

Embryonic kidney of E12-14 of age were used. The kidneys were fixed in 4% PFA at 4 degrees Celsius for 2 days. Afterwards the kidneys were processed

at room temperature for the following steps. They are washed in PBS two times for 15 minutes two times. Following that, the kidneys were immersed in 50% ethanol for 2 hours, followed by 70% ethanol for 2 hours times two, 95% ethanol for 2 hours, then 100% ethanol for minimum of two hour or overnight. Then the kidneys were immersed in histoclear solution for 30 minutes times two at room temperature. Following that, the kidneys were immersed in histoclear/wax mix at 65 degrees Celsius once, followed by wax immersion at 65 degrees Celsius for 1-hour times 6, then wax blocks were cooled to room temperature. The wax embedded tissues were sectioned by using a microtome at 5 to 10 micrometre thickness. Sections were then placed onto SuperFrost® Plus glass slides and left on a heating plate at 38° C overnight.

2.5.1.2. Cryofixation

The kidneys of were first immersed in 4% PFA at 4 degrees Celsius for 2 days. Then they are washed with PBS at room temperature for 15 minutes 2 times. Then the kidneys were immersed in 30% sucrose in PBS at 4 degrees Celsius for 2 days. Following that, the kidneys were embed in OCT compound and then stored at -80 (minus 80) degrees Celsius until needed to be used.

The OCT embedded kidneys were sectioned by using the cryostat microtome machine cut between 5 to 10 µm thickness. The sectioned tissues were placed onto glass slides and stored at -20° C before being stained.

2.5.2. Haematoxylin and Eosin (H&E) staining

H&E staining and commercial DPX (Distyrene, plasticizer, and xylene mixture) chemical was used for slide mounted sectioned tissues using the method below at room temperature.

The kidney sectioned from wax fixed procedure were used in this procedure. The sectioned kidneys were fixed first on glass slides. The slides were de-waxed by immersing in histoclear solution for 10 minutes. The sectioned were then hydrated through 100% ethanol for 2 minutes, then 80% ethanol for 2 minutes, then 50% ethanol for 2 minutes, then ddH2O for 2 minutes. Following

that, sectioned were then immersed in Harris haematoxylin for 2 minutes, then rinsed with tap water until the running water becomes clear. Then slides were immersed in eosin solution for 3 minutes, then rinsed with running tap water until running water becomes clear. The sectioned kidneys were then de-hydrated by immersion in 50% ethanol for 1 minute, then 70% ethanol for 1 minute, then 100% for 1 minute. Then the slides were immersed in histoclear solution for 10 minutes. Following that, the slides are covered with slide cover and DPX (Dibutyl Pthalate Xylene).

2.6. Molecular Biology

2.6.1. DNA preparation for genotyping:

DNA preparation from the pieces of the mouse ear clips. For each PCR reaction, 5µl of the DNA solution was used. Ear clip DNA solution for mice genotype were prepared as follows. Each ear clip pieces (1-2 mm diameter) were isolated in a 1.5ml tubes, can be kept at -20 (minus 20) degrees Celsius or processed as soon as ear clip were obtained. 60µl of 25 mM NaOH/0.2 mM EDTA ph 12 were added to the tube containing ear clip and kept in shaking thermocycler at temperature 95 degrees Celsius for 20 minutes. The tube was cooled afterwards and 60µl of 40 mM Tris-HCL ph 5 (not Tris base) were added in the tube and mix well by vortexing. The tubes were then centrifuge at max G for 1 minute.

2.6.2. PCR genotyping mix:

PCR genotyping method below was used for ear clip genotyping. Each PCR reaction contains (prepared and added in the following order):

AMOUNT	MATERIAL
5µL	DNA from ear clip
30.7µL	ddH_2O
10µL	x5 GOTAG flexi buffer

3µL	MgCl
1µL	dNTP mix (stock at 10mM each dNTP)
0.1µL	Oligonucleotide primers (stock at 1µg/µl)
0.2µL	Taq polymerase enzyme

Each PCR tube contains 50µl of reaction mix. For controls, positive and negative controls were used with addition of ddH_2O control.

Primers used:

NO	TARGET	SEQUENCE (5'- 3')
1	loxP For ex8	**ATGGCTTTTTTTCCAAGTCAG**
2	loxP Rev ex8	**CAGTGAGACACATAAGGCCGG**
3	Cre For	**TGCCACCAGCCAGCTATCAAC**
4	Cre Rev	**AGCCACCAGCTTGCATGATCT**
5	loxP For ex9	**CTGCTGTGAACCTAAGTTTC**
6	loxP Rev ex9	**CACTAGGAATGTCCTCAGTC**
7	DDS Ex9F2	**AGACCTTCTCTGTCCGTTTAG**
8	DDS neo52	**GATGCCTGCTTGCCGAATATCATGG**
9	**DDS CRE1R**	**TGTTCTGAATCTCCTGGACA**

**For the remaining primers, please refer to the appendix. These primer sequences were used for qRT-PCR to measure the expression of genes found to be expressed in the array, and normal PCRs.

Primers were designed using NCBI primer-BLAST (Available at http://www.ncbi.nlm.nih.gov/tools/primer-blast/index.cgi?LINK_LOC=BlastHome)

2.6.2.1. PCR conditions:

Below is the PCR conditions that being used for PCR in the PCR machine.

2.7.2.1.1. For PCR genotyping of Lox-P site and Cre site gene sequence, below is the PCR machine setup:

STAGE	TEMPERATURE	DURATION
HEATED LID	110° C	
HOT START	95° C	00:05.00
START CYCLE	-	30x
DENATURATION	95° C	00:00.05
ANNEALING	58° C	00:00.30
ELONGATION	72° C	00:00.30
END CYCLE		
TEMPERATURE	72° C	00:05.00
STORE	4.0° C	Infinite

2.6.2.1.2. For PCR genotyping of DDS/+ mice, below is the PCR machine setup for genotyping the exon 9 region of WT1,:

STAGE	TEMPERATURE	DURATION
HEATED LID	110° C	
HOT START	95° C	00:10.00
START CYCLE	-	32x
DENATURATION	94° C	00:00.30
ANNEALING	56° C	00:00.45
ELONGATION	72° C	00:00.30
END CYCLE		
TEMPERATURE	72° C	00:10.00
STORE	4.0° C	Infinite

2.6.3. DNA extraction using QIAGEN Tissue DNA Extraction Kit

QIAGEN commercial extraction kit was used to obtained pure DNA extraction as protocol below. 25mg tissue was placed in 1.5ml microcentrifuge tube. 180µl Buffer ATL was added with 20µl proteinase K and then mix by

vortexing. The microcentrifuge tube was incubated at 55° C overnight (or until tissues completely lysed). Afterwards, tubes were vortexed for 15 seconds and then incubated at 70° C for 10 minutes. 200µl 100% Ethanol was added and mix thoroughly by vortexing. Mixture was pipetted into DNeasy Minispin Column (QIAGEN) and placed in a 2ml collection tube, and then centrifuged at ≥6000g (8000rpm) for 1 minute. DNeasy Minispin Column was placed in a new 2ml collection tube and 500µl Buffer AW1 was added and centrifuged at ≥20000g (14000rpm) for 3 minutes, the flow-through was discarded. DNeasy Minispin Column was placed in a new 2ml collection tube, 500µl Buffer AW2 was added and then centrifuged at ≥20000g (14000rpm) for 3 minutes, the flow-through was discarded. DNeasy Minispin Column was placed in a new 1.5ml microcentrifuge tube, 200µl Buffer AE was pipetted directly onto the DNeasy Minispin Column membrane, incubate for 1 minute at room temperature, then centrifuged at ≥6000g (8000rpm) for 1 minute. The last step was repeated in a new collection tube if needed. Finally, DNA concentration and quality were checked by Nanodrop (ND1000, LabTech) and stored at -80°c to avoid degradation of DNA in long term.

2.6.4. RNA extraction

RNA extraction was done through general method of RNA extraction. Stored tissue for RNA extraction were stored at -80° C in 1ml of Invitrogen Trizol in 1.5ml microcentrifuge tube. Tubes with samples were allowed to thaw on ice, and then homogenized using homogenizer and left at room temperature for 5 minutes. Tubes were then centrifuge at 4° C at 12000rpm for 10 minutes. 200µl chloroform were added and vigorously shake for 15 seconds and incubate at room temperature for 3 minutes. Tubes were then centrifuge at 4° C at 12000rpm for 15 minutes. The top aqueous layer was transferred to a new clean Eppendorf tube (RNase free). 500µl isopropanol were added for RNA precipitation and left at room temperature for 10 minutes. Tubes were then centrifuge at 4° C at 12000rpm for 10 minutes. Tubes were then centrifuge at 4° C at 12000rpm for 10 minutes. The supernatant was removed and discarded. The

pellet was washed with 1ml 70% ethanol (with diethylpyrocarbonate (DEPC) water). Tubes were then centrifuge at 4° C at 7500rpm for 5 minutes. Supernatant was removed, and the pellet was air dried for 30 minutes. 30µl RNase free water was added to resuspend the pallet (RNA) and then stored at -20° C or use for RNA experiment of choice.

Alternatively, RNA was extracted using a RNeasy micro kit (Qiagen Cat No./ID 74004) following manufacturer protocol. Briefly, less than $1x10^7$cells or 30mg of tissues (Guan et al., 2006) were disrupted and homogenized in RLT buffer then ethanol was added for selected binding of RNA to the column. In the washing steps, all contaminants were washed efficiently. RNase-free DNase set (Qiagen) was applied to wash genomic DNA, in the case of using RNA samples for real time PCR.
Finally, RNA concentration and quality were checked by Nanodrop (ND1000, LabTech) and stored at -80°c to avoid degradation of RNA in long term.

2.6.5. Reverse Transcription – Polymerase Chain Reaction (RT-PCR) and **Quantitative PCR (qPCR):**

By using spectrometer equipment and the optical density (OD) value of RNA obtained from it, 2µg of RNA was added to dd H_2O to make a total volume of 11µl per sample. Then 1µl of 10mM dNTPs and 1µl of oligonucleotide dT primer were added. The mixture was then incubated at 65° C for 5 minutes. Afterward 4µl of Invitrogen 5x Buffer, 1µl of Dithiothreitol (DTT), 1µl of Invitrogen RNAse OUT and 1µl of Invitrogen Superscript III RNA polymerase were added. This mixture was then incubated at 50° C for 50 minutes and later at 70° C for 15 minutes. The cDNA product was stored at -20° C to be used later.

Alternatively, Promega (GoScript™ Reverse Transcription System, Cat A5001) kit were used for reverse transcription and method we followed as per kit instructions.

2.6.6. Quantitative PCR (qPCR):

The qPCR was performed on the cDNA synthesised from the mouse kidneys RNA, MEFs, and extracted DNA. All cDNA and DNA were quantified and equalized between controls and mutants prior to run. The mouse kidneys used were the second kidneys from the mice whose kidneys were used in the nephron counts. The primers used in the qPCRs were designed using the NCBI primer BLAST software and primer3 software, the primers were checked to ensure that they spanned at least one exon-exon junction and that the product produced was between 70-250 base pairs long. For each sample the genes GAPDH, HPRT and/or Beta-Actin genes were used as control/reference genes. Each qPCR was performed using Quantstudio 7 Flex Real Time PCR System (Life Technologies). For each well 9µl of a master mix and 1µl of the cDNA was used. The master mix was made up from 5µl of SYBR Select Master Mix (x2), 0.5µl of the forward primer (10µM), 0.5µl of the reverse primer (10µM) and 3µl of RNase free water. Alternatively, Fast SYBR™ Green Master Mix (4385612) were used.

2.6.7. Gel electrophoresis

To prepare a 2% agarose gel, the materials needed were 4gram Agarose powder (Sigma), 20ml of TAE solution, and 180ml of ddH_2O. The mixture is heated in microwave for 3 minutes. Then the gel was slightly cooled on running water. 20µl ethidium bromide was added and gel was then poured onto a running plate.

2.7. Immunostaining

2.7.1. Apoptosis/ TUNEL Staining for cryosectioned tissue samples

Commercial Roche in Situ Fluorescein Cell Death Detection Kit was used for apoptosis antibody staining. The previously cryosectioned kidney tissues were used. The methods used were from manual provided with the antibody. For one sample, 50µl of TUNEL mix was required. 50µl TUNEL mix equal to 5µl Enzyme solution plus 45µl Label solution. For one sample of negative control, 50µl of Label solution only was used. To induce a positive control, a wild type tissue section was incubated with a mixture of DNase 1 recombinant (3 U/ml), 50mM Tris-HCl ph 7.5 and BSA (1mg/ml) for 10 minutes. Tissue sections (cryosection) that was mounted on SuperFros® Plus glass slides were allowed for air dry for 1 hour. The general step started with sectioned tissue fixation with 4% PFA for 20 minutes, then wash with PBS for 30 minutes. Permeabilization solution Triton-X 0.2% then used on the tissue section for 2 minutes while the slides are on ice (cooled condition). Slide then rinsed with PBS 2x and dap/dry lightly of remaining PBS. Following that, TUNEL mix was added to sample and positive control while adding Label solution only to negative control. The slides were incubated in wet chamber at 37°C in the dark for 1 hour. The slides were then rinse with PBS 3x. The slides were then mounted with Vectashield DAPI mounting medium and cover slip. For evaluation by fluorescence microscopy use an excitation wavelength in the range of 450 – 500 nm (*e.g*., 488 nm) and detection in the range of 515 – 565 nm (green).

2.7.2. ***Apoptosis/ TUNEL Staining for paraffin/wax tissue samples***

The routine for TUNEL staining protocol is as follows. Slides having wax sectioned kidneys of choice were taken, and then de-paraffinized and rehydrated in histoclear for 10 minutes, 100% ethanol for 5 minutes, then 70% ethanol for 3 minutes, then 70% ethanol for 3 minutes, then 50% ethanol for 3 minutes, then water for 3 minutes. The slides were then immersed in 4% formaldehyde in PBS (Phosphate Buffered Saline) at room temperature for 15 minutes. Then the slides were washed in PBS for 5 minutes. The sections then were incubated at room temperature after adding 100µl of 20µg/ml Proteinase K solution onto each slide

for 8-10 minutes. Then slides were washed in PBS again for 5 minutes. Slides were then immersed in 4% formaldehyde in PBS for 5 minutes, then washed in PBS for 5 minutes. Then 100µl of equilibration buffer (Promega) was added to the slides and incubated for 5-10 minutes. Equilibration buffer was then removed and 50µl of rtdt incubation buffer was added, using a plastic cover slip to ensure even distribution of the reagent. During this step the slides were kept out of light and incubated at 37°C for 60 minutes in a humidified chamber. Following this the slides were immersed in 2X SSC solution (Promega) to end the rtdt reaction for 15 minutes. Then slides were washed 3x 5 minutes with PBS. Slides were then immersed in propidium iodide solution diluted to 1µg/ml in PBS (in dark area) for 15 minutes. Then slides were washed in deionised water 3x 5 minutes. Then a drop of Anti-Fade solution was added to the treated cells and a coverslip was added. Then the edges of the coverslip were sealed using clear nail polish. For evaluation by fluorescence microscopy use an excitation wavelength in the range of 450 – 500 nm (e.g., 488 nm) and detection in the range of 515 – 565 nm (green).

2.8 Cell Counts:

There were two different cell counts performed; an apoptotic cell count and a nephron count.

2.8.1 Apoptotic cell count:

This was performed on TUNEL stained kidney sections where events and bright events were counted. Double blinded approach was used to make sure no bias in selecting and counting the florescence signal. Until all slides were counted, the slide numbers were then cross checked with the actual sample label. Both counts were checked for differences, analysed for discrepancies, and average was taken. Florescent signal counting was done using the image J software.

2.8.2 Nephron count:

This was performed on PNA stained kidney (Peanut agglutinin (PNA)) sections where different stages of nephron development were counted, these were the glomeruli, S-shaped bodies and Comma shaped bodies, and they shaped were obvious under microscope when stained and easy to be identified especially PNA will stain the bodies different colour compared to the surrounding tissues. This was done using a light microscope with the nephrons being examined and counted using a 20x magnification, with each nephron stage being labelled, using a different colour, and counted. Five kidney sections were counted for each kidney, with each counted section being separated by roughly 15 sections to avoid counting the same structures twice. The total number of nephrons, glomeruli, comma shaped bodies and S-Shaped bodies was then obtained and for each value the total number of bodies for that structure was obtained using a method outlined by Cullen-McEwen (2011), by using PNA staining and formula , where N_{glom} is the total $N_{\text{glom}} = \text{SSF} * \frac{1}{2} * \frac{1}{2} * Q^{-}$ number of PNA-positive nephrons, and SSF is the number of slide in between sectioned, Q^{-} is the actual number of PNA-positive structures appearing and disappearing in between slides. The counting was made by 2 people and double blinded. The slides sample numbers were covered and randomly labelled. They were shuffled, and nephrons were counted independently by the 2 persons. Both counts were checked for differences, analysed for discrepancies, and average was taken and accepted as the true count for the subsequent analysis.

2.8.3 Analysis

To examine the research question of relationship between genotype and nephron number, a linear regression was conducted to investigate whether or not independent variable (in this case genotype) predicts dependent variable (the nephron number). A linear regression is an appropriate analysis when the goal of research is to assess the extent of a relationship between a dichotomous (genotype) predictor variable on an interval/ratio criterion variable. In this case, the predictor variable is the independent variable and the criterion variable is

the dependent variable. The following regression equation was used: y = b1*x + c; where y = estimated dependent variable, c = constant, b = regression coefficient and x = independent variable (as done through SPSS). The *F*-test was used to assess whether the independent variable predicts the dependent variable. *R*-squared reported and used to determine how much variance in the dependent variable can be accounted for by the independent variable. The *t*-test was used to determine the significance of the predictor and beta coefficients will be used to determine the magnitude and direction of the relationship. For statistically significant models, for every one-unit increase in the predictor, the dependent variable will increase or decrease by the number of unstandardized beta coefficients (positive or negative values). The assumptions of a linear regression —linearity and homoscedasticity—will be assessed. Linearity assumes a straight-line relationship between the predictor variables and the criterion variable and homoscedasticity assumes that scores are normally distributed about the regression line (as shown in appendix P-P plot of Regression Residual).

2.9 PNA Staining:

Slides having wax sectioned kidneys of choice were taken, and then de-paraffinized and rehydrated in histoclear for 10 minutes, 100% ethanol for 10 minutes, then 70% ethanol for 10 minutes, then 70% ethanol for 10 minutes, then 50% ethanol for 10 minutes, then water for 10 minutes. The slides then immersed in 2% methanol for 10 minutes. Following that, the slides were incubated with Neuraminidase (0.1 units/ml with 1% cacl2 in PBS) from Vibrio Cholerae (Sigma-Aldrich, N7885-2UN) at 37ºC for 30 minutes. Following that, the sections were immersed in 2% BSA, 0.3% Triton X-100 in PBS solution for 30 minutes. Then the slides were placed into a 20 µg/ml biotinylated PNA (Arachis Hypogaea, Sigma-Aldrich) diluted with 0.3% Triton X-100 in PBS, with 1mm cacl2/mncl2/mgcl2 solution and kept out of light for 2 hours. The slides were washed in PBS. Following that, the biotinylated PNA was visualised utilizing the Elite streptavidin/biotin amplification ABC Kit protocol (Vector Laboratories), the

reaction is then developed using Diaminobenzidine (DAB) and 0.01% H202 in PBS for 5-10 minutes. The slides were then washed again in PBS and counterstained using methyl green for 5-10 minutes. The slides were then washed and dehydrated for cover slip mounting with DPX solution.

2.10 Western blot

Western blot experiments follow the standard protocol. Samples were homogenised either in Laemmli buffer or tissue lysis buffer using needles (19G,23G,26G). Samples were centrifuged at 4°C for 15 minutes at medium to maximum g. This will pellet cell debris at bottom. Supernatant were removed and place into fresh tube. Sonication were done to shear the DNA. Samples were heated to 95°C for 5 mins. Samples were spin for 5 min at room temperature. Samples were loaded into wells of the polyacrylamide gel. The power-pac were set to run as follows; protein size 15 kDa (dye front) at voltage 115 for 1hr and protein size 40 at voltage 120 for 1hr 20 min.

Once the gel has run, the transfer set assembled: Sheet is soaked of extra-thick blot paper in transfer buffer and place on the anode plate assembly, the gel was place on top of the membrane, one more sheet was added of extra-thick blot paper on top, re-soak the sandwich in transfer buffer. Voltage was set to 15V, current max to 0.5A and time to 45 minutes. If set up correctly, at 15V the current should be around 0.2A. After the run, the transfer cell was disassembled, membrane was rinsed with water, Ponceau S red was added and soak for 2 minutes to visualize transfer. Membrane were washed 2x for 10 minutes with TBST. The membrane was blocked in 10% milk in TBST for 1-hour at room temperature. The membrane was put into primary antibody over night at 4°C. The membrane was rinse once with TBST. Then wash 3x 15 minutes in TBST on roller. The membrane then was put into secondary antibody for 90 minutes, then rinsed once with TBST and washed 3x 15 minutes in TBST on roller. The chemiluminescent substrate was mixed, and the West Dura is mixed 1:1. The membrane was placed inside a plastic pouch, added with substrate, and spread around. Second sheet of plastic was placed on top and

squeeze out excess with some blue roll. Membrane was placed into developing cassette and expose to film.

For buffers, following are the standard buffers for western blot. The tissue extraction buffer (10ml) was prepared with combination of 2.4g Urea, 2.5ml 0.5M Tris pH6.8, 2ml 20% SDS, 500µl β-mercaptoethanol, 2ml 50% Glycerol, 3ml H_2O, and then aliquoted into 0.5ml and freeze at -20°C. The 10X Running buffer (1L) was prepared with combination of 30.2g Tris, 188g Glycine and for each litre of 1X, 5ml 20% SDS was added. The 10X Transfer buffer (1L) was prepared with combination of 29g Glycine, 58g Tris and for each litre of 1X, 1.85ml 20% SDS and 200ml MeOH (methanol) were added. The 10X TBS (1L) was prepared with combination of Tris and Sodium Chloride, at pH to 7.5 and prepared up to 1L by adding dH_2O. For each L of 1X, 5ml 20% Tween was added. The Ponceau S Red (100ml) was prepared with combination of 0.1g Ponceau S red (0.1%), 5ml Acetic acid and then prepared to 100ml by adding dH_2O.

2.11 Alamar Blue Assay

This assay was designed to measure quantitatively proliferation animal cell. The indicator is H2O-soluble. It also can be used to establish relative toxicity of agents within various chemical classes. The system of reduction related to growth causes the REDOX (oxidation-reduction) indicator to change from oxidised form (non-fluorescent, blue) to reduced form (fluorescent, red). In order to prepare, 0.5 mM Resazurin sodium salt stock (R7017, Sigma-Aldrich) in PBS were obtained, 6.27925 mg of Resazurin sodium salt were put into 50 ml PBS and filtered, and then store at 4oC fridge until needed.

In order to use the assay, medium from culture plates were removed, and additionally, cells were washed with sterile PBS to remove cell debris. To prepare medium with Alamar Blue, 10% of stock were added to the medium, and shake well. The Alamar Blue medium were added to the cell culture plate as needed (about 2-4ml) and incubated as usual. Regularly check for colour changes or as the experiment was designed (usually every 30 minutes to 2-3 hours). The medium then were pipetted out and triplicated into a 96-well plate to read under

plate reader. It is read it using Spectro fluorometer machine (excitation: 530-560 nm; emission: 590 nm) or fluoroskan machine (excitation: 544 nm; emission 590 nm). If required, the number of cells can be determined using standard curve (done separately).

2.12 Cytochrome C Oxidase / Succinate Dehydrogenase (COX/SDH) Double-labelling Histochemistry

COX histochemistry

Cryosectioned slides were allowed to dry (about 1 hour) and were pun in slide-staining chamber with wet filter paper. 1X DAB, 100 µM cytochrome c in 0.1 M PBS pH=7.0 were prepared in chemical fumes hood and vortexed quickly. 2 µg bovine catalase (2 µg per ml) were added and vortexed to mix and break the catalase grains. 150- 200 µL of incubation medium were applied to each slide and spread evenly on the slide surface. It is let to incubate for 40 minutes at 37 °C. Excess solution is removed. Slides were washed 4 times in 0.1 M PBS pH=7.0. 10 minutes each. Slide were returned back to slide-staining chamber.

SDH histochemistry

1.5 mM NBT, 130 mM sodium succinate, 0.2 mM PMS, and 1.0 mM sodium azide in 0.1 M PBS pH=7.0. were prepared in chemical fume hood, shielded from sunlight and quickly vortexed. 150- 200 µL of incubation medium were applied to each slide and spread evenly on the slide surface. It is let to incubate for 40 minutes at 37 °C. Excess solution is removed. Slides were washed 4 times in 0.1 M PBS pH=7.0. 10 minutes each. Each slide is dehydrated through 70%, 70%, 95%, 95%, 99.5% ethanol for 2 minutes each, plus additional 10 minutes in 99.5% step. Slide is placed in xylene for 10 minutes, then mounted with coverslip. Slides were allowed to dry in ventilated area for 1-2 hours or overnight.

2.13 Copy number analysis

The measurement of mtDNA copy number is done by measuring the relative different from qPCR of mutants' controls/reference gene mtDNA (e.g. ND1, ND2, ND5) and the normal cell/mice controls/reference mtDNA copy number, and the differences of individual copy number relative to nuclear DNA copy number of control/reference genes. All mtDNAs were quantified using Nanodrop (ND1000, LabTech) and equalized/normalized between samples and controls prior to loading. Each qPCR was performed using Quantstudio 7 Flex Real Time PCR System (Life Technologies) and standard qPCR protocols were followed for protocols.

2.14 Mitochondrial isolation

Mitochondrial organelle was isolated using Thermo Scientific Mitochondrial Isolation Kit for Tissues (89801) and Mitochondrial Isolation Kit for Cultured Cells (89874).

2.14.1 Isolation of Mitochondria using Reagent-based Method for Cultured Cells

MEF cells were harvested from T25 flask and quantified. A pellet of 2×10^7 cells was harvested by centrifuging cell suspension in microcentrifuge tube at about 850 g for 2 minutes. Supernatant was carefully removed and discarded. 800 µL of Mitochondria Isolation Reagent A was added to the pallet and mixed with pallet by pipetting up and down. The tube was vortexed for 5 seconds at medium speed and then incubated on ice for exactly 2 minutes (do not exceed 2 minutes). 10 µL of Mitochondria Isolation Reagent B was added to the solution and vortex for 5 seconds at maximum speed. The sample tube was incubated on ice for 5 minutes and intermittently vortexed every minute at maximum speed. 800 µL of Mitochondria Isolation Reagent C was added to the sample tube and mix by inverting tube several times (but do not vortex). The tube was centrifuged at 700 g at 4°C.for 10 minutes Supernatant was transferred to a new 2ml tube and centrifuge at 12,000 g at 4°C for 15 minutes. The supernatant (cytosol fraction) is transferred to a new tube. Pallet at the bottom of the tube is the mitochondrial fraction. 500 µL of Mitochondria Isolation Reagent C ws added to

the pallet, centrifuged at 12,000 for 5minutes. Supernatants was discarded. The pallet was kept on ice prior to further experiment, or frozen at -80°C until needed for experimentation.

.

2.14.2 Isolation of Mitochondria using Dounce Homogenization for Tissues

50-200mg of tissue were washed 2x with 4ml of PBS, and PBS was discarded carefully. Tissues were cut into smaller pieces and 800µL of BSA/Reagent A Solution was added. Dounce homogenization was performed on ice. 800µL of Mitochondria Isolation Reagent C was added and mixed by inverted the tube few times. The tube was centrifuged at 700×g for 10 minutes at 4°C. The pallet was discarded. The supernatant was transferred a new 2mL tube, and centrifuged at 3,000×g for 15 minutes at 4°C. The supernatant (cytosols) were removed from the mitochondrial pellet and kept at 80°C until needed. 500µL of Wash Buffer was added to the pallet to perform a surface wash, then centrifuged for 5min at 12,000×g, and supernatant was discarded. The pallet was kept on ice prior to further experiment, or frozen at -80°C until needed for experimentation.

2.15. Preparation of fresh MEF for FACS with MitoTracker®

MEFs culture cells were made into single cell suspension using standard trypsin method and resuspended in DMEM only media. MEFs were transferred as the single cell suspension onto a 30-micron filter/cell strainer and let gravity filter it into a glass tube for FACS. Keep it on ice/dark until FACS, preferable as little lag time as possible to FACS. FACS LSRII (BD Biosciences) was applied to sort the cells based on MitoTracker(R) expression. The device was calibrated with the non-stained cells to set up the size gate, SSC and FSC of dot plots and baseline negative control for the fluorescent channels. LSRII (BD Biosciences) device was employed to detect the signals. Standard dead cell stain was used (e.g. Propidium iodide (PI) or DAPI) to detect dead cells. (DAPI – 1 microgram/ml is enough, detection at 355/450/50). Analysis was done with LSRII.

2.16 Seahorse mitochondrial analysis (XFe) - XF Cell Mito Stress Test

Day1; XF96 well cartridge is hydrated with standard XF solution, wrap with cling film and left in non-CO2 incubator for 24 hours. The desired number of cell plate are prepared and seeded as per optimisation (15000 cells per well) and left overnight in normal incubator to settle down in XF96 well plate with 200ul normal MEF media per well (spin for 1 minute at 1000 rpm as required).

Day 2; XF96 well plate containing the MEF was check for consistency and cells attached to the bottom of plate well under microscope. Media were replaced with XF Cell Mito Stress Test Media with final volume of 175ul per well and leave in non-CO2 incubator for 1 hour. Stock compounds/drugs were prepared as required concentration and 25ul of each are injected in the XF probe port A, B, C, or/and D as required.

a. Port A-Oligomycin 1 uM
b. Port B-FCCP 0.5 uM
c. Port C-FCCP 1 uM
d. Port D-Rotenon/Antimycin A (1uM each in combination)

The template in XFe machine were created for the experiment. XF probe plate are inserted into the machine and calibrated. Culture plate were inserted replacing the bottom plate of XF probe. Experiment then run accordingly. When finished, XFplate containing the cells are emptied and lysed for protein concentration assay using standard Bradford assay and values were calibrated and used for normalisation of assay signals in the XFe software.

2.17 Statistical analysis

Unless specifically stated, the significant of differences between mutants and wild-type mice were tested with ANOVA or unpaired student t-test using the SPSS software. Values are presented as mean +/- SE. P values were deemed significant when ≤0.05. Correlation coefficients were calculated using SPSS and stated as per in the result. For all experiment samples were relabelled or slides

blinded prior to analysis and then genotypes and sexed for uniformity and confirmation.

All experiments were approved by the animal ethics committee and were conducted in accordance with the UK code of practice for the care and use of animals and the Home Office Animals in Scientific Procedures act, 1985.

CHAPTER 3. DISRUPTED NEPHROGENESIS IN MURINE DENYS DRASH SYNDROME.

3.1 Introduction

In kidney development, the morphological stages of nephrogenesis are largely well documented. Studies on mutant and wild type mouse models, supported by analysis of human nephrogenesis have uncovered a deep insight into the contribution of some of the genes involves in the normal developmental processes. The nephron is the functional unit of a kidney, containing structures that filter blood within the glomerulus into solutes that at later segments are selectively reabsorbed and later excreted and concentrated as urine through the connected duct system, as required by the body. The Monash Series documents human nephron number analysis across 5 ethnic backgrounds, showing a 13-fold range from 210,000 to 2.7 million nephrons per kidney (Bertram et at., 2014) compared with between 11,000 and 19,000 nephrons per kidney in adult mice (Merlet-Bénichou et al., 1999). There are no new nephrons are formed in human kidneys after approximately 36 weeks' gestation, thus the final number of nephrons is determined prior to birth, whereas in mice, nephrogenesis carries on for several days after birth. However, the process of nephrogenesis itself is most similar between these two species and involves almost the same genes (Cheval et al., 2012). In the adult mammalian kidney, the renal tubular network and multiple glomerular structures undergo constant cell renewal as a consequence of aging and injury but there is no evidence for the generation of new nephrons (Humphreys et al., 2008; Vogetseder et al., 2005).

Although quite a number of studies shown a relationship between lower nephron number and various diseases, for example, hypertension and CKD (Luyckx et al., 2011), the underlying mechanism is not known. Variation of nephron numbers in adult are determined by the nephron number at the end of nephrogenesis and the rate of nephron loss during postnatal life and also other age-related loss of glomeruli due to glomerulosclerosis, disease affecting kidneys, hypertensive status and other attributes of health (Nyengaard and Bendsen 1992, Hoy et al., 2008, Bertram et al., 2011).

The total number of glomeruli (nephrons) in a kidney is an important microanatomical parameter for at least three reasons. First it provides an index of the success/extent of nephrogenesis. Second, low nephron number has been linked to an increased risk of cardiovascular and renal disease in adulthood and third, the knowledge of quantitative kidney microanatomy can illuminate our understanding of physiological mechanisms in health and disease (Bertram et al, 2013). Although low nephron number is implicated in hypertension and renal diseases, the mechanisms that determine nephron number are obscure.

Numerous studies have indicated that Wt1 mutation, both dominant-negative and haploinsufficiency, cause glomerulosclerosis (GS) in mouse models but the underlying mechanisms remain to be identified (Patek et al., 1999). In the adult kidney, Wt1 expression is strikingly restricted to the podocyte cells of the glomeruli and, given that mutation of podocyte genes, such as CD2AP, podocin, podocalyxin etc, also causes GS (Guo et al., 2002), it has been assumed that Wt1 mutation causes GS by disrupting downstream podocyte-specific gene expression. However, no such pathway has been identified to date and evidence, from studies of mouse chimaeras, indicates that Wt1 mutation is neither necessary nor sufficient for GS to develop at the level of individual glomeruli (Patek et al., 2003).

It has recently been shown that DDS/+ Wt1 mutant mice present with a 20% deficiency in nephron number at 4 weeks of age, prior to the onset of overt GS. Furthermore, this deficiency is physiologically relevant as mutant mice exhibit compensatory glomerular hypertrophy and increased activation of the renin-angiotensin pathway, thus it was suggested that Wt1 mutation causes abnormal nephrogenesis that results in a failure to develop a full complement of nephrons, leading to hypertensive changes that ultimately cause GS (Wroe et al., 2009). However, nephron loss is a common feature of GS, i.e., sclerotic glomeruli undergo atrophy and reabsorption (Denic at al., 2016), so a deficiency in nephron number at 4 weeks of age does not prove that a developmental abnormality affecting nephrogenesis underlies GS in murine DDS.

Given the increasing evidence that Wt1 mutations are a significant factor contributing to GS in patients, it is important to determine whether Wt1-mediated

nephron underdosing is due to abnormal development or post-natal nephron loss. In order to address this question, kidneys from wholly inbred DDS/+ mice were examined at P0 (post-partum day 0, newborn) – a time at which nephrogenesis is ongoing in the mouse, therefore all key stages of nephron development can be assessed.

3.2 Results

The interdisciplinary field concerned with quantitative analysis of three-dimensional (3-D) objects utilising two-dimensional (2-D) data aspects is called stereology and is widely employed in the analysis of nephrogenesis (Kelli et al., 2000). In order to precisely analyse nephrogenesis in Wt1 DDS/+ mice, kidneys were isolated from newborn (P0), sex-matched (female), wholly inbred (129/Ola) wild type and DDS/+ mice. Accurate measurements of kidney size (length and cross-sectional area) can provide an indication of abnormal development (Bridgette et al., 2010) but a more detailed approach is to use stereological techniques to count the absolute number of nephrons. In this current study, nephron number counts were extended to include different stages of nephrogenesis normally present in the newborn mouse kidney (glomeruli, comma- and s-shaped bodies).

Kidney size measurements were taken under light microscopy to give length (pole-to-pole) and cross-sectional area, using AxioVision software, as illustrated in Figure 3.2.1 below. The kidneys were not weighed.

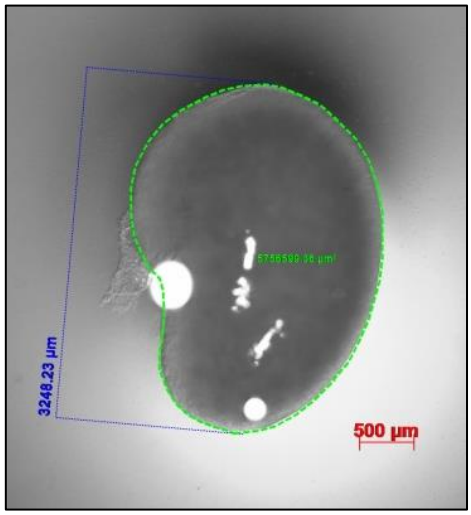

Figure 3.2.1: Representative figure depicting the P0 (new born) mice kidney. Measurements taken were length (length pole-to-pole) (blue numbering) and cross-sectional area of the kidneys.

In order to facilitate nephron counting, peanut agglutinin (PNA) staining was employed, with methyl green counterstaining of sections. In contrast to counting nephrons in an adult kidney, where glomeruli can be readily detected under conventional light microscopy, nephrons within the developing kidney are typically in one of three distinct states, immature glomeruli, comma-shaped body, and s-shaped body, that are more difficult to distinguish. Figure 3.2.2 and Figure 3.2.3 shows examples of developing nephrons following PNA/methyl green staining from the most immature comma-shaped body, through s-shaped body to the mature glomerulus.

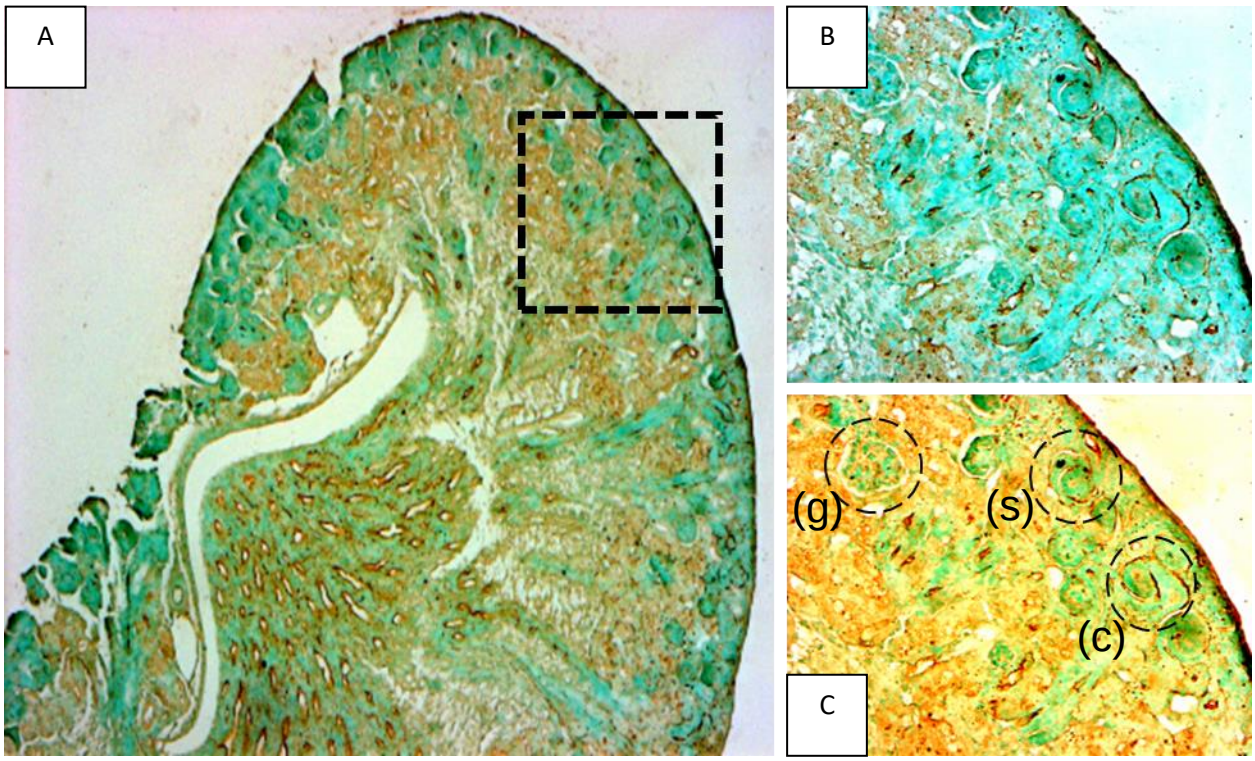

Figure 3.2.2: A. Representative section of P0 kidney stained with PNA/methyl green (5X magnification). B & C. Expanded view of boxed area from A under different contrasts to highlight a glomerulus (g), comma-shaped body (c) and s-shaped body (s) within the cortical region (20X magnification).

Immature and mature nephrons were counted on 5 kidney sections, separated by 15 sections, located towards the centre of the kidney (passing through the renal pelvis), for each kidney, under 40X magnification. Figure 3.2.2(C) shows representative images of PNA/methyl green stained kidney sections highlighting comma-shaped bodies, s-shaped bodies and glomeruli. As can be seen, nephrogenesis occurs at the periphery of the kidney cortex, with more mature structures (glomeruli) being situated towards the inside of the cortex, with comma- and s- shaped bodies occupying the periphery, marking the “nephrogenic zone”.

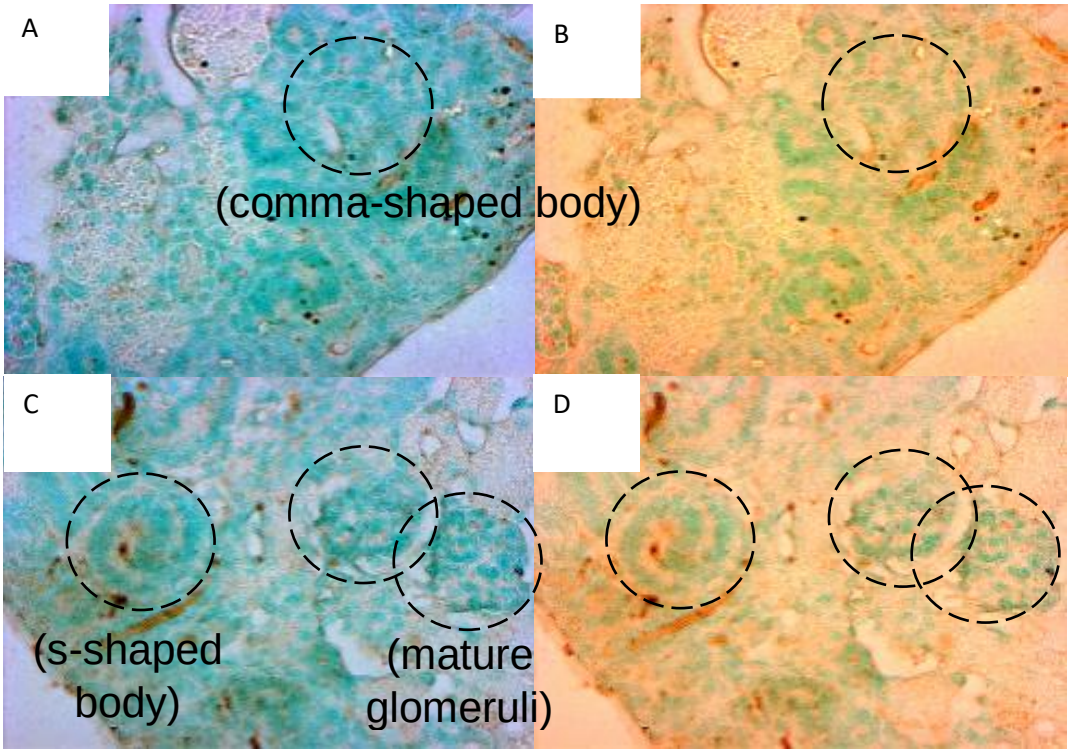

Figure 3.2.3: Representative diagram of P0 kidney section stained with PNA/methyl green (40X magnification) under different contrasts, A & B. Highlight comma-shaped body. C & D. S-shaped body and glomeruli highlighted on P0 kidney section stained with PNA/methyl green (40X magnification). Note S-shaped body found peripheral to glomeruli, within the "nephrogenic zone".

The counting was made by 2 people and double blinded. The slides numbers were covered and randomly labelled. They were shuffled, and nephrons were counted independently by the 2 persons. The values were compared and calculated for the significance of the different between the counts. For all stages of nephron, the calculated p-value were significantly >0.05, indicating no difference between the 2 blind counts. The counted nephron numbers were averaged and were accepted as the true count for the subsequent analysis.

	GENOTYPE	
	Wild type (n=7)	***DDS/+ (n=7)***
LENGTH POLE-TO-POLE (LPP)	3557.96 ± 107.07	3501.29 ± 108.17
LONGITUDINAL CROSS-SECTIONAL AREA (CSA)	6780549.73 ± 397093.94	6286498.87 ± 295393.36
$\mathbf{N_{NEPHRON}}$	4268.57 ± 126.45	3561.71 ± 171.00
$\mathbf{N_{GLOMERULI}}$	3068.57 ± 104.06	2667.43 ± 135.12
$\mathbf{N_{S\text{-}SHAPED}}$	268.57 ± 20.27	109.14 ± 13.26
$\mathbf{N_{COMMA}}$	931.43 ± 35.13	785.14 ± 51.18

Table 3.2.1: Summary of measurements/counts carried out on P0 female kidneys. All values expressed as means ± standard error of the mean (SEM). Length pole-to-pole /µm, Longitudinal cross-sectional area / µm^2.

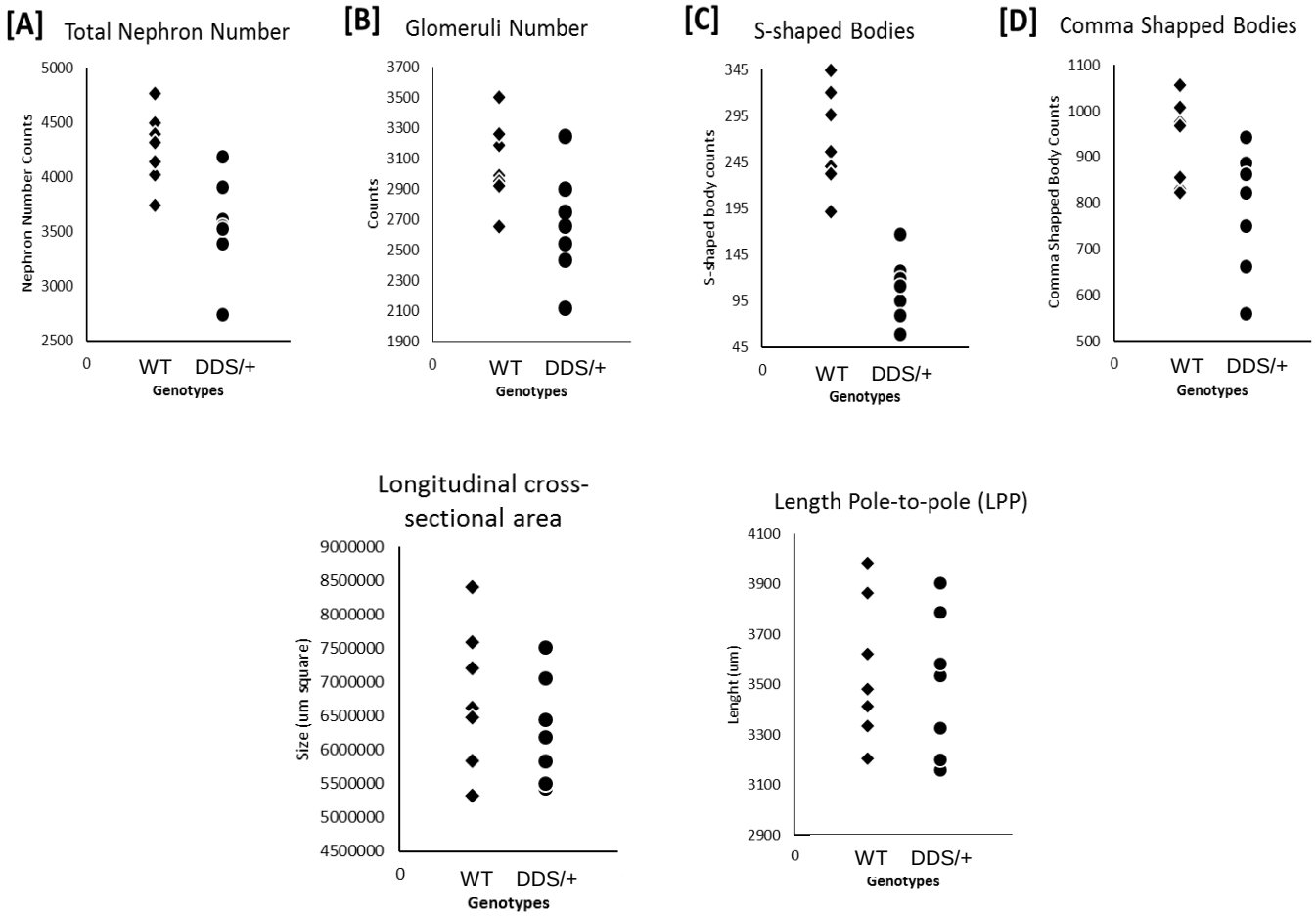

Figure 3.2.4: Summary of measurements/counts carried out on P0 female kidneys showing distribution of values of each genotype. Wild type (WT) = diamonds, DDS/+ = circles.

The data seems to provide evidence that nephron number is reduced in DDS/+ mice at birth, with all stages of nephrogenesis under-represented, particularly the s-shaped body stage. However, the analysis of kidney stereology requires rigorous statistical analysis due to the influences of environmental factors that can confound such studies, even with the use of age- and sex- matched wholly inbred mice.

In order to verify the distribution of data prior to statistical analysis, assessments of normality were carried out. Assessment of the normality of data is a prerequisite for many statistical tests because normal data is an underlying assumption in parametric testing.

Tests of Normality

	Kolmogorov-Smirnov[a]			Shapiro-Wilk		
	Statistic	df	Sig.	Statistic	df	Sig.
LengthPoleToPole	.119	14	.200*	.939	14	.409
LongCrossSection	.130	14	.200*	.953	14	.607
TotalNephronNumber	.090	14	.200*	.974	14	.921
GlomeruliNumber	.110	14	.200*	.984	14	.992
CommaBodies	.185	14	.200*	.952	14	.595
SshapedBodies	.171	14	.200*	.941	14	.429
Genotypes	.332	14	.000	.646	14	.000

*. This is a lower bound of the true significance.

a. Lilliefors Significance Correction

Table 3.2.2 Results of the Kolmogorov-Smirnov Test and the Shapiro-Wilk Test of normality, indicating that all datasets follow a normal distribution (p-value >0.05).

The Shapiro-Wilk test is more appropriate for small sample sizes (<50 samples) and, under these conditions, a Sig. value below 0.05 indicates that the data deviates significantly from a normal distribution. The normality of the datasets can be presented graphically, by using the output of a normal Q-Q Plot. If the data are normally distributed, the data points will be close to the diagonal line. If the data points stray from the line in an obvious non-linear fashion, the data are not normally distributed. As we can be seen in Figure 3.2.5, the normal Q-Q plot below, the data is normally distributed.

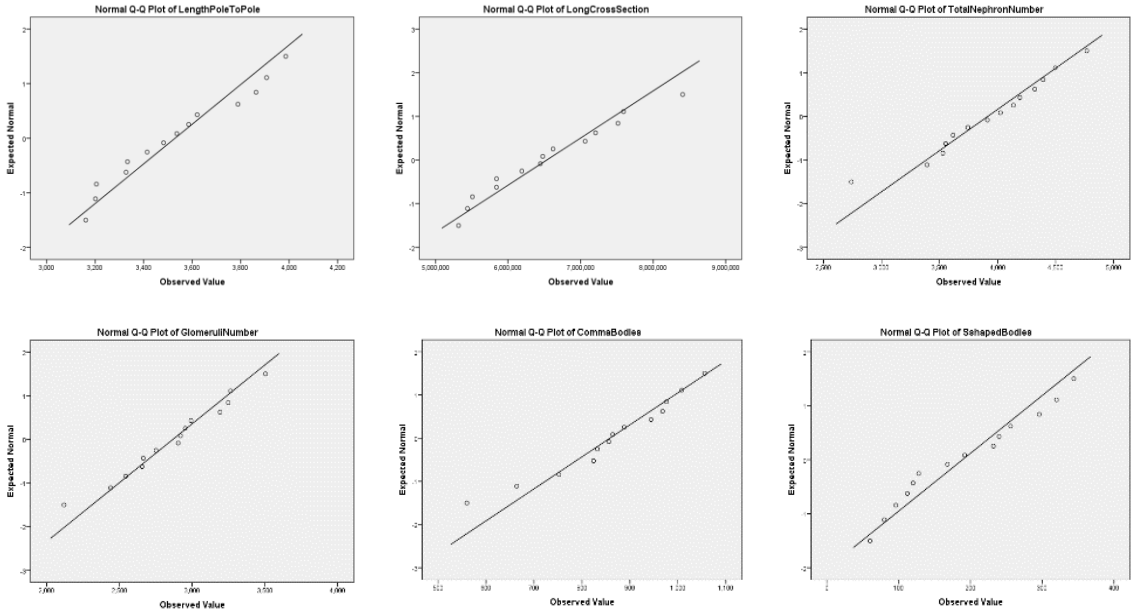

Figure 3.2.5: Q-Q plots for data normalisation. Everything is within acceptable margin.

Having confirmed the datasets follow a normal distribution, further testing was carried out to investigate homogeneity of variance and means. This analysis adds further rigour and stringency and is designed to identify any “outlying” data points that fall within a normal distribution. These tests will inform whether parametric or non-parametric analyses are most appropriate.

The assumption of homogeneity of variance is an assumption of the ANOVA that assumes that all groups have the same or similar variance. The ANOVA utilizes the *F* statistic, which is robust to the assumption, as long as group sizes are equal. Equal group sizes may be defined by the ratio of the largest to smallest group being less than 1.5. If group sizes are vastly unequal and homogeneity of variance is violated, then the *F* statistic is considered liberal when large sample variances are associated with small group sizes. When this occurs, the alpha value is greater than the level of significance. This indicates that the null hypothesis is being falsely rejected.

The test statistic for Levene’s test is calculated by diverging the data for each group from the group mean, and then comparing the absolute values. Levene’s test is

presented with the *F* statistic, as an ANOVA is conducted to compare the absolute values. A *p* value less than .05 indicates a violation of the assumption. If a violation occurs, it is likely that conducting the non-parametric equivalent of the analysis is more appropriate.

Test of Homogeneity of Variances

	Levene Statistic	df1	df2	Sig.(P-value)
LengthPoleToPole	.004	1	12	.949
LongCrossSection	.574	1	12	.463
TotalNephronNumber	.074	1	12	.790
GlomeruliNumber	.173	1	12	.685
CommaBodies	.951	1	12	.349
SshapedBodies	2.162	1	12	.167

Table 3.2.3: Results of the Levene Test indicating the datasets show homogeneity of variance (Sig. value >0.05)

Table 3.2.3 indicates that all parameters measured in this study show equal variance between groups (Levene Test is not significant, Sig.>0.05), thus ANOVA can be carried out with confidence without the need for non-parametric testing or log-transformation of data. Analysis of variance (ANOVA) tests the hypothesis that the means of two or more populations are equal. ANOVAs assess the importance of one or more factors by comparing the response variable means at the different factor levels. The null hypothesis states that all population means (factor level means) are equal while the alternative hypothesis states that at least one is different.

ANOVA

		Sum of Squares	df	Mean Square	F	Sig.
LengthPoleToPole	Between Groups	11240.211	1	11240.211	.139	.716
	Within Groups	972877.378	12	81073.115		
	Total	984117.589	13			
LongCrossSection	Between Groups	854301897755.114	1	854301897755.114	.997	.338
	Within Groups	10287515022089.006	12	857292918507.417		
	Total	11141816919844.120	13			
TotalNephronNumber	Between Groups	1748764.571	1	1748764.571	11.046	.006
	Within Groups	1899753.143	12	158312.762		
	Total	3648517.714	13			
GlomeruliNumber	Between Groups	563204.571	1	563204.571	5.532	.037
	Within Groups	1221595.429	12	101799.619		
	Total	1784800.000	13			
CommaBodies	Between Groups	74898.286	1	74898.286	5.554	.037
	Within Groups	161828.571	12	13485.714		
	Total	236726.857	13			
SshapedBodies	Between Groups	88961.143	1	88961.143	43.317	.000
	Within Groups	24644.571	12	2053.714		
	Total	113605.714	13			

Table 3.2.4: Results of ANOVA and the P-value of each measurements are to the right side of the table.

Rigorous statistical analysis confirms that all stages of nephrogenesis are under-represented in P0 DDS/+ female kidneys, whereas there are no differences in kidney size – either pole-to-pole length or cross-sectional area. The means of length pole-to-pole and longitudinal cross-sections were equal and show no difference between groups (genotype). Whereas the other variables, total nephron number, glomerular number, s-shaped and comma-shaped bodies have unequal means, indicating that they are different between genotypes. The data can now be visualised, as summarised, below.

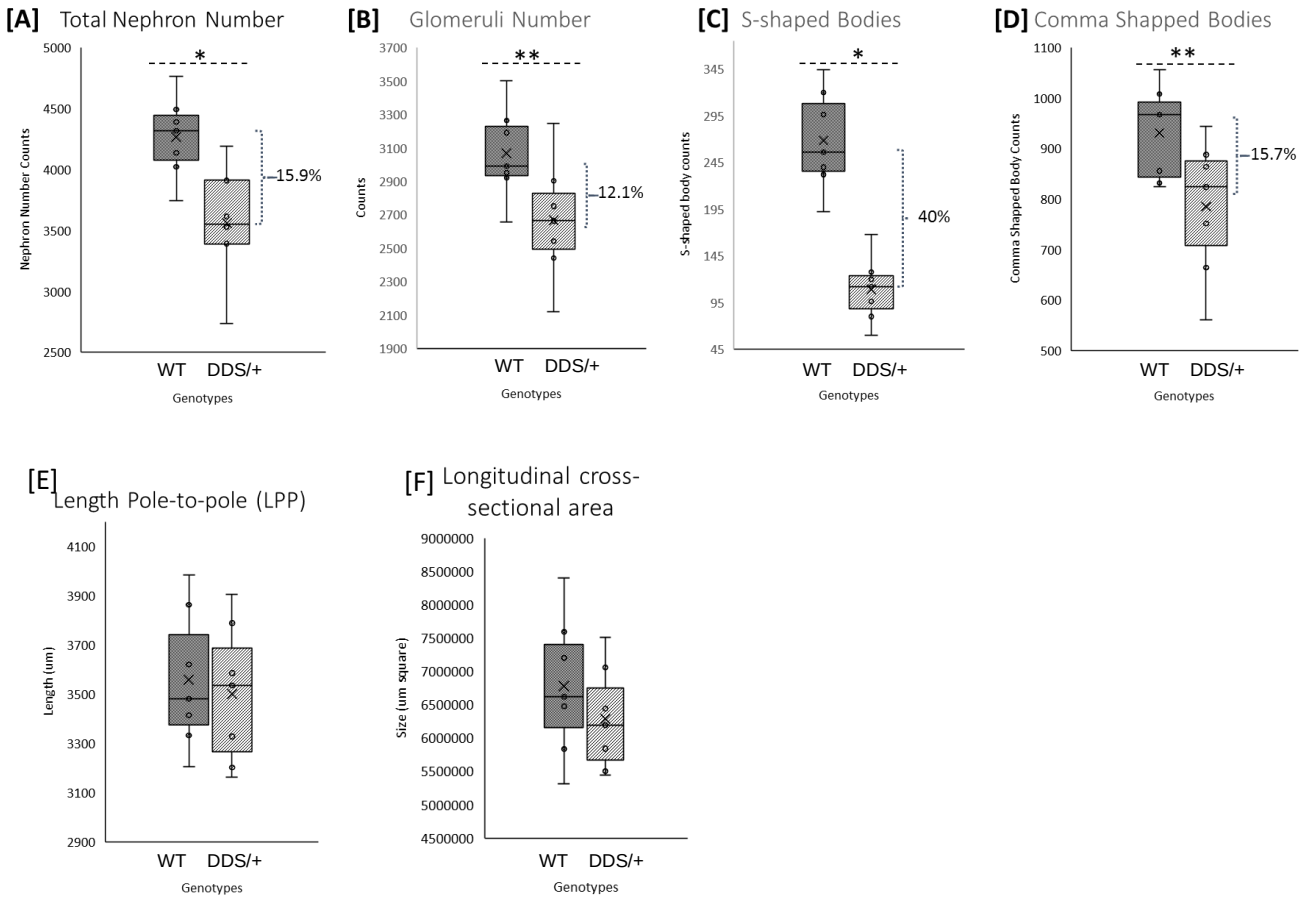

*Figure 3.2.6: Box-whisker plots of data showing nephron number and nephron precursor number at P0 (newborn) age between wild type and DDS/+ mice. A- Difference between the total nephrons number in DDS/+ mice, *p<0.05. B- Difference between the glomerular number in DDS/+, **p<0.05. C- Difference between the number of S-shaped bodies in DDS/+ mice, * P<0.05. D- Difference between the number of comma shaped bodies in DDS/+ mice, **p<0.05. Figure E and F p>0.05. In all cases n=7 both genotypes, female littermates, p value calculated by unpaired student t-test.*

All data were then analysed using IBM SPSS version 23 for Windows. All data have been tested for normality using a Shapiro-Wilk test (and Kolmogorov-Smirnov test if ones preferred), and homogeneity of variance prior to analysis of variance ANOVA (Table 3.2.2). All data were found to be normally distributed. To compare stereology data at termination of treatment, a one-way analysis of variance (ANOVA) was performed with a post hoc analysis to determine differences between groups. A probability of 0.05 or less was considered statistically significant.

Correlation Analysis and regression statistic

Correlations

		Genotypes	LengthPoleToPole	LongCrossSection	TotalNephronNumber	GlomeruliNumber	CommaBodies	SshapedBodies
Pearson Correlation	Genotypes	1.000	-.107	-.277	-.692	-.562	-.562	-.885
	LengthPoleToPole	-.107	1.000	.928	-.095	-.091	-.204	.113
	LongCrossSection	-.277	.928	1.000	.125	.109	.006	.267
	TotalNephronNumber	-.692	-.095	.125	1.000	.955	.823	.695
	GlomeruliNumber	-.562	-.091	.109	.955	1.000	.651	.507
	CommaBodies	-.562	-.204	.006	.823	.651	1.000	.645
	SshapedBodies	-.885	.113	.267	.695	.507	.645	1.000
Sig. (1-tailed)	Genotypes	.	.358	.169	.003	.018	.018	.000
	LengthPoleToPole	.358	.	.000	.373	.379	.243	.351
	LongCrossSection	.169	.000	.	.335	.355	.491	.178
	TotalNephronNumber	.003	.373	.335	.	.000	.000	.003
	GlomeruliNumber	.018	.379	.355	.000	.	.006	.032
	CommaBodies	.018	.243	.491	.000	.006	.	.006
	SshapedBodies	.000	.351	.178	.003	.032	.006	.
N	Genotypes	14	14	14	14	14	14	14
	LengthPoleToPole	14	14	14	14	14	14	14
	LongCrossSection	14	14	14	14	14	14	14
	TotalNephronNumber	14	14	14	14	14	14	14
	GlomeruliNumber	14	14	14	14	14	14	14
	CommaBodies	14	14	14	14	14	14	14
	SshapedBodies	14	14	14	14	14	14	14

Table 3.2.5: Pearson correlation (r) matrix of all factors calculated against each other. Significant p value was taken as p<0.05 1-tailed. Positive Pearson's correlation value (top part of the table, in red box) indicate positive correlation (describes the relationship between X and Y perfectly, which Y increases as X increases), and negative values indicate negative correlation (which Y decreases as X increases). The Sig. value is the significance for each Pearson's value. N is the total number of items in the calculation. The ranges of correlation coefficient is −1 to 1. No linear correlation between the variables indicated with value of 0.

The correlation table shows decomposition of each unique variables and each shows some level of unique predictive capacity towards respective variables from Pearson's correlation calculations.

Multiple regression is quite a sophisticated technique. Regression calculation was done on all predictive factors (not including genotype) towards glomerular number as dependant to see if any of these factors have the highest contributing predictive value with high level of accuracy towards nephron number using stepwise method in SPSS regression calculation. Stepwise method will choose the independent variable that has the largest Pearson's correlation with the dependant variable, in this case glomerular number, and next will look at the next highest predictor from Pearson correlation matrix and continue the calculation and so on.

ANOVA[a]

Model		Sum of Squares	df	Mean Square	F	Sig.
1	Regression	2.847	5	.569	6.973	.009[b]
	Residual	.653	8	.082		
	Total	3.500	13			

a. Dependent Variable: Genotypes

b. Predictors: (Constant), SshapedBodies, LengthPoleToPole, GlomeruliNumber, CommaBodies, LongCrossSection

Table 3.2.6: ANOVA of statistically significance of the model for prediction indicating potential predictors that can be used to assess nephron number.

Model Summary[b]

Model	R	R Square	Adjusted R Square	Std. Error of the Estimate	Change Statistics				
					R Square Change	F Change	df1	df2	Sig. F Change
1	.885[a]	.783	.765	.25154	.783	43.317	1	12	.000

a. Predictors: (Constant), SshapedBodies

b. Dependent Variable: Genotypes

Table 3.2.7: Result of stepwise method for significant predictor for nephron number.

Stepwise method gave the S-shaped bodies as the most significant predictors for representation of final glomerular number in this case at this stage of renal development, $F(1,12) = 43.317$, $p<0.005$, $R^2 = 0.783$. This points out that this stage gives a significant indication and contribution towards final glomerular number, adding to the technical aspect of it to be easily recognised when counting.

To see whether the correlation between the two genotype groups is significantly correlated, regression calculation was done. The total number of nephron, and glomeruli number was set separately up as dependant variable and the genotype was the dichotomous independent variable in both calculations by default method (enter), result as shown below.

ANOVA[a]

Model		Sum of Squares	df	Mean Square	F	Sig.
1	Regression	1748764.571	1	1748764.571	11.046	.006[b]
	Residual	1899753.143	12	158312.762		
	Total	3648517.714	13			

a. Dependent Variable: TotalNephronNumber

b. Predictors: (Constant), Genotypes

ANOVA[a]

Model		Sum of Squares	df	Mean Square	F	Sig.
1	Regression	563204.571	1	563204.571	5.532	.037[b]
	Residual	1221595.429	12	101799.619		
	Total	1784800.000	13			

a. Dependent Variable: GlomeruliNumber

b. Predictors: (Constant), Genotypes

Table 3.2.8: ANOVA of statistically significance of the model for prediction for both glomeruli and total nephron number.

3.3 Summary of key findings:

I. Nephron number is decreased at birth in DDS/+ mice. Thus, it is abnormal development and not the disease state that leads to fewer nephrons in DDS/+ mice.
II. DDS/+ kidneys do not differ in size from wild type at birth.
III. There is a differential effect (can be recognized and identified) on different stages of nephrogenesis, with s-shaped body as the most significant.
IV. Indication of factors contributing to the nephron number start before parturition (i.e. genotype or other factors)
V. S-shaped body is both easy to be recognised technically and predictive of the nephron number.

3.4 Discussion

The exact pathways governing the end of nephron formation is not yet understood, although some genes have been implicated with specific spatial expression. Two possible mechanism initiating the ending of nephrogenesis have been proposed. First, the birthing or post birth processes trigger a system involving glycolytic pathways and the increase in oxygen tension, a theory based on differential gene expression changes (Brunskill et al, 2011). Second, the process of nephrogenesis gradually loses the progenitors' stem cells capacity and exhausted itself, ultimately leads to differentiation into various specified cells types and loses progenitor attributes, thus ending the nephrogenic processes (Brunskill et al., 2011, Hendry et al., 2011).

It has been documented that infants below 10th percentile of birth weight shown to have smaller kidneys plus fewer nephron number indicating possibility of relationship between body size, kidney weight, kidney size and nephron number (Hoy et al., 2003, Merlet-Benichou et al., 1999). In addition, correlation has been shown to exist between adult height and body surface area (Hoy et al., 2006), and between kidney weight, kidney volume and glomerular volume (Hughson et al., 2003). Mice with a lower birth

weights were documented to be are born with smaller kidney and kidney surface area (Murawski et al., 2010).

It is well known that nephron number in humans can vary more than tenfold from 200,000 to 1.8 million (Hughson et al., 2003) while in mice varies from 11,000 to 19,000 per kidney (Merlet-Benichou et al., 1999). The end of nephrogenesis in human was documented to be at 36 weeks of gestation (Hinchliffe et al., 1991) and around one week (P6) after birth in mouse (Rumballe et al., 2011). It is thought that this variation of nephron number, with lower counts having higher risk and highly associated with predisposition to renal disease (Brenner and Anderson, 1992; Luyckx and Brenner, 2010.).

Whilst the studies describe the association of nephron number and those factors, some have shown relationship of those to hypertension or chronic renal failure, and some have not (Hoy et al., 2003, Hughson et al., 2006, McNamara et al., 2008). This suggest the existence of other possible parameters that are independent, or maybe interdependent that obscure the relationship by means of multiple variations in gene expressions and environments.

The wild type and DDS/+ mutant mice are of similar strain and background, with uniform exposure to surrounding environment making this model ideal for various comparison studies. Newborn mice (P0) were culled and the kidneys were isolated, measured for cross-sectional area (CSA) and pole-to-pole length (LPP) then prepared for nephron number counting. Kidney weight were previously shown to be correlated positively with kidney surface area suggesting that these measurements are interchangeable. (Murawski et al., 2010).

Although it seems logical to assume if there was reduction of nephron number, the kidney should be smaller for the volume reduction. In this study, DDS/+ mice had slightly smaller kidneys than wild type mice measured as planar surface area and LPP, but insignificant statistically. This insignificant different might be as a result of supervening compensatory hypertrophy of the remaining nephron and glomeruli as adult DDS/+ mice have been shown to have significantly larger mean glomerular volume (MGV) compared to wild type (Wroe et al., 2009).

The study of the relationship between kidney size and nephron number came mostly from rat models. The relationship studies of naturally occurring low birth weight rat (Wistar rat) shows 20% reduction of nephron number and normal size kidneys with increase in glomerular volume (Schreuder 2007, Jones et al., 2001), while another strain of naturally occurring low birth weight rat (Sprague-Dawley rats) do not have a significant nephron number different and kidney weight or size (Jones et al., 2001). On the other hand, a study on mice kidney shows size correlates with birth weight, but nephron number does not correlate with birth weight or kidney size, and that the differences in nephron number cannot be predicted by a change in kidney size or body weight and that nephron number is an independent variable (Murawski et al., 2010). Unfortunately, the kidneys were not weighed prior to processing to correlate this previous finding. While other studies showed correlation between nephron number and kidney size with up to 5-fold correlated difference (Hoy et al., 2003, Nyengaard et al., 1992, Hoy et al., 2006, McNamara et al., 2008), it is suspected that large comparative difference is needed of at least 2-fold to show any significant correlation between kidney size and nephron number (Murawski et al., 2010). Even though hypoplastic kidneys (small kidneys) were seen to be the results of multiple genetics and also environmental factors, it is not always reflected as kidney size abnormality for nephron number differences (Cain et al., 2010). These highlights the challenges and importance of understanding the underlying morphogenetic and molecular process of the kidney development.

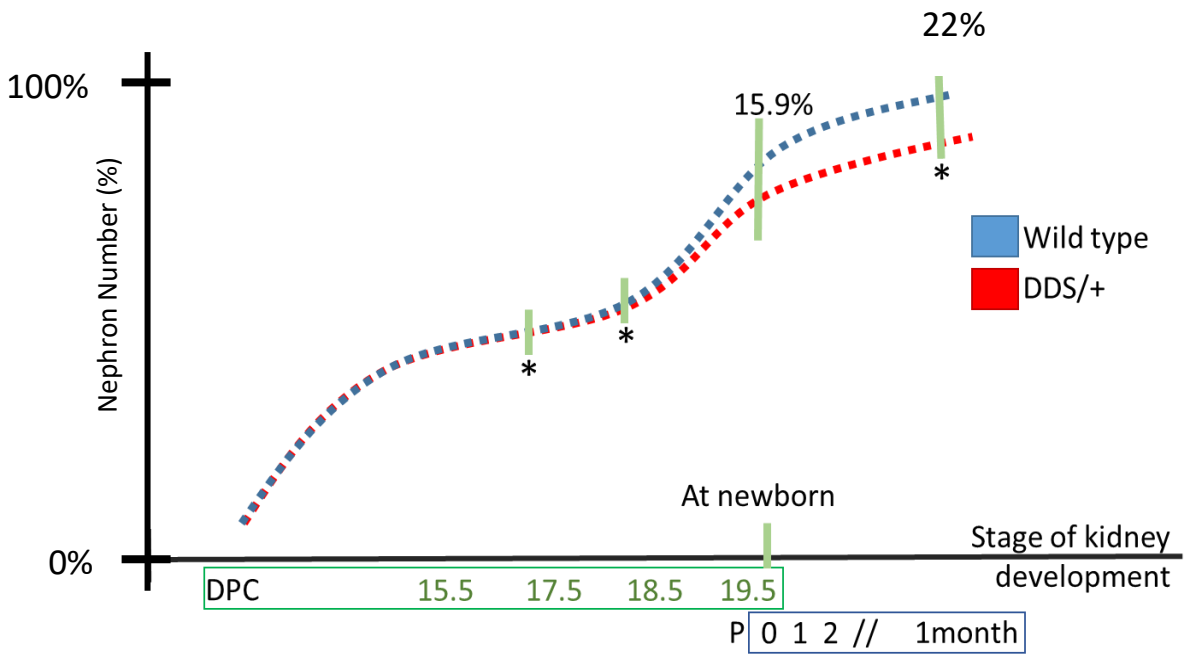

*Figure 3.4.1: Projection of nephron number (current counts at 15.9% and *Miles Lab unpublished data and 22% Wroe et al., 2009, Figure 1.8.2.1) at various stages of development between wild type and DDS/+ (Wt1tmT396/+) mice adapting the nephron number trend from Short et al., 2014. At e17 and e18, there were no gross different of total counts. At P0 there is observable reduction of 15.9% and at one month a 20% reduction on nephron number, p<0.05.*

The pattern of nephron formation, morphological segmentation and functions are guided partially by ureteric epithelium and the rest by the interstitial tissue and vasculature surrounding it (Costantini and Kopan, 2010 and Little and McMahon, 2012). Even the interaction is known, the complexity of alteration of one factor affecting another is still not predictable, let alone the relative changes they affect the stages of nephrogenesis are unknown. Contrary to logical impression of timely repeated synchronous growth, renal morphogenesis exhibits temporal discontinuity of its conserve branching growth, not to mention the branching and proliferation reduces over time (Short et al., 2013).

It is known that cap mesenchymal (CM) cells may either aggregates and differentiate itself into nephrogenic epithelial cells or self-renew to support the growth of

ureteric tip (UT) while another UT contributes to the nearby duct formation. A morphometric analysis measuring the initial exit rate of the CM and UT of this branching processes was showing unbalance with CM niche show early depletion, displaying a heterogenous growth between the cell populations at the first half of nephrogenesis, though become balance in later half postnatally with exponential CM growth that resulting in final loss of the cell niche (Short et al., 2013).

This confirms the previous finding of CM showing heterogenous growth (Mugford et al., 2009), with unequal depletion of fast rapid turn-over CM niche that thought to undergo differentiation, that later imparted the predominant possible observation of having more than 50% nephron originated from this rapid turn-over CM niche (Short et al., 2013). Nevertheless, lineage tracing indicates all CM would end up contribute to nephron formation (Boyle et al., 2008 and Kobayashi et al., 2008) which indicates that the remaining slow turn-over CM niche eventually contribute to nephron. This observation corroborates the hypothesis of decisive trigger prompted CM depletion by differentiation at parturition (Rumballe et al., 2011) implying possible CM sub-niche exist as progenitor in certain ration, decreasing by time denoting dissimilarity of early CM and later CM. This elucidate the study having disparate gene expression profiles of early CM and later CM after birth (Brunskill et al., 2011).

S-shaped bodies show greater difference between wild type and DDS/+. This seems to indicate a dynamic difference in the process of nephrogenesis, in addition to fewer comma-shaped bodies developing. Could there be compensatory acceleration of nephrogenesis through the s-shaped body stage to counteract the reduction in nephrons being produced, i.e., spending less time at the s-shaped body stage is a possibility. This seems to affect the last wave of nephrogenesis post parturition.

It is possible that pax-2 determines epithelial tubule specialization, whereas WT1 determines glomerular visceral epithelial specialization in the developing nephron. WT1 have also suggested suppression not only of transcription of early growth response gene (EGR-1), IGFII and platelet-derived growth factor-A (PDGF-A) (Drummond et al., 1992) but also the transcriptional activation of WT1 itself (Wang et al., 1993). It does not appear to contribute to development of the other epithelial tubular cells of the nephron. However, in Wilms tumours, WT1 is over expressed in dysplastic tubular epithelium

(Yeger et al., 1992). WT1 serve as transcriptional repression of growth factor and receptor genes like IGFII, PDGF-A, CSF-1, TGF-13, IGF1R and transcription factors like RARct (Dey et al., 1994, Drummond et al., 1992). Under some circumstance transcriptional activation of these and other genes may also occur (Madden et al., 1991, Wang et al., 1993).

Although nephrogenesis was seen to initiate early (12.5 dpc), the majority of nephrons (>50%) form once branching has ceased. Consequently, variability in final nephron number may not necessarily reflect variations in final branch generation number. Perhaps of greater interest is the clear sub sectioning of the CM into distinct populations based on cell-cycle length, with the slower cycling population representing those portions of the CM containing the highest level of Six2 protein. (Short et al., 2013), which Six2 together with WT1 are involve in early nephron formation. There are more questions than answers at this stage, perhaps there are other contributing factors to it such as effect of programmed cell death, or maybe abnormal differentiation or proliferation in affect?

From Figure 3.4.1, it is postulated that the most likely time point suitable for investigation of gene expression would be between e17.5 to e18.5. This would give a list of genes that would give an idea towards the role of WT1 gene and its downstream affecting the formation of new nephron. Next chapter would explore more on this in interesting time point of what genes change when WT1 was disrupted that would lead to phenotype of low nephron in DDS/+.

CHAPTER 4. ALTERED GENE EXPRESSION PATTERNS DURING KIDNEY DEVELOPMENT IN MURINE DENYS DRASH SYNDROME

Introduction

The role of multiple systemic disease processes in the pathogenesis of chronic kidney disease (CKD) has been recognised, for example in ageing DDS/+ mice (Patek et al., 2008), and the concept of a 'first hit' in renal disease is becoming widely accepted (Hershkovitz et. al., 2007). This concept has developed such that kidney diseases are now thought to often be associated with low nephron number (LNN), in particular as a mechanism involved in CKD development and progression. Multiple observations on intrauterine growth restricted (IUGR) babies initially led to this conceptual formulation (Hershkovitz et. al., 2007). Consistent with these observations, many studies in rats induced to have LNN by protein restriction diet resulted in animals with impaired renal function (Woods et. al., 2004, Bauer et. al., 2002). This positive correlation has also been documented from studies involving mortality of stillborn and infants within the first year of life (Manalich et. al., 2000). Thus, an individual with the 'first hit' LNN kidney then later becomes vulnerable to various forms of renal injury, the 'second hits', thus enhancing the development toward CKD.

As been shown in previous chapter, DDS/+ mutant mice have lower nephron compared to wild type. In order to investigate the gene expression changes directly related to this abnormal kidney development, kidneys were taken for analysis at e17.5, prior to any gross differences being apparent, such as reduction in nephron number that has been discussed in previous chapter. The e17.5 to e18.5 timing is taken because it is just before birth of the mice (Figure 3.7), and this is the timing assumed to be a crucial turning point for nephron development. Instead of using RNA-seq, I have opted for microarray for several reasons, namely it is a test with proven clinical utility, cost efficient, and is a direct measurement of annotated genes.

4.1 Microarray data and analysis of DDS/+ mice e17.5 kidneys versus wild type

Foetal kidneys from *DDS*/+ mice were compared with age- and sex-matched wild type littermates was carried out in order to identify molecular pathways disrupted by Wt1 mutation.

The overall quality of the analysis was determined by Source Bioscience for RNA integrity and array signal optimisation and normalization. As can be seen below, only minimal normalisation was necessary across the 8 hybridisations:

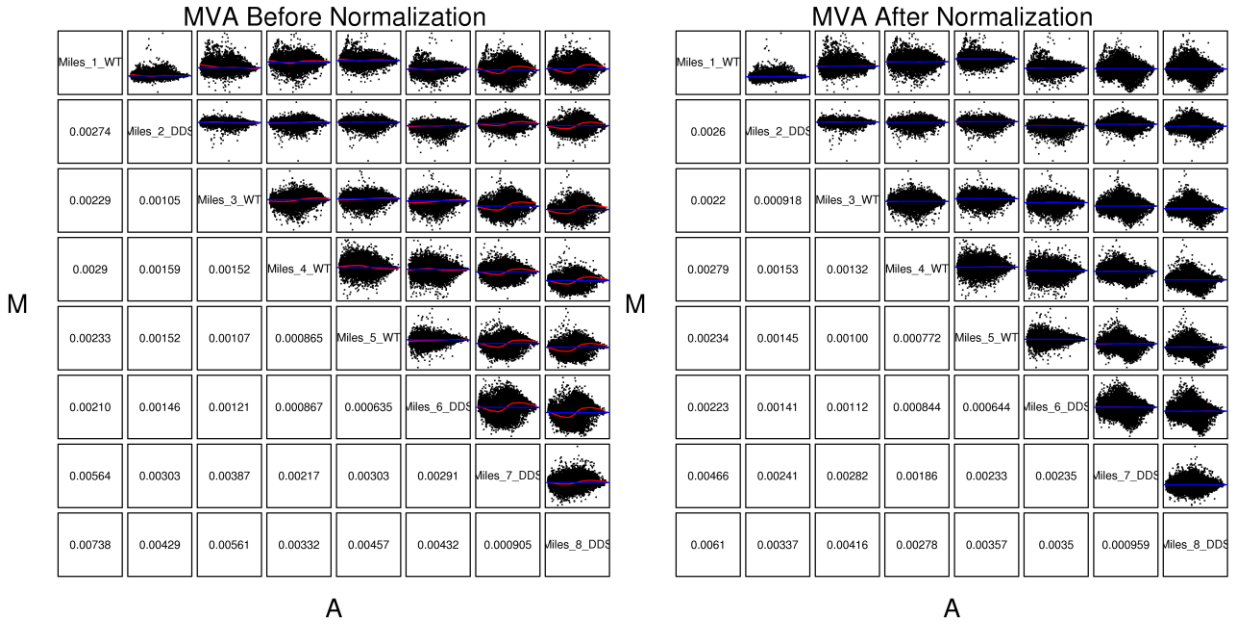

Figure 4.1.1: A chip-to-chip comparison before and after normalization. The plots on the diagonal show the names of the chips compared. The plots above the diagonal show the comparison of the data of two chips. After normalization, the red line should be close to zero (the blue line). The plots below the diagonal show the variance of the ratios. The variance equals zero, if the compared chips are identical.

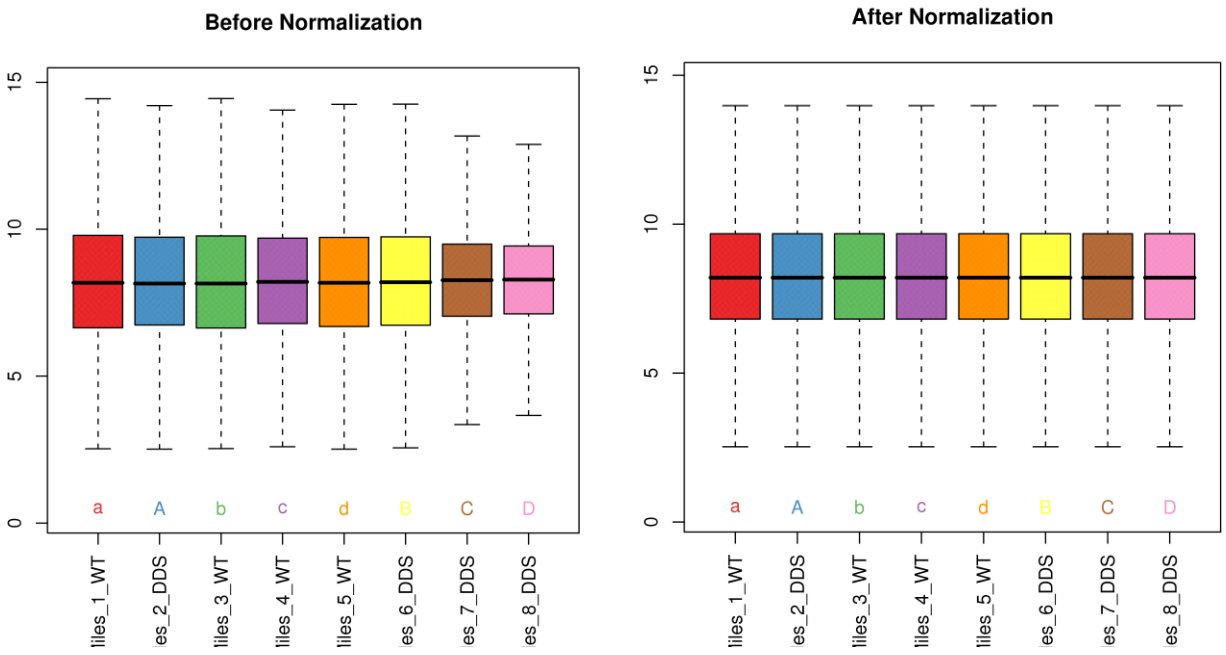

Figure 4.1.2: Boxplots of log2 transformed expression values before and after normalization.

Unbiased Principal Component Analysis revealed the global differences in gene expression between wild type and mutant samples (wild type red triangles, mutant blue crosses) and the hierarchical clustering of the top 50 differentially expressed genes is depicted by the heat map below:

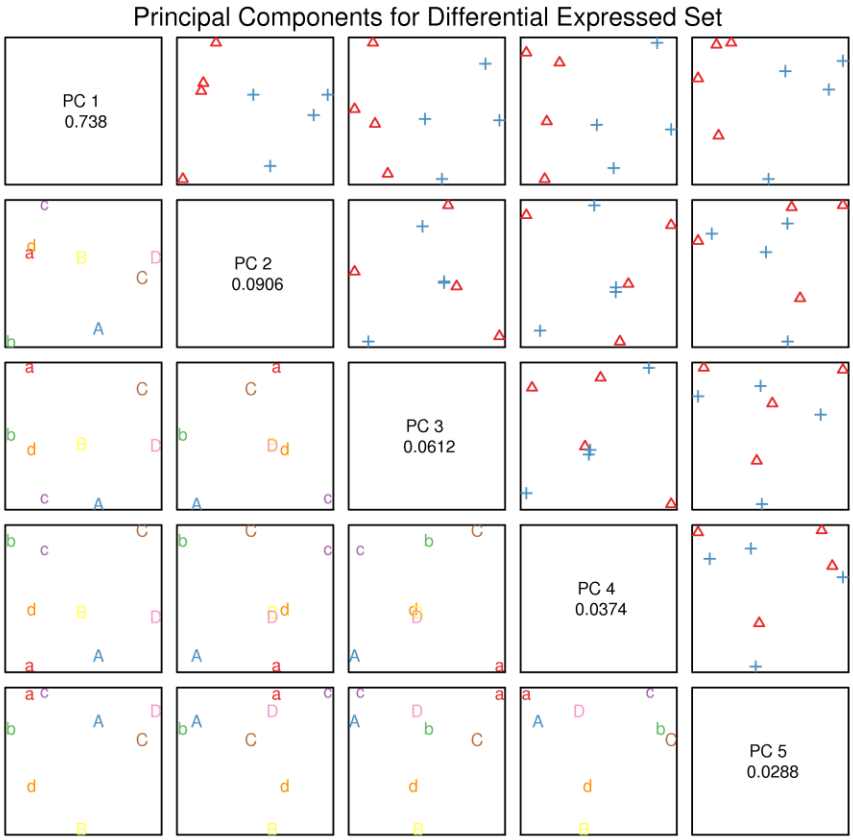

Figure 4.1.3: PCA of expression values for normalized and filtered genes for the arrays. First four principal components (PCs) are plotted against each other. The numbers in the diagonal show the proportion each PC contributes to the overall differences between the arrays.

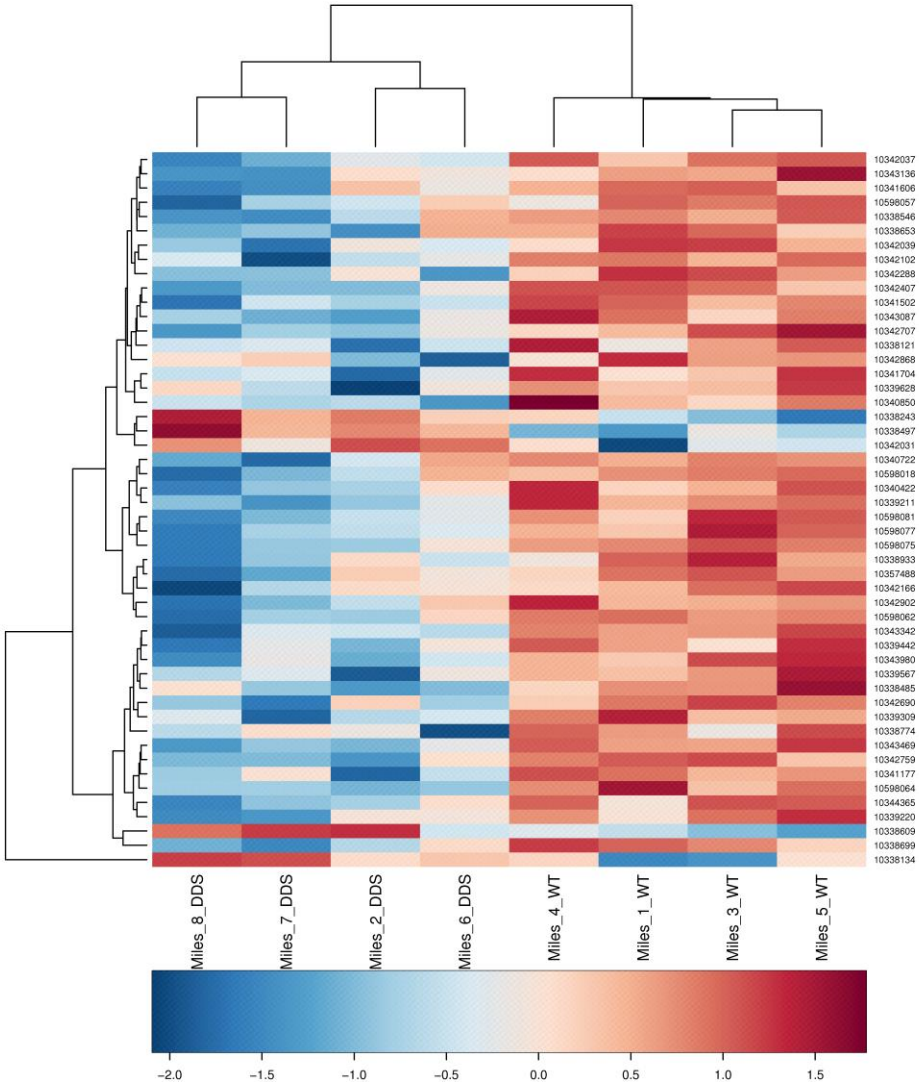

Figure 4.1.4: The heatmap shows a two-dimensional clustering of the top 50 genes. Expression intensities are normalised row wise by the Z-score: Row Mean - Value / Row-Standard Deviation. Those Z-score values are represented by red and blue, for high and low intensities, respectively. White indicates medium intensities.

The top 120 differentially expressed genes, ranked by fold change are listed below (with transcripts lacking annotation removed for clarity):

		Lfc (negative-down regulated, positive-up regulated)	**p-value**	***Genes***
1	**10598075**	-2.22903	0.00083	*tRNA-Ala*
2	**10598081**	-2.12106	0.025774	*tRNA-Tyr*
3	**10598077**	-1.85398	0.031739	*tRNA-Asn*
4	**10598062**	-1.53878	0.003805	*tRNA-His*
5	**10598064**	-1.51768	0.012982	*tRNA*
6	**10598057**	-1.18111	0.022606	*tRNA-Arg*
7	**10598018**	-1.08121	0.027798	*tRNA-Phe*
8	**10357488**	-0.91549	0.019895	*Cd55*
9	**10536401**	0.841199	0.010346	*Nxph1*
10	**10419559**	-0.78621	0.005714	*Rnase12*
11	**10578413**	0.765265	0.018589	*Gm5346*
12	**10492300**	-0.7533	0.042471	*Aadac*
13	**10386093**	-0.75041	0.017522	*Snord1c*
14	**10382844**	-0.74899	0.017813	*Snord1c*
15	**10344897**	-0.7368	0.009932	*Sulf1*
16	**10385770**	-0.73139	0.040264	*Olfr1372-ps1*
17	**10472235**	-0.7077	0.032637	*Dapl1*
18	**10528207**	-0.70188	0.043533	*Cd36*
19	**10601598**	-0.68867	0.048529	*3110007F17Rik*
20	**10478383**	-0.68431	0.018082	*R3hdml*
21	**10372139**	-0.68268	0.036528	*Nts*
22	**10344981**	-0.67303	0.043962	*Pi15*
23	**10472400**	-0.67012	0.010298	*Scn2a1*
24	**10511631**	-0.66949	0.01448	*Slc26a7*
25	**10371740**	-0.64001	0.015135	*Ano4*
26	**10554547**	-0.62115	0.033853	*Mir1839*
27	**10366640**	-0.61023	0.041946	*Llph*
28	**10389759**	-0.59724	0.004574	*Ankfn1*
29	**10528015**	-0.59716	0.038962	*Steap1*

30	**10390080**	0.596323	0.007788	*Tmem92-ps*
31	**10601867**	0.593682	0.029672	*Kir3dl1*
32	**10536216**	-0.58981	0.036545	*Gng11*
33	**10351039**	-0.5882	0.041848	*Gas5*
34	**10447885**	-0.57518	0.040072	*Acat3*
35	**10603746**	-0.57487	0.014565	*Maob*
36	**10417408**	-0.5672	0.042637	*D830030K20Rik*
37	**10414545**	-0.56683	0.007217	*Eddm3b*
38	**10536405**	0.566299	0.007919	*Nxph1*
39	**10450363**	-0.55038	0.049447	*Snord52*
40	**10559179**	-0.53265	0.024009	*E330027M22Rik*
41	**10462922**	-0.51966	0.039754	*Plce1*
42	**10522788**	-0.51921	0.016472	*Stap1*
43	**10429128**	-0.51376	0.009071	*Sla*
44	**10547664**	0.511662	0.018797	*Clec4e*
45	**10472531**	-0.51108	0.005387	*G6pc2*
46	**10368970**	-0.50362	0.028189	*Prdm1*
47	**10587988**	-0.50303	0.044305	*Gk5*
48	**10346164**	-0.49389	0.034008	*Sdpr*
49	**10579958**	-0.49364	0.044267	*Il15*
50	**10458122**	-0.49156	0.034577	*Nme5*
51	**10455123**	-0.48945	0.038048	*Pcdhb19*
52	**10494821**	-0.48898	0.040524	*Tspan2*
53	**10368907**	0.483124	0.012591	*Nr2e1*
54	**10478461**	0.481125	0.04532	*Svs3a*
55	**10504664**	-0.48021	0.01283	*E230008N13Rik*
56	**10354563**	-0.47177	0.03986	*Dnahc7b*
57	**10510191**	-0.46746	0.040806	*Zfp600*
58	**10401068**	0.465756	0.033258	*Spnb1*
59	**10514313**	0.465296	0.022729	*Gm13280*
60	**10458725**	0.464576	0.035711	*Spink11*
61	**10462818**	-0.46375	0.009839	*Hhex*
62	**10494281**	0.459147	0.038373	*Hormad1*
63	**10538802**	-0.45823	0.039896	*A930038C07Rik*
64	**10407707**	-0.45796	0.031596	*Gm10336*
65	**10574598**	0.457852	0.040883	*Ces3a*
66	**10493896**	0.456502	0.010185	*Lce3b*
67	**10351873**	0.45483	0.016871	*Pyhin1*
68	**10506213**	-0.45475	0.044067	*Ube2u*

69	**10572097**	-0.45371	0.022646	*Sh2d4a*
70	**10346321**	-0.45346	0.039115	*Gm10561*
71	**10473557**	0.453405	0.008877	*Olfr1131*
72	**10472366**	-0.45205	0.025266	*Scn2a1*
73	**10466932**	-0.45186	0.01664	*Insl6*
74	**10408629**	-0.45106	0.026002	*1300014I06Rik*
75	**10471912**	-0.44212	0.037525	*Kynu*
76	**10496457**	-0.44209	0.041203	*Adh6b*
77	**10399027**	0.440232	0.047945	*Adam6a*
78	**10434845**	-0.43881	0.038171	*Il1rap*
79	**10530536**	-0.43858	0.040619	*Tec*
80	**10555894**	0.436814	0.005808	*Dub1*
81	**10439651**	-0.43644	0.047642	*Cd200*
82	**10442779**	0.435282	0.012199	*Prss29*
83	**10507152**	-0.43451	0.011948	*Cyp4a12b*
84	**10458875**	-0.43399	0.011031	*Dtwd2*
85	**10427461**	-0.43391	0.029826	*Ptger4*
86	**10347033**	-0.43302	0.04243	*Crygf*
87	**10401968**	-0.43197	0.03626	*Galc*
88	**10352497**	-0.4315	0.011979	*Snora36b*
89	**10554745**	0.431012	0.026423	*Vmn2r78*
90	**10542414**	-0.43009	0.020478	*Ptpro*
91	**10461820**	0.429948	0.031995	*Olfr1489*
92	**10432278**	-0.42948	0.007339	*Ddn*
93	**10493114**	-0.42787	0.006861	*Nes*
94	**10591749**	0.427276	0.005877	*1810064F22Rik*
95	**10536697**	-0.42686	0.035286	*Asb15*
96	**10445909**	-0.42603	0.040321	*Kat2b*
97	**10361265**	0.425487	0.001135	*Mir205*
98	**10400510**	-0.4246	0.027049	*Clec14a*
99	**10371578**	0.424148	0.013115	*Ascl1*
100	**10356457**	-0.42269	0.034074	*Dnajb3*
101	**10491106**	-0.4207	0.020578	*Pld1*
102	**10602896**	-0.41864	0.022076	*Gpr64*
103	**10497197**	0.416634	0.01406	*5330432E05Rik*
104	**10492281**	0.416094	0.007682	*4930449A18Rik*
105	**10489545**	0.412805	0.046791	*Tnnc2*
106	**10431585**	-0.41191	0.049342	*Chkb*
107	**10515828**	0.41188	0.039201	*Olfr1335*

108	**10603807**	0.410597	0.031278	*Mir222*
109	**10374777**	-0.40916	0.02635	*Efemp1*
110	**10554778**	0.408558	0.028678	*Grm5*
111	**10427918**	-0.40345	0.034643	*Fam105a*
112	**10420362**	-0.40302	0.049286	*Gjb2*
113	**10396402**	-0.402	0.04288	*Prkch*
114	**10471945**	-0.39995	0.027294	*Gm13476*
115	**10395733**	-0.39883	0.00993	*Npas3*
116	**10523451**	-0.3987	0.040458	*Anxa3*
117	**10407126**	-0.39684	0.04899	*Plk2*
118	**10502042**	-0.39427	0.021116	*Alpk1*
119	**10368918**	0.393518	0.000809	*Sobp*
120	**10574098**	0.393368	0.04925	*Nlrc5*
1040	10474295	0.339383	0.027389	*Wt1*

Table 4.1.1: List of significant differentially expressed genes ($p < 0.05$) with highest fold ratio from microarray analysis of DDS/+ ($Wt1^{tmT396}$/+) foetal kidneys. The negative values in Lfc column are downregulated gene expression, the positive values in Lfc column are upregulated genes expression.

The microarray has provided us with an interesting list of novel genes that change between mutant and the wild type that are strong candidates that play important role in kidney development, in particular in terms of regulating nephron endowment that may give clues towards the initiation of the renal stress leading to CKD. When compared, the expression profiles of the mutant and wild type sample RNA showed that many genes would have been identified as genes up- or downregulated and need to be validated. 626 genes have been found upregulated and 511 downregulated. For some an example, genes such as Sulf1 has been shown previously to be regulated by WT1 (Ratelade et al., 2010). Nonetheless, many other genes have yet to be identified for association with WT1 regulation in renal development.

4.2 Reduction in tRNA expression levels, but not ND5, confirmed in independent DDS/+ (*Wt1*^{tmT396}/+) mutant kidney samples.

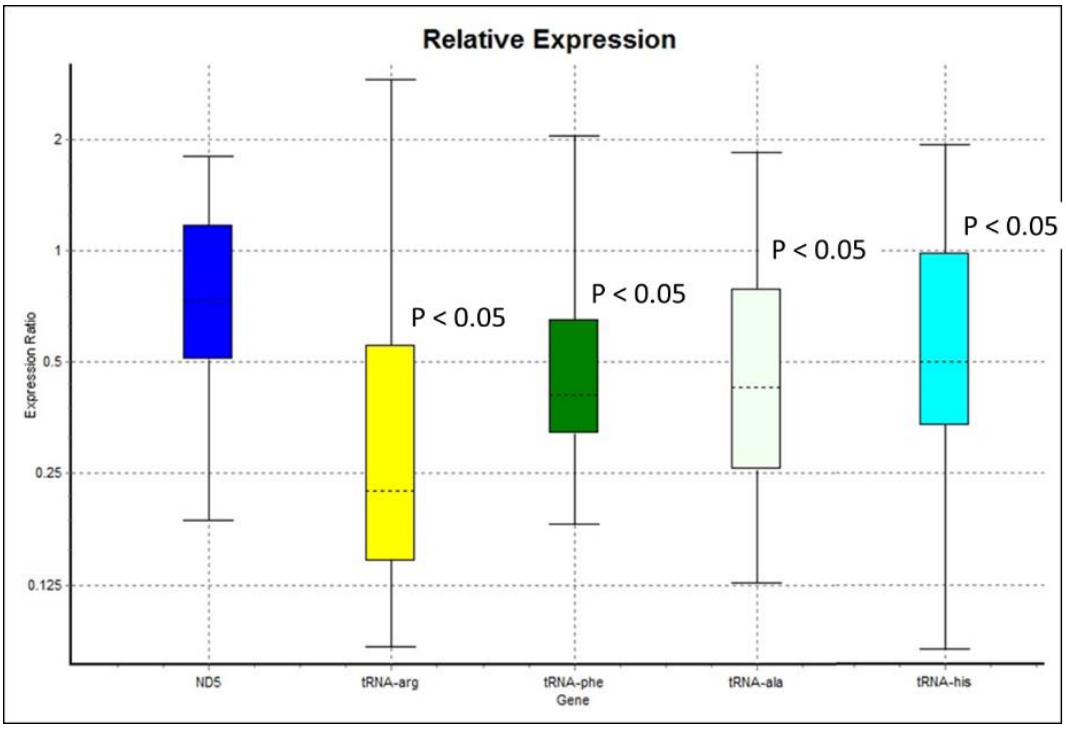

Figure 4.2.1: Whisker-Box plot of qRT-PCR analysis of independent samples showing mitochondrial tRNA expression levels being reduced in DDS/+ foetal kidneys compared with wild type. ND5 is a mitochondrially encoded gene, suggesting the downregulation is specific for tRNAs. N=3 wild type vs 3 mutants, with technical triplicate each.

Given the striking representation of mitochondrially encoded tRNAs in the differentially expressed gene lists, qRT-PCR was employed to verify these findings. Of the mitochondrial tRNAs, PCR primers were able to be designed for 4 and the specificity of the PCR reactions confirmed by conventional PCR and gel electrophoresis.

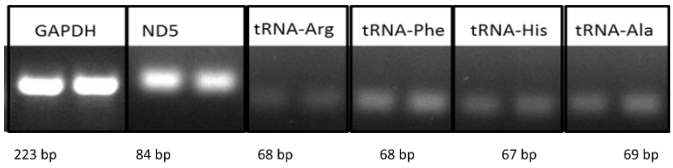

Figure 4.2.2: *Representative gel electrophoresis of qRT-PCR analysis of each primer pairs for mitochondrial genes.*

qRT-PCR confirmed down regulation of all 4 mitochondrial tRNA genes (Figure 4.2.1).

Gene	P-value	Result
ND5	0.079	No change
tRNA-arg	0.001	DOWN
tRNA-phe	0.003	DOWN
tRNA-ala	0.004	DOWN
tRNA-his	0.009	DOWN

Table 4.2.3: *Table: Show the non-normalized data obtained from qRT-PCR analysis of 5 genes in the mitochondria. ND5 sample group is not different to control group. tRNA-arg, tRNA-phe, tRNA-ala and tRNA-his are DOWN-regulated in sample group (in comparison to control group).*

As there was no significant different between the controls and the samples for the gene ND5 (which is a gene that is conserved and almost constant in mitochondria, given no mutation in those gene), ND5 may be used as a reference (housekeeping gene in the mitochondrial genome). To evaluate indirectly mitochondrial copy number (based on ND5 expression) between the two groups, the ND5 was analysed in reference to the nuclear housekeeping genes, GAPDH and B-actin.

Gene	P-value	Result
GAPDH		
B-actin		
ND5	0.088	No change

Table 4.2.4: *ND5 sample group is not different to control group.*

As there are no significant different of expression of ND5 gene seen between the two groups, this may reflect that there was no significant change with regard to mitochondrial copy number. We then chose to use ND5 can act as the reference for the expression of the other mitochondrial genes of interest.

Given the small, circular nature of the mitochondrial genome and the extremely high copy number of the mitochondrial genome compared with the nuclear genome, we conducted a further control to ensure that the mitochondrial tRNA signals were derived from RNA and not contaminating mitochondrial DNA. As tRNAs have no introns, we carried out qRT-PCR on cDNA and compared this with qRT-PCR carried out on an equivalent amount of RNA without reverse transcription (cDNA). This confirmed that the signals detected by the microarray and our qRT-PCR were derived from RNA (Figure 4.2.5).

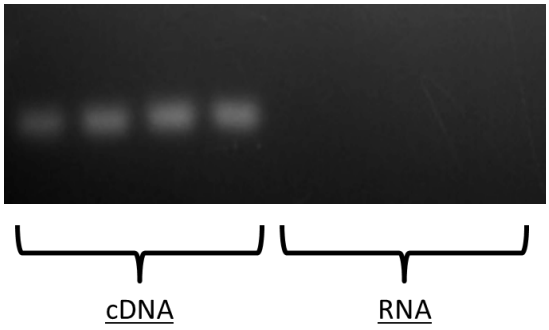

Figure 4.2.5: *Gel electrophoresis of qRT-PCR products from cDNA (lanes 1-4) and from equivalent amounts of pure RNA stock, without reverse transcription (lanes 5-8). This indicates that the tRNA signals do not arise as a result of mitochondrial DNA contamination of the original RNA preparation.*

The most statistically significant fold changes are seen in member of the tRNAs that are involved in mitochondrial functions. In human, mitochondrial mRNAs are translated by the mitochondrial protein synthesis mechanism that utilize the 22 species of mitochondrial tRNAs (mt tRNAs) encoded by mtDNA (Taanman, 1999). The structural features of mt tRNAs is unique in comparison to cytoplasmic tRNAs bearing the canonical cloverleaf structure. mt tRNAs genes are prone to point mutations and are linked with a wide range of pathologies related to mitochondrial disease. Various nuclear factors implicated in the biogenesis and function of mt tRNAs have been recognized. These include tRNA-modifying enzymes and processing endonucleases indicating the nuclear-mitochondrial interaction and the importance of mt tRNAs for mitochondrial activity (Suzuki et al. 2011). Given that mt tRNA genes change in the microarrays suggest it is possible that WT1 has some regulatory influence on those genes in particular that may play a role during kidney development and contribute to the reduced nephron number endowment that subsequently predisposes to a higher risk of renal disease.

4.3 Nuclear genes with the largest fold-change were also confirmed in independent *Wt1*^{tmT396}/+ mutant kidneys. qRT-PCR for 4 out of the top 5 nuclear genes ranked by fold-change are shown below – confirming reduced expression of Aadac (red), CD55 (blue) and Rnase12 (white), and increased expression of Nxph1 (green).

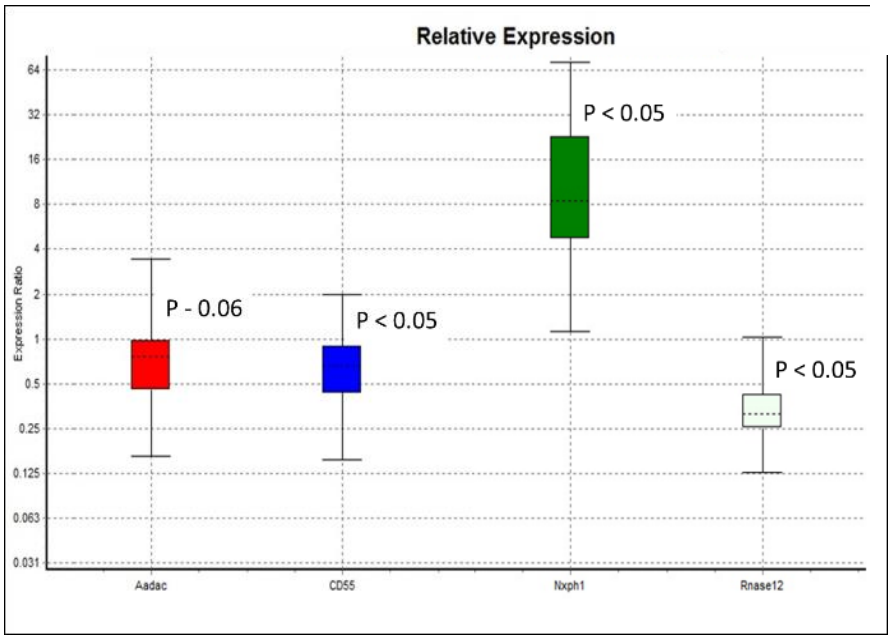

Figure 4.3.1: Whisker-Box plot of qRT-PCR showing nuclear genes expression level. N=3 wild type vs 3 mutants, with technical triplicate each.

It is of interest that amongst the most differentially expressed genes, the four nuclear genes that showed significant differences have not previously been linked with Wt1 in any way. AADAC gene is arylacetamide deacetylase that goes up against the action of cytosolic arylamine N-acetyltransferase, which involve in heterocyclic amine carcinogens pathways. It also has been proposed to be involved in triglyceride catabolic process and the protein product are localize in various of cells (Nourbakhsh et al. 2013). Rnase12 is ribonuclease RNase A family 12. Not much known of its function in mice. In human, it is annotated as RNA phosphodiester bond hydrolysis, has endonucleolytic endoribonuclease activity, and related to extracellular region nucleic acid binding (Carbon et al. 2009). Nxph1 is Neurexophilin 1, is a highly conserved secreted protein that forms a very tight complex with alpha neurexins, which may resemble neuropeptides signalling molecules (Kinzfogl et al. 2011).

4.4 Selected genes within the top 150 ranked by fold change were verified by qRT-PCR.

Gene	P value	Result
HPRT		
NES	0.03	DOWN
GAPDH		
EFEMP1	0	DOWN
ANKFN1	0	DOWN
SULF1	0	DOWN

Table 4.4.1: qRT-PCR of selected genes in the microarray list for verification. Sulf1 – rank #16, Ankfn1 – rank #32, Nes – rank #113, Efemp1 – rank #132 could all be verified. N=3 wild type vs 3 mutants, with technical triplicate each.

The total number of significant differentially expressed genes with $p<0.05$ is 1137. Although the largest difference was seen in mitochondrial tRNA genes, we tested a selection of genes down the list randomly to verify the overall accuracy of the microarray analysis. Even the gene ranked #132 has been shown to be changed by qRT-PCR analysis of gene expression in independent samples. Thus, the microarray data appears robust and appropriate for further, detailed analysis.

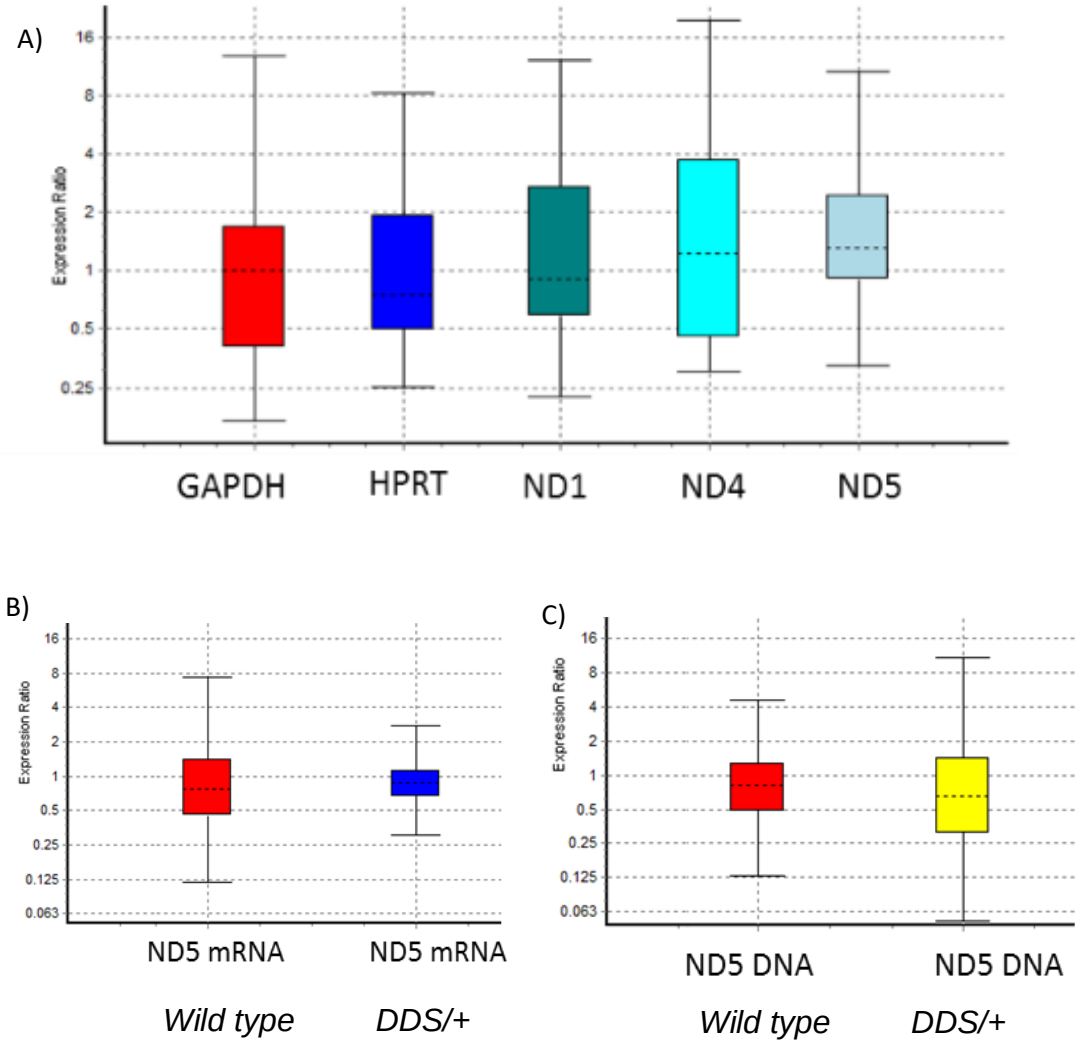

Figure 4.4.2: A) A selection of reference genes used in qRT-PCR, GAPDH and HPRT for nuclear genes and ND1, ND4 and ND5 for mitochondrial reference genes comparing between wild type kidney and DDS/+ e17.5 kidneys, show no different of expressions. B) ND5 expression level between wild type and DDS/+ e17.5 kidneys. C) ND5 gene copy number reading between wild type and DDS/+ e17.5 kidneys. All show no significant different, (p>0.05). N=3 wild type vs 3 mutants, with technical triplicate each.

4.5 Ingenuity Pathway Analysis (IPA)

Given the robust nature of the microarray data, assembly of genes networks and Ingenuity pathway analysis (IPA) was conducted on the differentially expressed gene list. Their corresponding diagrams of the calculated networks connections are shown in Figure 4.5.1. IPA can generate a network of interactors based on the recognized relations among target genes. It will not just show discovered pathways, but also give ideas towards new experiments through the utilization of the established network.

Multiple WT1 signalling pathway target genes were suggested in the overlay of connectivity networks. There were multiple genes dysregulated in the heterozygous (DDS/+) kidneys. Overlaying our WT1 regulated signalling pathways on to the connectivity networks of differentially expressed genes demonstrated that directional changes in gene expression patterns (up or down) in multiple networks of adjacent gene nodes (Figure 4.5.1) could be a result of WT1 signalling.

To show how WT1 affected the gene network, we over-laid gene expression in the IPA network system (Figure 4.5.1). Various shapes of gene nodes are displayed representing the class of the gene product. Two main colours are shown in our original gene list, green represent down regulation of gene expression and red signifies up regulation of gene in which the colour intensity shows their significance in the network. The interactions shown in Figure 4.5.1 also consist of other colours that represent inconsistency and unpredicted from the IPA knowledgebase. This might give more insight towards WT1 up and downstream genes and it proposed potential interactions.

Utilising the Ingenuity Pathway Analysis software to analyse our gene list, we identified multiple molecular networks of genes differentially expressed in relation to our microarray of e17.5 kidneys. These inter-connections between genes are developed from literature that was assimilated into the system, describing the physical or functional interactions of the molecules. The gene networks with the most significant are shown in Figure 4.5.1, depending on their cellular functions and imputed interaction of the molecules.

Functional analysis using the Ingenuity Pathway Analysis system were also performed together. These data demonstrated functional clustering of differentially

expressed genes within known canonical pathways, and highlighted tRNA splicing and renal related responses as mechanisms for disease (Figures 4, 5).

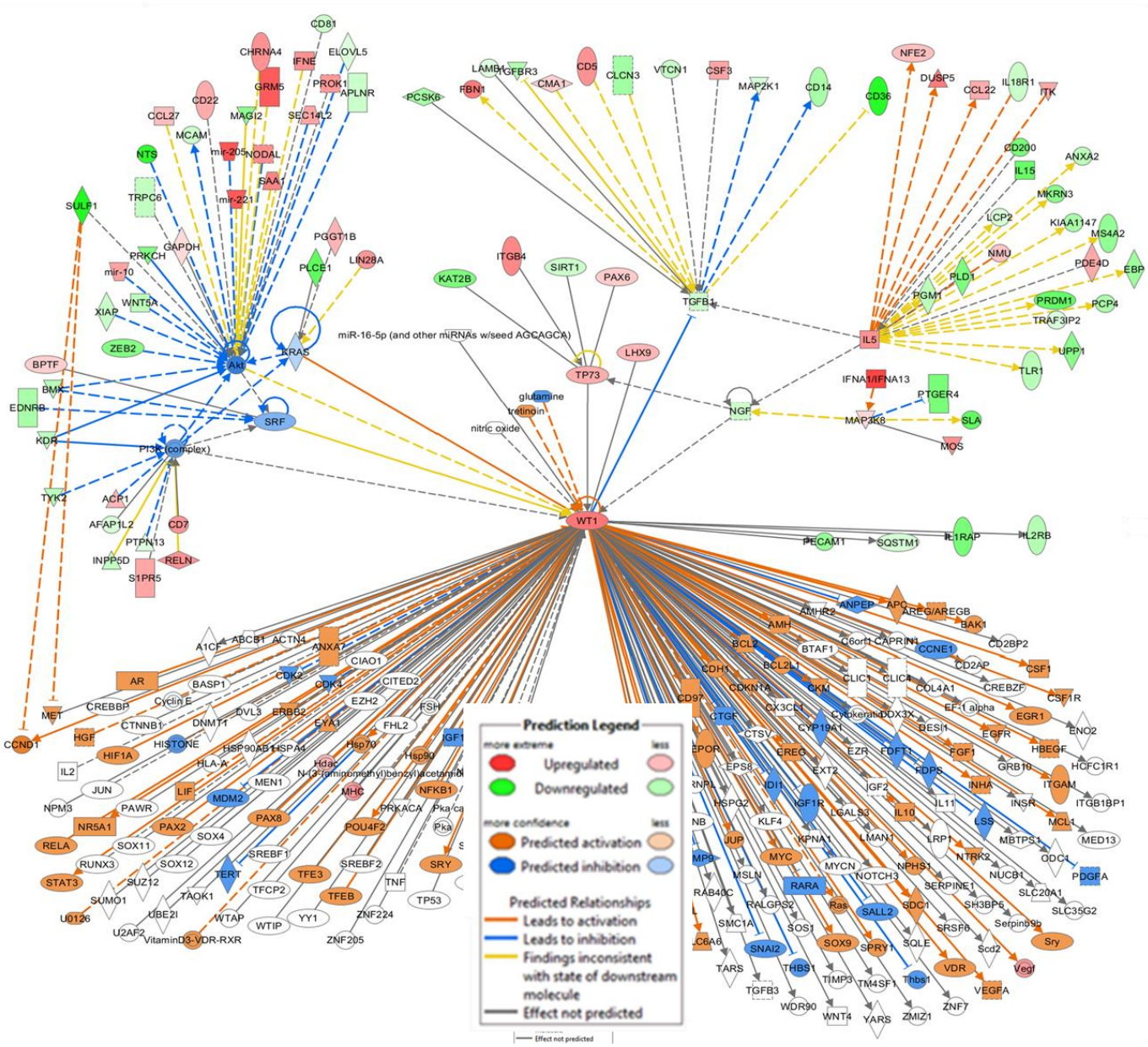

Figure 4.5.1: Ingenuity Pathway Analysis showing networks of interacting molecules, overlapping our array data and IPA databases of genes from publication. The upper half of the picture (molecules/genes in shades of green or red) are genes from our microarray data, meanwhile the lower half (molecule/genes with white or brown) are from IPA databases, and unchanged in our data.

The IPA in figure 4.5.2 were the genes from array with p value < 0.05 were put into IPA analysis. There are 1137 genes to be included for network generation with log fold changes ranging from -2.2 log fold change (lfc) down-regulation to 0.8 lfc up-regulation. IPA suggested that our gene list is associated with the canonical pathways listed in Figure 4.5.2-A. The tox list in Figure 4.5.2-B, is an analysis that convey a focused toxicity and safety assessment of targeted compounds uncovering the biological mechanisms that are associated to toxicity on particular molecules. Interestingly this analysis show mutation in WT1 gene has negative impact of renal glomerulus. When the genes with p value < 0.005 that constitute of 51 genes included for network generation with log fold changes ranging from -2.2 log fold change (lfc) down-regulation to 0.4 lfc up-regulations. Among the top canonical pathways, the most intriguing are genes are related to tRNA splicing, in which we seen at the top of our microarray gene list.

A **Top Canonical Pathways**

Name	p-value	Ratio
Hematopoiesis from Multipotent Stem Cells	1E-02	3/12 (0.25)
Glycogen Biosynthesis II (from UDP-D-Glucose)	1.68E-02	2/12 (0.167)
Role of Cytokines in Mediating Communication between Immune Cells	1.79E-02	5/55 (0.091)
Thioredoxin Pathway	2.46E-02	2/8 (0.25)
Tryptophan Degradation to 2-amino-3-carboxymuconate Semialdehyde	2.46E-02	2/18 (0.111)

B **Top Tox Lists**

Name	p-value	Ratio
Renal Glomerulus Panel (Human)	5.75E-04	5/17 (0.294)
Increases Cardiac Dysfunction	1.42E-02	5/35 (0.143)
Renal Ischemic Resistance Panel (Rat)	6.58E-02	2/10 (0.2)
Increases Cardiac Proliferation	7.84E-02	4/41 (0.098)
Hepatic Stellate Cell Activation	1.67E-01	3/35 (0.086)

C **Nephrotoxicity**

Name	p-value	# Molecules
Renal Inflammation	5.35E-03 - 4.35E-01	6
Renal Nephritis	5.35E-03 - 4.35E-01	6
Glomerular Injury	3.96E-02 - 2.27E-01	6
Kidney Failure	4.29E-02 - 5.69E-01	9
Nephrosis	4.29E-02 - 4.35E-01	4

D **Top Molecules**

Log Ratio up-regulated

Molecules	Exp. Value
KIR3DL2	↑0.594
CLEC4E	↑0.512
NR2E1	↑0.483
Svs3a/Svs3b	↑0.481
SPTB	↑0.466
IFNA1/IFNA13	↑0.465
HORMAD1	↑0.459
CES3	↑0.458
Ifi204 (includes others)	↑0.455
Olfr1131	↑0.453

Log Ratio down-regulated

Molecules	Exp. Value
Cd55/Daf2	↓-0.915
AADAC	↓-0.753
SULF1	↓-0.737
DAPL1	↓-0.708
CD36	↓-0.702
NTS	↓-0.683
SLC26A7	↓-0.669
STEAP1	↓-0.597
GNG11	↓-0.590
GAS5	↓-0.588

E **Top Upstream Regulators**

Upstream Regulator	p-value of overlap
PARK2	2.45E-04
BCL2	4.64E-04
REST	6.65E-04
NGF	8.26E-04
leteprinim	1.65E-03

Figure 4.5.2: Table show IPA analysis of genes list from our microarray with p < 0.05 values.

These results suggest that WT1 may play a noteworthy coordinated regulation in the pathways. Further evaluation of these genes is necessary to clarify their role in kidney nephron endowment.

Focussing on differentially expressed genes with a stringent p-value <0.05, IPA revealed some significant pathways linked to renal glomerulus panel (Figure 4.5.2). Figure 4.5.2-D confirms the previous findings of the microarray analysis (note CD55, Aadac and Sulf1 amongst the top downregulated genes) and indicates that the settings applied to the IPA suite are appropriate and that the outcomes are likely to be biologically relevant.

4.6 Comparative Database Analysis

As described before, multiple differentially expressed genes and molecular pathways were identified that differ between DDS/+ and wild type mice using whole kidney microarray expression profiling analysis of e17.5 kidneys. Some have been described and associated with IPA, revealing functional clustering of these genes. The microarray data was shown to be of high quality and shown to be robust.

However, despite the identification of known Wt1 target genes, such as Sulf1, and IPA clusters consistent with Wt1 mutation and a target of such functions, such as hematopoietic stem cell differentiation, the data did not highlight known genes critical to normal nephrogenesis. For example, the following genes are not differentially expressed: Wnt4, Wnt11, Six2, Cited1, Gdnf, Pax2, Pax8, and c-Ret.

The array provided a global view of gene expression within a developing kidney. This has given me some insights into genes regulated by WT1 in nephron development. To get a deeper understanding of these genes listed in the microarray, I have compartmentalized the list of genes from the expression microarray. I compared E17.5 differentially expressed gene list ($p<0.05$) to few other arrays from isolated glomerulus, podocytes and isolated cells from kidneys from public databases. This comparison provided me with genes list that suggested being glomerular specific WT1 regulated genes (Figure 4.6.1).

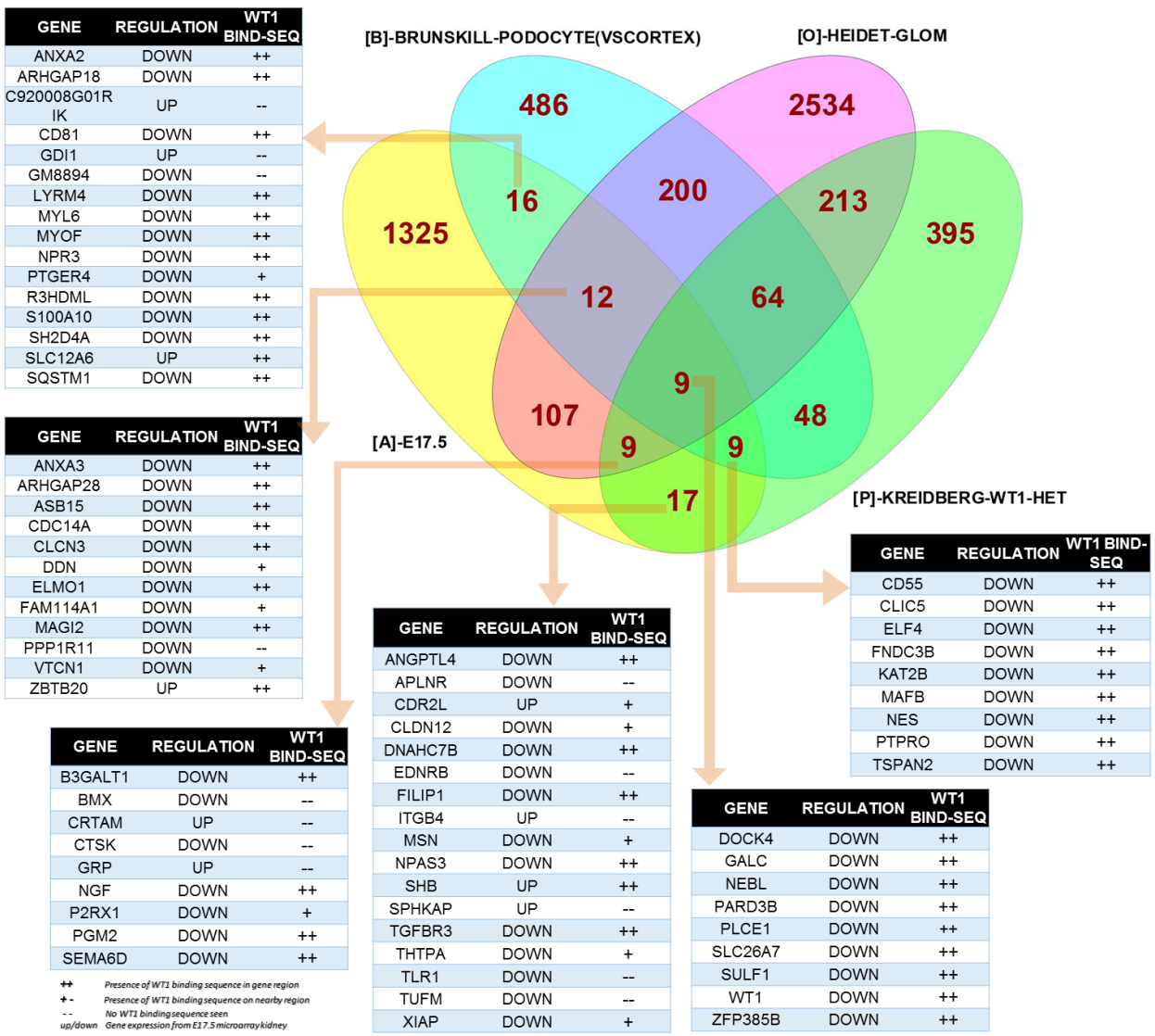

GENE	REGULATION	WT1 BIND-SEQ
ANXA2	DOWN	++
ARHGAP18	DOWN	++
C920008G01RIK	UP	--
CD81	DOWN	++
GDI1	UP	--
GM8894	DOWN	--
LYRM4	DOWN	++
MYL6	DOWN	++
MYOF	DOWN	++
NPR3	DOWN	++
PTGER4	DOWN	+
R3HDML	DOWN	++
S100A10	DOWN	++
SH2D4A	DOWN	++
SLC12A6	UP	++
SQSTM1	DOWN	++

GENE	REGULATION	WT1 BIND-SEQ
ANXA3	DOWN	++
ARHGAP28	DOWN	++
ASB15	DOWN	++
CDC14A	DOWN	++
CLCN3	DOWN	++
DDN	DOWN	+
ELMO1	DOWN	++
FAM114A1	DOWN	+
MAGI2	DOWN	++
PPP1R11	DOWN	--
VTCN1	DOWN	+
ZBTB20	UP	++

GENE	REGULATION	WT1 BIND-SEQ
B3GALT1	DOWN	++
BMX	DOWN	--
CRTAM	UP	--
CTSK	DOWN	--
GRP	UP	--
NGF	DOWN	++
P2RX1	DOWN	+
PGM2	DOWN	++
SEMA6D	DOWN	++

GENE	REGULATION	WT1 BIND-SEQ
ANGPTL4	DOWN	++
APLNR	DOWN	--
CDR2L	UP	+
CLDN12	DOWN	+
DNAHC7B	DOWN	++
EDNRB	DOWN	--
FILIP1	DOWN	++
ITGB4	UP	--
MSN	DOWN	+
NPAS3	DOWN	++
SHB	UP	++
SPHKAP	UP	--
TGFBR3	DOWN	++
THTPA	DOWN	+
TLR1	DOWN	--
TUFM	DOWN	--
XIAP	DOWN	+

GENE	REGULATION	WT1 BIND-SEQ
CD55	DOWN	++
CLIC5	DOWN	++
ELF4	DOWN	++
FNDC3B	DOWN	++
KAT2B	DOWN	++
MAFB	DOWN	++
NES	DOWN	++
PTPRO	DOWN	++
TSPAN2	DOWN	++

GENE	REGULATION	WT1 BIND-SEQ
DOCK4	DOWN	++
GALC	DOWN	++
NEBL	DOWN	++
PARD3B	DOWN	++
PLCE1	DOWN	++
SLC26A7	DOWN	++
SULF1	DOWN	++
WT1	DOWN	++
ZFP385B	DOWN	++

Figure 4.6.1: A Venn diagram showing overlap of comparison database of 3 microarrays ($p<0.05$). [A] is E17.5 whole kidney microarray, [O] is DDS/+ heterozygous adult isolated podocyte glomerulus kidney microarray from Ratelade et al., 2010, and [P] is WT1 heterozygous mutant adult isolated glomerulus kidney microarray from Schumacher et al., 2011, and [B] genes in Brunskill et al., 2011 listing genes involve in patterning and development of podocytes to become part of nephron. Adjacent tables showing the respective overlap list of differentially expressed genes in mutant mice together with regulation status and listed indication for presence of WT1 transcriptional binding. These datasets reveal several within my array that suggested specific to glomerulus

I then compare the 1136 hits (comparison in Venn diagram differ in number due to the redundant names for some genes) from my array to a dataset from Kann et al., 2015. This dataset was derived from ChIP-seq of WT1 bound genes in podocytes of adult kidneys. They validated the WT1 binding domains to two other ChIP-seq of WT1 targets sequence derived from embryonic kidneys (Hartwig et al., 2010, Motamedi et al., 2014). Their data show specific role of WT1 in regulating transcriptome through the target genes promoter and enhancers region. The domain of WT1 targets were found in promoter region of target genes (21%), 5' UTRs region (7%), genic sites; Intron, Exons, 3' UTRs (29%) and mostly in intergenic sites (43%). This highlighted the role of WT1 in regulating genes at non-promoter sites.

There are 216 genes from my array list that contains WT1 binding domain. These genes are involved in various parts of the kidney, including apoptosis and mitochondrial related genes.

[A]

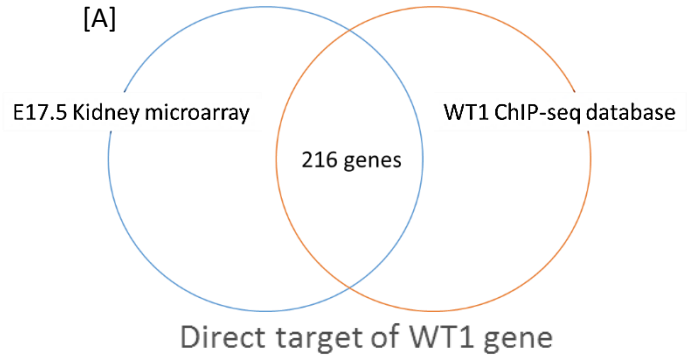

Direct target of WT1 gene

[B]

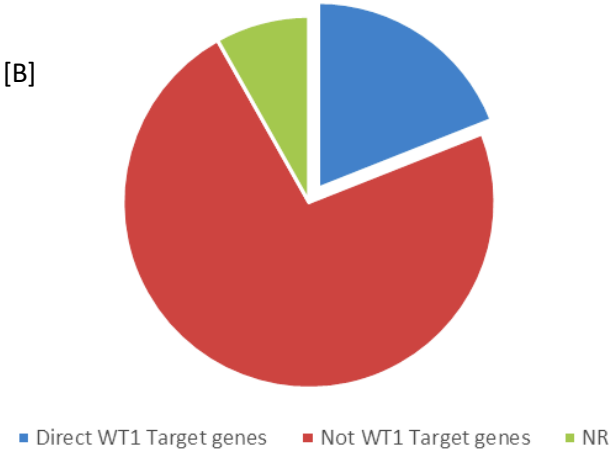

[C]

216	*WT1 Target domain*
828	*Not WT1 Target domain*
93	*NR (No record)*

Figure 4.6.2: Comparison of WT1 ChIPseq datasets in embryonic kidneys and podocytes (Kann et al., 2015) to my array list of significant genes. A) Venn diagrams showing overlap of the two datasets. Within a single diagram, circles are drawn disproportionally. B and C) the fraction and number of genes contain WT1 binding domains and tables of their respective numbers. Appendix Table A-4.6.2 show the list of 216 gene having WT1 target domain.

The referred dataset was taken from Brunskill et al 2014. They describe experiment conducted on precursor cells of nephron (metanephric mesenchyme, and to some extend cap mesenchyme) from age e11.5 to e15.5 delineating comparison of groups of individual precursor cells that were expressing (induced) genes that known to develop more differentiated cells. These include cells that will differentiate into renal vesicles, renal epithelial cells, stroma and podocytes. Induced are cells that express genes like Six2, Foxd1, or/and Cited1. Uninduced are the cells of similar origin without the expression of those genes (Figure 4.6.3).

The dataset from Brunskill et al 2014 gave sets of genes list that were differently expressed that was hypothesized to be the genes that responsible for the differentiation of precursor cells into specific type of cells within the nephron structures, defining the changing pattern of gene expression propelling nephrogenesis. As such, we found several tissues specific WT1 regulated genes from my array involved in this mechanism (Figure 4.6.4)

Comparing with dataset from Brunskill et al 2014, there are several genes listed from my array that involved in the metanephric mesenchyme differentiation into renal epithelial cell/ nephron, genes involved in differentiation of cap mesenchyme into renal vesicles, genes involve in differentiation into stroma and genes involved in proximal tubule formation.

The list of genes in overlapping area are those of glomerular specific. When compared to metanephric mesenchyme induced cells, Pgm2 gene is listed. Sulf1 was listed from cap mesenchyme induced cells genes list. Sulf1 contain WT1 target sequence is a well-known WT1 target and nephron related genes.

Given that I am able to compartmentalize some of the differentially expressed genes from my array into more specific part of kidneys, and 19% of the listed genes (of $p < 0.05$) in my array have WT1 target sequence, it is undoubtedly containing genes responsible to parts of renal development. Isolating the genes involved in nephron number endowment would not be easy. It will take time to get more structured connection of the genes toward better understanding of nephron number genes.

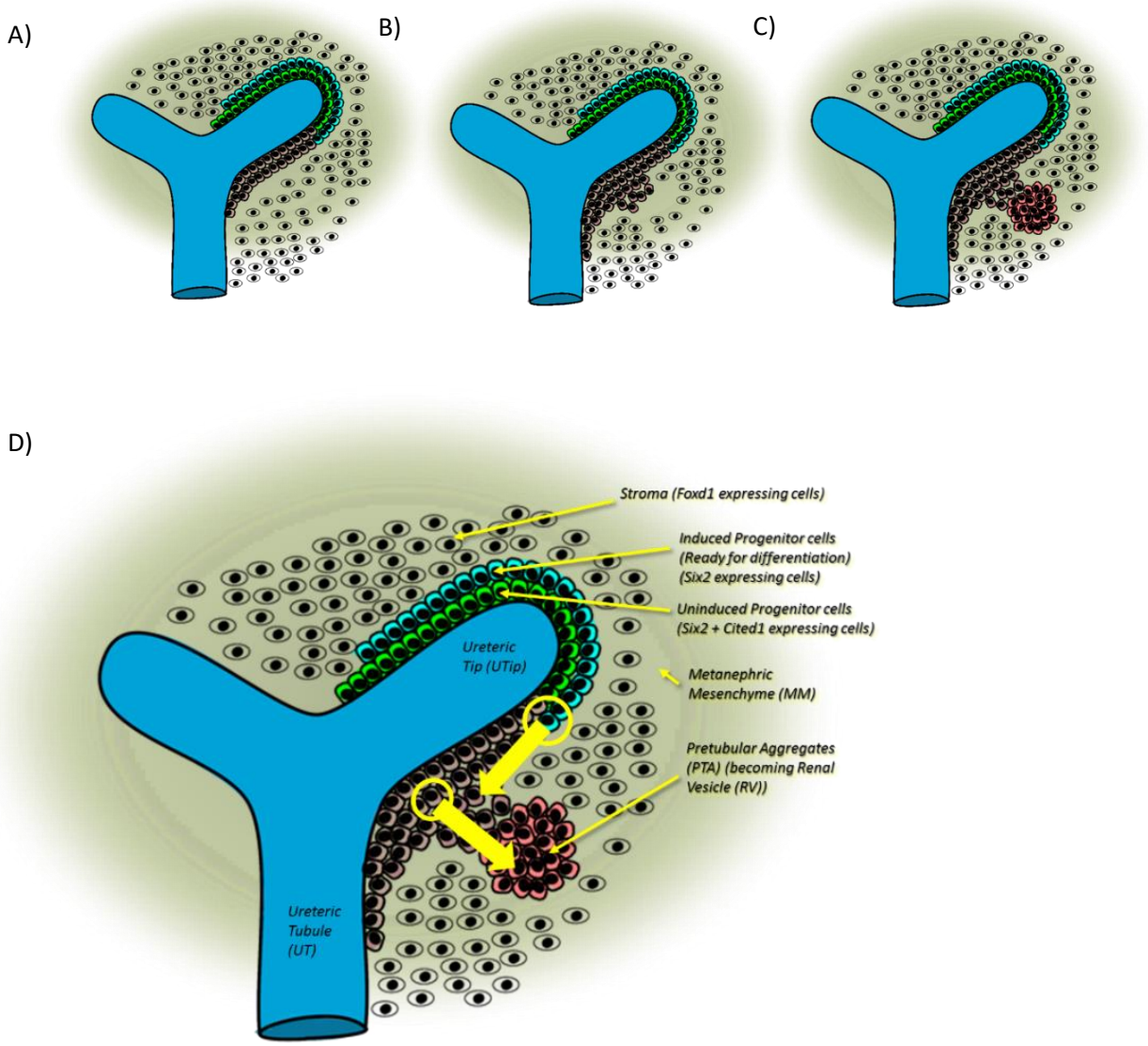

Figure 4.6.3: A model representation of nephrogenic area of developing kidney. A) to C) are diagrammatic representation of cellular development nearby nephron niche. D) depicting the cellular components of the tubule and the nephron niche with main gene expression that differentiate the cells, Stroma/Interstitium (Foxd1), stem cell progenitor (uninduced progenitor cells, expressing both Six2 and Cited1), induced progenitor cells (Six2 expressing cells) that will proliferate and differentiates to be a component of pretubular aggregates (PTA) later becomes the nephron.

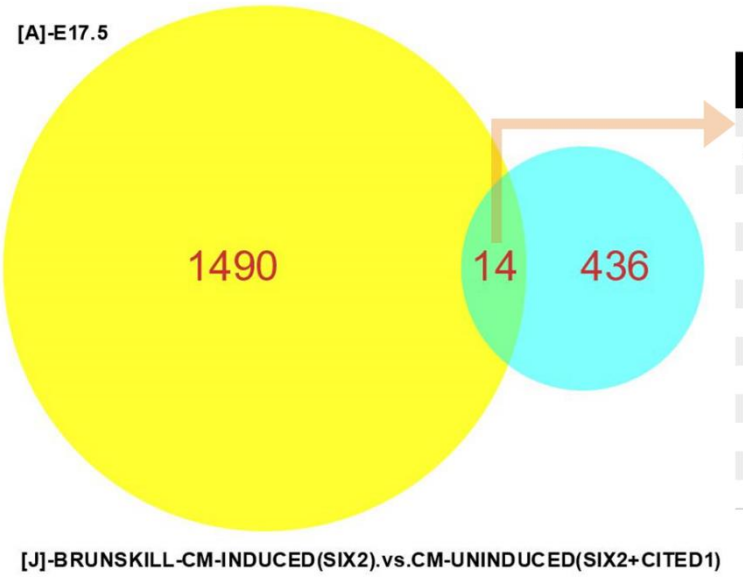

GENE	REGULATION	WT1 BIND-SEQ
1810031K17RIK	DOWN	+
2610204G22RIK	UP	--
ADAM11	UP	++
ANGPTL4	DOWN	++
AP1S1	DOWN	++
CCL27A	UP	--
CREB3	DOWN	++
CRYM	UP	--
KAT2B	DOWN	++
LLPH	DOWN	--
PTPN13	DOWN	++
SULF1	DOWN	++
TGFBR3	DOWN	++
WNT5A	DOWN	--

++ Presence of WT1 binding sequence in gene region
+ - Presence of WT1 binding sequence on nearby region
- - No WT1 binding sequence seen
up/down Gene expression from E17.5 microarray kidney

Figure 4.6.4: Comparison database Venn diagrams showing overlap of the two datasets of different constituents. [A] Represent overlaps of genes listed E17.5 array (listing gene names are redundant for alternative gene names, p<0.05) and [J] Represent overlaps of genes listed in Brunskill et al 2014 from differential expression of genes in cap mesenchyme (Six2 versus Six2+Cited1 cells, giving the genes involve in CM induction to become nephron, p,0.05). Overlapping are listing 14 genes that are identical in both, giving a list of genes from E17.5 array that are involve in CM induction and differentially expressed in mutant mice (table) with listed indication if those genes contain sequences for WT1 transcriptional binding.

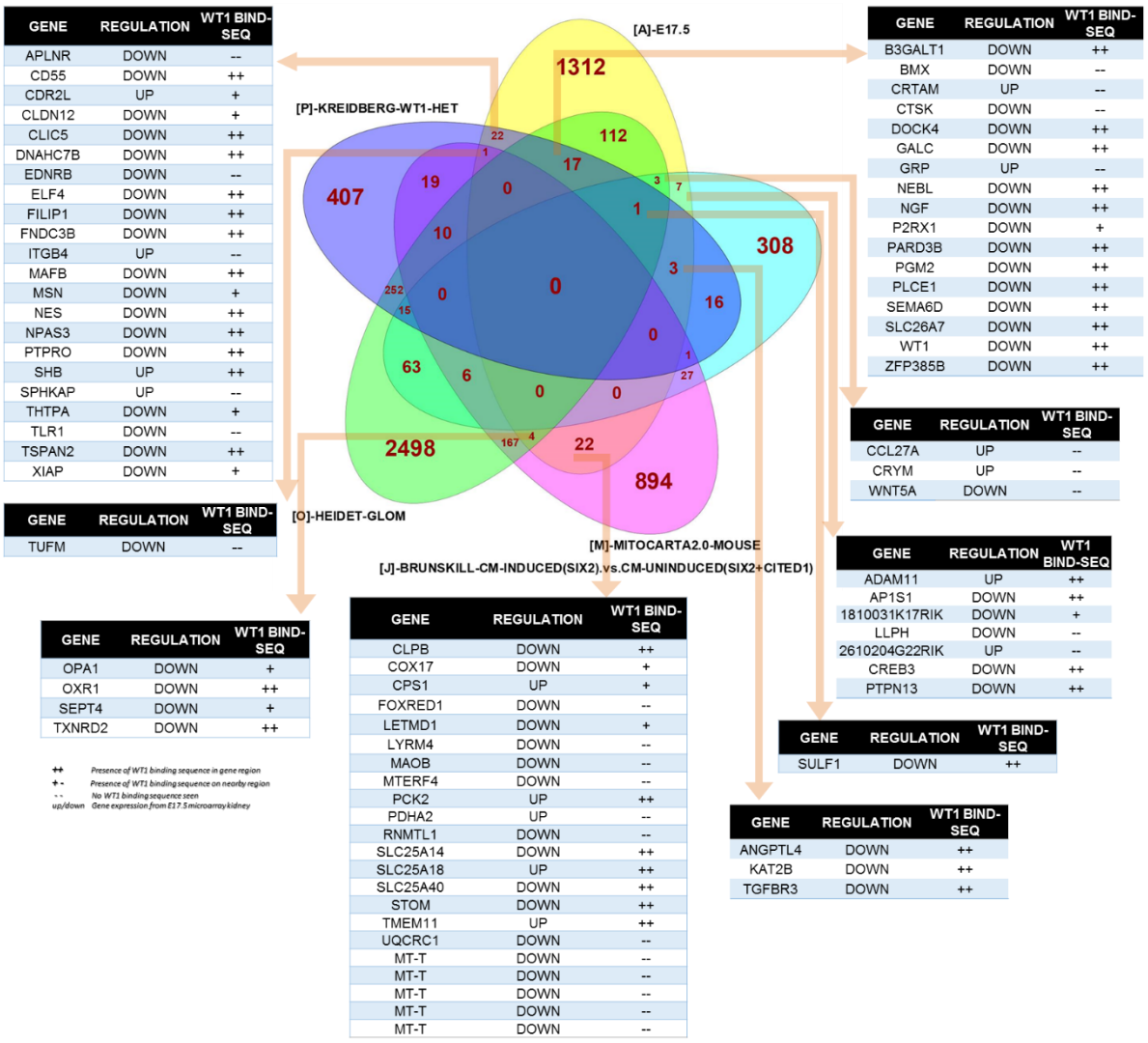

GENE	REGULATION	WT1 BIND-SEQ
APLNR	DOWN	--
CD55	DOWN	++
CDR2L	UP	+
CLDN12	DOWN	+
CLIC5	DOWN	++
DNAHC7B	DOWN	++
EDNRB	DOWN	--
ELF4	DOWN	++
FILIP1	DOWN	++
FNDC3B	DOWN	++
ITGB4	UP	--
MAFB	DOWN	++
MSN	DOWN	+
NES	DOWN	++
NPAS3	DOWN	++
PTPRO	DOWN	++
SHB	UP	++
SPHKAP	UP	--
THTPA	DOWN	+
TLR1	DOWN	--
TSPAN2	DOWN	++
XIAP	DOWN	+

GENE	REGULATION	WT1 BIND-SEQ
B3GALT1	DOWN	++
BMX	DOWN	--
CRTAM	UP	--
CTSK	DOWN	--
DOCK4	DOWN	++
GALC	DOWN	++
GRP	UP	--
NEBL	DOWN	++
NGF	DOWN	++
P2RX1	DOWN	+
PARD3B	DOWN	++
PGM2	DOWN	++
PLCE1	DOWN	++
SEMA6D	DOWN	++
SLC26A7	DOWN	++
WT1	DOWN	++
ZFP385B	DOWN	++

GENE	REGULATION	WT1 BIND-SEQ
CCL27A	UP	--
CRYM	UP	--
WNT5A	DOWN	--

GENE	REGULATION	WT1 BIND-SEQ
TUFM	DOWN	--

GENE	REGULATION	WT1 BIND-SEQ
ADAM11	UP	++
AP1S1	DOWN	++
1810031K17RIK	DOWN	+
LLPH	DOWN	--
2610204G22RIK	UP	--
CREB3	DOWN	++
PTPN13	DOWN	++

GENE	REGULATION	WT1 BIND-SEQ
OPA1	DOWN	+
OXR1	DOWN	++
SEPT4	DOWN	+
TXNRD2	DOWN	++

GENE	REGULATION	WT1 BIND-SEQ
CLPB	DOWN	++
COX17	DOWN	+
CPS1	UP	+
FOXRED1	DOWN	--
LETMD1	DOWN	+
LYRM4	DOWN	--
MAOB	DOWN	--
MTERF4	DOWN	--
PCK2	UP	++
PDHA2	UP	--
RNMTL1	DOWN	--
SLC25A14	DOWN	++
SLC25A18	UP	++
SLC25A40	DOWN	++
STOM	DOWN	++
TMEM11	UP	++
UQCRC1	DOWN	--
MT-T	DOWN	--
MT-T	DOWN	--
MT-T	DOWN	--
MT-T	DOWN	--
MT-T	DOWN	--

GENE	REGULATION	WT1 BIND-SEQ
SULF1	DOWN	++

GENE	REGULATION	WT1 BIND-SEQ
ANGPTL4	DOWN	++
KAT2B	DOWN	++
TGFBR3	DOWN	++

Figure 4.6.5: A Venn diagram showing overlap of comparison database of 3 microarrays (p<0.05). [A] is E17.5 whole kidney microarray, [O] is DDS/+ heterozygous adult isolated podocyte glomerulus kidney microarray from Ratelade et al., 2010, and [P] is WT1 heterozygous mutant adult isolated glomerulus kidney microarray from Schumacher et al., 2011, [M] (pink) MitoCarta2.0 that listing genes that directly related to the mitochondrial and [J] (light blue) genes listed in Brunskill et al 2014 listing genes involve in CM induction to become nephron. Adjacent tables showing the respective overlap list of differentially expressed genes in mutant mice together with regulation status and listed indication for presence of WT1 transcriptional binding.

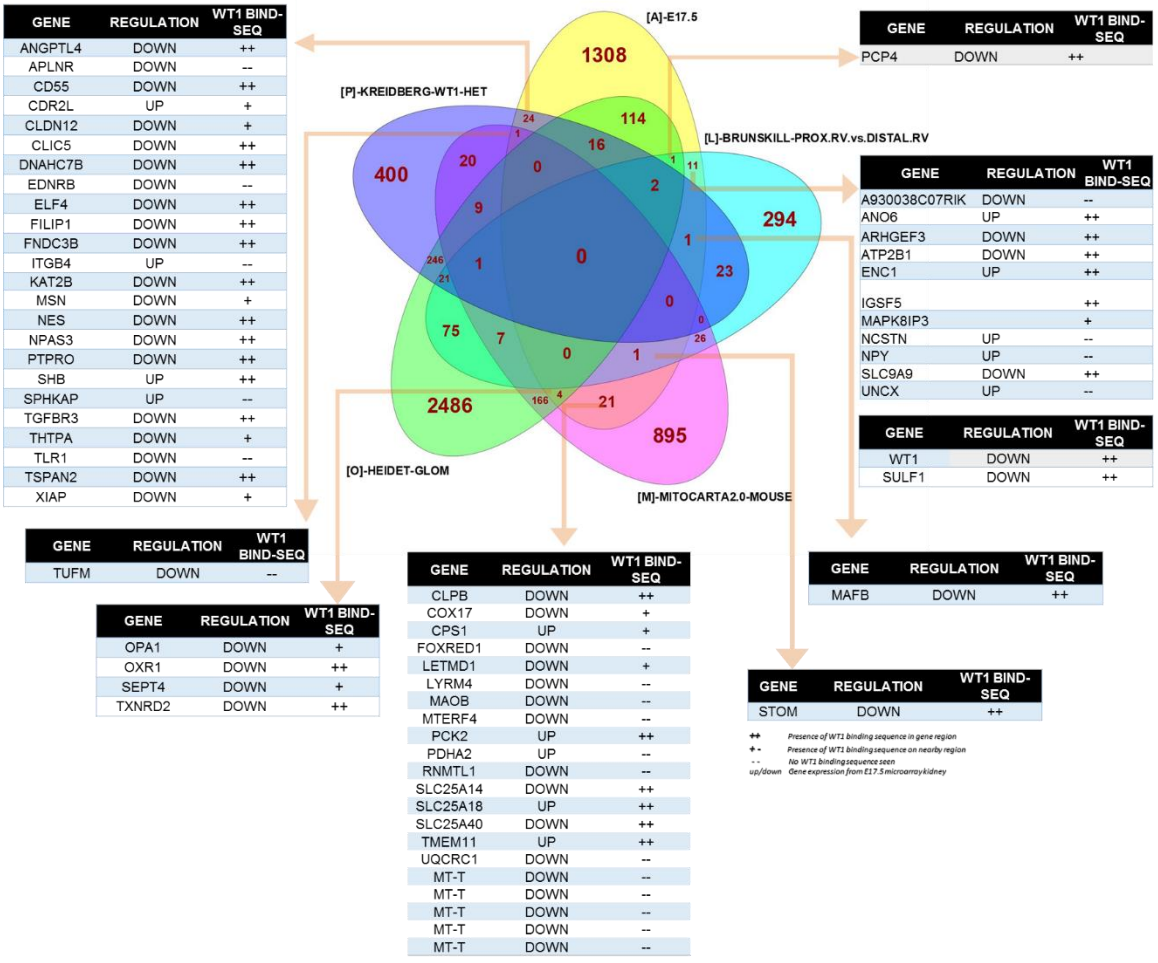

GENE	REGULATION	WT1 BIND-SEQ
ANGPTL4	DOWN	++
APLNR	DOWN	--
CD55	DOWN	++
CDR2L	UP	+
CLDN12	DOWN	+
CLIC5	DOWN	++
DNAHC7B	DOWN	++
EDNRB	DOWN	--
ELF4	DOWN	++
FILIP1	DOWN	++
FNDC3B	DOWN	++
ITGB4	UP	--
KAT2B	DOWN	++
MSN	DOWN	+
NES	DOWN	++
NPAS3	DOWN	++
PTPRO	DOWN	++
SHB	UP	++
SPHKAP	UP	--
TGFBR3	DOWN	++
THTPA	DOWN	+
TLR1	DOWN	--
TSPAN2	DOWN	++
XIAP	DOWN	+

GENE	REGULATION	WT1 BIND-SEQ
PCP4	DOWN	++

GENE	REGULATION	WT1 BIND-SEQ
A930038C07RIK	DOWN	--
ANO6	UP	++
ARHGEF3	DOWN	++
ATP2B1	DOWN	++
ENC1	UP	++
IGSF5		++
MAPK8IP3		+
NCSTN	UP	--
NPY	UP	--
SLC9A9	DOWN	++
UNCX	UP	--

GENE	REGULATION	WT1 BIND-SEQ
WT1	DOWN	++
SULF1	DOWN	++

GENE	REGULATION	WT1 BIND-SEQ
TUFM	DOWN	--

GENE	REGULATION	WT1 BIND-SEQ
OPA1	DOWN	+
OXR1	DOWN	++
SEPT4	DOWN	+
TXNRD2	DOWN	++

GENE	REGULATION	WT1 BIND-SEQ
CLPB	DOWN	++
COX17	DOWN	+
CPS1	UP	+
FOXRED1	DOWN	--
LETMD1	DOWN	+
LYRM4	DOWN	--
MAOB	DOWN	--
MTERF4	DOWN	--
PCK2	UP	++
PDHA2	UP	--
RNMTL1	DOWN	--
SLC25A14	DOWN	++
SLC25A18	UP	++
SLC25A40	DOWN	++
TMEM11	UP	++
UQCRC1	DOWN	--
MT-T	DOWN	--
MT-T	DOWN	--
MT-T	DOWN	--
MT-T	DOWN	--
MT-T	DOWN	--

GENE	REGULATION	WT1 BIND-SEQ
MAFB	DOWN	++

GENE	REGULATION	WT1 BIND-SEQ
STOM	DOWN	++

Figure 4.6.6: (Continuation as not enough space to list all) A Venn diagram showing overlap of comparison database of 3 microarrays (p<0.05). [A] is E17.5 whole kidney microarray, [O] is DDS/+ heterozygous adult isolated podocyte glomerulus kidney microarray from Ratelade et al., 2010, and [P] is WT1 heterozygous mutant adult isolated glomerulus kidney microarray from Schumacher et al., 2011, [M] MitoCarta2.0 that listing genes that directly related to the mitochondrial and [L] genes listed in Brunskill et al 2014 listing genes involve in patterning and polarizing renal vesicle development to become nephron. Adjacent tables showing the respective overlap list of differentially expressed genes in mutant mice together with regulation status and listed indication for presence of WT1 transcriptional binding.

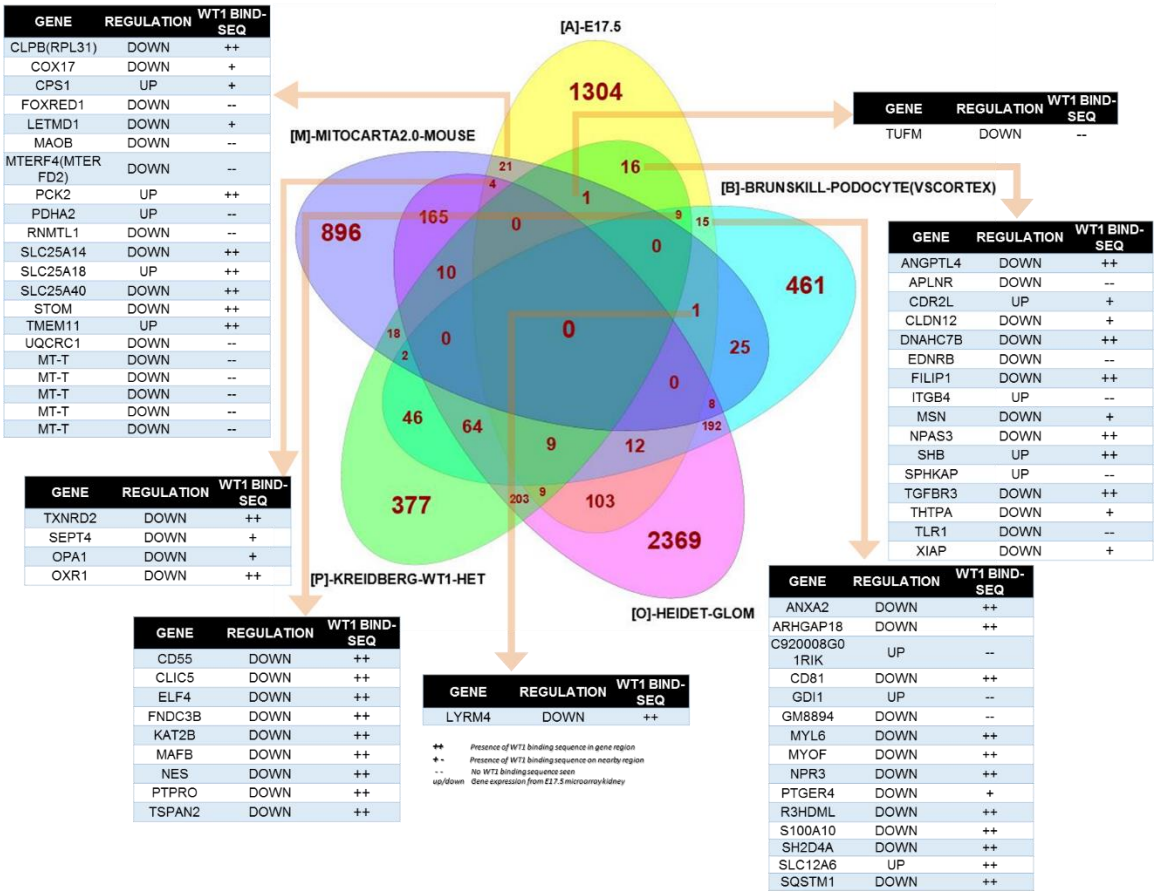

GENE	REGULATION	WT1 BIND-SEQ
CLPB(RPL31)	DOWN	++
COX17	DOWN	+
CPS1	UP	+
FOXRED1	DOWN	--
LETMD1	DOWN	+
MAOB	DOWN	--
MTERF4(MTERFD2)	DOWN	--
PCK2	UP	++
PDHA2	UP	--
RNMTL1	DOWN	--
SLC25A14	DOWN	++
SLC25A18	UP	++
SLC25A40	DOWN	++
STOM	DOWN	++
TMEM11	UP	++
UQCRC1	DOWN	--
MT-T	DOWN	--
MT-T	DOWN	--
MT-T	DOWN	--
MT-T	DOWN	--
MT-T	DOWN	--

GENE	REGULATION	WT1 BIND-SEQ
TUFM	DOWN	--

GENE	REGULATION	WT1 BIND-SEQ
ANGPTL4	DOWN	++
APLNR	DOWN	--
CDR2L	UP	+
CLDN12	DOWN	+
DNAHC7B	DOWN	++
EDNRB	DOWN	--
FILIP1	DOWN	++
ITGB4	UP	--
MSN	DOWN	+
NPAS3	DOWN	++
SHB	UP	++
SPHKAP	UP	--
TGFBR3	DOWN	++
THTPA	DOWN	+
TLR1	DOWN	--
XIAP	DOWN	+

GENE	REGULATION	WT1 BIND-SEQ
TXNRD2	DOWN	++
SEPT4	DOWN	+
OPA1	DOWN	+
OXR1	DOWN	++

GENE	REGULATION	WT1 BIND-SEQ
CD55	DOWN	++
CLIC5	DOWN	++
ELF4	DOWN	++
FNDC3B	DOWN	++
KAT2B	DOWN	++
MAFB	DOWN	++
NES	DOWN	++
PTPRO	DOWN	++
TSPAN2	DOWN	++

GENE	REGULATION	WT1 BIND-SEQ
LYRM4	DOWN	++

GENE	REGULATION	WT1 BIND-SEQ
ANXA2	DOWN	++
ARHGAP18	DOWN	++
C920008G01RIK	UP	--
CD81	DOWN	++
GDI1	UP	--
GM8894	DOWN	--
MYL6	DOWN	++
MYOF	DOWN	++
NPR3	DOWN	++
PTGER4	DOWN	+
R3HDML	DOWN	++
S100A10	DOWN	++
SH2D4A	DOWN	++
SLC12A6	UP	++
SQSTM1	DOWN	++

Figure 4.6.7: (Continuation as not enough space to list all) A Venn diagram showing overlap of comparison database of 3 microarrays (p<0.05). [A] is E17.5 whole kidney microarray, [O] is DDS/+ heterozygous adult isolated podocyte glomerulus kidney microarray from Ratelade et al., 2010, and [P] is WT1 heterozygous mutant adult isolated glomerulus kidney microarray from Schumacher et al., 2011, [M] MitoCarta2.0 that listing genes that directly related to the mitochondrial and [B] genes in Brunskill et al., 2011 listing genes involve in patterning and development of podocytes to become part of nephron. Adjacent tables showing the respective overlap list of differentially expressed genes in mutant mice together with regulation status and listed indication for presence of WT1 transcriptional binding.

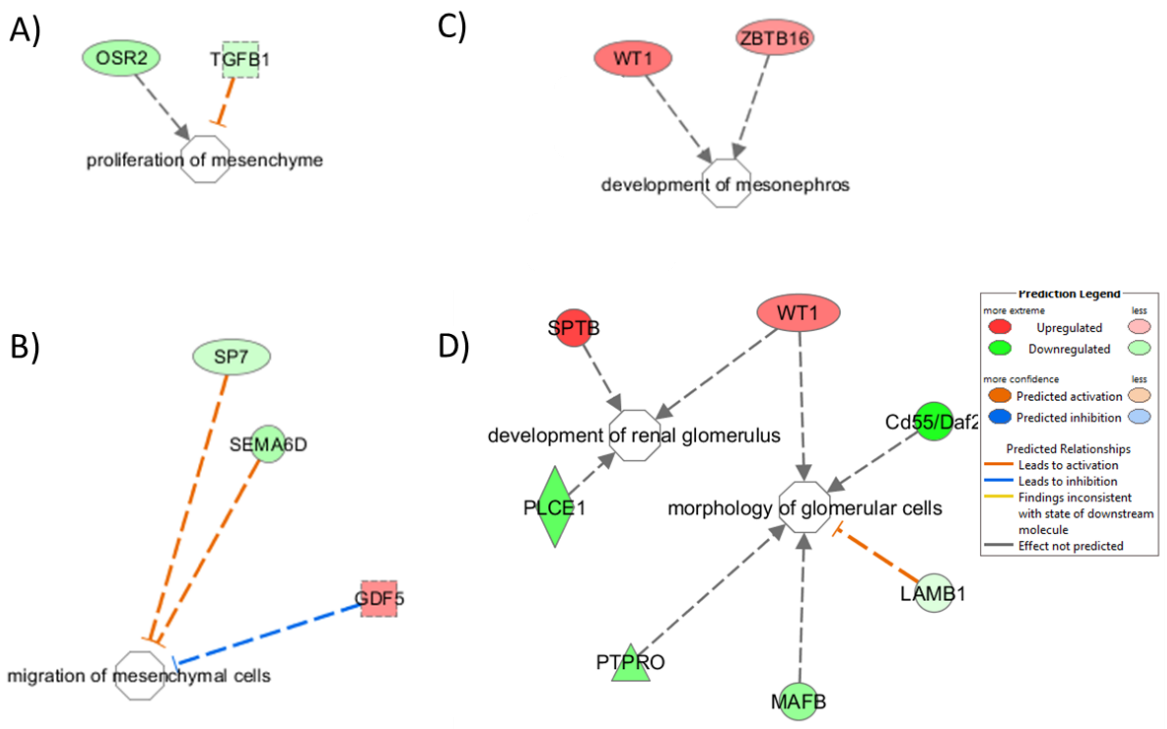

Figure 4.6.8: IPA functional analysis in relation to nephron and glomerular development. The array list of p<0.05 were put into IPA system, and selected for renal related functional analysis. A) and B) are those involved in mesenchymal cells, C) in development of early kidney and D) genes involved in glomerular development. All of these genes have sequences in the gene region for WT1 binding while Sp7 and Gdf5 have the sequence adjacent to their gene sequences.

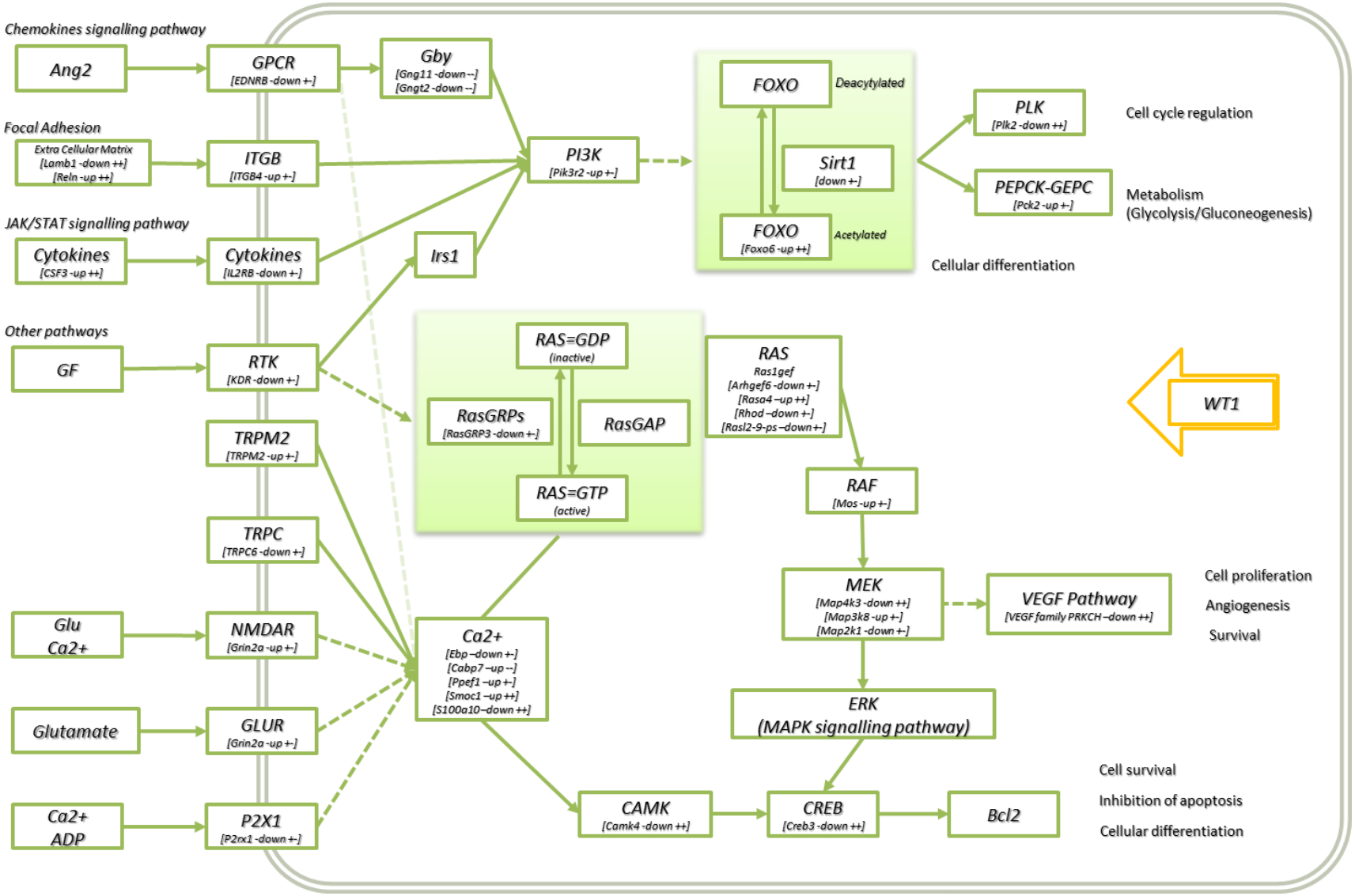

Figure 4.6.9: Adaptation of KEGG pathway (combination of multiple KEGG pathway in relation to WT1 gene) analysis reflecting the genes changes in E17.5 array with the genes involved documented together with respective up or down regulation and with indication of presence or absence of gene sequence for WT1 binding (+ for presence, - for absence).

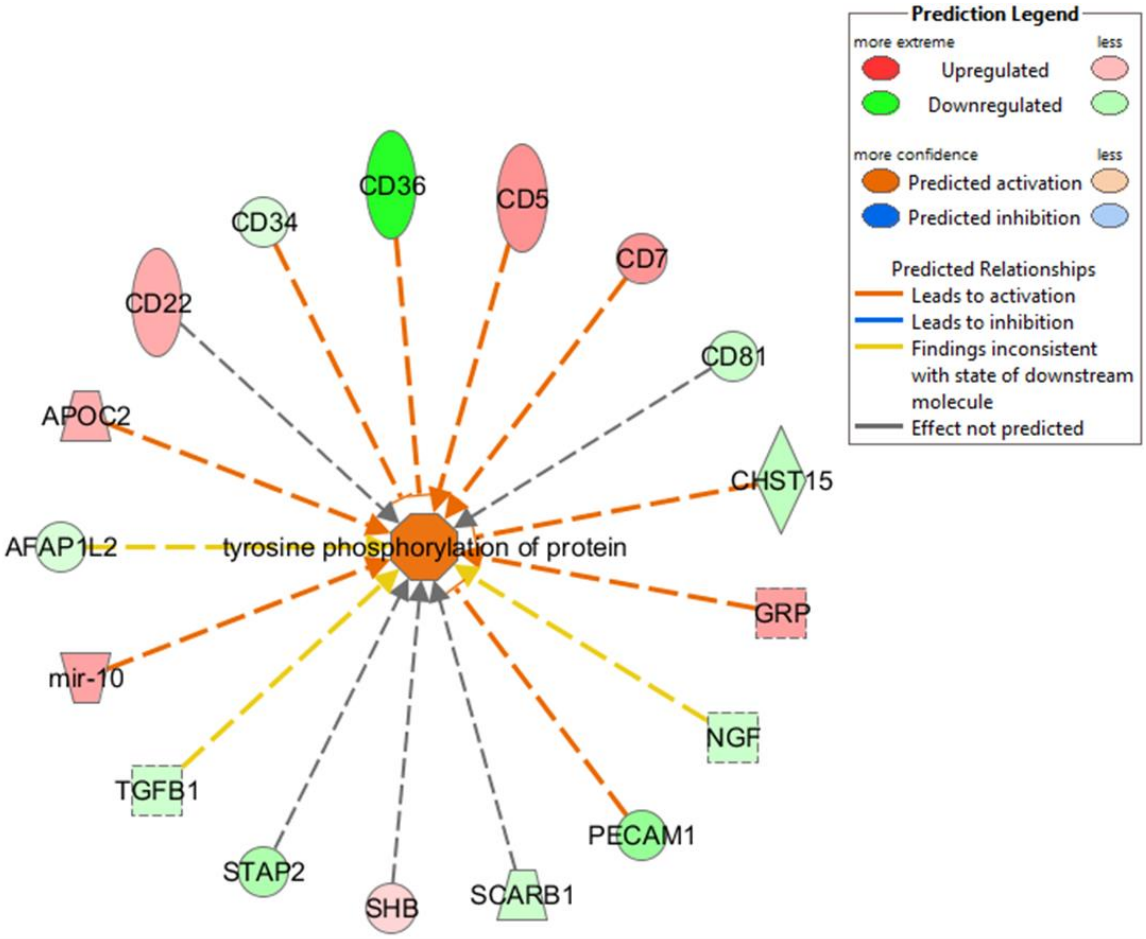

The filtering found 1 Functions for Post-Translational Modification There are 17 unique molecules selected

	Category	Diseases or Functions Annotatio	p-Value	Predicted Activ	Activation z-sc	Molecules	# Molecules
☑	Post-Translatio	tyrosine phosphorylation of pro	4.64E-03		1.797	AFAP1L2, APOC2, CD22, CD34, CD36, CD5, CD7, CD81, CHST15, GRP all 17	17

Figure 4.6.10: IPA functional analysis for genes associated with post-translational modification via tyrosine phosphorylation (of phosphate). This type of post-translational modification has been shown previously to be associated with mesenchymal-epithelial modification which play an important role in 'budding' of nephron progenitors in kidney development.

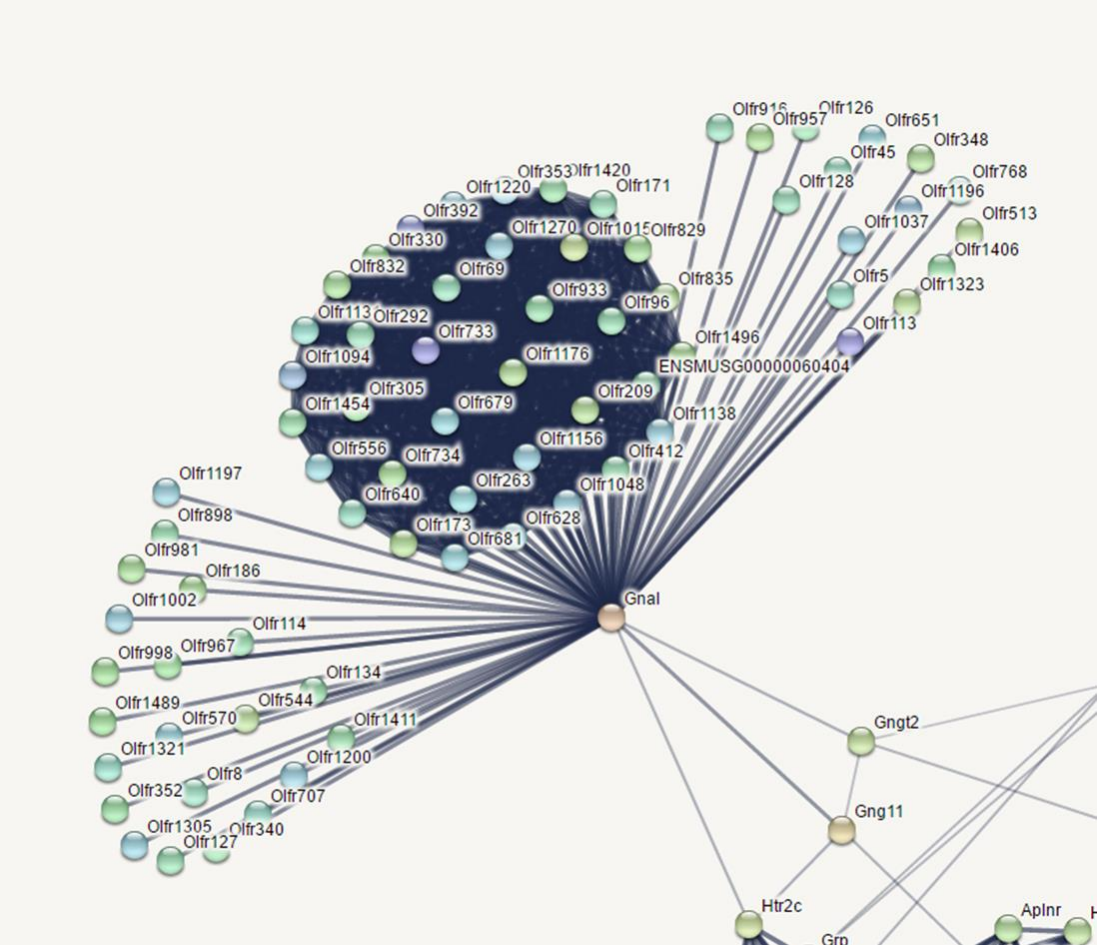

Figure 4.6.11: STRING diagram showing olfactory related genes differentially expressed in E17.5 kidney array. Reduction of WT1 +KTS isoforms has been link to disruption of olfactory products. Gnal (down, ++). This related back to the basic of WT1 mutation in DDS/+mice, which resulting in imbalance on +KTS and -KTS isoforms of WT1 protein. Disruption in exon 9 region of WT1 contribute to less +KTS isoform with the loss of fourth zinc finger region. This is to show that the array gene list does portray the outcome of WT1 mutation.

4.7: Summary of key findings

I. Microarray data were analysed and validated.
II. Gene expression profile of e17.5 DDS/+ kidney and wild type revealed novel genes underlying development and biochemical interaction in foetal kidney development in relating to WT1 gene.
III. Changes seen in mitochondrial tRNA and its alteration give clues towards more complex interaction between nuclear genes, mitochondria and WT1.
IV. Comparative databases analysis shows confirmation of some genes that were found to be involved in nephron formation.
V. Ingenuity Pathway Analysis (IPA) showing networks of interacting molecules and biological functions related to WT1

4.8: Discussion

Our hypothesis is that the dominant negative mutation in the Wilms' tumour suppressor 1 regulatory gene carried by DDS/+ mice will alter the expression of downstream genes in the developing kidney. As there is no comprehensive list of Wt1 target genes, we chose to carry out a microarray experiment to identify these genes. In order to identify genes involved in the earliest known kidney phenotype (reduced nephron number) of the DDS/+ ($Wt1^{tmT396}$/+) mice, we elected to analyse foetal (e17.5) kidneys from 4 DDS/+ mice and 4 wild type controls. At this stage, mutant and wild type kidneys are indistinguishable under light microscopy, so we do not assume that any gene expression changes will be large, nevertheless any changes between mutants and wild types are more likely to be directly causative, as opposed to secondary.

Prior to our array, both RNA and raw frozen e17.5 kidneys were sent to Source Bioscience for RNA extraction. In both cases, RNAs were analysed for RNA integrity prior to running through the array, and the best of those were used. In our setting, initially cDNA was prepared using Invitrogen RNAse OUT and 1µl of Invitrogen Superscript III, but the result seems to be not as consistent when run for qRT-PCR. Changing to a complete kit setup improved the result obtained. The complete kit setup may influence the quality of cDNA and crucial for getting a confidence result.

Recent advancements have shown that the mitochondrial system is an important cellular component that is essential for maintaining normal health. Additionally, a large proportion of mitochondrial disease mutations have been found in mt-tRNAs (Moreno-Loshuertos et al. 2011). However, the situation is complicated by the fact that even similar homoplasmic tRNA mutations cause variable phenotypes and variable penetrance, likely through compensatory expression of metabolic pathways or by upregulating mitochondrial biogenesis (Fernández-Ayala et al. 2010) or may also increase the expression of tRNA-interacting genome loci (Perli et al. 2012). In fact, it has been shown previously that expression of nuclear-encoded genes is known to modify mitochondria related disease (Francisci et al. 2011). Thus, the combined mitochondrial-nuclear interaction at tRNAs and their target may have much more pronounced effects than previously known.

Analysis of the microarray data showed that these tRNAs were expressed less in the mutant. Validation of these findings was carried out by qRT-PCR for the four tRNAs that could be successfully amplified and ND5 as a mitochondrial encoded gene not appearing on our differentially expressed lists. ND5 is part of an enzyme complex for transducing energy in the respiratory chain in mitochondria. Its function is the transfer of electrons and protons from NADH to ubiquinone across the membrane. (Walker, 1992, Yagi & Matsuno-Yagi, 2003, Brandt, 2006, Zickermann et al., 2009). In mice, mtDNA ND5 is tightly controlled and its regulation can compensate for its needs in harsh expression variation NADH dehydrogenase-dependent respiration rate (Bai et. al., 2000).

Given the unexpected nature of this result, we sought to interrogate the finding thoroughly. Some tRNAs are known to have nuclear analogues, pseudogenes (Mishmar et al., 2004). We sought to investigate if the tRNA species identified by the microarray and verified by qRT-PCR were nuclear pseudogenes or true mitochondrially encoded tRNAs. A series of BLAST searches were conducted spanning the entire tRNA sequence covered on the array and by qRT-PCR which revealed that two of the four validated tRNAs have no nuclear pseudogene (whereas 2 clearly have nuclear pseudogenes with 100% sequence similarity on Chr 1 and Chr 2). See figures 4.8.1 below.

A - *tRNA-his*

ary (click arrow to hide)

Select rows to include in table, and type of sort
(Use the 'ctrl' key to select multiples)

refresh

Query	Subject	Chromosome	Scaffold	Contig	Stats	Sort By
off	_off_	_off_	_off_	_off_	_off_	>Score
Name	Name	Name	Name	Name	Score	<E-val
Start	Start	Start	Start	Start	E-val	>E-val

Links	Query Start	Query End	Ori	Chromosome Name	Chromosome Start	Chromosome End	Ori	Stats Score	E-val	P-val	%ID	Length
[A] [S] [G] [C]	1	25	-	Chr:MT	11572	11596	+	25	7.7e-06	7.7e-06	100.00	25
[A] [S] [G] [C]	1	25	+	Chr:2	69355584	69355608	+	25	7.7e-06	7.7e-06	100.00	25
[A] [S] [G] [C]	1	22	-	Chr:7	99026626	99026646	+	18	0.45	0.36	95.45	22
[A] [S] [G] [C]	4	21	-	Chr:14	71593565	71593582	+	18	0.45	0.36	100.00	18
[A] [S] [G] [C]	8	24	+	Chr:1	25994048	25994064	+	17	2.2	0.89	100.00	17
[A] [S] [G] [C]	1	17	-	Chr:X	35911902	35911918	+	17	2.2	0.89	100.00	17
[A] [S] [G] [C]	1	17	+	Chr:5	70992121	70992137	+	17	2.2	0.89	100.00	17
[A] [S] [G] [C]	3	23	-	Chr:13	67105248	67105268	+	17	2.2	0.89	95.24	21
[A] [S] [G] [C]	3	19	-	Chr:16	59909154	59909170	+	17	2.2	0.89	100.00	17
[A] [S] [G] [C]	9	25	-	Chr:19	12058684	12058700	+	17	2.2	0.89	100.00	17
[A] [S] [G] [C]	1	16	-	Chr:2	73346564	73346579	+	16	10.	0.99995	100.00	16
[A] [S] [G] [C]	2	17	-	Chr:1	134407444	134407459	+	16	9.9	0.99995	100.00	16

B- *tRNA-phe*

ry (click arrow to hide)

e in table, and type of sort
(Use the 'ctrl' key to select multiples)

refresh

Query	Subject	Chromosome	Scaffold	Contig	Stats	Sort By
off	_off_	_off_	_off_	_off_	_off_	>Score
Name	Name	Name	Name	Name	Score	<E-val
Start	Start	Start	Start	Start	E-val	>E-val

Links	Query Start	Query End	Ori	Chromosome Name	Chromosome Start	Chromosome End	Ori	Stats Score	E-val	P-val	%ID	Length
[A] [S] [G] [C]	1	25	-	Chr:MT	1	25	+	25	7.7e-06	7.7e-06	100.00	25
[A] [S] [G] [C]	9	25	-	Chr:11	91603847	91603863	+	17	2.2	0.89	100.00	17
[A] [S] [G] [C]	4	19	+	Chr:1	131072966	131072981	+	16	9.9	0.99995	100.00	16
[A] [S] [G] [C]	8	23	-	Chr:1	146238203	146238218	+	16	9.9	0.99995	100.00	16

B- *tRNA-phe*

ry (click arrow to hide)

e in table, and type of sort
(Use the 'ctrl' key to select multiples)

refresh

Query	Subject	Chromosome	Scaffold	Contig	Stats	Sort By
off	_off_	_off_	_off_	_off_	_off_	>Score
Name	Name	Name	Name	Name	Score	<E-val
Start	Start	Start	Start	Start	E-val	>E-val

Links	Query Start	Query End	Ori	Chromosome Name	Chromosome Start	Chromosome End	Ori	Stats Score	E-val	P-val	%ID	Length
[A] [S] [G] [C]	1	25	-	Chr:MT	44	68	+	25	7.7e-06	7.7e-06	100.00	25
[A] [S] [G] [C]	1	18	-	Chr:11	42531373	42531390	+	18	0.45	0.36	100.00	18
[A] [S] [G] [C]	3	19	+	Chr:1	3959467	3959483	+	17	2.2	0.89	100.00	17
[A] [S] [G] [C]	3	19	+	Chr:14	81473045	81473061	+	17	2.2	0.89	100.00	17
[A] [S] [G] [C]	2	18	-	Chr:14	29898013	29898029	+	17	2.2	0.89	100.00	17
[A] [S] [G] [C]	9	24	+	Chr:1	122477695	122477710	+	16	9.9	0.99995	100.00	16
[A] [S] [G] [C]	3	18	+	Chr:2	68901604	68901619	+	16	10.	0.99995	100.00	16
[A] [S] [G] [C]	4	19	-	Chr:X	89171676	89171691	+	16	10.	0.99995	100.00	16
[A] [S] [G] [C]	4	19	-	Chr:X	89075380	89075395	+	16	10.	0.99995	100.00	16
[A] [S] [G] [C]	4	19	-	Chr:X	67191311	67191326	+	16	10.	0.99995	100.00	16

Figure 4.8.1: *TBLASTN output from ENSEMBL for* ***(A)****, tRNA-his Affymetrix probe showing 100% identity to chromosome 2,* ***(B)*** *tRNA-phe Affymetrix probes minimal nuclear chromosomal identity.*

There has been little previous research into mitochondria and tRNAs in the developing kidney, however, nephrogenesis is likely to be a very high-energy requiring process with rapid cell divisions and differentiation. Hence the reduced amount of mitochondrial tRNAs may reflect a general reduction in mitochondria or a specific reduction in those tRNAs. The expression data suggests that the mitochondrial copy number is not reduced based upon ND5 expression data. Further confirmation needed to be done.

In terms of what is known of Wt1 biology, it is plausible that reduced levels and/or the presence of the DDS mutation could affect RNA. As we know, Wt1 can interact with splicing factors (Davies et al., 2004), can localise within a cell with splicing factors (Larsson et al., 1995), and also involved in regulating other alternative splicing such as Vegf (Cunningham et al., 2013), though Vegf did not significantly change in the array. In addition, it is noteworthy that two independent probe sets for a small nucleolar RNA species are differentially expressed (2 probe sets maybe self-validating) along with RNase12 and several other RNAs, in which increase our confidence in these data.

In our gene expression analyses, mitochondrial tRNA genes show significant differential expression in foetal kidneys from DDS/+ mice compared with wild type littermates. This finding raises the question as to the involvement of these tRNAs in the physiopathology of renal disease development, in particular nephron endowment. Our data suggest that there might be some interruption of mitochondrial tRNA gene expression. A much more in-depth analysis needed to be done to confirm these finding. No published data that we know of shows any correlation between WT1 and mitochondrial genes. These unexpected findings raise two questions: what is the role of mitochondrial tRNA genes in nephrogenesis, and by what mechanism does Wt1 mutation affect mitochondrial tRNA levels? In terms of a role for tRNAs in nephrogenesis, it is intriguing to note that mitochondrial tRNAs do show differential spatial levels of expression in different components of the developing kidney (Figure 4.8.2).

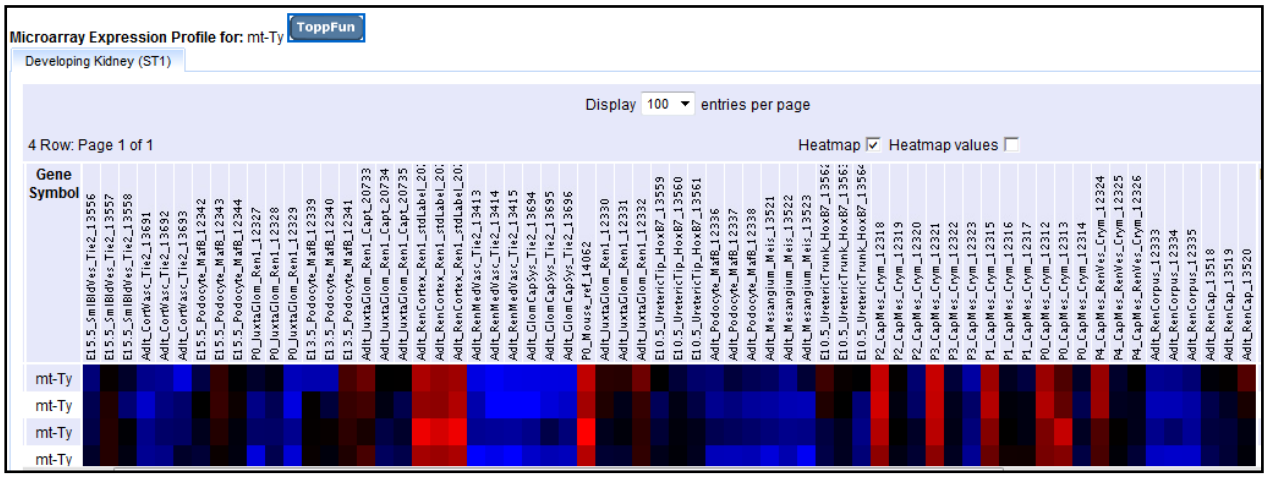

Figure 4.8.2: *A diagram of expression analysis from GenitoUrinary Development Molecular Anatomy Project (GUDMAP) website showing tRNA-tyr expression in developing kidney, a representative example of mitochondria tRNA displaying strong tissue-type specificity of expression. Red area indicates positively expressed.*

It has previously been documented that mitochondrial abnormalities may instigate abnormalities in various organs. Mitochondrial respiratory chain deregulation has been correlated with chronic kidney disease (CKD) and in those patients going to haemodialysis (HD) via analysis of their peripheral blood mononuclear cells (Granata et. at., 2009). Although other publications shown various mutations in the mtDNA that relates to end-stage renal disease, our microarray of DDS/++ mutant mice imply that deregulation in the nuclear genome, in this case the Wilms Tumor 1 gene, may actually involve in mtDNA expression in kidney development that may lead to nephron number endowments and subsequent higher risk to renal disease.

Decay-accelerating factor (DAF) also known as CD55 is a Glypiated (GPI)-linked membrane complement regulator. It has a protective role to the plasma membrane of cell and associated with classical and alternative complement activation pathways and also expressed widely in mammals, including the kidney. In adult human, it was found in glomeruli and in glomerular visceral epithelial cells (GEC) culture. In adult rats, it was exclusively seen on the apical surfaces of GEC via antibody staining (Bao et al., 2002). Recent research suggests that CD55 expression has a protective effect on kidney, reducing the intensity of insults on the glomerulus (Sogabe et al., 2001, Bao et al., 2009)

and show increase survival in transplanted kidney (Brodsky et al., 2009). There is very little research so far investigating the role of CD55 in mice embryonic kidney. However, there are data of specificity of CD55 when the expression pattern in developing kidney is examined (via GUDMAP). It can be seen that high levels of CD55 are found in developing podocytes and renal corpuscle (Figure 4.8.3). In our array, CD55 (downregulated) is at the top of the list of significantly change gene from the nuclear genes group.

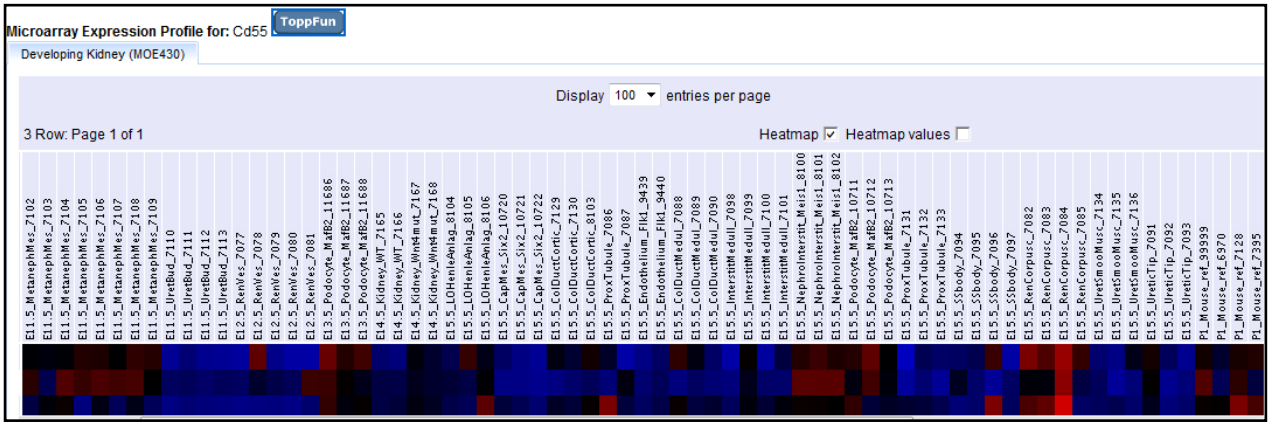

Figure 4.8.3: *A diagram of expression analysis from GenitoUrinary Development Molecular Anatomy Project (GUDMAP) website showing CD55 expression in developing kidney, a representative example A displaying strong tissue-type specificity of expression. Red area indicates positively expressed, notably within the renal corpuscle (the condensing nephron mesenchyme, coincident with Wt1).*

Two other genes that of particular prospects are FGF9 (upregulated from the array) and FGF20 (upregulated) which are profound prosurvival genes, show such increases in my array list. These genes are especially important and critical for maintaining nephron progenitor survival in transgenic mouse models, and mutation in FGF20 is implicated in severe renal dysplasia (Barak et al., 2012). To what extend these two genes exerts its function to progenitor nephron survival is yet unknown.

The pathway analysis such as Database for Annotation, Visualization and Integrated Discovery (DAVID), Ingenuity Pathway Analysis (IPA) or KEGG (Kyoto

Encyclopaedia of Genes and Genomes) were considered and used because of ease of access and robust database, having Causal Network Analysis comprehensively identifies upstream molecules that control the expression of the genes helps to build and better identify the pathway. IPA has contributed to the possible interaction on WT1 gene and the genes from the array. Even though this array dataset is of kidney origin, it is noteworthy (Figure 4.5.2-A) that IPA has highlighted pathways that are consistent with known functions of WT1, such as Haematopoiesis from multipotent stem cells (see Cunningham et al., 2013). Given the Wt1 expressing cells within e17.5 kidneys are differentiating mesenchymal stem cells, the similarities with hematopoietic stem cells may reflect similar underlying mechanisms in both sets of differentiating stem cell. Whilst the Tox List (Figure 4.5.2-B) is not a direct measurement of biological function, the identification of renal, cardiac and hepatic systems can be seen as consistent with the known roles of Wt1 in development (Carmona et. al., 2010).

Given the insight that the main mechanism on nephron formation and mesenchymal-epithelial transformation was disrupted, it is of interest to see whether the mechanism of controlled cell death during the kidney is disrupted, as this is also a possible mechanism in which the early nephron niche was lost during this developmental stage which might contributes to the lack of nephron number. Comparing known apoptosis related genes to the array list, quite a number of genes were listed and can be group in two, apoptotic gene upregulated, anti-apoptotic genes downregulated. I further analysed the overview of apoptosis event in foetal kidneys.

CHAPTER 5. APOPTOSIS IN DEVELOPING KIDNEYS OF MURINE DENYS DRASH SYNDROME MICE AND DISRUPTION OF MOUSE EMBRYONIC FIBROBLAST CELLULAR METABOLISM

Introduction

The first nephrons are seen at embryonic stage e12.5 in the mouse, then branching continues, increasing nephron number until e15.5 where nephrogenesis slows almost to a plateau but that later there is a rapid acceleration of nephrogenesis between P0 to P4 (after birth) (Short et al. 2013). This emphasizes the rapid two-stage nature of nephrogenesis during embryonic stages and then postnatally in mice. The mechanism which regulates both of these two rapid phases will determine the final nephron number. We know DDS/+ mutants have 20% less nephrons in the adult. If we know the number of nephrons at the plateau phase (between the rapid phases), that might give us a clue as to which part of prenatal or postnatal development that WT1 is significantly involved in nephron number regulation and thus nephron endowment. Previously it has been shown that nephron endowment is a potent modulator of the risk of developing renal disease (Walker et al. 2012).

Mutations of p53 and Pax2 in embryos from mouse models shows lower expression of these genes in nephron progenitors and an increase in apoptotic activity (Saifudeen et al. 2012). In other studies, mutation in genes Bmp2 and Smad4 mice, demonstrated reduced mesenchymal proliferation, also in Bmp7 mice demonstrating metanephric mesenchyme cell apoptosis (Dudley and Robertson, 1997; Hartwig et al., 2005). There are other examples of gene mutations associated with apoptosis in developing kidneys at various stages of development; these include Wnt9b (Karner et al. 2011), Mdm2 (Saifudeen et al. 2002) and MMP9 (Arnould et al. 2009). There are also a few genes that show no evidence of apoptosis pertaining to nephron development. These includes examples like gene mutations in Alk3 (Giovanni et al. 2011), Cv2 (Ikeya et al. 2010), and Ptc1 (Cain et al. 2009). Some of these were associated with delayed maturation of the nephron (e.g. MMP9). These highlight the possible pathways relating to the development of nephrons from nephron progenitors to mature glomerulus.

Short et al. 2013 highlight the lack of evidence for cell death within the cap mesenchyme in early normal physiological renal development. This suggests that apoptosis might not be part of normal renal development and the lack there-off in normal nephron growth afterwards. As in our data, few known pro-apoptotic genes were upregulated, and anti-apoptotic genes were shown to be both down regulated and upregulated. As to question how these are related is not yet known and very interesting to be uncovered.

Results

5.1 Apoptosis gene list

Of the 1136 genes hit list from the array, there are a number of genes that were listed to have roles in apoptosis. Various known potential genes related to apoptosis were listed and compared to our array genes list and shortlisted as in table below.

Mechanism in Apoptosis System	*Genes*	*WT1 target Domain*	*Array*	*Log fold change*
Induction of Apoptosis by Extracellular Signals	Adora1	yes	up	0.174696015
Induction of Apoptosis by Extracellular Signals	Cd5	yes	up	0.26880245
Induction of Apoptosis by DNA Damage	Trp73	no	up	0.204253675
Other Genes Involved in Induction of Apoptosis	Map3k10	no	up	0.103516552
Other Genes Involved in Anti-apoptosis	Map3k10	no	down	-0.491563283
Other Genes Involved in Anti-apoptosis	Polb	no	down	-0.215526653
Other Genes Involved in Anti-apoptosis	Tgfb1	no	down	-0.158113741
Other Genes Involved in Anti-apoptosis	Xiap	no	down	-0.175726026
Positive Regulation of Anti-apoptosis	Opa1	no	down	-0.155242003
Caspase Inhibitors	Xiap	no	down	-0.175726026
TRAF Domain Proteins	Traf7	no	down	-0.11277985

Inhibitor of apoptosis	Sirt1	no	down	-0.169357687
Inhibitor of apoptosis protein (array)	Naip2	no	down	-0.33938724

Table 5.1.1: Listed are the genes related to apoptosis that were significantly changed in my array, with respective column indicating the presence of direct WT1 binding sites and array changes.

This list indicates that there is a role for apoptosis in the development of nephron. It is logical to assume that organ development requires a huge number of cells to divide and at some points, some have to be programmed to die. What is most surprising is that WT1 has transcriptional target domains on two of the genes. What and how exactly WT1 regulates the apoptotic mechanism are yet unknown.

5.2 Apoptosis staining

To further validate the possibility of dysregulation of apoptosis mechanism deregulated in these developing kidneys, I performed TUNEL (Terminal deoxynucleotidyl transferase (TdT) dUTP Nick-End Labelling) apoptosis screening test to observe any different between the wild type and DDS/+.

5.2.1 Localizing apoptotic segment of developing nephron of P0 kidney

On general notes, there were quite a number of fluorescence signal seen within sections of both wild types and DDS/+. In most circumstances, these signals were seemed to be generalised within the kidneys, mainly the tubular structures. This is understandable given the role of the renal tubules' roles in urine production. Working with kidney sections allow one to be able to discern with eyes the structure of nephron on kidney sections, especially the identifiable arrangement/appearance of mature glomerulus, s-shaped bodies and comma shaped bodies. What I am interested is the area where the renal glomerulus develops, the cortex and nephrogenic zone. This area shows quite a number of TUNEL signals. On higher magnification, specifically on the

developing structures of glomerulus, these TUNEL signals were seen mainly at the elongated tail region of the comma-shaped bodies. These were seen in both wild types and DDS/+.

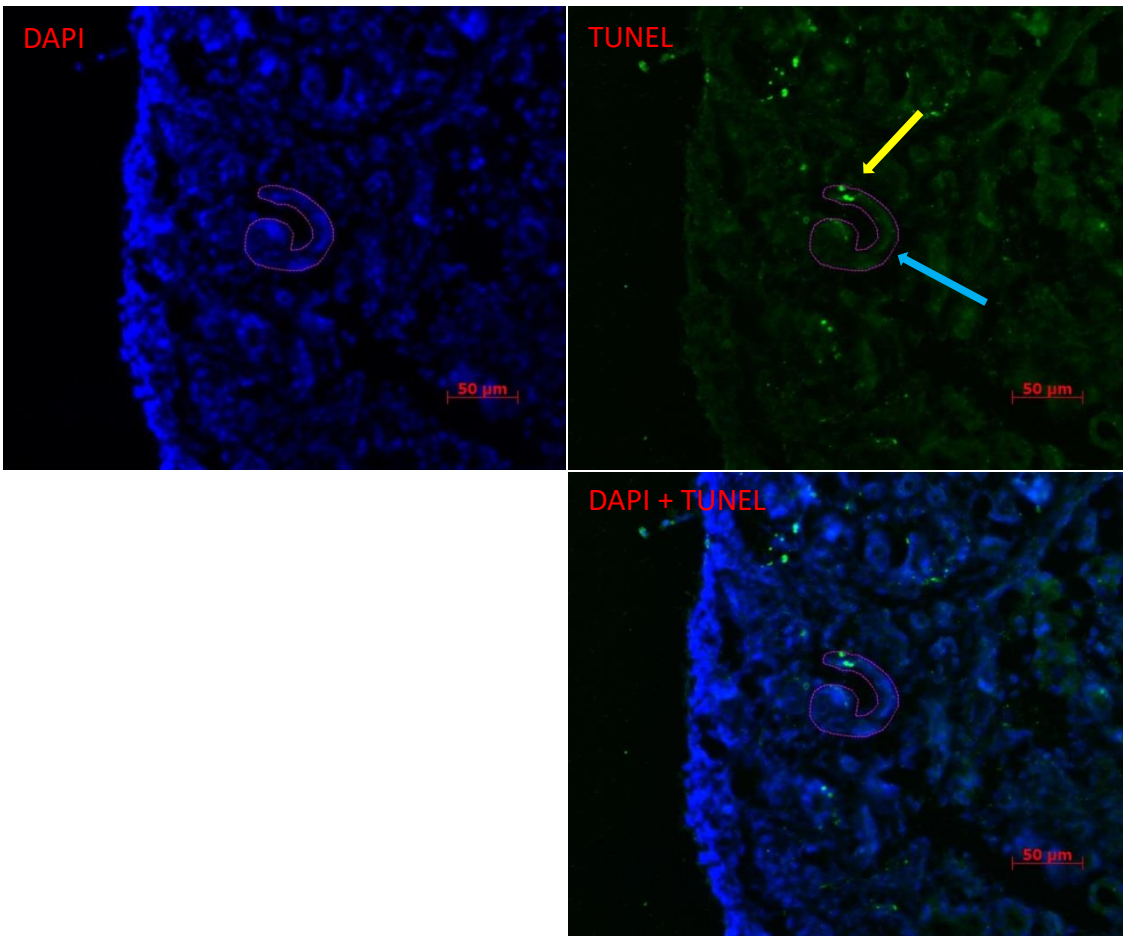

Figure 5.2.1: Representative figure wild type kidney showing the Immunofluorescence of TUNEL staining (Life Technologies) to detect the presence of DNA fragments cause by programmed cell death. The Sections are viewed at 20x magnification showing a 'comma shaped' body of a developing nephron indicated by blue arrow. TUNEL signal were seen at the tail of the comma shaped body, indicated by yellow arrow. N=3 P0 kidneys of wild type and N=3 of DDS/+ were examined.

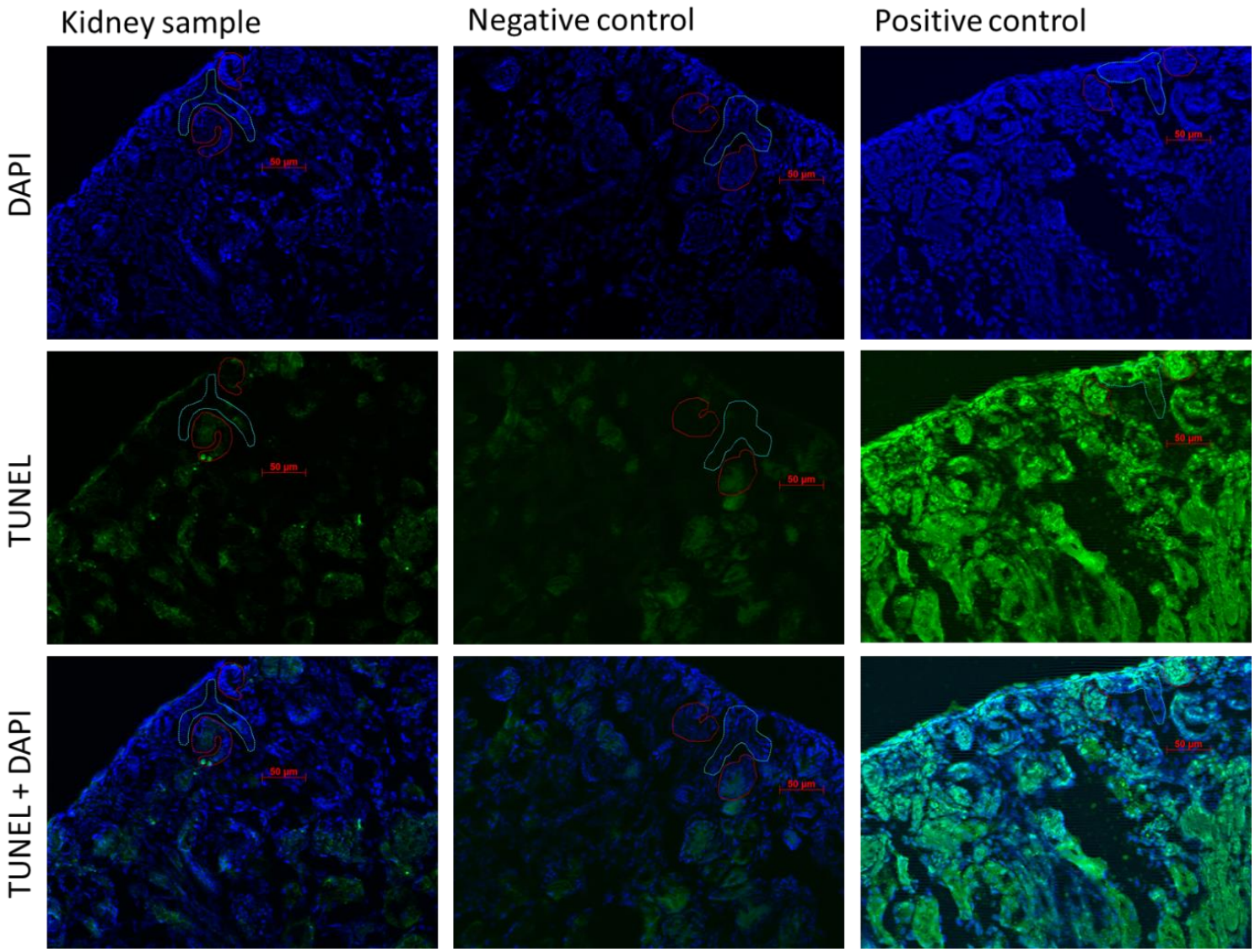

Figure 5.2.2: Immunofluorescence of TUNEL staining (Life Technologies) to detect the presence of DNA fragment caused by programmed cell death. The Sections showing the controls, positive and negative control of the staining procedure.

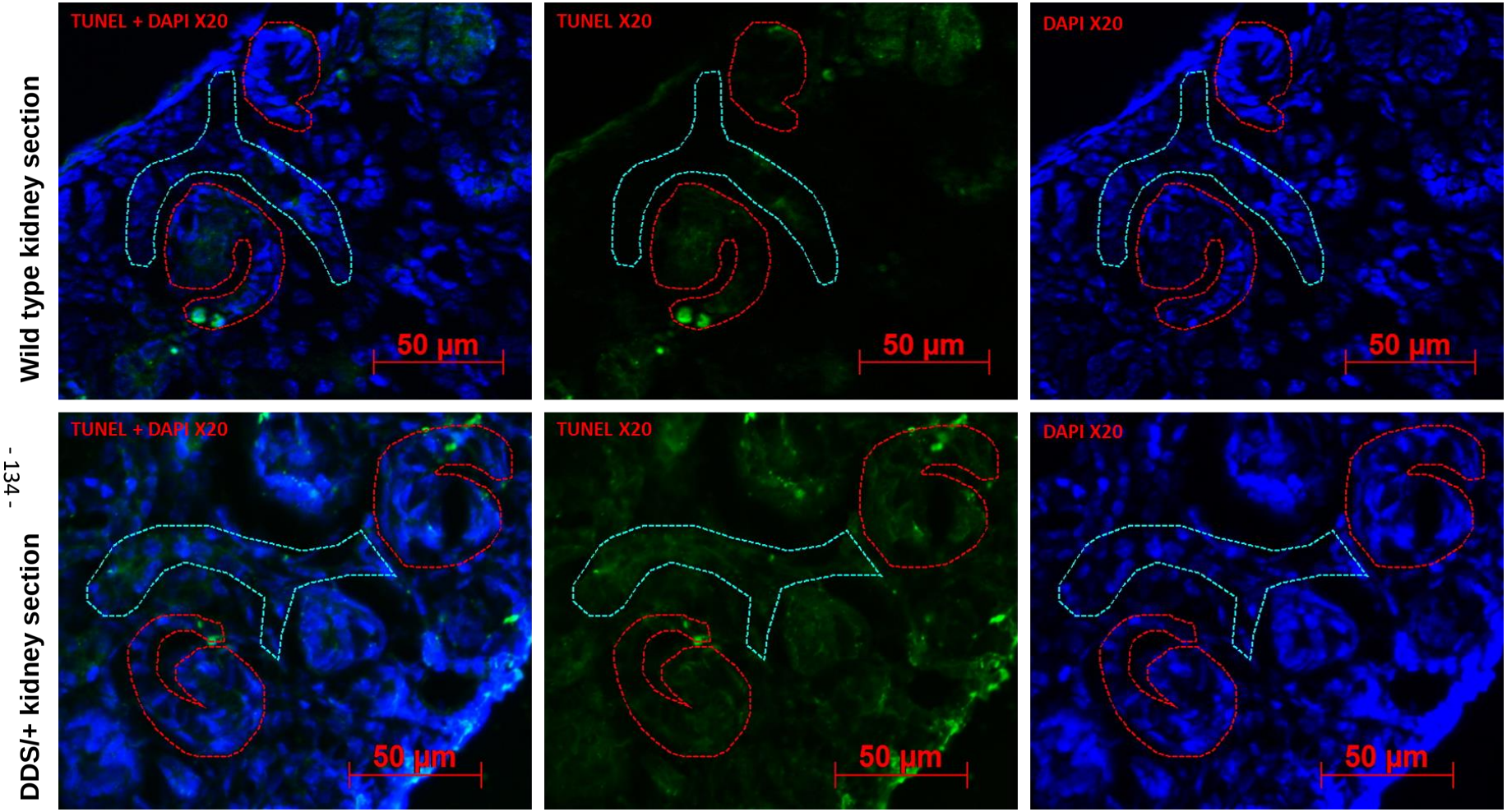

Figure 5.2.3: Immunofluorescence of TUNEL staining (Life Technologies) to detect the presence of DNA fragment caused by programmed cell death. The Sections showing comma shaped bodies with ureteric trunk. TUNEL signal were seen at the tail of the comma shaped bodies in both wild type control and DDS/+, showing similar pattern of TUNEL fluorescence signals.

5.2.2 Quantifying the TUNEL signals on cortex region of P0 kidney section

In general overview of the kidney sections, there were no significant different of the placement of the TUNEL signal. I then counted the signal to investigate further if there is any increment or decrease of signals seen between wild types and DDS/+. Counting was done (by double blinded counting by two persons) in the cortex region delineated by the line drawn at 200um from the edge of the kidney section (as this was determined by the subjective observation of the developing glomerulus. This will be repeated after the exact delineation can be obtained from PNA staining of the same stage of kidney development later on). Longitudinal kidney section region can be divided into 3 (three) region in general, the cortex which is the outermost region, medulla which is the middle region and the renal pelvis which is the urine outflow from the kidney. Kidney cortex region is where the nephrogenic zone is located, where nephron is developing, is where the interest of this study lies.

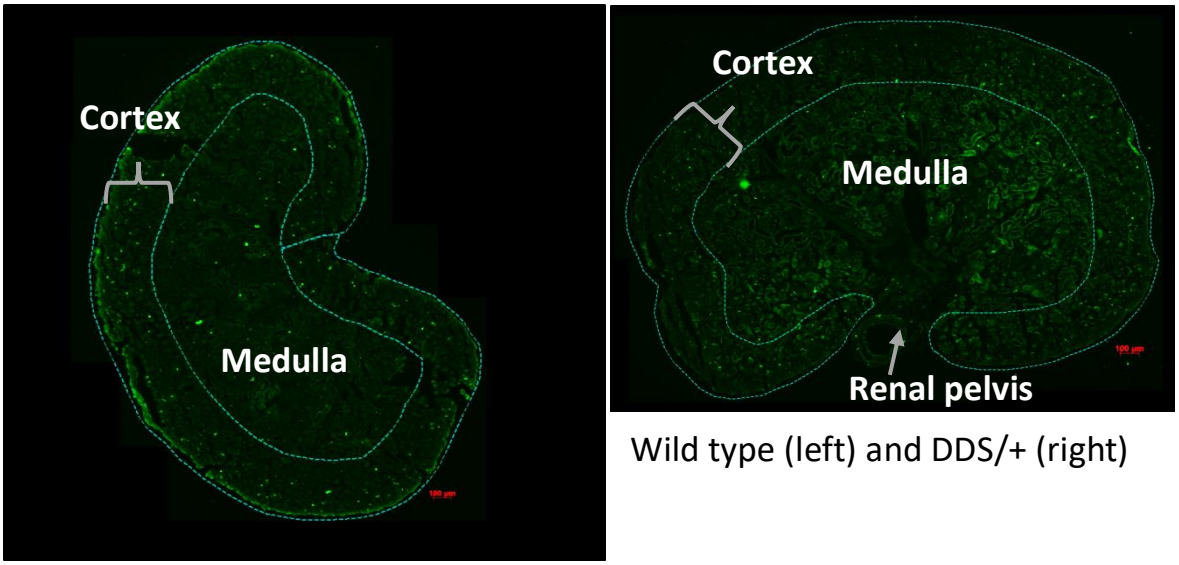

Wild type (left) and DDS/+ (right)

Figure 5.2.4: Representative figures of TUNEL staining of P0 kidneys. All TUNEL staining were done with DAPI co-staining (not shown). Images show multiple green dots of overall pattern of program cell death in the kidneys. (These above images were slightly edited to enhance the colour due to pixel lost when resized)

The counting was done using ImageJ software, and repeated by another person by double blinded counting, the two groups of count were assessed for significant difference with t-test, and the difference were of no significant ($p>0.05$) for each section, and the average was taken as the final count. As for the counts, they are divided into all signals, high intensity signals alone and low intensity signals alone from individual perspective. These counting were then calculated for their significance. In all those circumstances, there were no significant difference of TUNEL signals ($P > 0.05$) between the wild type and DDS/+ (Figure 5.2.5). Caspase 3 staining on the kidneys previously (Wroe 2009) support my finding, which uses the same DDS/+ strain mice at similar time frame of development.

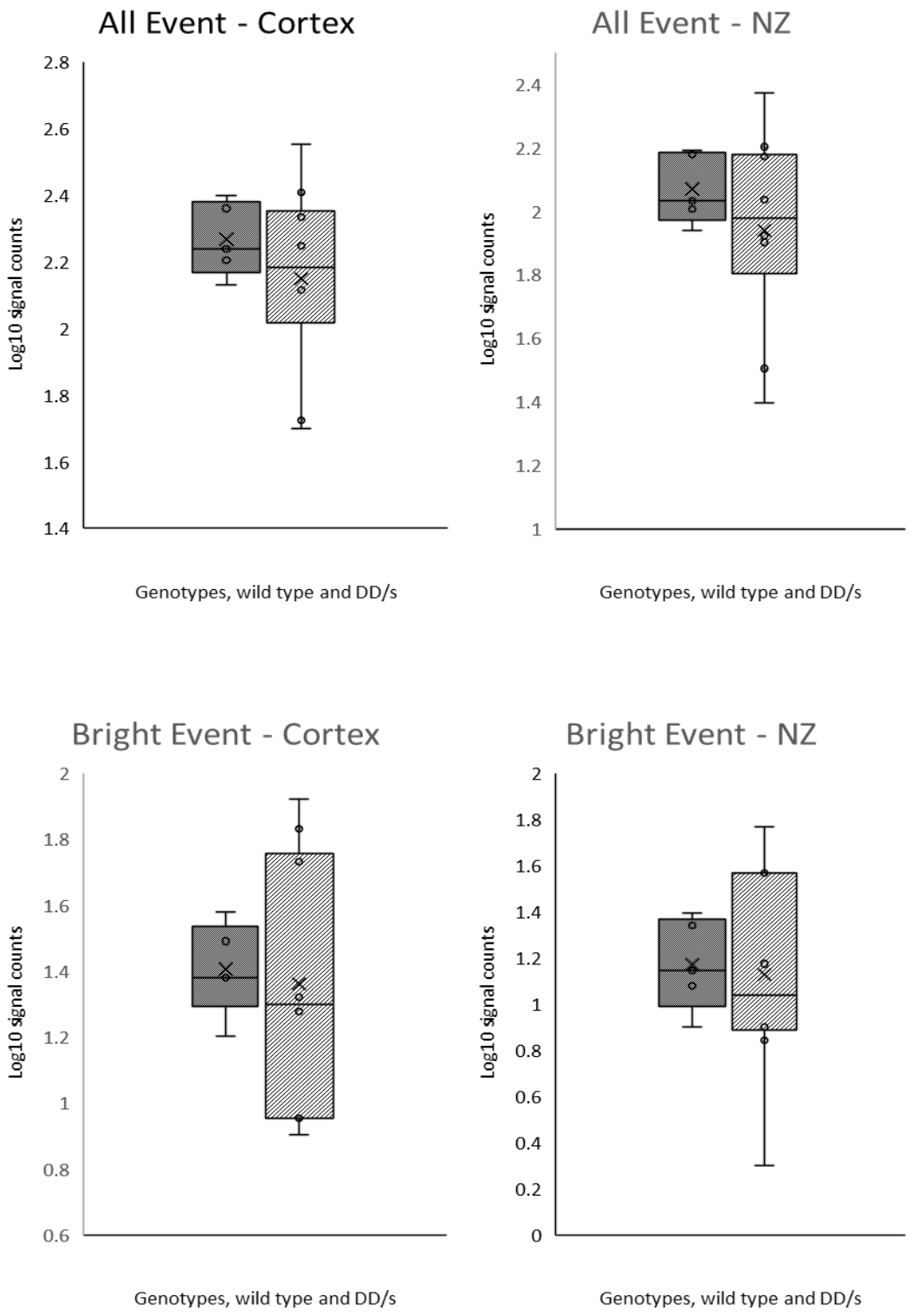

Figure 5.2.5: Counts (normalized by log10) of TUNEL signals (events) from sections of newborn kidney (p0) od wild type mice versus DDS/+ (N=6 wild type vs N=6 mutant kidneys). NZ = nephrogenic zone.

ANOVA

		Sum of Squares	df	Mean Square	F	Sig.
All_Cortex	Between Groups	.043	1	.043	.660	.434
	Within Groups	.709	11	.064		
	Total	.752	12			
All_NZ	Between Groups	.053	1	.053	.676	.429
	Within Groups	.856	11	.078		
	Total	.909	12			
BE_Cortex	Between Groups	.006	1	.006	.051	.825
	Within Groups	1.306	11	.119		
	Total	1.312	12			
BE_NZ	Between Groups	.006	1	.006	.036	.852
	Within Groups	1.830	11	.166		
	Total	1.836	12			

Table 5.2: SPSS calculation using one-way ANOVA of the TUNEL signal counts normalized to log10. The differences between wild type and DDS/+ is insignificant (p>0.05).

5.3 Mouse Embryonic Fibroblast impairment of cellular metabolism

In order to investigate the effect of WT1 mutation on cellular viability, I opted to use the Alamar Blue assay. This assay has been shown able to elicit deficit of cell viability in mitochondrial related conditions, albeit not specifically (Rampersad 2012). The active ingredient of alamarBlue® (resazurin) is a nontoxic, cell permeable compound that is blue in colour and virtually nonfluorescent. Upon entering cells, resazurin is reduced to resorufin, which produces very bright red fluorescence. Viable cells continuously convert resazurin to resorufin, thereby generating a quantitative measure of viability and cytotoxicity over time. In order to see the effect of WT1 mutation on live cells, given the fact that the DDS/+ mice are difficult to breed and the introduction of a bias in cell growth due to the inherent mutation, I choose to use mouse embryonic fibroblasts (MEF) derived from DDS20 (Chapter 2.1), utilising the cells inducible Cre-loxP system. The Cre-loxP system is a method to overcome early embryonic lethality in mice in conventional knockout systems. Cre is a 38 kDa recombinase protein from bacteriophage P1 that mediates site specific recombination between compatible loxP sites. In addition, by fusing Cre to a mutated oestrogen receptor ligand-binding domain, the Cre recombinase is able to be expressed with exposure to the synthetic oestrogen homologue, Tamoxifen (Indra et al., 1999). In order cultivate the cells free of influence of mutation, I opted for this DDS20 strain rather than DDS/+ strain mice. This would prevent the WT1 mutation influencing the growth of the cells prior to experiment. This DDS20 mice was shown to have similar characteristics of DDS/+, in which it causes chronic kidney disease (CKD) in mice (Ahzad MSc 2010).

5.3.1 Tamoxifen-induced MEF versus normal MEF

MEF were cultured and divided into two, one was given Tamoxifen while the other were kept as control. The number of cells were kept at 500000 per well of a 6 well plate. 6 cell lines were used, 3 for MEF control (MEF (no Tamoxifen)) while other 3 was given Tamoxifen (MEF (Tamoxifen)) 48hour prior to experiment and the cells were taken for PCR assessment of Cre-loxP recombination event of 100% (all cells were induced for loxP exonal deletion). The media were measured for absorbance in triplicate per well of cell culture plate after the intended exposure to Alamar Blue containing medium.

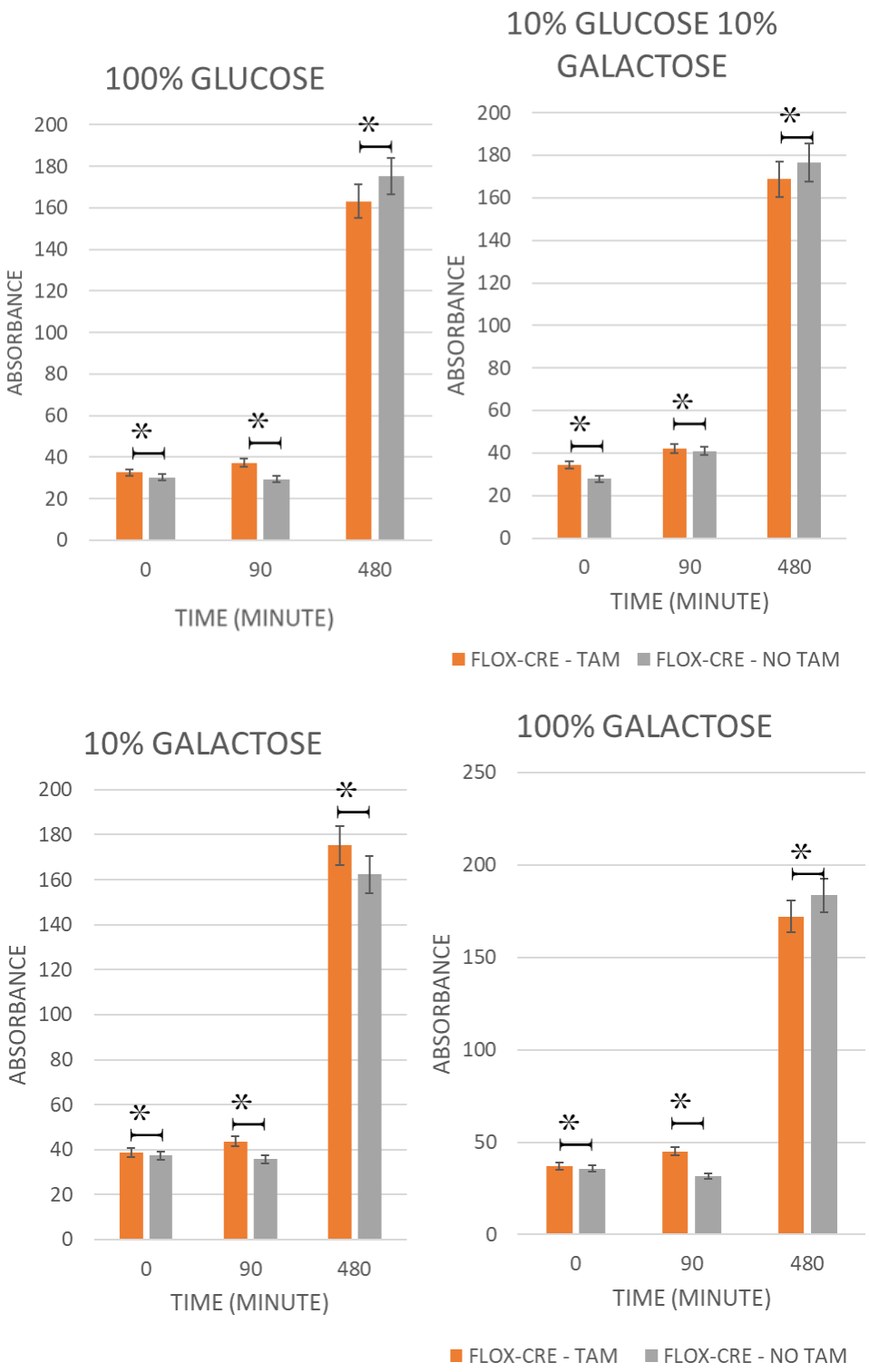

*Figure 5.3.1: Bar chart depicting the absorbance value of Alamar Blue according to time of MEF culture after addition of Alamar Blue. Four different medium preparation were done. P-value were calculated using T-test, *p-value were >0.05 which is insignificant. N=3 MEF (no Tamoxifen) vs N=3 MEF (Tamoxifen).*

The bar charts (Figure 5.3.1) show the absorbance values changes at different time points, immediate (within 15 minutes after introducing media), at 90 minutes and at 480 minutes in four different medium preparation. The control is the MEF without giving any Tamoxifen induction. From the data, there was no significant different seen in normal culture condition at 37°C.

5.3.2 Oxygen deprived MEF (Tamoxifen)

Given there was no significant different seen in normal culture of MEF (no Tamoxifen) versus MEF (Tamoxifen), MEF were exposed to oxygen deprivation to induce stress conditions. In order to simulate a stressful situation to the cells in which oxygen is deprived, subsequent cull culture was overlaid with a superficial layer of mineral oil on the surface of the medium after adding Alamar Blue containing medium.

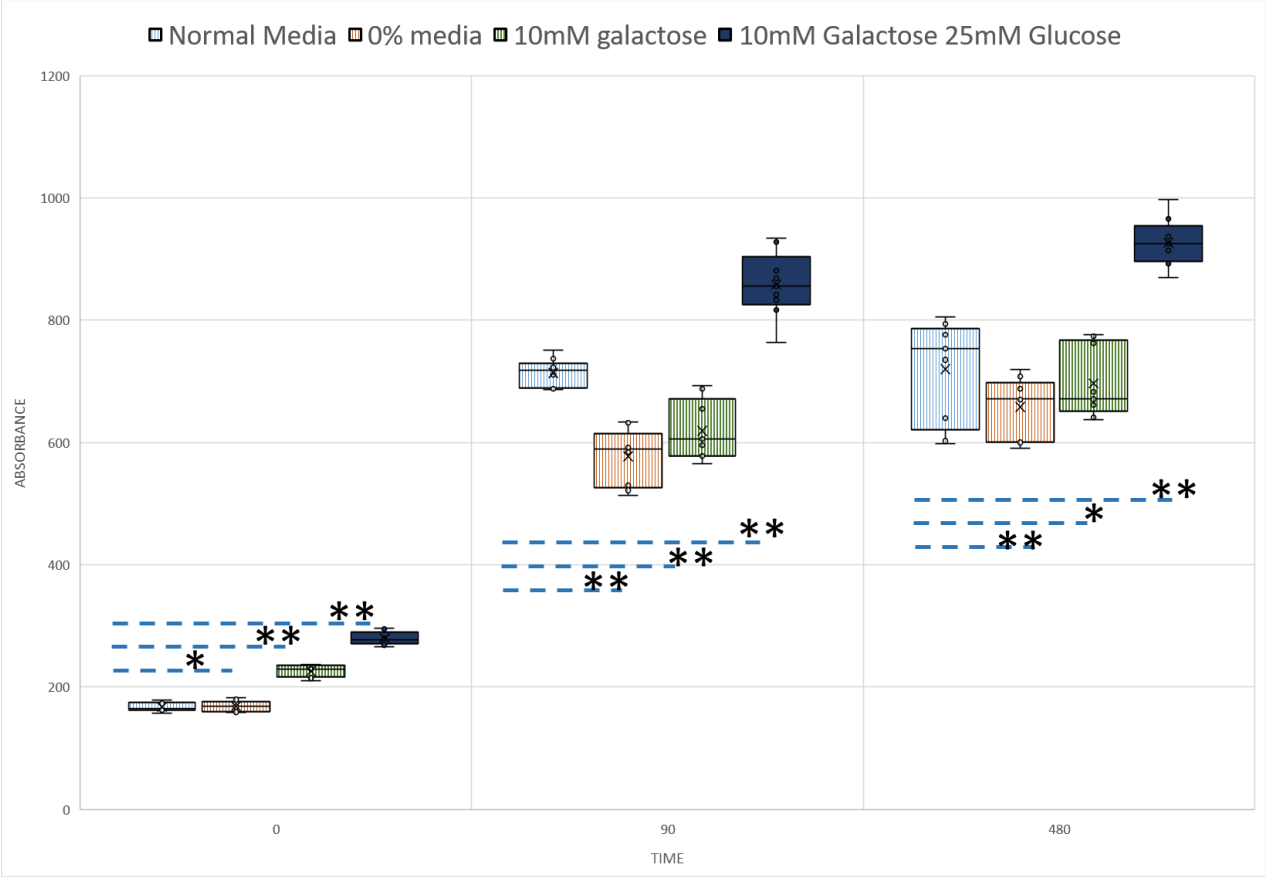

Figure 5.3.2: Box-plot chart depicting the absorbance value of Alamar Blue according to time of MEF culture after addition of Alamar Blue. Four different medium preparation

*were done. P-value were calculated using T-test and MEF with normal media were used as referenced, *p-value were >0.05 which is insignificant. **p-value <0.05, which is significant. All MEF were given Tamoxifen, N=9 technical replicates times four different media. Each well was read with triplicates.*

The box plot chart (Figure 5.3.2) show the absorbance values changes at different time points, immediate (within 15 minutes after introducing media), at 90 minutes and at 480 minutes in four different medium preparation, namely normal media, media without substrate (0% media), media with only galactose as substrates, and media with galactose and glucose as substrates. All the MEF used were exposed Tamoxifen prior experiment and were checked for 100% recombination.

From the data, there are some significant differences in absorbance at all time points. For the immediate time point (0), the different might be attributed to the delay due to preparation of culture plates. But the changes seen at 90 minutes and 480 minutes (8 hours) are significant, as this MEF experiment were repeated 3 times on 3 different MEF with 9 technical replicates each and seen similar pattern at 90 and 480 minutes. There was a higher absorbance value seen in galactose plus glucose media compared to normal media (contain glucose only), galactose only media and no substrate media (0% media) as time went by. This shows when deprived of oxygen, there is disruption of cellular physiology of MEF (Tamoxifen) when deprived of certain substrate, presumably for energy production.

5.4 Summary of key findings:

I. There are genes related to apoptosis dysregulated from microarray data.
II. No different of pattern of apoptosis seen between wild type immature nephron and DDS/+ P0 kidney.
III. No evidence of disruption of apoptosis seen in cortex region of renal sections in both wild type and DDS/+ P0 kidneys.
IV. There is disruption of normal cellular physiology in MEF (Tamoxifen) when in an unfavourable environment (different substrates and oxygen deprived).

5.5 Chapter Discussion

Given the number of studies showing the role of apoptosis in the kidney development, it was hypothesised that the apoptosis might be playing a significant role in nephron number endowment. In this case, there were no increase in TUNEL positive cells in association with the finding of lower nephron number in DDS/+ kidneys at this stage of development. This opens the possibility of another mechanism that determined their number, or the possibility that the nephron number that were determined via apoptosis, if true, were at a slightly earlier stage of kidney development then what I see here, at P0. It is unfortunate that e17 to e18 mice kidneys were not able to be assessed for apoptosis as they are too small for successful sectioning. Although the technique of counting the TUNEL positive signal is from slide section was performed, I would be more convinced if a volumetric assessment could have been done for the kidney. This would give a much more comprehensive data for the whole kidney. Hopefully there will be a better quantification technique that can be applied for apoptosis detection in the small kidneys in the future.

However, given the list of genes involved in apoptosis mechanism are significantly different in the e17.5 kidneys, there might be another possibility. A recent study suggested that in some specific conditions, there is the possibility of incomplete activation of apoptosis (mitochondrial) pathway, in which the incomplete apoptosis activation was shown to be a part of survival mechanism of the cells (Yee et al., 2014). They provided some interesting insights into a unique pattern of gene expression triggered when there is mitochondrial dysfunction, ultimately providing a protective mechanism against stress. The genes from the Table 5.1.1 are possibly involved in this postulated mechanism. The pro-apoptotic genes Adora1, Cd5, Trp73 and Map3k10 that was all upregulated might be balanced out by the antiapoptotic genes Nme5, Polb, Tgfb1, Xiap, Opa1, Xiap, Traf7, Sirt1 and Naip2 as a protective measure. Seeing the list of pro-apoptotic generally upregulated and anti-apoptotic generally down regulated, it really is plausible that somehow in mutated form of WT1 caused this imbalance, and somehow a nephron precursor would die prematurely before it can develop further. Hopefully this can be the aim of another experiment in the future. In a normally developing kidneys, these two mechanisms are always in balance in order for cells to have normal spatial expansion and tissue growth in timely manner. As this array

suggested changes to these genes, this really does imply that imbalances occur within the system. Although no evidence of apoptosis was seen, the implication of involvement of proliferation related factors might be very important in this context of renal nephrogenesis. It might be a circumstantial indication of reduce survivality or survival factors and the balance between it and apoptosis. In depth experiments are needed to further elucidate their involvement in renal nephrogenesis and nephron number.

This disruption of balance might affect the cellular viability. In order to assess this, Alamar Blue assay was used, primarily as it can also give indication of involvement of mitochondrial and non-toxic. The resazurin dye in Alamar Blue assay would go to the electron transport chain and perform as an intermediate electron acceptor without interference of the normal function (Page et la., 1993). There are several reasons why multiple substrate options were used. It has been shown that galactose enhances mitochondrial metabolism and is a good substrate to use to study mitochondrial dysfunction in cultured cells (Aguer et al., 2011). Usually through production of pyruvate from glycolytic metabolism, 2 net ATP is yielded. However, if galactose were used, no net ATP produced, and thus for cells to get ATPs, the cells would need to rely on oxidative phosphorylation (OXPHOS) from mitochondria (Marroquin et al., 2007, Bustamante and Pedersen 1977). Thus, for the cells, there would be increase of oxygen consumption for increment of aerobic state and would have to rely on the capacity of OXPHOS (Rossignol et al., 2004). If the cell mitochondrial do not function normally, it would not survive for long in galactose medium (Robinson et al., 1992).

Fluorometric absorbance value between normal MEF and MEF (Tamoxifen) show no significant different in normal culture environment, thus suggesting that in normal condition without stress, the cell could function close to normal without obvious observable abnormality (Figure 5.3.1). But when stressful situations were introduced, these cells would be unable to cope. From result of Figure 5.3.2, normal media, media without substrate (0% media), media with only galactose as substrates, and media with galactose and glucose were used. The use of galactose was to redirect the reliance of cells to OXPHOS within mitochondria. The MEF in galactose and glucose medium provide higher absorbance value compared to MEF in normal medium (have glucose only) was to be expected, as galactose enhance the process of producing ATP from the readily available glucose, thus reflected in the faster increment of absorbance value.

Where as in galactose only medium, although the MEF were enhance with presence of galactose to produce more ATP, as there was no glucose available, the cellular function was reduced, the change of absorbance value is lower, close to the value of MEF without any substrate (0% medium) and the process of producing ATP is disrupted. This clearly shows that MEF (Tamoxifen) that was induced for WT1 exon 9 deletion would decrease the capacity of cell to cope with stress, specifically in this experiment oxygen and substrate changes.

Given this insight that WT1 mutation does affect normal functions in mitochondria, to clarify further how WT1 relates to mitochondria and it effect in DDS/+ and DDS20 MEF, various experiments were done in subsequent chapter.

CHAPTER 6. A MITOCHONDRIAL ROLE FOR WT1

Introduction

In our gene expression analyses, mitochondrial tRNA genes show significant differential expression in foetal kidneys from DDS/+ mice compared with wild type littermates. This finding raises the question as to the involvement of these tRNAs in the physiopathology of renal disease development, in particular nephron endowment. My data suggest that there might be some interruption of mitochondrial tRNA gene expression. A much more in-depth analysis needed to be done to confirm these finding. No available data that I know of shows any direct correlation between WT1 and mitochondrial genes.

In terms of what is known of Wt1 biology, it is plausible that reduced levels and/or the presence of the heterozygous WT1 mutation could affect RNA expression. As was previously published, Wt1 can interact with splicing factors (Davies et al., 2004), can localise within a cell with splicing factors (Larsson et al., 1995), and also involved in regulating other alternative splicing such as VEGF (Cunningham et al., 2013).

There has been very little research into mitochondria roles in the developing kidney. However, it is presumed that nephrogenesis is likely to be a very high-energy requiring process with rapid cell divisions and differentiation. Hence the reduced amount of mitochondrial tRNAs may reflect a general reduction in mitochondria or a specific reduction in those tRNAs. Measurement of mitochondrial DNA copy number (qPCR) analysis data suggests that the mitochondrial copy number is not reduced based upon ND5 DNA measurement.

These unexpected findings raise two questions: what is the role of mitochondrial tRNA genes and other mitochondrial genes in nephrogenesis, and by what mechanism does Wt1 and Wt1 mutation affect mitochondrial gene expression levels? In terms of a role for tRNAs in nephrogenesis, it is intriguing to note that mitochondrial tRNAs do show differential spatial levels of expression in different components of the developing kidney (GUDMAP data).

It has previously been documented that mitochondrial abnormalities may instigate abnormalities in various organs (Stepien et. al., 2017). Mitochondrial respiratory system deregulation has been correlated with chronic kidney disease (CKD) and in those patients going to haemodialysis (HD) via analysis of their peripheral blood mononuclear cells (Granata et. at., 2009). Although other publications shown various mutations in the mtDNA that relates to end-stage renal disease, our microarray of DDS/+ mutant mice imply that deregulation in the nuclear genome, in this case the Wilms Tumor 1 gene, may actually involve in mtDNA expression in kidney development that may lead to nephron number endowments and subsequent higher risk to renal disease.

In cells, 99% of the mitochondrial proteins are imported from cytosol, where they are synthesized. The preproteins that were synthesized interact with chaperone and carried towards mitochondria, where they interact with various mitochondrial outer membrane translocase (Tom) complex, as the main entry gate into mitochondria (Fan et al., 2006), then later involve the translocase of the inner membrane (Tim) complex to transport preproteins across the inner membrane and mitochondrial intermembrane space import and assembly (Mia) complex. Different complexes will direct the preproteins to their respective destination and compartment in mitochondria. The proteins interplay is crucial to the import machinery of mitochondrial proteins which are encoded by nuclear gene.

Among the differentially expressed genes from my array, some of them are among the nuclear genes encoding mitochondrial proteins, and at least five of them have the sequence for direct targeting of WT1 genes (Table 6.1.2.1). This further strengthens the hypothesis that WT1 may have a more direct function in mitochondria system than previously thought.

In order to determine the role of WT1 gene in mitochondria system, further analysis was performed.

6.1 Mitochondrial related functional analysis, Public and Published Cross-Databases Analysis

6.1.1 ToppGene®

Ingenuity Pathway Analysis (IPA) is no doubt among the main choice for functional analysis for selections of interest genes, however, to increase confidence in the findings of this analysis, the microarray data was further analysed using the ToppGene Suite (http://toppgene.cchmc.org). Among the main uses of ToppGene® are to list out the functional enrichment for the selected genes, network analysis or functional annotation of candidate genes, and novel candidate gene identification for related diseases. The system uses several algorithms to compute any similarity between genes, then statistically combining individual scores and random sampling of whole genome to give p-values.

: Disease [Display Chart] 4092 annotations before applied cutoff / 16149 genes in category

	ID	Name	Source	pValue	FDR B&H	FDR B&Y	Bonferroni	Genes from Input	Genes in Annotation
1	cv:C0751651	Mitochondrial diseases	Clinical Variations	4.537E-10	1.857E-6	1.651E-5	1.857E-6	10	21
2	540000	MITOCHONDRIAL MYOPATHY, ENCEPHALOPATHY, LACTIC ACIDOSIS, AND STROKE-LIKE EPISODES; MELAS	OMIM	1.308E-5	2.324E-2	2.067E-1	5.354E-2	6	17

: GO: Cellular Component [Display Chart] 630 annotations before applied cutoff / 19061 genes in category

	ID	Name	Source	pValue	FDR B&H	FDR B&Y	Bonferroni	Genes from Input	Genes in Annotation
1	GO:0031226	intrinsic component of plasma membrane		2.052E-5	6.939E-3	4.874E-2	1.292E-2	96	1714
2	GO:0005887	integral component of plasma membrane		2.256E-5	6.939E-3	4.874E-2	1.422E-2	93	1651
3	GO:0098552	side of membrane		3.304E-5	6.939E-3	4.874E-2	2.082E-2	38	510

Figure 6.1.1.1: Cellular component and disease list categories annotated from e17.5 kidney array list processed through ToppGene website, showing the significant genes related to the individual components, listing the p-values, and the genes from input and annotated.

The two highest and the only significant (p-value < 0.05 with post hoc Bonferroni correction) disease list in this algorithmic analysis is of the mitochondrial disease. 10 out of 21 annotated genes accounts for this list, including all tRNAs that changed in the array list and complex 1 subunit. This further implicates mitochondrial function as one of

the most important mechanisms in the mutant model. The highest listed significant (p-value < 0.05 with post hoc Bonferroni correction) changes are the component of plasma membranes, either integral, intrinsic and the sides. Most of these have to do with transportation of molecules between the two sides of membranes. This can be considered logical as kidney function is to filter in and out selected molecules, and changes of these genes might implicate some abnormality in regard to its ability to maintain normal function that might later on predispose to secondary and progressive damage by stress throughout life.

6.1.2 MitoCarta 2.0

To directly assess the potential mitochondrial involvement of differentially expressed genes in DDS/+ foetal kidneys, the e17.5 array list (converted to ENSM gene ID) was cross-referenced to the MitoCarta 2.0 Mouse gene list that was updated recently. The MitoCarta 2.0 database represents a comprehensive, highly curated, representation of seven proteomic analyses of mitochondrial sub-compartments.

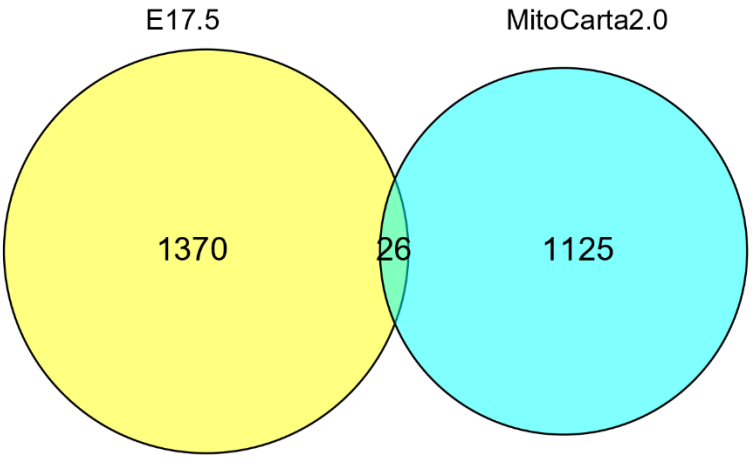

Figure 6.1.2.1: Venn diagram of E17.5 array gene list and mitochondria MitoCarta 2.0 Mouse gene list (latest update and last accessed September 2016).

The e17.5 array genes total to 1396 when converted from Affy_Mogene_1_0_St_V1 gene ID to Ensembl Gene ID (ENSMUST) and MitoCarta 2.0

Mouse consist of 1151 genes as September 2016. The common genes of the two databases are listed on table below, together with any presence of WT1 bindings sequence and the array expressions of each genes, together with the full names.

E17.5 vs MitoCarta2.0	***WT1 interacting sequence (developing kidney ChIP)***	***WT1 interacting sequence (podocyte ChIP)***	***Lfc***	***Array expression***	
LYRM4	*yes*	*No*	-0.1795036	*down*	*Mus musculus LYR motif containing 4*
SLC25A40	*yes*	*No*	-0.3736200	*down*	*Mus musculus solute carrier family 25, member 40 (Slc25a40), nuclear gene encoding mitochondrial protein*
SLC25A14	*yes*	*Yes*	-0.2687070	*down*	*Mus musculus solute carrier family 25 (mitochondrial carrier, brain), member 14 (Slc25a14), nuclear gene encoding mitochondrial protein*
CLPB / Rpl31	*yes*	*No*	-0.3278431	*down*	*Mus musculus ribosomal protein L31, mRNA*
TXNRD2	*yes*	*Yes*	-0.0973281	*down*	*Mus musculus thioredoxin reductase 2 (Txnrd2), nuclear gene encoding mitochondrial protein*
OXR1	*yes*	*No*	-0.1604140	*down*	*Mus musculus oxidation resistance 1 (Oxr1)*
STOM	*yes*	*Yes*	-0.3308239	*down*	*Mus musculus stomatin (Stom)*
tRNA-His	*no*	*No*	-1.5387803	*down*	*NC_005089 ::: gi|34538597|ref|NC_005089.1|:11546-11612*
tRNA-Arg	*no*	*no*	-1.1811108	*down*	*NC_005089 ::: gi|34538597|ref|NC_005089.1|:9808-9875*
MTERF4 / Mterfd2	*no*	*No*	-0.2057496	*down*	*Mus musculus MTERF domain containing 2 (Mterfd2)*
FOXRED1	*no*	*No*	-0.1813044	*down*	*Mus musculus FAD-dependent oxidoreductase domain containing 1 (Foxred1)*
RNMTL1	*no*	*No*	-0.1580168	*down*	*Mus musculus RNA methyltransferase like 1 (Rnmtl1)*

PCK2	*no*	*Yes*	0.1363217	*up*	*Mus musculus phosphoenolpyruvate carboxykinase 2 (mitochondrial) (Pck2), nuclear gene encoding mitochondrial protein*
COX17	*no*	*No*	-0.3244111	*down*	*Mus musculus cytochrome c oxidase, subunit XVII assembly protein homolog (yeast) (Cox17)*
PDHA2	*no*	*No*	0.1667518	*up*	*Mus musculus pyruvate dehydrogenase E1 alpha 2 (Pdha2)*
TUFM	*no*	*No*	-0.1765575	*down*	*Mus musculus Tu translation elongation factor, mitochondrial (Tufm), nuclear gene encoding mitochondrial protein*
UQCRC1	*no*	*no*	-0.1394423	*down*	*Mus musculus ubiquinol-cytochrome c reductase core protein 1 (Uqcrc1)*
LETMD1	*no*	*Yes*	-0.1472563	*down*	*Mus musculus LETM1 domain containing 1 (Letmd1)*
TMEM11	*no*	*Yes*	0.1277565	*up*	*Mus musculus transmembrane protein 11 (Tmem11)*
SLC25A18	*no*	*Yes*	0.3162048	*up*	*Mus musculus solute carrier family 25 (mitochondrial carrier), member 18 (Slc25a18), nuclear gene encoding mitochondrial protein*
CPS1	*no*	*No*	0.0853237	*up*	*Mus musculus carbamoyl-phosphate synthetase 1 (Cps1), nuclear gene encoding mitochondrial protein*
OPA1	*Yes**	*No**	-0.1552420	*down*	*Mus musculus optic atrophy 1 homolog (human) (Opa1), nuclear gene encoding mitochondrial protein*
MAOB	*no*	*No*	-0.57487	*down*	*Mus musculus monoamine oxidase B (Maob), nuclear gene encoding mitochondrial protein*

Table 6.1.2.1: List of genes with description of nuclear gene encoding mitochondrial protein, mRNA. Listed also the presence of direct WT1 target sequences and changes

*of their respective expression in DDS/+ kidneys. Developing kidney Wt1 ChIP (https://www.ncbi.nlm.nih.gov/geo/query/acc.cgi?acc=GSE58179), Podocyte Wt1 ChIP (https://www.ncbi.nlm.nih.gov/geo/query/acc.cgi?acc=GSE64063). *Note: Opa1 has 3 Wt1 binding sites in both developing kidneys and podocytes identified by ChIP that are between 50-80Kb downstream of the gene.*

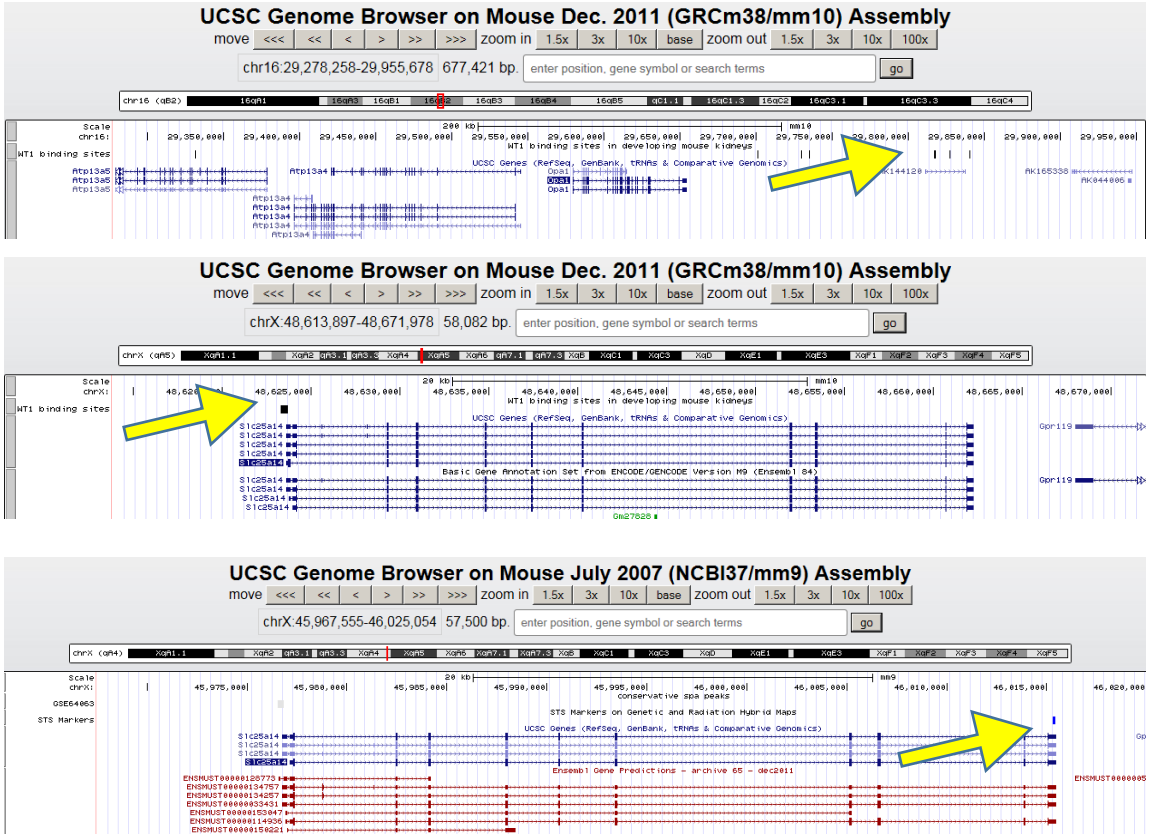

Figure 6.1.2.2: ChIP data visualised using UCSC Genome Browser: Downstream elements associated with Opa1 are shown, plus the more typical pattern of Wt1 binding sites at transcription start site, shown for Slc25A14 (developing kidney upper panel, black bar, podocyte lower panel, grey bar).

Thus, several nuclear genes encoding mitochondrial proteins that are potentially regulated by Wt1 are differentially expressed in DDS/+ kidneys. However, none of these have previously been identified as *bona fide* Wt1 target genes prior to this, but the positive findings from ChIP-seq represents strong evidence (Table 6.1.1.1).

6.1.3 STRING database

Given that none of the identified genes has previously been studied in the context of Wt1, further *in silico* analysis was carried out to further investigate the relationship, if any, between these genes using the STRING online website. STRING (Search Tool for the Retrieval of Interacting Genes/Proteins) is a web resources for biological database used for predicting protein–protein interactions and network interactions (Lehmann et al., 2000). The STRING database contain experimental data, computational algorithmic prediction and public data collections. The system also highlights functional enrichments of user listed genes and proteins, incorporating other functional classification systems including GO, Pfam and KEGG.

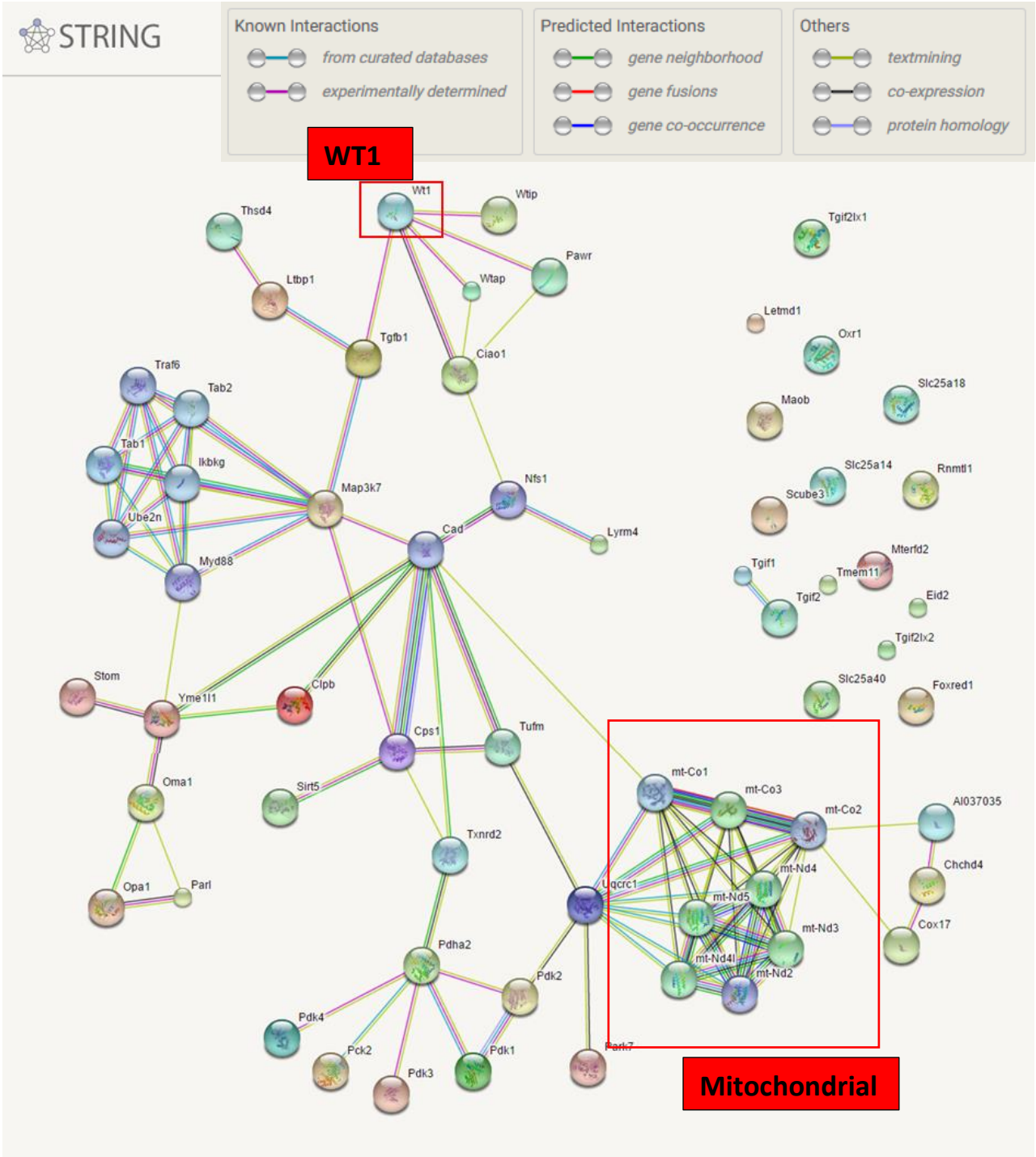

Figure 6.1.3.1: STRING analysis of mitochondrial related genes. 26 cross-database listed genes plus additional system genes (up to 10 interactor gene setting) to fill in the gap of network. See appendix for each gene annotated functions. WT1 is highlighted in the red box, showing its permutated downstream interactions with mitochondrial genes

at the bottom right of the figure. The meaning of each coloured connection is in the legend at the top of the figure. Please refer to appendix Table A-6.1.3.1 for gene annotation for STRING analysis.

In the figure 6.1.3.1 showing STRING analysis, there are strong nodes of interaction featuring Map3k7 and mt-ND3, for example, however, the genes that contain Wt1 binding sites within their promoters are randomly distributed across the network, either not clustering or in many cases showing no interactions (individual node not connected to other node). It should be noted that Wt1 links to the major nodes via TGFß1 or a single link between Ciao1 and Nfs1 (both are not significantly changed in the array, but both have WT1 binding region from developing kidney ChiP). Association analysis like this were hoped give meaning and show specificity, such as those that share common function, however those does not necessarily bind close to each other. STRING database include a lot of sources, including public text, experimental data, and those predicted by computational algorithm. It is a tool and resource for further experiment and analysis.

Whilst this analysis indicates the evidence for Wt1 involvement in known gene networks is weak, this most likely reflects the novelty of the findings and, without experimental verification, these results must be treated with caution.

6.2 Mitochondrial function: Succinic dehydrogenase (SDH) and Cytochrome oxidase (COX) staining

In order to observe mitochondrial activity within the developing kidney, COX-SDH staining was performed on cryostat sections from e18 of DDS/+ and wild type kidneys. This staining is done in conjunction with the Mitochondrial Group at Institute of Genetic Medicine. This specific staining method of mitochondrial activity has previously been optimized for muscle fibres. Complex IV, or cytochrome c oxidase (COX) reflects indirectly the mtDNA integrity, as the catalytic subunits of COX are encoded by mtDNA and are essential for assembly of the complex. Thus, proper synthesis and function are largely based on mtDNA integrity by observing the activity of the respiratory complex. Complex II, or succinate dehydrogenase (SDH), is entirely encoded by nuclear DNA.

And its activity is usually not associated directly to mtDNA dysfunction, however abnormalities in SDH may reflect abnormalities in mitochondria biogenesis (Tanji and Bonilla, 2001).

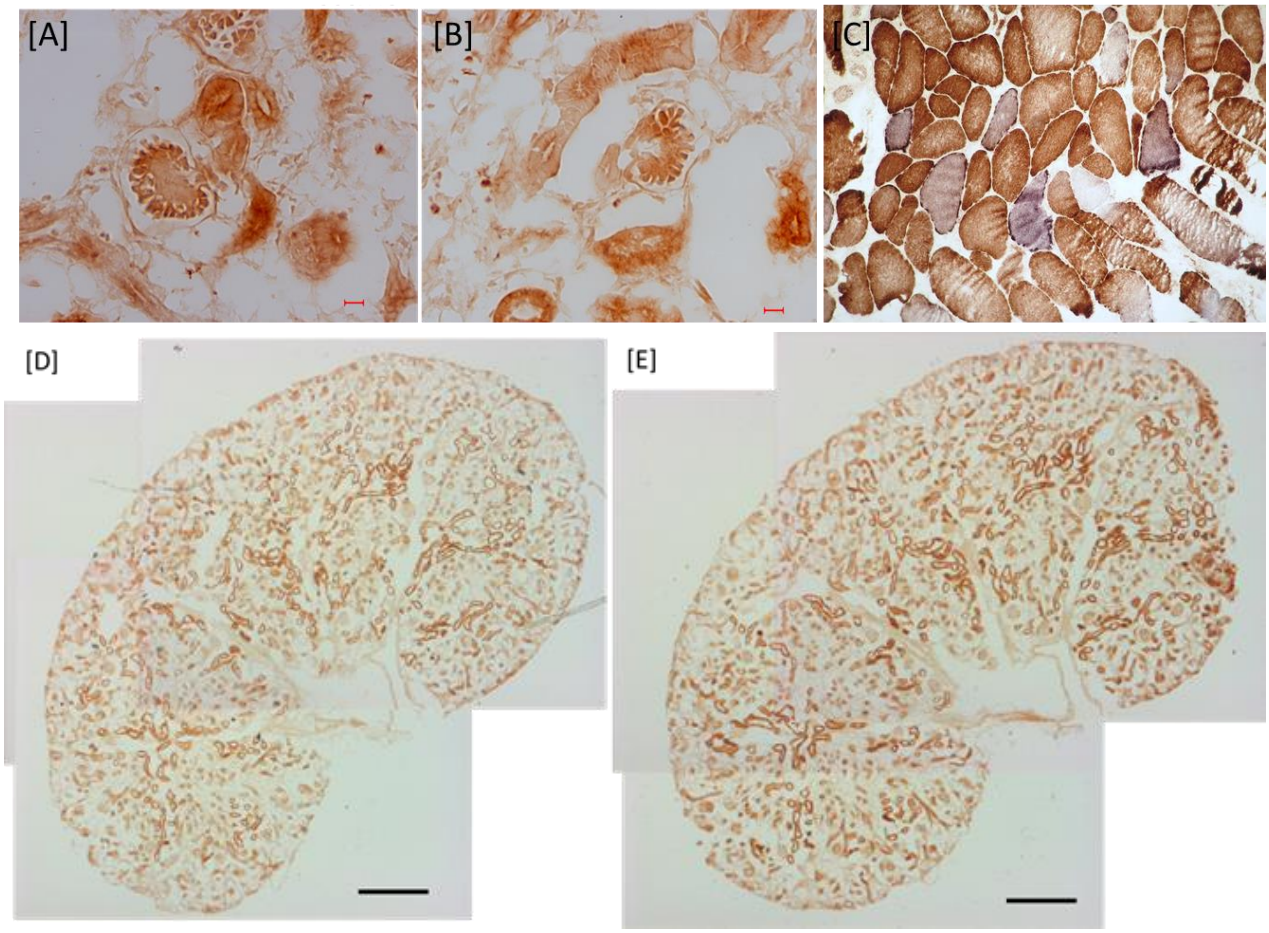

Figure 6.2.1: *Representative figures of Succinic dehydrogenase (SDH) and Cytochrome oxidase (COX) staining of e18 male mice kidneys of [A] wild type and [B] mutant. COX staining will show brown colouration and SDH staining show bluish staining if positive as in [C] muscle staining of myopathy. [D] Whole section of wild type, [E] whole section of mutant. Note there is no gross difference of the staining between the two glomeruli. Thank you to Jensflorian for positive control of Image [C]. N=3 wild types vs N=3 mutants.*

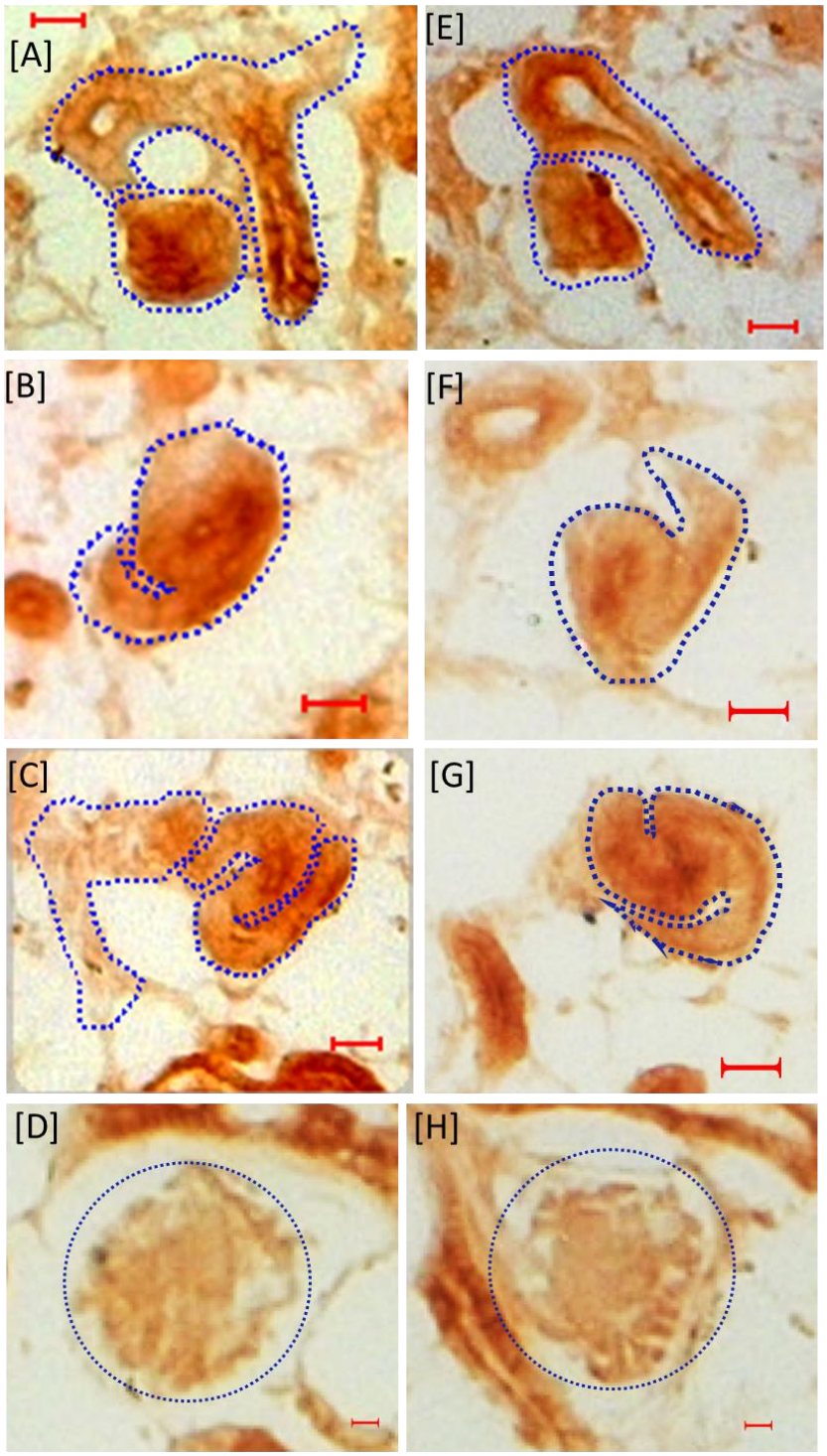

Figure 6.2.2: *Representative figures of COX-SDH staining of foetal kidney for every stage of nephron development from pre-tubular aggregates (PTA), comma shaped body, S-shaped body and glomerulus, Wild type [A] to [D], mutants [E] to [H]. [A] and [E] Pre-tubular aggregates, [B] and [F] comma-shaped bodies, [C] and [G] S-shaped bodies, [D] and [H] mature glomerulus. N=3 wild types vs N=3 mutants.*

Mutant and wild type glomeruli of similar developmental stage (blue arrows) show no differences in COX/SDH staining (Figure *6.2.1* and 6.2.2). Examining the overall patterns of COX/SDH staining of whole kidney cross sections and specific stages of nephron development (Figure 6.2.2), there were no dramatic alterations of those enzymatic staining in any kidney compartment comparing mutant to wild type. However, there is higher concentration of COX brownish staining, suggesting evidence of high mitochondrial activity within the developing nephron (comma- and S- shaped bodies) and in condensing mesenchyme at the ureteric bud tips, suggesting these stages of nephrogenesis may be sensitive to mitochondrial abnormalities. As for doing it during the e18 instead of e17.5, there should not be much of a different in physiology of the kidneys as it is still in the fast pace of nephron development, and any changes would be obviously reflected in these stages of nephron growth. In overall, there is no difference between wild type and mutant kidney, however, as this technique has not previously been applied to kidney, alternative analyses may be needed to draw a definite conclusion.

6.3 *ex-vivo* system for WT1

To create an ex-vivo system for WT1 dysfunction in cultured cells, mouse embryonic fibroblasts (MEFs) were isolated from homozygous “floxed” Wt1 embryos that carried a tamoxifen inducible, constitutively active, Cre recombinase transgene (R26-Cre-ERT2). Deletion of exon 9 of Wt1 resulting in truncation of zinc finger 3, transforming into a null allele in these mice. Whilst this is not the exact situation in *DDS*/+ mice, we reasoned that a complete loss of function may prove informative in terms of a potential role for Wt1 in mitochondria.

6.3.1: DDS20 is a null allele.

In order to determine if the DDS20 Wt1 “floxed” mice were comparable with DDS/+ mice, homozygous DDS20 containing the inducible Cre-loxP system were bred. When the female mouse pregnant at e19, a dose of tamoxifen was given subcutaneously to induce deletion of exon 9 in the littermates. Kidneys of littermates were taken, genotyped, and qRT-PCR was used to measure expression of several of the differentially expressed genes previously identified by microarray analysis of DDS/+ kidneys in newborn kidneys of DDS20 mice treated with tamoxifen. The most significantly downregulated genes in DDS/+mice were all similarly downregulated in newborn DDS20 mice. The comparison is between mice given tamoxifen and mice not given tamoxifen.

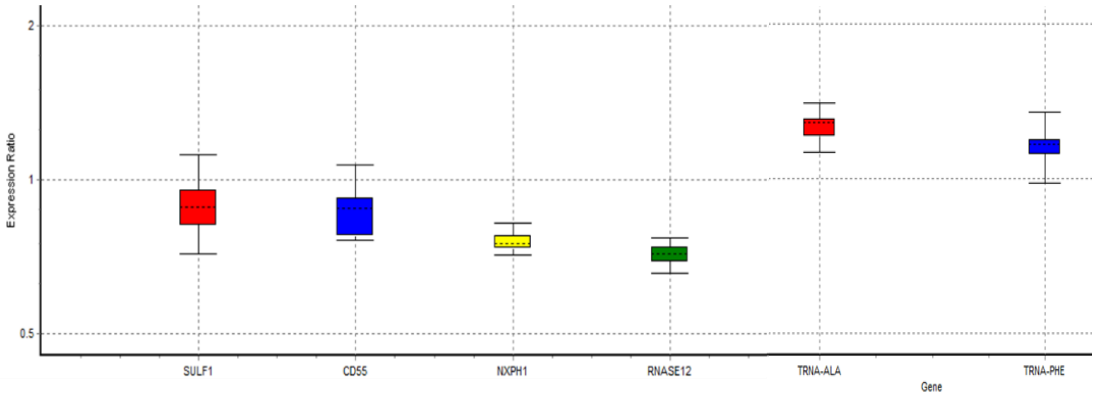

Figure 6.3.1.1: qRT-PCR of day one newborn mice kidney after injection of Tamoxifen at e19 of pregnant mice. Nuclear genes Sulf1, CD55, Nxph1, and Rnase12 show significant downregulation with p-value<0.05 (normalised to GAPDH, B-actin, HPRT) and mitochondrial genes tRNA-Ala and tRNA-phe show upregulation (p<0.05) (normalised to ND5).

Sulf1, CD55, Nxph1, and Rnase12 genes were chosen as target for this qRT-PCR because Sulf1, CD55 and Rnase12 are at the top of the list in micro array and Nxph1 is at the bottom region and gene changes in the array (p>0.05). Sulf1 is a direct target of WT1 binding and inhibits signalling by heparin-dependent growth factors, diminishes proliferation, and facilitates apoptosis in response to exogenous stimulation. CD55 is a WT1 target from developing kidney ChiP dataset and involved in the

regulation of the complement cascade. Nxph1 is a WT1 target from developing kidney ChiP dataset and part of a group of proteins that promote adhesion between dendrites and axons. Rnase12 has no known WT1 target site and involve in nucleic acid binding and ribonuclease activity. The reason e19 was chosen as a time because by experience, injection at earlier time points contribute to early sudden death of pregnant mouse and littermates.

6.3.2 DDS20 Mouse Embryonic Fibroblast

However, analysis of Wt1 conditional-null mouse embryonic fibroblasts isolated from DDS20 mice and treated with tamoxifen revealed dramatic differences in the response to Wt1 mutation in kidneys compared with MEFs. Most notably, those downregulated genes were, in fact, upregulated upon Wt1 inactivation and mitochondrial tRNA genes also showed some discrepancies. Although discrepancies were seen, these discrepancies still involve the genes that were dysregulated from the array list. MEF was chosen because it was intended to be a replacement system to investigate changes downstream to WT1 genes, as a result from WT1 mutation. The reason replacement is needed because DDS/+ strain mice have a very serious problem of breeding difficulties. Although DDS20 strain used for MEF do breed slowly, it is still acceptable in order to be used as replacement.

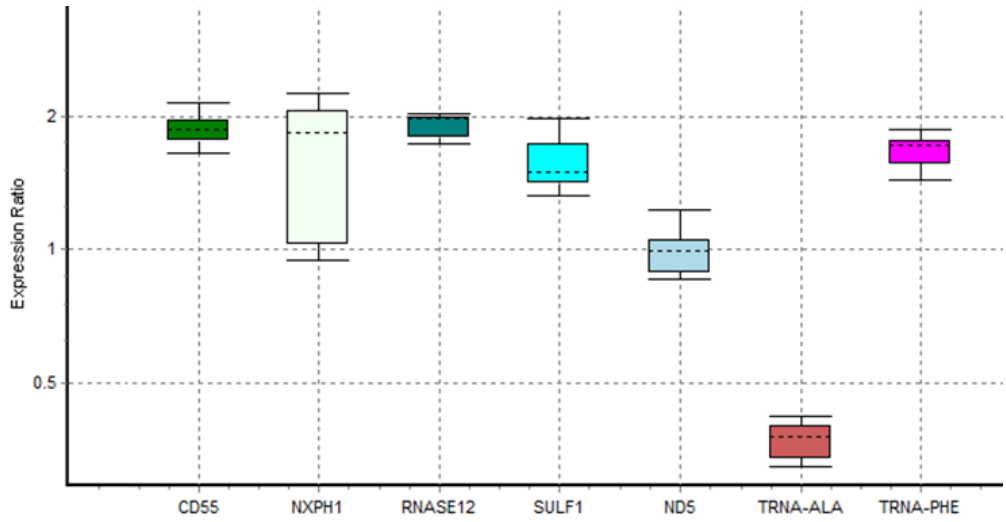

Figure 6.3.2.1: qRT-PCR of mouse embryonic fibroblast (MEF) after cultured, and introduction of Tamoxifen for 48 hours for exonal deletion and confirmed for of exon 9 deletion by PCR genotyping. Nuclear genes Sulf1, CD55, Nxph1, and

Rnase12 show significant downregulation with p-value<0.05 (normalised to GAPDH, B-actin, HPRT), except for ND5 which was unchanged (used for normalisation of mitochondrial genes).

The dramatic cell-type specific differences most likely reflect the mode of action of Wt1 itself – recently it has been shown that Wt1 protein can occupy the same genomic location (bind the same sequence of a specific gene) but contribute to either gene activation or repression depending upon cell type.

Furthermore, examination of gene expression profiles of MEF cells available via GEO (https://www.ncbi.nlm.nih.gov/geo/query/acc.cgi?acc=GSE15325) reveals that both Sulf1 and CD55 are, in fact, upregulated in Wt1 mutant MEFs, consistent with the findings on DDS20 MEFs.

ID	P.Value	logFC	Gene.symbol	Gene.title
1436319_at	1.10E-04	0.5591	Sulf1	sulfatase 1
1418762_at	0.008024	2.529887	Cd55	CD55 molecule, decay accelerating factor for complement
1443906_at	0.012715	2.412084	Cd55	CD55 molecule, decay accelerating factor for complement
1460242_at	0.009413	2.31916	Cd55	CD55 molecule, decay accelerating factor for complement

Table 6.3.2.1: Gene expression profiles of Sulf1 and CD55 from MEF cells available via GEO (https://www.ncbi.nlm.nih.gov/geo/query/acc.cgi?acc=GSE15325) showing the changes of expression in MEF with WT1 mutation.

Whilst it appears that tRNA-Ala and tRNA-Phe behave in different ways, it should be noted that tRNA-Ala $P<0.009$, whereas tRNA-Phe is far less significant $P<0.046$. This may reflect the fact that tRNA-Ala is encoded by the mitochondrial Light strand, whereas tRNA-Phe is encoded by the Heavy strand.

Despite differences between MEF cells and developing kidney, DDS20 MEFs will provide a cell-culture based system with which to investigate the consequences of Wt1 loss of function on mitochondria using various methods.

As the MEF cells were different from DDS/+ mutant mouse foetal kidney, we analysed the expression pattern of selected genes in MEF and compare it to our e17.5 foetal kidney. Expression of tRNA-Ala (the gene with the highest fold change in kidneys) was reduced in MEFs lacking Wt1. This MEF system was initially intended for us to use to represent the finding seen in our e17.5 DDS/+ kidney. Regardless of the dissimilarity of in-vivo and in-vitro system, the finding relating to the mitochondrial cannot be disregard.

MEF system in this case was not intended to look upon similarity to the actual kidney microarray data, but to look into the feasible separate *ex vivo* system can show changes when WT1 is knock-out. In this case, yes, this MEF system provide another tool to investigate the upstream and downstream genes regulation of WT1 gene. We have the intention of proceeding with another microarray or gene sequencing specifically for MEF in this case to look deeper into WT1 gene regulation, specific to MEF knockout.

6.3.3: MitoTracker® staining

In order to investigate the role of WT1 in mitochondrial biology in mouse embryonic fibroblast (MEF) in more detail, mitochondrial network analysis was undertaken using MitoTracker® in order to visualise mitochondrial networks following fluorescent staining. This technique is typically used to study monolayer cells growing in culture as it involves staining live cells. The mitochondrial probe MitoTracker® does not florescent in aqueous solution. Upon uptake and accumulation in the mitochondria, it will give a red fluoresce signal, without any effect from mitochondrial membrane potential. MitoTracker® allows observation of the mitochondrial morphology in these cells in the

presence/absence of functional Wt1. Wild type MEF (no Tamoxifen) acted as the control, showing normal appearance of MitoTracker® within cells and MEF flox-Cre (Tamoxifen), Cre induced floxed exon 9 deletion of WT1 genes would be the subject of interest.

The mitochondrial staining shows clustering and fragmentation of MitoTracker® in mutant that differentiates it from the wild type. It is interesting to see that mutation of WT1 and disruption of its function leads to aggregation of mitochondria in the MEF. MitoTracker® staining of MEF cells with and without Cre activation revealed multiple clustering of mitotracker signals seen in the cytoplasm of MEF Flox-Cre, ie, those lacking Wt1 (Figure 6.3.3.1).

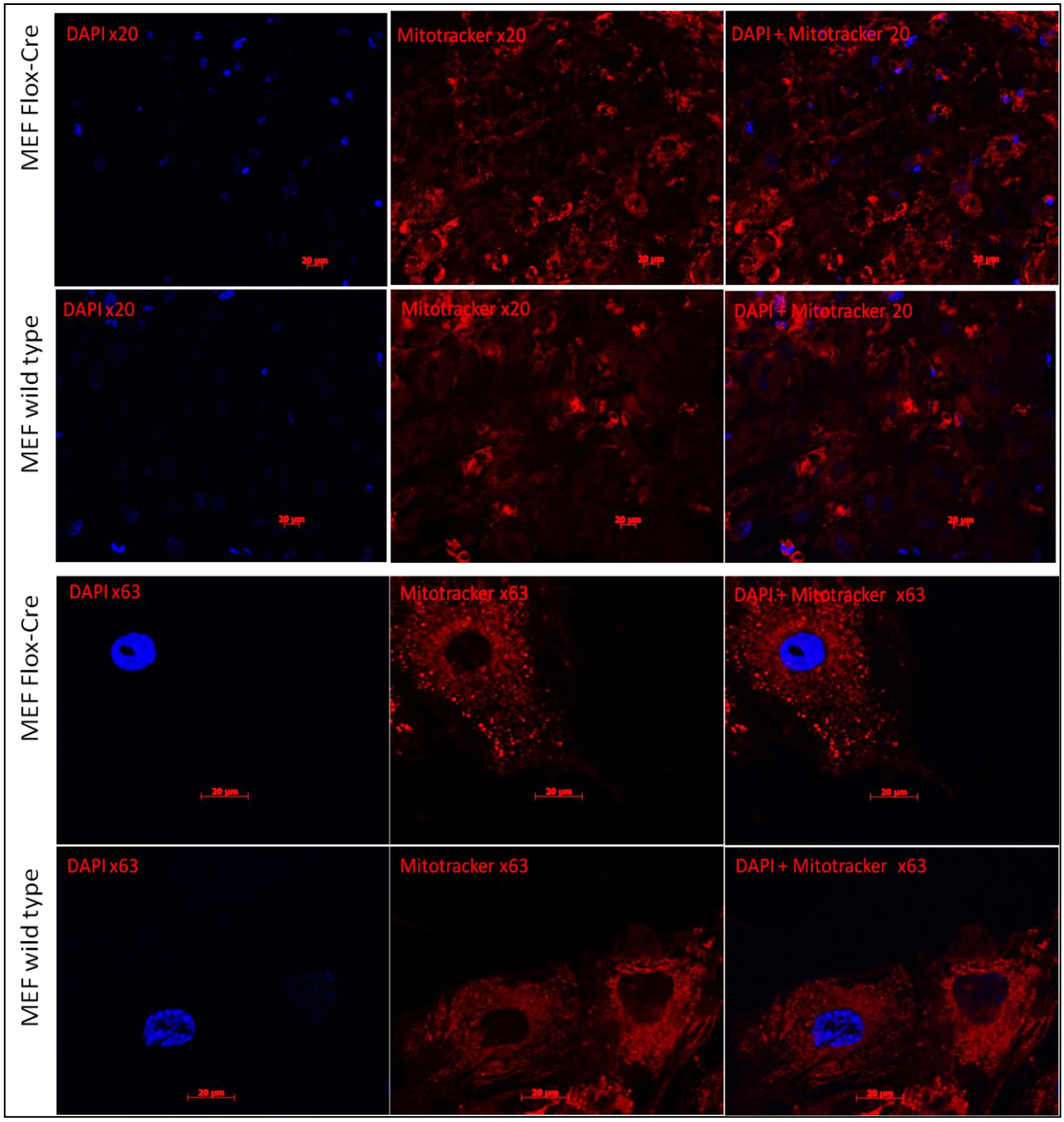

Figure 6.3.3.1: Immunofluorescence of mouse embryonic fibroblasts (MEFs) showing mitotracker staining in wild type MEF (no Tamoxifen) and MEFflox-Cre (Tamoxifen), Cre induced floxed exon 9 of WT1 genes, showing the appearance of fragmentation. x20 magnification. N=4 wild type (as control) vs N=4 mutant MEF, repeated on 3 different batched of MEFs.

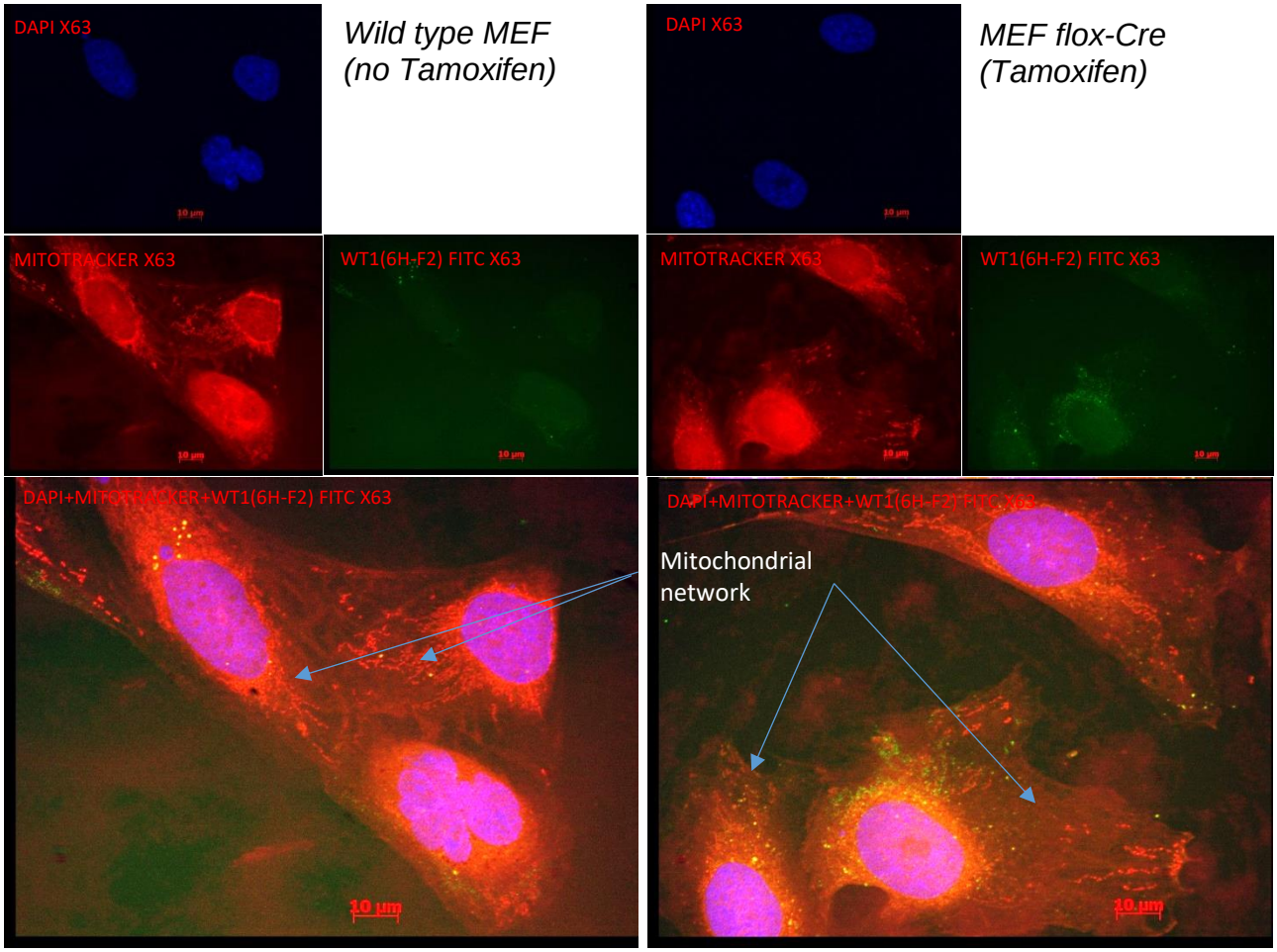

Figure 6.3.3.2: Representative figure showing disruption of mitochondrial network / Double immunostaining. X63 magnification. N=4 wild type (as control) vs N=4 mutant MEF, repeated on 3 different batched of MEFs.

In normal wild type, when stained for mitochondria using MitoTracker®, the mitochondrial network would show continuous trail of 'connecting' beads, this is what is referred to mitochondrial networks. In MEF (Tamoxifen), this network shows discontinuity, and seems to cluster in small groups. This is the most likely reason why it seems to be fragmented/clustered when seen at lower magnification. These finding correlates with the downregulation of Opa1, as mutation in Opa1 has been shown to cause fragmentation (Wai et al., 2015).

6.3.4: Flow cytometry analysis

In order to quantify and confirm the aggregation of MitoTracker® signal that was evident in under fluorescence microscopy in MEF cultured cells, flow cytometry was used. From visual observation of MEFs under the microscope, the mutant MEF (Tamoxifen) is easier to recognised and identified as it shows more florescence signal compared to wild type MEF (no Tamoxifen) at similar exposure setting.

Two batches of MEF cells (wild type and “floxed Wt1”) were treated with Tamoxifen for 48 hours and then further diluted and passaged until passage five to eliminate any residual Tamoxifen. The disruption of Wt1 by Cre-loxP mediated recombination was confirmed and the cells were stained with MitoTracker® and then analysed.

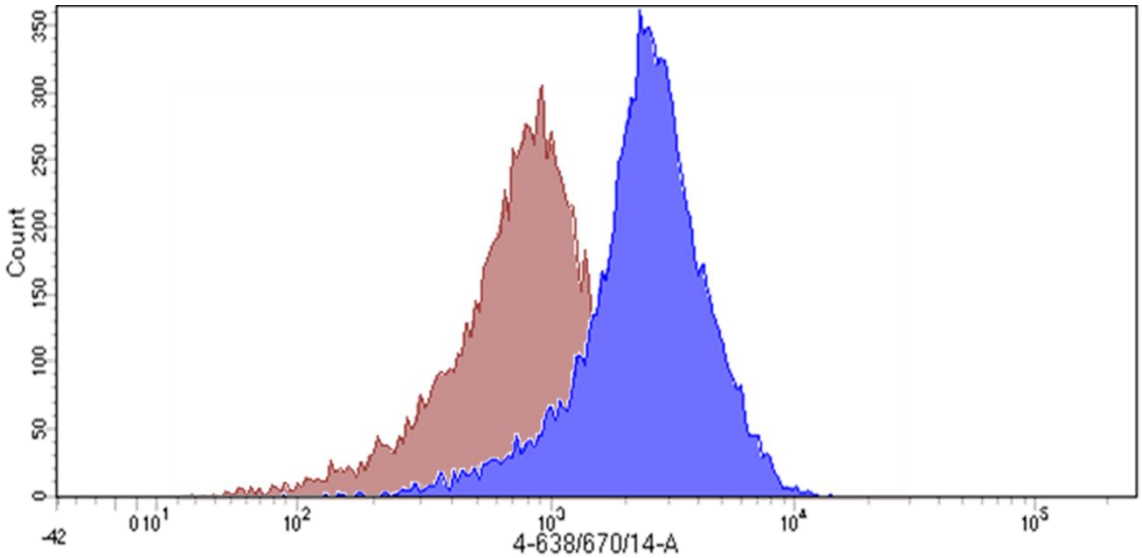

Figure 6.11: Figure showing MFI (Mean florescence intensity) of flow cytometry analysis of wild type + TAM (dark red) and WT1ex9-/- cre + TAM (blue) MEF cells labelled with Mitotracker® Deep Red. Fluorescence intensity is displayed on the x-axis (logarithmic), with the number of cells containing that fluorescence level plotted on the y-axis). N=4 wild type vs N=4 mutant MEF. This experiment was repeated two times with N=7 different MEF on the second run, with similar finding seen.

From the figure, there is a clear different between the two groups of cells. The wild type cells show an average fluorescence intensity of ~800 (red graph), whereas the mutant cells show an average fluorescence intensity of ~2500 (blue). The MitoTracker® seems to be retained more and aggregate inside the mutant cells, consistent with the fluorescence microscopy. Given the mechanism of MitoTracker® which permeates through the mitochondrial membrane, to see more signals in the mutant indicates some level of abnormal function of the membrane system or changes towards the membrane potential or may also indicates increment of mitochondrial mass.

6.4 – WT1 localisation within mitochondria

6.4.1 – WT1 localisation in e17.5 kidney fraction

Although there is a lack of very strong evidence that Wt1 regulates expression of nuclear-encoded mitochondrial proteins, multiple mitochondrial tRNA species were within the top differentially expressed genes in DDS/+ kidney when ranked in terms of fold-change or p-value. As Wt1 is known to encode a multifunctional protein that has been linked to transcription, RNA processing and translation, and has been shown to shuttle between nucleus and cytoplasm, it is possible that Wt1 exerts a direct effect on tRNA expression within mitochondria. In order to test whether WT1 protein is present and, thus has the potential to directly interact with mitochondrial protein inside mitochondria, western blotting was carried out on fractionated mouse fetal kidneys. Mitochondria were isolated using a commercially available mitochondrial isolation kit (Thermo Fisher) to provide isolated mitochondrial, nuclear and cytoplasmic protein fraction.

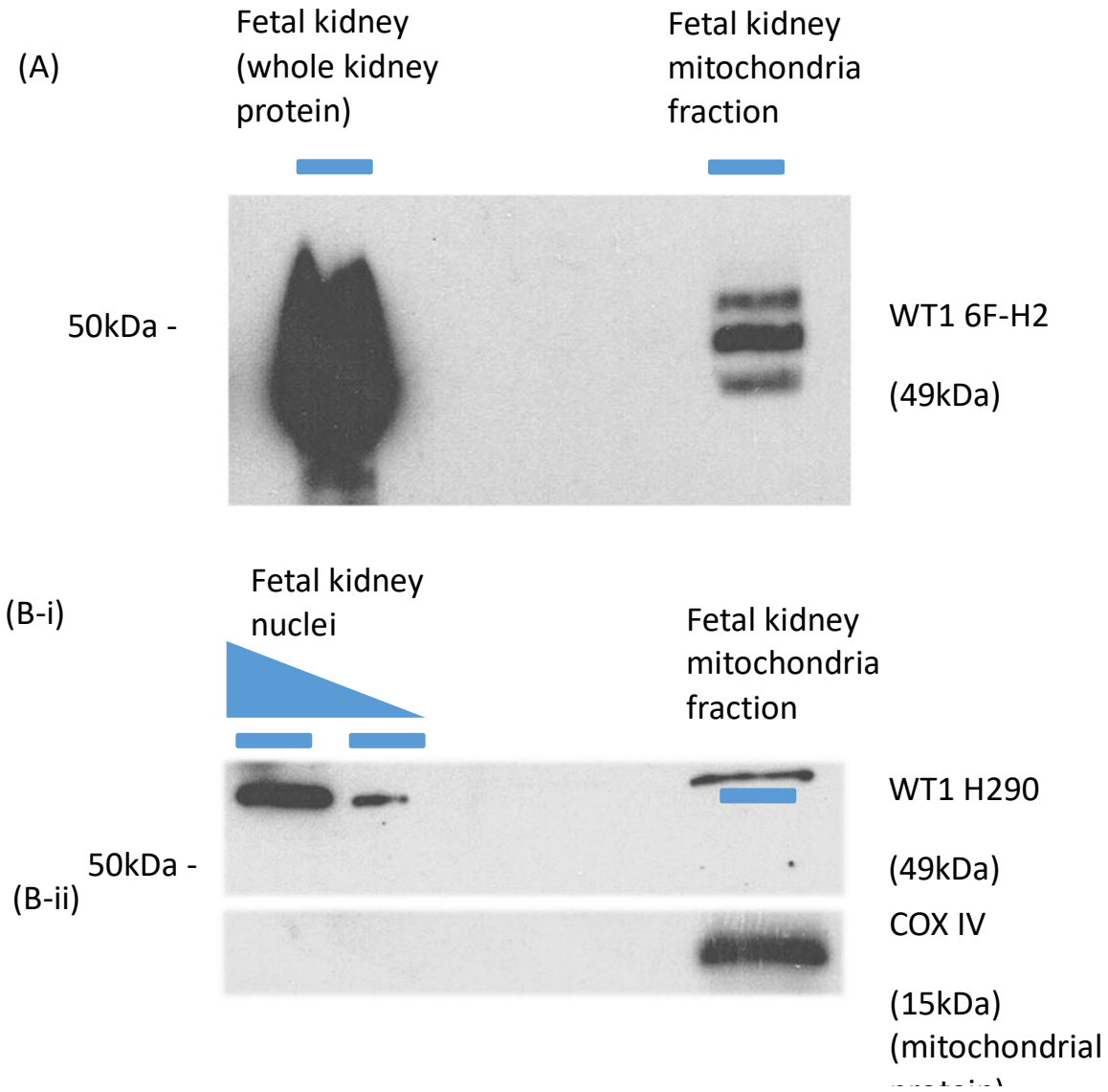

Figure 6.4.1.1: Western blots of wild type e17.5 foetal kidneys, isolated foetal kidney nuclei, and isolated mitochondrial. Three antibodies were used, A) WT1 6F-H2, B-i) WT1 H290, B-ii) COXIV (mitochondrial) antibody were used to confirm the presence of mitochondrial protein. Figure A is overexposed.

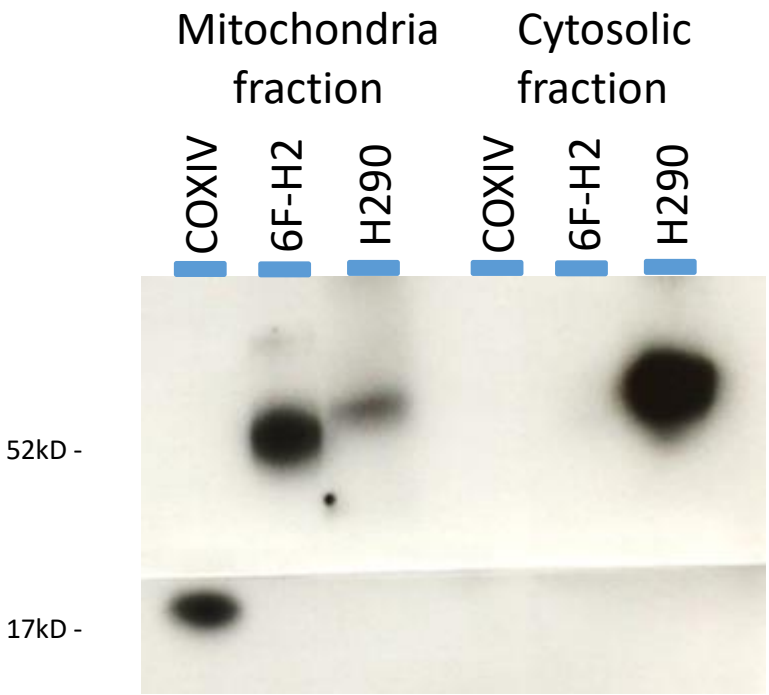

Figure 6.4.1.2: Western blots of wild type e17.5 foetal kidneys, isolated foetal kidney cytosolic fraction. Three antibodies were used, WT1 6F-H2, WT1 H290, COXIV (mitochondrial) antibody was used to confirm the presence of WT1 protein inside mitochondrial fraction. No COXIV band seen in cytosolic fraction. The blot been cut separately for ease of staining of primary and secondary antibody.

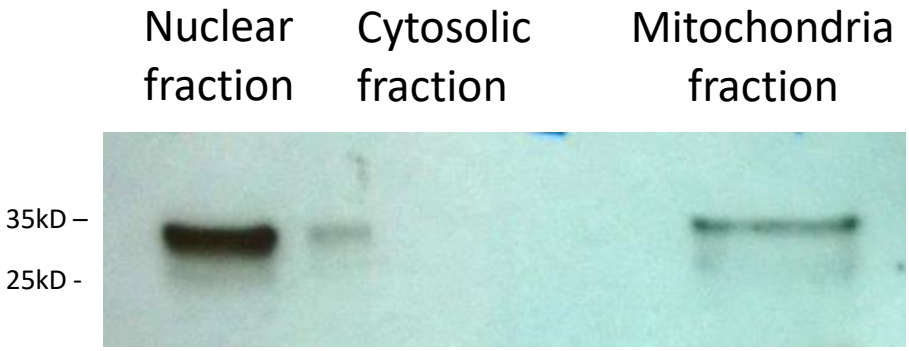

Figure 6.4.1.3: Western blots of wild type e17.5 foetal kidneys, isolated foetal kidney cytosolic fraction, nuclear fraction and mitochondrial fraction of PCNA antibody, intended as control for nuclear fraction.

The western blots show two different WT1 antibodies that were used to identify WT1 proteins from the mitochondrial isolates. 6F-H2 antibodies bind to N-terminal region of protein whereas H290 bind to middle part of WT1 protein. COXIV antibodies were used to confirm the presence of mitochondrial proteins. Although Figure 6.4.1.1-A is overexposed, it is suggestive of similar weight of protein seen. Figure 6.4.1.2 shows similar antibodies in cytosolic fraction and mitochondrial fraction. Only anti-H290 band was seen in cytosolic fraction, and this most likely due to its binding in the middle site of WT1protein compared to 6F-H2 which bind to N-terminal side, or maybe WT1 protein too diluted in cytosol to be detected with 6F-H2 antibody. Figure 6.4.3 show PCNA antibody staining, initially intended for nuclear control as it was the only nuclear antibody I have at the time of experiment. However, PCNA antibody may stained minimally in cytoplasm and in mitochondria (Naryzhny and Lee 2010). Given the option in the future, other nuclear antibody can be look into and tested on fractions as not all nuclear specific antibodies commercially available stained specifically only to nuclear fraction.

For these western blots, only wild type mice foetal kidneys were used, due to the difficulties in obtaining more DSS/+ mice within the timeframe of the project. This was because the DDS/+ strain of mice are very difficult to breed as they have the inherent problem of sexual organ development. When we need e17.5 kidneys, each pregnant female mouse must be killed too plus littermate count are usually varied from 1 to 5, disregarding the genotype that one-third of the time are wild types. In addition, the size of e17.5 kidneys are very small, about 2mm in length, therefore a number of e17.5 kidneys are required in order to get enough biological samples for a number of different experiments. This is a real challenge, due to the physiological nature of this mice. Due to this inherent difficulty, experiments with e17.5 kidneys are difficult to repeat.

The localization of WT1 protein in mitochondria (Figure 6.4.1.1 and 6.4.1.2*)* suggests a direct function for WT1 in mitochondria and interactions with mitochondrial proteins and processes, but more evidence is needed to support this hypothesis. In doing this western blot, although the centrifugation technique used to separate the nuclei, cytoplasm and mitochondrial components is reliable, there is still a possibility of minimal contamination of different fraction extracts. With limited number of foetal kidneys available due to slow breeding and few adult mice available, extra repeats of the experiment were not plausible.

6.4.2 – Mouse Embryonic Fibroblast fraction comparison

Given that western blotting of cytoplasmic, nuclear and mitochondrial extracts derived from foetal kidneys had previously suggestive of Wt1 protein to be present within mitochondria, MEF cells were similarly fractionated into nucleus, cytoplasm and mitochondria. In order to see the differences in protein expression between the mutant and wild type condition, Western blot were done on MEF (no Tamoxifen) and MEF (Tamoxifen). Loading of protein fraction were calculated based on protein concentration measured on Nanodrop protein reader.

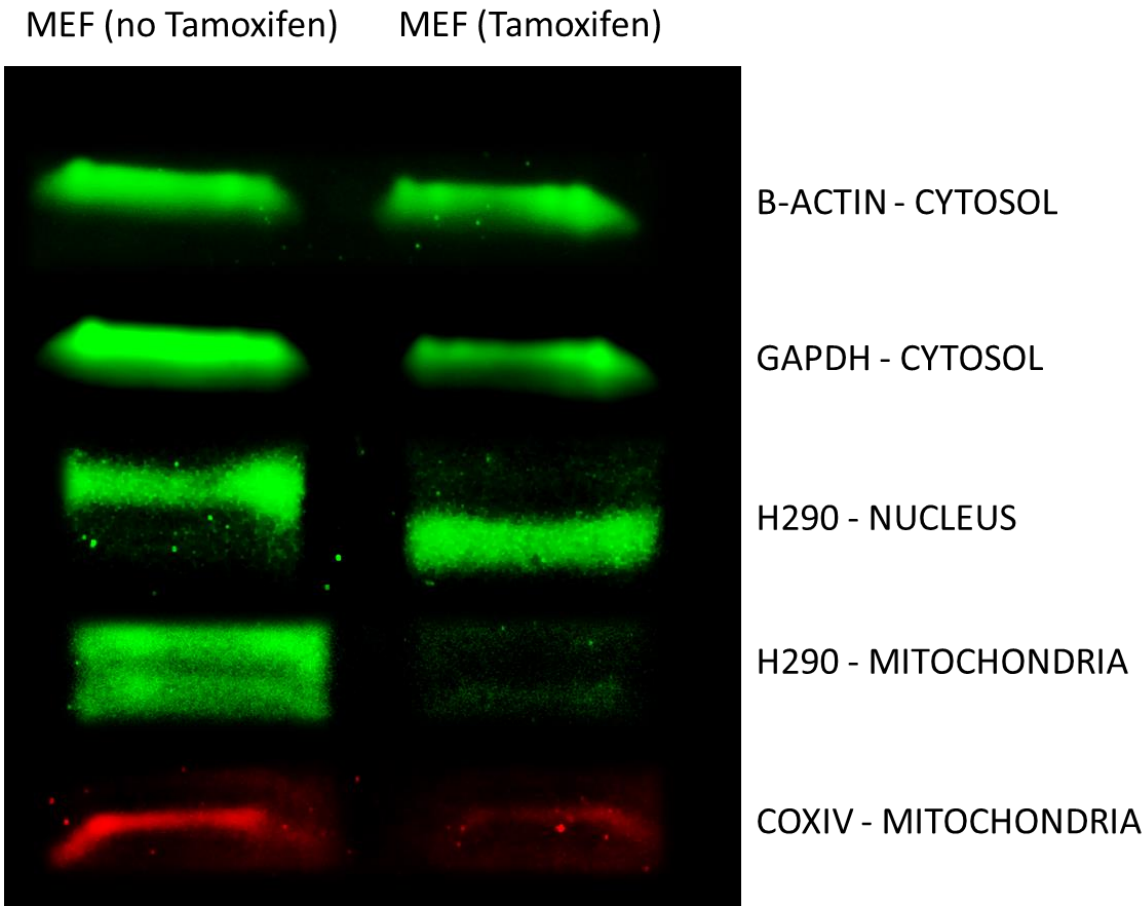

Figure 6.4.2.1: Western-blot (with florescence secondary antibody) of MEF (no Tamoxifen) and MEF (Tamoxifen) cell isolate of cytosols, nucleus and mitochondria. B-actin, Gapdh, H290 (WT1), and CoxIV were used. Protein were first quantified via nanodrop, and similar concentration were loaded for Western blotting for each fraction.

Note: To get an appropriate concentration of mitochondrial proteins for each run, similar fractions of each genotype were pooled together and quantified.

When western blotting is done comparing MEF (no Tamoxifen) and MEF (Tamoxifen), there are some differences that can be seen. The WT1 protein seems smaller in the nucleus as this can be attributed to the truncated mutant proteins with less pronounce band of normal WT1 protein allele. In mitochondrial, there seems to be less WT1 protein as compared to wild type mitochondrial isolates. COXIV protein expression also seems to be less in mutant compared to wild types when compared with ß-actin. To get an appropriate concentration of mitochondrial proteins, fractions were pooled of at least 8 tubes per run. This exhausted the fresh MEF fraction significantly, and difficult to control cross contamination of fraction. To get absolute isolated fraction at higher concentration is very difficult, but side-to-side comparison would give a better general idea of the differences between control and mutant.

It is also reasonable that fractionation procedure may introduced contamination of each fraction to one another. This is also an issue to keep in mind. To overcome this, the most appropriate way I think plausible is to increase the protein concentration of each fraction and introduced fewer primary antibodies. But in my case, it is almost not plausible to test this method given the limited amount of protein fractioned per each very small kidneys, the breeding difficulty, and also limited number and lifespan of primary MEF cultured (to remind, MEF is cultured from body of e14 mice, taken from culling pregnant mice, thus downsizing the breeding pool of the mice, not to mention only small number of MEF carried heterozygous Cre and loxP sequence).

With many of the mitochondrial gene expression to be lowered compared to the wild type, it is not surprising to see lowered protein expression in mutant mitochondrial. However, to see a lowered content of WT1 might attributes to the normal dysregulated of its normal role within mitochondrial system. This might be due to lowered normal WT1 protein inside mitochondrial, or it can also be attributed to the possibility of malfunction mutant protein (dominant negative effect), it is uncertain at this moment. More evidence is needed to make a conclusive summary.

Given that Wt1 “conditional knockout” MEFs display evidence of mitochondrial abnormality, these cells could be subjected to a more rigorous examination of mitochondrial function.

6.5 Comprehensive mitochondrial analysis using metabolic profiling

Previously, in other studies, in order to assess mitochondrial function in cultured cells, methods utilising probes to detect oxygen consumption were carried out on intact mitochondrial organelles and enzyme activities were measured in lysates. However, those methods required extensive manipulations such as cell lysis that risk disturbing the biological function that one intends to measure. The ability to measure actual live intact cells provides insight into the actual physiological function of the mitochondria (Will et al., 2006, Brand et al., 2011). Currently the standard protocol to measure changes of oxygen consumption of cultured cells use an electrode called Clark electrodes (Clark et al.,1953). Recent advancement has miniaturised and adapted oxygen consumption probes into improved fluorimetric systems for adherent cells in culture (Wu et al., 2007, Ferrick et al., 2008, Gerencser et al., 2009).

The Seahorse XFe96 Analyzer from Seahorse Bioscience Agilent Technologies allows for measurement of Oxygen Consumption Rate (OCR) which reflects oxidative phosphorylation and Extracellular Acidification Rate (ECAR) which reflects glycolysis with measurement of O_2 and protons (pH) in cell culture of live intact cells in a 96-well plate and accurately quantify mitochondrial function in intact cells (Dranka et al., 2010, Hill et al., 2009, Hill et al., 2010, Perez et al., 2010). These indicators are the main indicators of mitochondrial respiration and glycolysis, and comparable to data acquired using the Clark-type electrode. These readings will supply a systems-level view of cellular metabolic function of ex vivo live cells mitochondrial physiological functions.

The system provides invaluable data on normal physiological and pathological of mitochondrial function in cellular setting toward various stressors, including changes of cellular bioenergetics by various oxidative stress (Ferrick et al., 2008, Wu et al., 2007).

The Seahorse XFe96 Analyzer capable of measuring 96 wells total (92 samples and 4 blank controls) at one time with four injection ports per well probe. These four

ports allow for sequential injections of selected inhibitor or compound of interest in order to elucidate the defect and differences between cells of interest.

In order to elucidate physiological mitochondrial changes in WT1 mutant MEF as compared to wild type, cells were incubated in non-buffered Seahorse media with glucose and pyruvate substrates, and four inhibitors were introduced sequentially into the wells, allowing the Seahorse XFe96 Analyzer to measure 1) basal OCR, 2) ATP-linked OCR, 3) proton leak OCR, 4) maximal OCR, 5) reserve capacity OCR, and 6) non-mitochondrial OCR. These parameters are shown below.

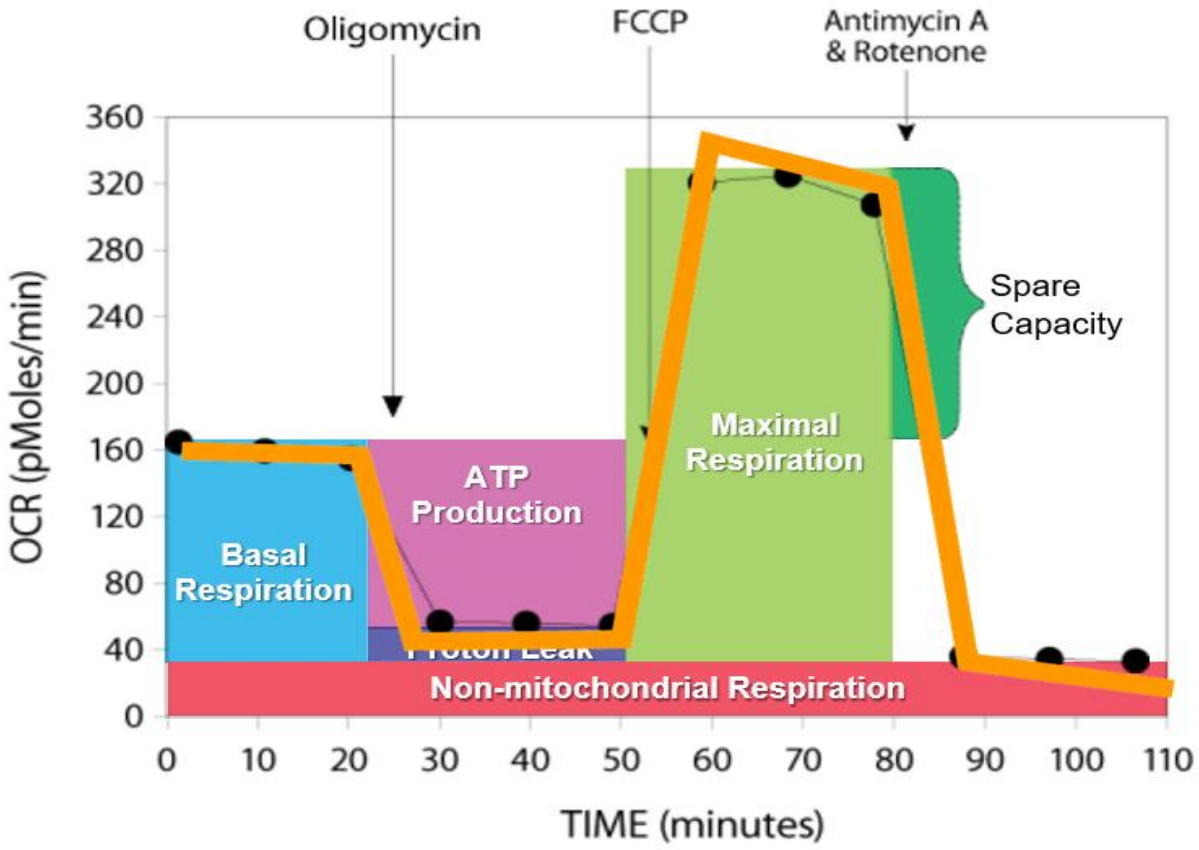

Figure 6.5.1: XF Cell Mito Stress Test time points and compartments for experimental representation (figure from Seahorse Bioscience website). This figure will be a reference in order to understand the meaningful data from Figure 6.5.2.

The inhibitors that were used are oligomycin (ATP synthase inhibitor), carbonyl cyanide *p*-(trifluoromethoxy) phenylhydrazone (FCCP) (uncoupling of mitochondrial inner membrane allowing for maximum electron flux through the electron transport chain (ETC) / protonophoric uncoupler), rotenone (complex I inhibitor) and antimycin A (complex III inhibitor) (*Seahorse Bioscience website*).

Three groups of MEFs were analysed to provide adequate controls:

1. $Wt1^{loxP/loxP}$ (FF no TAM) – wild type for WT1, no tamoxifen.
   - This is wild type MEF control
   - Coloured purple in the XF Cell Mito Stress Test graph in Figure 6.5.2
2. $Wt1^{loxP/loxP}$ +Tamoxifen (FF plus TAM)
   - this is wild type control for WT1, with addition of tamoxifen control as control measures to make sure tamoxifen does not affect normal cell physiology.
   - Coloured green in the XF Cell Mito Stress Test graph in Figure 6.5.2

3. $Wt1^{loxP/loxP}$: $RosaCre^{ERT2}$ +TAMOXIFEN (FFC plus TAM)
   - MEF of interest with deletion of exon 9 of WT1 gene.
   - Coloured blue in the XF Cell Mito Stress Test graph in Figure 6.5.2

Total sample well N=92 for wild type MEF (FF noTAM) – coloured purple, wild type MEF plus Tamoxifen (FF – (no Cre) plus Tam) – coloured green, and mutant MEF (FFC plus TAM, deleted exon 9) – coloured blue, and 4 wells as blank control as standard procedure. Biological MEF replicates: wild type MEFs (no Tamoxifen) control N=3, wild type MEFs (with Tamoxifen) control N=2, Mutant MEF N= 3. They are divided in multiple technical replicates (at least 10 wells each) per run. Experiment was repeated 3 times with different biological MEF cultures.

[A]

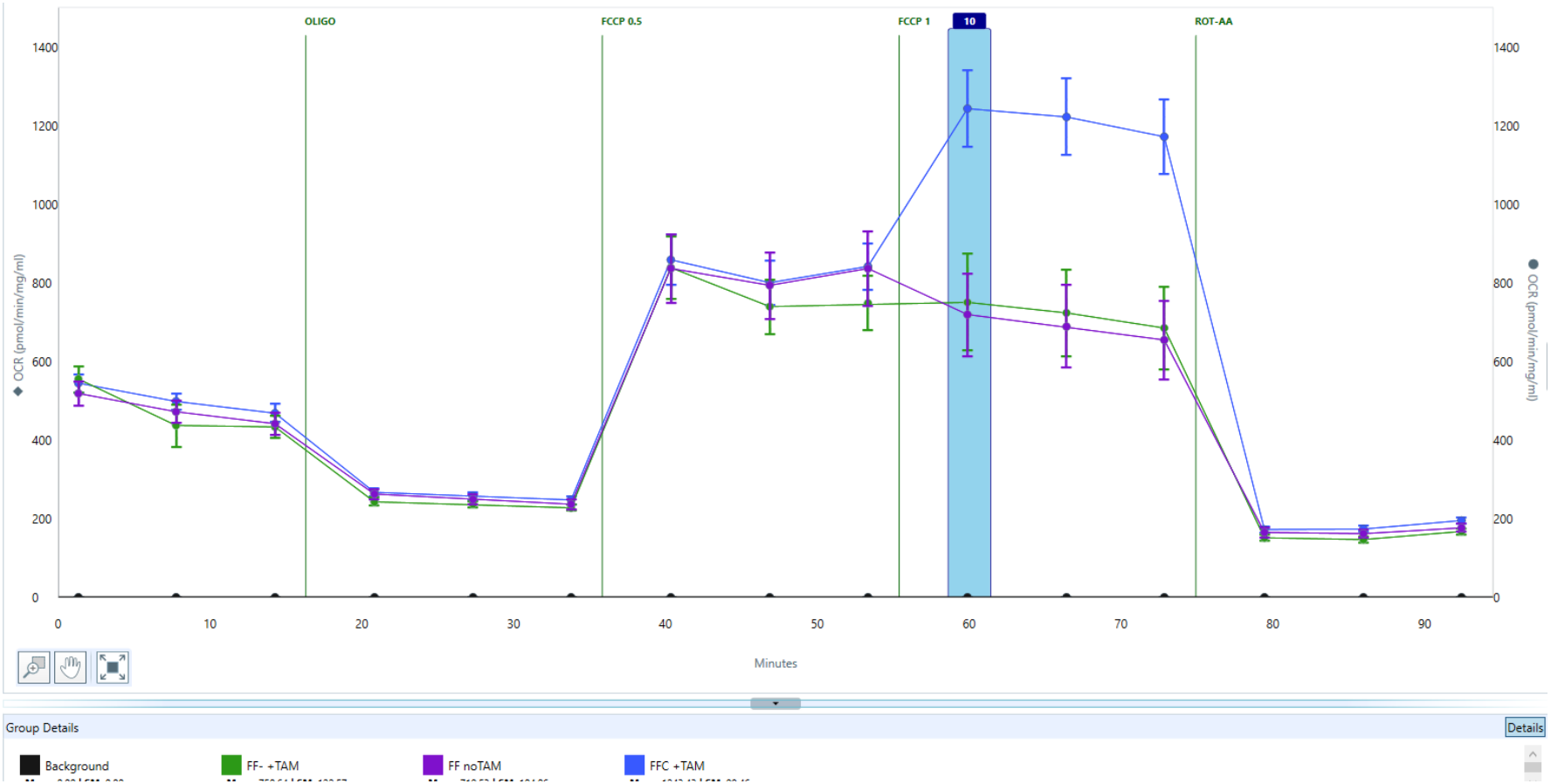
OLIGO
FCCP 0.5
FCCP 1
10
ROT-AA
OCR (pmol/min/mg/ml)
Minutes
Group Details
Details
Background
FF- +TAM
FF noTAM
FFC +TAM

[B]

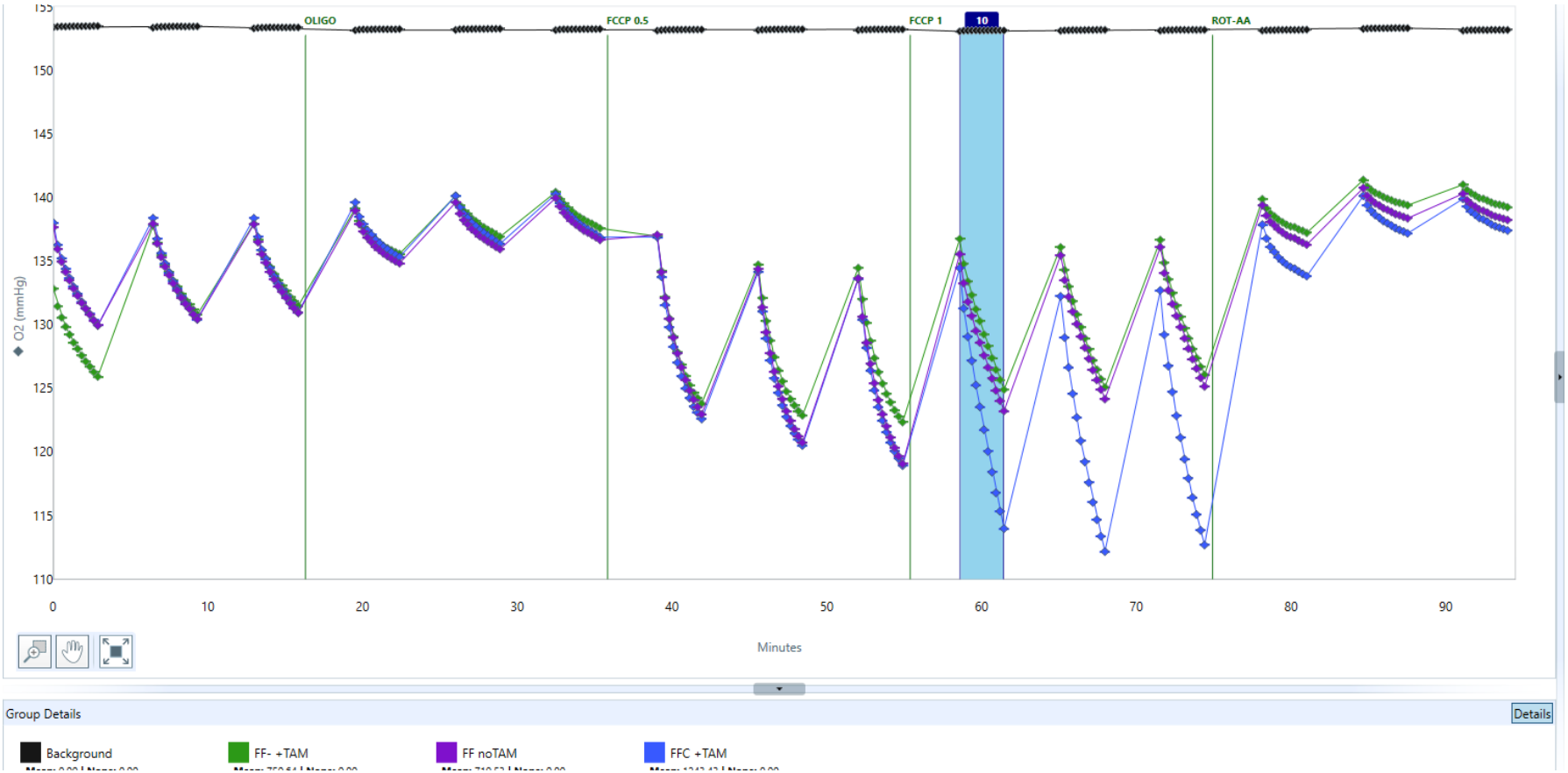
OLIGO
FCCP 0.5
FCCP 1
10
ROT-AA
O2 (mmHg)
155
150
145
140
135
130
125
120
115
110
0
10
20
30
40
50
60
70
80
90
Minutes
Group Details
Details
Background
FF- +TAM
FF noTAM
FFC +TAM

[C]

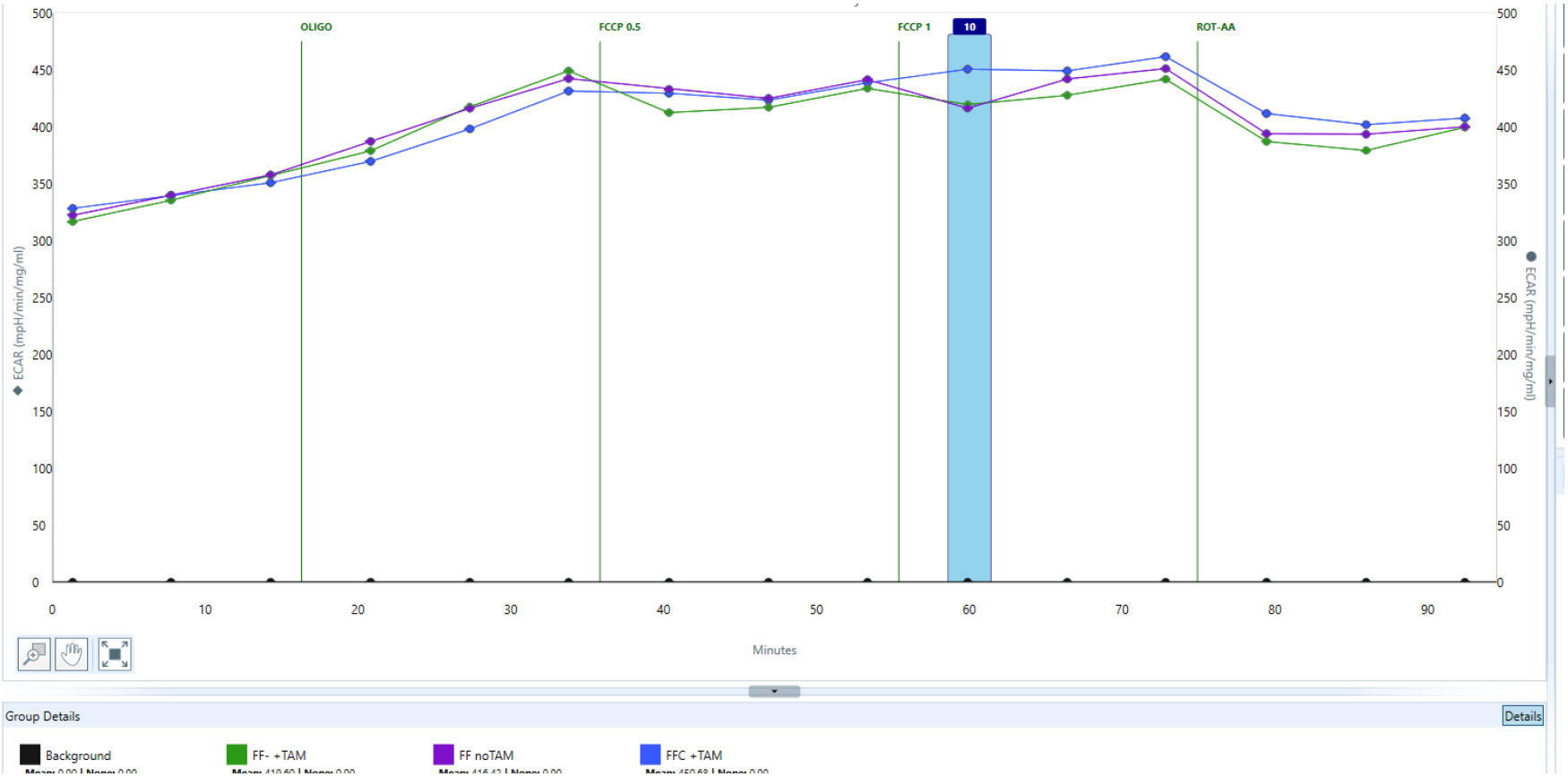
OLIGO
FCCP 0.5
FCCP 1
10
ROT-AA
ECAR (mpH/min/mg/ml)
Minutes
Group Details
Details
Background
FF- +TAM
FF noTAM
FFC +TAM

Figure 6.5.2: Figures of XF Cell Mito Stress Test. Multiple time points readings of A) Oxygen Consumption Rate (OCR), B) Oxygen Consumption Level (Measured) and C) Extracellular Acidification Rate (ECAR) for mouse embryonic fibroblast (MEF) at passage six post Tamoxifen at passage one. Total sample well N=92 for wild type MEF (FF noTAM) – coloured purple, wild type MEF plus Tamoxifen (FF – (no Cre) plus Tam) – coloured green, and mutant MEF (FFC plus TAM, deleted exon 9) – coloured blue, and 4 wells as blank control as standard procedure. Biological MEFs variation: wild type MEFs (no Tamoxifen) control N=3, wild type MEFs (with Tamoxifen) control N=2, Mutant MEF N= 3. They are divided in multiple technical replicates (at least 10 wells each). Experiment was repeated 3 times with different biological MEFs cultures.

Using the Seahorse data, it is possible to calculate the difference of oligomycin-insensitive OCR and basal OCR is equivalent to ATP-linked OCR at resting (Jekabsons and Nicholls, 2004) and the balance OCR is the proton leak and non-mitochondrial OCR. Both of these are unchanged ($p > 0.05$) in MEF.

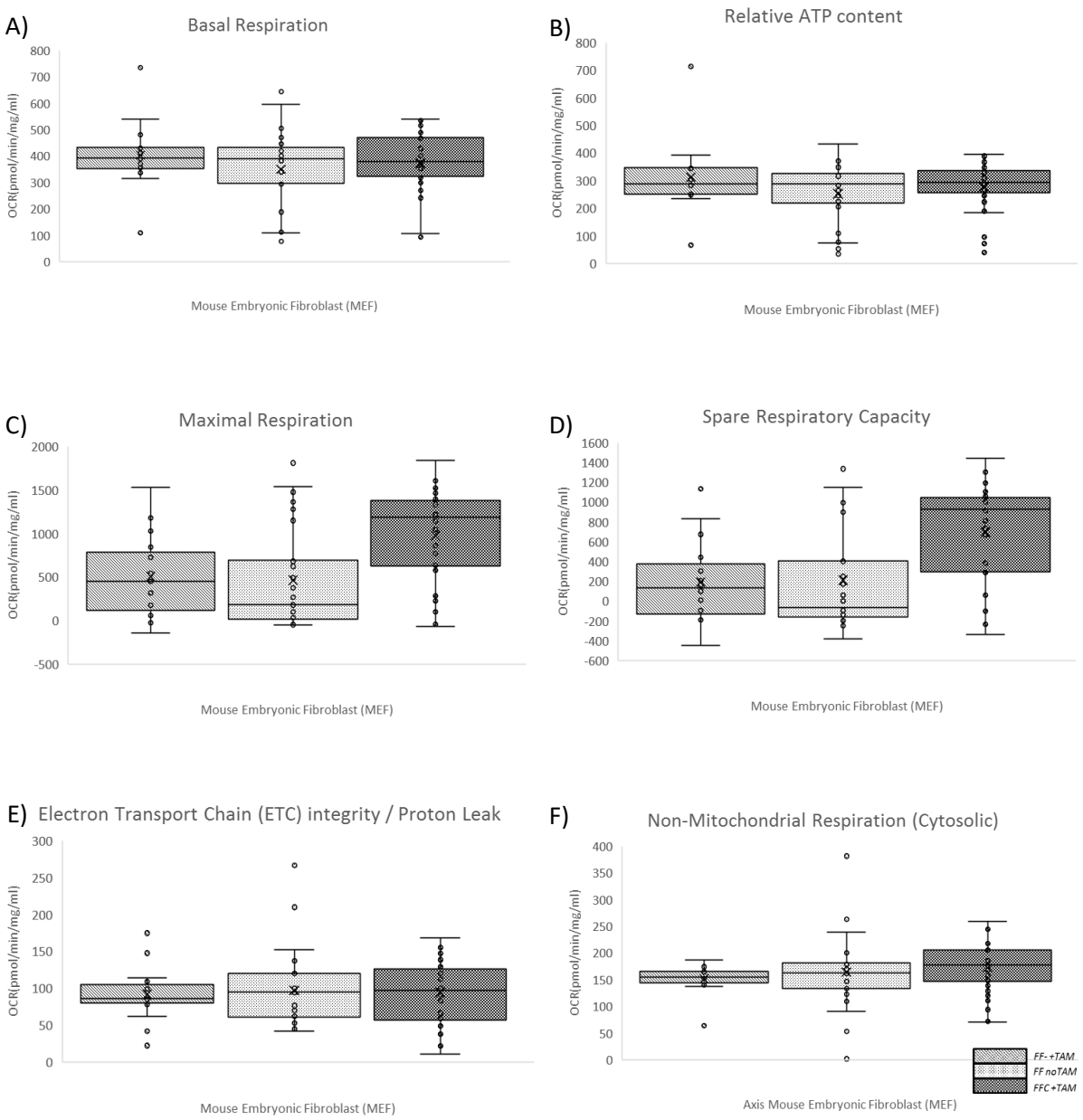

Figure 6.5.3: Box-Plot charts showing the important time points/sections of XF Cell Mito Stress Test. This is the calculation for significance of Figure 6.5.2-[A], in reference to Figure 6.5.1 as which part of the graph is called. A) Basal respiration, no different between groups ($p > 0.05$), B) Relative basal ATP content between groups ($p > 0.05$), C) Maximal respiration showing significant different between MEFs Cre-Floxed WT1 and controls ($p < 0.05$), D) Spare respiratory capacity showing significant different between MEFs Cre-Floxed WT1 and controls ($p < 0.05$), E) Proton leak / Electron transport chain, no different between groups ($p > 0.05$), and F) Non-mitochondrial respiration / cytosolic, no different between groups ($p > 0.05$).

Subsequently, FCCP were injected, depleting the mitochondrial membrane potential by inhibited the proton movement across the inner membrane. The first was 0.5uM showing no difference, followed by 1uM FCCP to completely uncouples the protons. This uncoupling resulted in electron to flow uninhibited through the mitochondrial respiratory chain. This will cause increment of oxygen consumption and its maximum limit by complex IV (cytochrome c oxidase). This process measures the OCR that which is not ATP/ADP transport dependant (Jekabsons and Nicholls, 2004). The maximal OCR was seen to be significantly higher compared to MEF wild type ($p < 0.05$).

The difference of the basal OCR and maximal OCR (FCCP OCR) will compute for the mitochondrial spare respiratory capacity (reserve capacity), which is significantly high in mutant MEF ($p < 0.05$). This spare respiratory capacity is the available amount of oxygen consumption capacity when cells is in dire need of ATP increment or demand during cellular stress (Dranka et al., 2010).

The fourth and last sequence is the injection of both rotenone (complex I inhibitor) and antimycin A (complex III inhibitor), both are electron transport inhibitor, inhibiting electron from going through respective complex. This resulted in complete blocked of mitochondrial system preventing oxygen from being consumed at complex IV and the OCR reading is the result of non-mitochondrial OCR (cytosolic) (Jekabsons and Nicholls, 2004).

Equally important readings are the Extracellular acidification rate (ECAR) which can have the same rate and pattern as proton production rate (PPR) which was measured the exact time as respective OCR under the same time and condition. ECAR is an indirect indicator of glycolytic flux. In this experiment, at all-time points, ECAR does not show any significant changes. Even though not changed significantly, at point at which second FCCP (1uM) was introduced, there was no difference ($p = 0.4$).

6.6. Conditionally immortalised human podocyte cells

In order to extend the findings of Wt1 mutation causing mitochondrial abnormalities in mouse kidneys and primary MEF cells, human podocyte cells were obtained. These human podocyte cells were derived by Saleem *et al*., 2002 from nephrectomy specimens from DDS patients, transfected with a temperature-sensitive SV-40 large T-antigen. At 33°C, podocytes are dedifferentiated, proliferate, and do not express podocyte-specific markers such as synaptopodin. Following 1 to 2 weeks of in vitro differentiation at 37°C, the immature podocytes acquire an arborized morphology and express synaptopodin, such of those found in mature podocyte in adults. Unfortunately, these cells quickly became infected and only a single experiment was possible. We are not sure of what infected these cells, or if it has been originally infected prior to arrival in our laboratory. However, initial culture showed no abnormal artifacts when viewed under microscope.

In order to determine if these cells also have changes in the mitochondrial membranes, MitoTracker® staining was done. The MitoTracker® staining on those immature podocytes reveals multiple clustered signals, predominantly seen in the DDS patient cells. This further confirms what I previously saw in Cre-MEF cells.

Previously double immunofluorescence of WT1 antibodies with COXIV show overlap signals that suggested direct interaction between the two proteins. This lead to the hypothesis that WT1 may actually directly involved in the mitochondrial system and processes. To further prove this, the MitoTracker® was double stained with WT1 antibodies.

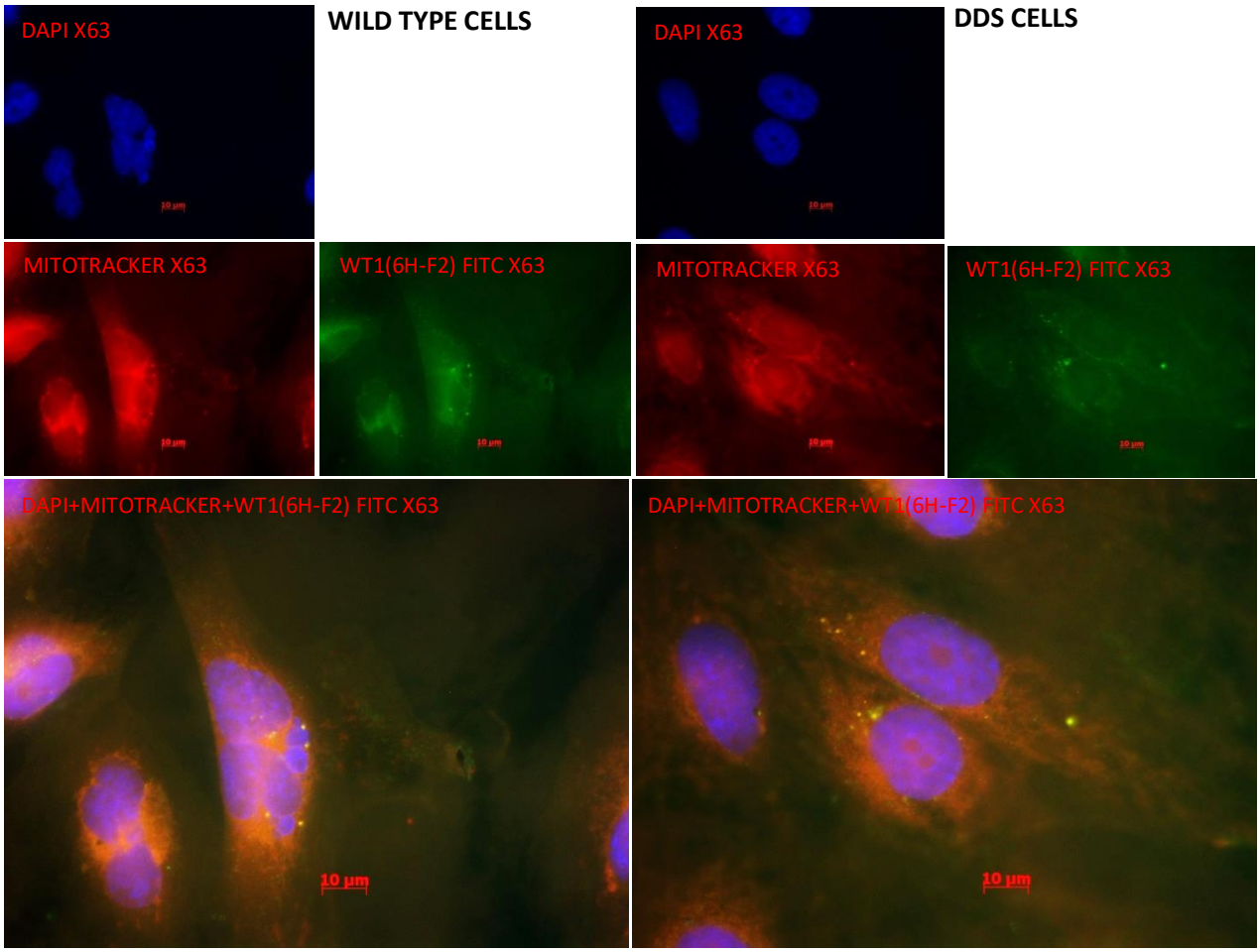

Figure 6.6.1: Double immunofluorescence staining of MitoTracker® and WT1 antibody (6F-H2) of human podocyte cells from Saleem et al., 2002 from nephrectomy specimens from DDS patients. 6F-H2 shows overlapping signals with MitoTracker® and DDS cells show more clustering/fragmentation compared to wild type human cells.

The double immunofluorescence shows overlap signals of MitoTracker® and WT1 antibodies. This further strengthens my hypothesis of the localization of the WT1 and co-localization with mitochondrial proteins. Aside from immunostaining, other experiment cannot be explored as all the cells were infected unfortunately. I do very much like to do Western blot, flowcytometry analysis, XF Cell Mito Stress Test and various expression analysis on these cell lines.

6.7. Summary of key findings

I. *In silico*, meta-analyses of provide evidence for the involvement of Wt1-regulated, nuclear-encoded mitochondrial genes in “mitochondrial” and “membrane” processes.

II. Wt1 protein is found in mitochondria in developing kidney, primary mouse embryonic fibroblasts (MEF), and human podocyte cells.

III. Wt1 mutation causes mitochondrial network abnormalities (Mitotracker)

IV. Wt1 mutation causes elevated maximal oxygen consumption rate (OCR, Seahorse) in MEF.

6.8. Chapter discussions

In these experiments, MEF were introduced in with the intention of replacing kidneys as the source of tissues to investigate the effect of Wt1 mutation on cellular biology. In an optimised world, we do want to use kidneys as they would provide the direct effect seen without making any conjectures and the need to re-do experiment done on MEF. However, unfortunately the feasibility of getting pre-parturition kidneys will take a considerable time and lives of the mice, as for each time kidneys were needed, the pregnant mouse has to be killed. Usually these DDS/+ do not have more than 5 littermates, with the most common are within the range of 1 to 3 and it is hard to get DDS/+ genotype as most of the time show wild type genotype. The advantages of MEFs are obvious. They are easy to culture and are physiological relevant to represent the changes that occur as the result of mutation. Although these MEFs were from different strain (DDS20), it is still physiologically relevant as the genes from the array were shown to be changes as the result of Wt1 mutation. To culture DDS/+ MEF, the mutation is already in place, not inducible as in DDS20 MEF. The initial mutation will cause unneeded secondary changes as MEF were prepared and cultured. Investigation of these cells might not be an indication of the actual causative effect of WT1 mutation, rather it will be the secondary effect of the initial change.

Mutant and wild type SDH/COX staining uses slightly different age kidney. Instead of e17.5, there should not be much of a different in physiology of the kidneys at e18 (different of less than a day) as it is still in the fast pace of nephron development, and any changes in nephron will still be reflected and obviously seen in these stages of nephron growth. In overall, there should be not much of a different as we are focusing on the individual developing nephron itself, though preferable we like to do at e17.5 but limited to the timing and availability of kidney sections at the time frame. It was not our first choice to use kidneys at e18, but we were limited by the availability of the kidney at the time of the time of experiment as the mice have innate difficulty of breeding. Physiologically from sectioned and nephron developmental stages, there would not be much different between e17 and e18 kidneys.

The fractionation process to get each cellular fraction, the nuclear, cytoplasmic and mitochondrial fraction uses chemical and centrifugation methods. Whilst it is

effective, it also has some concerns that needed to be addressed. It is understandable that when fractionation is performed, there might be some parts of each fraction which contaminate one another. What we can do to minimise the effect is to strictly follow the protocol and use of appropriate amount of tissues or cells. Another way is by doing a comparison between wild type and mutant, while loading the similar amount of protein concentration. This would just be an indicator towards the change of protein expression. To get absolute amount, more rigorous technique such as protein mass spectrometry is needed to be done.

Among the most significant changes in the array are of the mitochondrial related genes. Listed out when compared to MitoCarta 2.0 Mouse list are various mitochondrial genes, some of which reside in the mitochondria such as the tRNAs, and others are nuclear encoded protein coding mitochondrial genes (Figure 6.1.2.1). Some of these even have probable binding sequences for WT1 to regulate gene expression directly. Given the wide array of WT1 functions, this gene has been implicated to be among the most important in kidney development.

WT1 was seen to be co-localised with at least two mitochondrial markers, COXIV and MitoTracker® Red and Deep Red, in human cells and mouse. It was surprising to see as no studies to-date has shown this. Western blotting of isolated mitochondria both from developing kidneys and MEF have been shown to contain WT1 protein and differences in the bands are seen in MEF mutant. Although it is not confirmed if this mutant WT1 protein is functional or not, the changes of WT1 was seen to contribute significantly to the mitochondrial function as observed in the XF Cell Mito Stress Test, which reflects the actual live physiological conditions of cellular metabolic functions and mitochondrial metabolism.

Mitochondrial metabolism is becoming an important topic in developmental biology and cancer metabolism. One particular is the intermediary macromolecules in tricarboxylic acid (TCA) cycle activity that are important for cellular macromolecules biosynthesis. There are increasing evidence that this synthesis requires energy from mitochondria to metabolize particular substrates (such as pyruvate and glutamine) in rapidly dividing cells (Halestrap and Price, 1999). The functional association of cellular

proliferative capacity and mitochondrial respiration has been ascertained (Dranka et al., 2010).

In glycolytic metabolism, 2 ATP molecules are produced per glucose molecules where as in mitochondrial OXPHOS produced 38 ATP molecules, though the prior provides better advantage for growth (reviewed in Weinberg et al., 2010). Among the most significant is the rate of ATP production which is faster compared to OXPHOS, providing advantage for rapid energy requirement and rapid substrate biosynthesis during rapid proliferation (Spitz et al., 1990, Kim and Lemasters, 2011), plus advantage for cells when under low oxygen tension and hypoxic environment (Newsholme et al., 1985).

This concept of different substrate for energy supplementation for rapidly dividing cells is supported by various reports. When compared to glucose, different substrates such as pyruvate and glutamine, supplemented through mitochondrial OXPHOS and TCA system shown to support cells growth with rapid proliferation such as cancer cells (Perez et al., 2010, Halestrap and Denton, 1975) though lactate alone as a substrate is not supportive of cell growth (Diers et al., 2012). The different substrate is even more important given the pathways provides substrates for various biosynthesis of nucleic acids, protein and lipids in rapidly dividing cells (Kim and Lemasters, 2011).

One of the ways to see how much different substrate influence the mitochondrial OXPHOS and TCA cycle is by analysing the extracellular acidification rate (ECAR). It is an indicator of glycolytic flux. It has been shown that rapidly dividing cells such as cancer cells, cells with complete media with glucose and pyruvate shown to have biggest reserve capacity (OCR), cells with pyruvate only media show small reserve capacity, whereas cells with glucose only media show no reserve capacity and lactose does not support any reserve capacity, whereas for ECAR, it was shown to increase in glucose containing medium and decrease with pyruvate media (Diers et al., 2012). In my XF Cell Mito stress test readings, even though there is a significant increase in maximum and reserve capacity, there are no significant difference in the ECAR reading at same time point. This may be due to the media containing both glucose and pyruvate. Even if the substrate changed, and there are changes in mitochondrial function, it is not equated to ATP and ADP levels (Diers et al., 2012). As mentioned before, alteration of

mitochondrial function correlates with proliferative potential, even more so, pyruvate is the preferred fuel to drive mitochondrial into overdrive for highly proliferative cells, had little effect on basal OCR, ATP linked OCR, ETC, non-mitochondrial OCR, no effect on cell viability, and not contribute to overt cell death (Diers et al., 2012).

The importance with regard to the ability of mitochondria to have the ability and have the extra reserve capacity will give the extra flexibility needed in those cells to response to multiple cellular stress (Sonveaux et al., 2008). It has been shown that losing the reserve capacity in cancer is associated with initiation of cells into mitochondrial activated apoptosis mechanism (Pinheiro et al., 2010) and cancer cell that gain the ability to increase its reserve capacity is less responsive to anticancer agents (Gerencser et al., 2009). In a condition where there is oxygen stress, this hypoxic cell rely more on glucose as fuel for oxidative metabolism, and shown to decrease cancer size (Diers et al., 2012). The combination of inadequacy of certain substrate plus hypoxia may drive cells into apoptosis, rather than proliferation. This thin balance just makes a difference between having one more cell or no cell at all (cell death). In MEF with Wt1 mutation in this study, the mutation most likely causes similar situation to occur, where in non-stressful condition, the cellular machinery already runs at a fast and demanding level. When stress is induced (e.g. increase in oxygen demand), the processes were pushed to ‘break-neck’ level and showed as higher rate of oxygen consumption (Figure 6.5.2-A). This kind of ‘break-neck’ performance of cellular machinery will most likely cause cells to die if demand is not met, or in the long run causes exhaustion of cellular processes, damaging the cells and tissues.

From this study, it seems that the cells that are required for rapid proliferation, such as developmental cells and cancerous cells have this characteristic. This facilitates the energy and substrates requirement to grow and proliferate, but also at the same time they are predisposed to exaggerated response when stressed and go into death mode. Two important genes for pyruvate metabolism are changed in the array list. Those are Pck2 and Pdha2, which were upregulated. It is not surprising to see these genes changes if this mechanism does contribute to the inadequacy of nephron endowment. To explore this further, other specific experiments may possibly be done by introducing drugs that can block Pck2 and Pdha2 in the XF Cell Mito Stress Test. Other way is to

introduce RNAi or Crisper Cas9 to inhibit the function of these genes *in vivo* during nephrogenesis process and repeat the nephron counting to confirm the hypothesis.

6.9. Conclusion

Wt1 plays a role in mitochondrial function. However, it remains unclear if this is due to the regulation of nuclear-encoded mitochondrial genes or to a function of Wt1 within the mitochondria, or a combination of both.

Consideration of the Mitotracker and Seahorse data leads to a feasible explanation for the results observed. The elevated OCR corresponds to an increase in “reserve capacity” within mitochondria and this is consistent with stronger Mitotracker staining. Aggregation of the mitochondrial network can be caused by reduced membrane potential (and an increase in “reserve capacity”). Whilst these cells are not compromised, the reduced membrane potential results in increased Mitotracker staining.

It is tempting to speculate that the decrease in tRNA levels reflect a compensatory mechanism to prevent overactivity/overproduction in the presence of a decreased membrane potential.

It is noteworthy that Pck2 is elevated in the DDS/+ microarray, as Pck2 is a rate-limiting factor in the production of glucose, such that an increased “reserve capacity” would require higher glucose, hence increased Pck2.

The developing kidney can be considered to be under stress, potentially leading to amino acid limitation and thus increased Pck2. Increased glucose can lead to decreased membrane potential that results in reducing amino acid transport by decreasing levels of tRNAs. It is intriguing to note many members of the Slc25 family of solute carriers are down-regulated in DDS/+ kidneys. Some studies seem to clearly show that a decrease in membrane potential causes a rise in Pck2 expression and subsequent elevation of glucose levels.

Thus, the most likely scenario is that Wt1 mutation affects mitochondria leading to a decrease in membrane potential triggering the effects seen in Wt1 mutant kidneys and cells.

CHAPTER 7. GENERAL DISCUSSION

7.1 General discussion

I have analysed and validated a microarray profile of e17.5 *DDS*/+ kidney and wild type and investigated the expression changes. The analysis revealed novel genes underlying development and relating to the role of the Wt1 gene during renal development. Changes seen in mitochondrial tRNA genes were surprising and those alterations gives clues towards more a complex interaction between nuclear genes and mitochondria and nephrogenesis. This analysis nevertheless confirmed some genes that have previously been found that are involved in nephron formation. More importantly, more new candidate genes suggest more complex molecular interactions than previously thought are involved. More investigation will help further in uncovering the various pathways involved in final nephron endowment, and potential candidates in management and early identification of risk factors for CKD.

The role of multiple systemic disease processes in the pathogenesis of chronic kidney disease (CKD) has been recognised, for example in ageing DDS/+ mice (Patek et al., 2008), and the concept of a ‘first hit’ in renal disease is becoming widely accepted (Hershkovitz et. al., 2007). This concept has developed such that kidney diseases are now thought to often be associated with low nephron number (LNN), in particular as a mechanism involved in CKD development and progression. Multiple observations on intrauterine growth restricted (IUGR) babies initially led to this conceptual formulation (Hershkovitz et. al., 2007). Consistent with these observations, many studies in rats induced to have LNN by protein restriction diet resulted in animals with impaired renal function (Woods et. al., 2004, Bauer et. al., 2002). This positive correlation also has been documented from studies involving mortality of stillborn and infants within the first year of life (Manalich et. al., 2000). Thus, an individual with the ‘first hit’ LNN kidney then later becomes vulnerable to various forms of renal injury, the ‘second hits’, thus enhancing the development toward CKD.

In my study, nephron number is decreased at birth in DDS/+ mice as a result of abnormal development and not the disease state that leads to fewer nephrons in DDS/+ mice. Although DDS/+ kidneys do not differ in size from wild type at birth, there is a differential effect on different stages of nephrogenesis, indication of factors contributing to the nephron number start before parturition.

Given the insight that the main mechanism of nephron formation and mesenchymal-epithelial transformation was disrupted, in the absence of obvious apoptosis event in foetal kidneys, the mechanism of controlled cell death during the kidney was not disrupted, it is unlikely that nephron niche dies to contribute to the lack of nephron number. WT1 was shown to exerts important function in renal progenitors (Figure 7.1.1), with a possibility of altering mechanisms in the early stage of nephron formation such as reduction of proliferation and survivality, thus altering the total nephron number at the end of nephrogenesis (Figure 7.1.2).

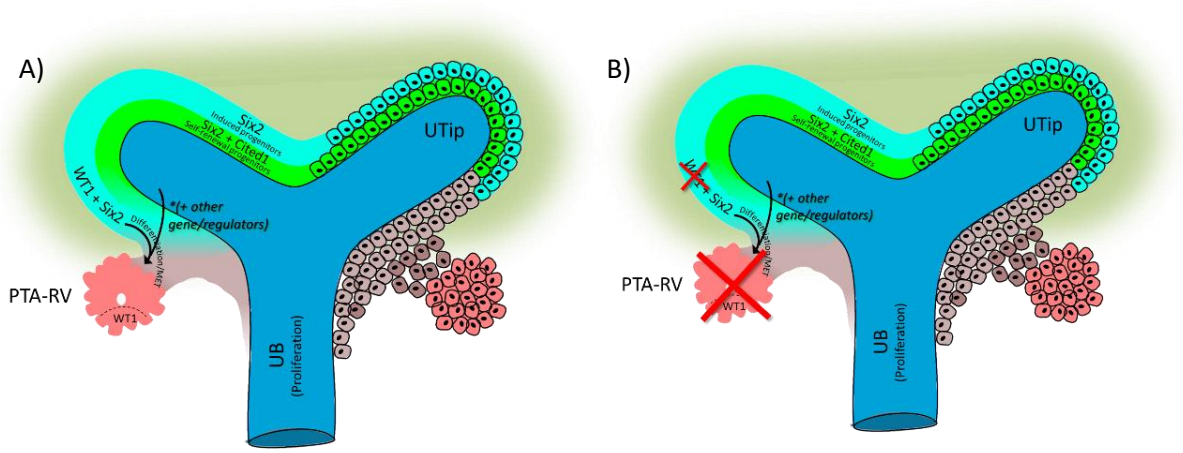

Figure 7.1.1: A) and B) depicting the summation of role of WT1 in formation of pretubular aggregates / renal vesicle (PTA-RV). My study postulates that with the loss of normal WT1 function, the cascade of abnormally expressing gene would result in loss of nephron precursor (PTA-RV, pretubular aggregates/ renal vesicle) when introduced to stressed as a result from the tissue inability to adequately cope to the stressful event.

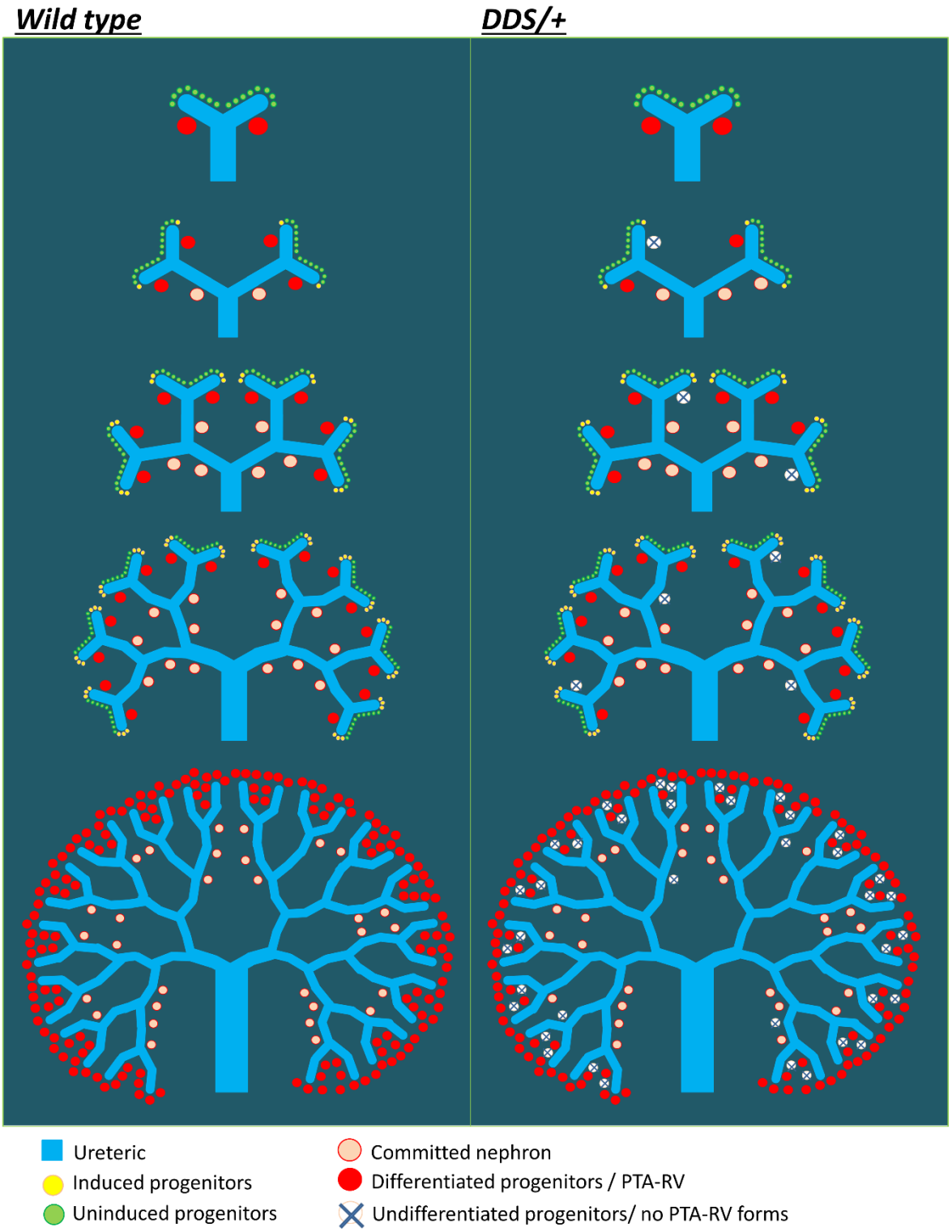

Figure 7.1.2: A model depicting the proposed mechanism of nephron endowment in DDS/+ mouse kidney. The total reduction shown in this diagram represented about 22%

reduction in numbers. Each branching morphogenesis step from top to bottom show increasing induced progenitors (yellow circle), decreasing uninduced progenitors (green circle), and appearance of PTA-RV formation (solid red circle) followed by committed nephron (red outlined circle with dull red centre). Final stage of nephron (triggered on parturition) involved induction of all remaining progenitors to be nephron.

Various other mechanism of LNN development in kidney have been postulated by various studies. We hypothesise that in WT1 mutant (DDS/+), the observable reduction of nephron number and accelerated maturation of nephrons may induce a premature cessation of nephrogenesis leading to a reduced nephron number due to Wt1 haploinsufficiency via a yet unknown mechanism. In addition, increasing cell turn over in IUGR babies, attempting to 'catch up' by accelerated growth has been suggested to induce LNN kidney, shortening the telomeres (Jennings et. al., 1999, Hales 2001), and depleting the progenitor stem cells, increasing the risk for kidney diseases (Welham el. al., 2002).

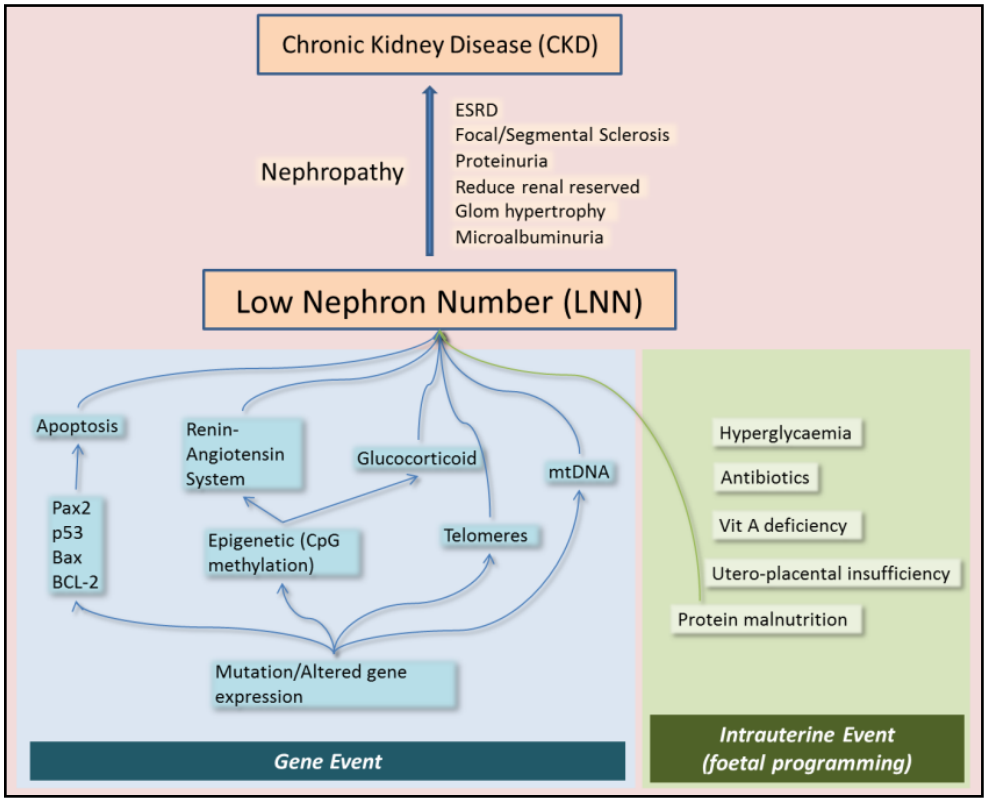

Figure 7.1.3: Potential mechanisms of factors related to low nephron number (LNN) and its subsequent progression towards adult kidney disease. (Adapted from Zandi-Nejad et. al., 2005, Hershkovitz et. al., 2007).

Further correlation between nephron endowment and the increased tendency towards kidney disease can be seen in some clinical studied, where patients with a solitary kidney (lower nephron number per individual) show a higher incidence of chronic renal failure when compared to normal subjects (Rugiu et. al., 1986, Thorner et. al., 1984, Zucchelli et. al., 1985). Solitary kidney transplants originating from ethnic groups having naturally lower nephron number show higher incidence of graft failures after 3 years and allograft nephropathy (Terasaki et. al., 1994, Azuma et. al., 1997, Heemann et. al., 1994, Mackenzie et. al., 1996). Whilst these examples are rather extreme cases, it is likely that even a modest reduction in nephron number will increase the risk of developing CKD and the associated complications.

I showed that loss of WT1 causes segregation or fragmentation of mitochondria and a profound metabolic state, which could drive the accelerated nephron maturation (differentiation). The WT1 mutation is postulated to cause stem-cell self-renewal deregulations and impairment of regenerative potential. Comparable deduction of my mitochondrial findings in nephron and MEF to a recent study in f rapid ageing hematopoietic stem cells (Ho et al., 2017), in which they showed that increased autophagy in this type of cells clears healthy mitochondria, in effect it maintains quiescence and stemness by supressing stem cell metabolism and functions to preserve the regenerative capacity in the ageing process.

My findings have stimulating implications for WT1 as they recognize a novel cellular characteristic that has the potential to be directly targeted to improve kidney function and preserve the health of renal system. In this setting, understanding of why/how WT1 activates the mitochondrial system, as well as finding the extra drivers for this differential adaptive response, will help supplement our understanding of nephron endowment, and develop more targeted approaches for improving kidney health during development and disease.

7.2 Summary

To summarize, nephron number is decreased at birth in DDS/+ mice. Thus, it is abnormal development and not the disease state that leads to fewer nephrons in DDS/+ mice with indication of factors contributing to the nephron number start before parturition (i.e. genotype or other factors).

This study achieved the first objective of utilising WT1 mutant mice to uncover molecular mechanism underlying nephron number and second objective of understanding the pathway that would eventually lead these mice into a diseased state. Gene expression profile of e17.5 DDS/+ kidney and wild type revealed novel genes underlying development and biochemical interaction in foetal kidney development in relating to WT1 gene. Changes seen in mitochondrial tRNA and its alteration give clues towards more complex interaction between nuclear genes, mitochondria and WT1.Databases analysis including Ingenuity Pathway Analysis (IPA) shows confirmation of some genes that were found to be involved in nephron formation. There are also genes related to apoptosis dysregulated from microarray data. Although no difference in the pattern of apoptosis was seen between wild type immature nephrons and DDS/+ P0 kidney, there is disruption of normal cellular physiology in MEF (Tamoxifen) when in an unfavourable environment (different substrates and oxygen deprived). *In silico*, meta-analyses provide evidence for the involvement of Wt1-regulated, nuclear-encoded mitochondrial genes in “mitochondrial” and “membrane” processes. Wt1 protein is found in mitochondria in developing kidney, primary mouse embryonic fibroblasts (MEF), and human podocyte cells. Wt1 mutation causes mitochondrial network abnormalities (Mitotracker). Wt1 mutation causes elevated maximal oxygen consumption rate (OCR, Seahorse) in MEF and various evidence suggesting this would lead to diseased state.

The finding in this study highlighted the WT1 is crucial in determining the nephron number and it does this through pre-natal period. This indicates the important role of keeping pregnancy stress-free and the need to have better *ex-vivo* detection method to determine nephron number and indirectly higher risk of kidney disease. This would be one of the next steps of research. If given the chance, I would like to get a better understanding of WT1 molecular mechanism in MEF buy doing expression analysis. This would make MEF better served as an important mechanism and means to search

for potential markers and medium of trial of therapy for WT1-caused low nephron number in mammals.

To conclude, this thesis has shown there is a previously uncharacterised significant developmental, role for WT1 role in the murine DDS/+ model. Analysis of DDS/+ mice has revealed novel functions of WT1 in normal kidney development, dysfunction of which contributes to kidney disease.

Table A-2.6.3: List of Primers used

	Gene / region	Sequence
1	Acaa2 F	CCCCAGCAAAACCAATGTGAG
2	Acaa2 R	TTTCCACCTCGACGCCTTAAC
3	Ankfn1 F	CGACACCAGGCAAGGAACTT
4	Ankfn1 R	GAGTGCGGGGTGTAAGGATT
5	Arhgef12 FWRD SET1	CGACTTCCCTCCTCCTCTATTA
6	Arhgef12 FWRD SET2	CCGAGAGTCACCAACAGATAAG
7	Arhgef12 REV SET1	GCTCATCCTCACTCTGACTTTC
8	Arhgef12 REV SET2	GCGCTGAACAAGACCATAGA
9	Arhgef6 F	TGGCTCGGTGGAGAAGTATTG
10	Arhgef6R	ACCTTGGAGAAATTGGCCCC
11	Asb15 F	GAATCCATTGAAGCGAGCCAG
12	Asb15 R	AGCTCAAAAATGCGACCTTGC
13	B-ACTIN F1 HUMAN	CTCGTCGCCCACATAGGAAT
14	B-ACTIN F1 HUMAN	CGTGCTCAGGGCTTCTTGT
15	B-ACTIN F2 HUMAN	CCACCAGAAGAGGTAGCGGG
16	B-ACTIN R2 HUMAN	CGACATGGAGAAAATCTGGCAC
17	Bmp4 F	TCCGTCCCTGATGGGATTCTC
18	Bmp4 R	GGAATGGCTCCATTGGTTCCT
19	Ccdc141 FWRD	AGCCCTTTACAAGGCATCTC
20	Ccdc141 FWRD SET2	CGTTGTGAGAGTTGGGAAGTA
21	Ccdc141 REV	CCAGATCACCACAGGACATAAA
22	Ccdc141 REV SET2	GGCACCGAGGGAGTAATAAA
23	Ccnyl1 FRWD SET2	GACCAGGCTGTATGGAATGTAG
24	Ccnyl1 FWRD SET1	GTGTTTGGAGCCATAGAGAGAG
25	Ccnyl1 REV SET1	CAGAGGATGAGAAGCACCATTAG
26	Ccnyl1 REV SET2	ACTGGAGTAGCTCCAAGAAATG
27	CD55 F1 HUMAN	GTGCCGTCCAGGTTACAGAA
28	CD55 F2 HUMAN	TGCCGTCCAGGTTACAGAAG
29	CD55 F3 HUMAN	CCATCTGGTGTTTGGGGGAA

30	CD55 R1 HUMAN	TTTCCCCCAAACACCAGATG
31	CD55 R2 HUMAN	ATTTCCCCCAAACACCAGATG
32	CD55 R3 HUMAN	TGACACTCATGGTCCTATCAAGA
33	CD55-F	GACAGACAGACAGACAGACATAC
34	CD55-R	GTCTCCAACCACTTCCTCTTAAT
35	CITED1 F	CTTCTGAGCACCTGAGACCAAC
36	CITED1 R	GTGCAGGCCTCGACATAGTT
37	Cldn16 FWRD SET1	CCTACCTGATGACCCACAAATTA
38	Cldn16 FWRD SET2	GCAAGAGGGATGTGAGGAAA
39	Cldn16 REV SET1	CCACAGCATACCACACAGAA
40	Cldn16 REV SET2	CTATGGGCCTCTGTTGCTATT
41	Clec4g F	TCTCCAGAGGGCAATTGGGA
42	Clec4g R	GTGCTCAGAATGAGAGCCCA
43	Clic5 F	CCAAACAACAGAACAATGCTG
44	Clic5 R	GTTGGTGTCAATCTCCTCTG
45	Cre1R (DDS20/MEF)	TGTTCTGAATCTCCTGGACA
46	Ex9F2 (DDS20/MEF)	AGACCTTCTCTGTCCGTTTAG
47	neo52 (DDS20/MEF)	GATGCCTGCTTGCCGAATATCATGG
48	Crym F	CCACAAAGCTGTTGAAGCCC
49	Crym R	GCGGTTCCACATTCTCACCT
50	Ddn F	TTATAGTCGTCGCGCTCCTTC
51	Ddn R	CCTACACGTGCGGCTCTG
52	Dlg1 F	GTTCCTCCCTCCTCTCCCAT
53	Dlg1 R	GGAGGAGGATTTGCCTGTGG
54	Etos F	AGGACTACCTCAGTCTCATACC
55	Etos R	TCCTCCAGTATCTGCCTTACT
56	EYA1 F	CCCACATATTCTCCCTACCCCT
57	EYA1 R	GCCCACAATGCACCATAGGA
58	GAPDH F1 HUMAN	CCACACTGAATCTCCCCTCC
59	GAPDH F2 HUMAN	CCCACCACACTGAATCTCCC
60	GAPDH F3 HUMAN	GAGCCGCACCTTGTCATGTA
61	GAPDH R1 HUMAN	CTTGACACAAGCCCAGCTTC
62	GAPDH R2 HUMAN	TCTGCCCCAGACCCTAGAAT
63	GAPDH R3 HUMAN	CTCACCTTGACACAAGCCCA

64	GDNF F	TGGGTCTCCTGGATGGGATT
65	GDNF R	CGGCGGCACCTCGGAT
66	Gm5346-F	TCAGCAAGTCTGTTCTGGTAAG
67	Gm5346-R	GGTGGTTCCCATGTGTTAGT
68	intronID10338497-F	GGAGTCCAGAGAACACAAGAAA
69	intronID10338497-R	CCATGGTGCTCATGTGAAGA
70	Iyd F	CACTGCAGAATGCAGGGCT
71	Iyd R	CCACAGGAAGTAGCACCAACA
72	Jarid1_sexChrom_Revs	CCACTGCCAAATTCTTTGG
73	Jarid1_sexCrom_Fwd	CTGAAGCTTTTGGCTTTGAG
74	Llph F	TGTCTCTCAGGTGAAGCATGG
75	Llph R	TTAGAGCATCCCCGTCCACT
76	Mafb F	CAGGGCTGGTTTGGAATCCT
77	Mafb R	TTGGCTCAATGGGAGCTCAG
78	Magi2 F	AAGTAGGCGTCCAGATTATAAGG
79	Magi2 R	GCTGTCCAGGTTCATCTCCC
80	mAldh1a2 ex2 for	GAGCAAGTGTGTGAAGTTCA
81	mAldh1a2 ex4 rev	AGCTTGCAGGAATGGCTTAC
82	Mcu F	TTGTGCCCTCTGATGACGTG
83	Mcu R	CCTCCTCTTGCAGTTGTCGT
84	Me3 F	CATGAGCGCCCTATCGTCTT
85	Me3 R	CAAAGATTCCTCGGCCCTCG
86	Mfap5 F	TTCACCAGTTTACGGCGCAT
87	Mfap5 R	ACAGGGAGGAAGTCGGAAGT
88	Micu3 F	TGACACTGACGGAAATGAGATGG
89	Micu3 R	CCATAAAGTTGAAGACGCAGCAT
90	Mir24-2 FWRD	CCTCCCGTGCCTACTGA
91	Mir24-2 REV	GGGCTGGACTCCTGTTC
92	Mrpl54 F	GTACCCCACATGGCTGTTCC
93	Mrpl54 R	CTGTTTGCGAAGTAGTCGCC
94	mWnt4 ex2 for	CAGGTGCAGATGTGCAAAC
95	mWnt4 ex3 rev	GCTGAAGAGATGGCGTATAC
96	Myo18b FWRD SET1	CTGGTTCGAGAGACAGAGAAAG
97	Myo18b FWRD SET2	CATCATCTGTGACCTGGAGAAC

98	Myo18b REV SET1	GAACTGCTGGGATCTCTACTTC
99	Myo18b REV SET2	GAGACAACTCTTCACCCATCTT
100	ND1 mito FWD	GCCGTAGCCCAAACAATTTC
101	ND1 mito RVS	CAGGCTGGCAGAAGTAATCATA
102	ND4 mito FWD	CTCAGTTAGCCACATAGCACTT
103	ND4 mito RVS	GGAGTTTGCTAGGCAGAATAGG
104	ND5 F1 HUMAN	CACACCGCACAATCCCCTAT
105	ND5 F2 HUMAN	TCGCTTCCCCACCCTTACTA
106	ND5 mito FWD	CTGGCAGACGAACAAGACA
107	ND5 mito RVS	GCTTCCGATTACTAGGCATGAT
108	ND5 R1 HUMAN	TGGAGGTGGAGATTTGGTGC
109	ND5 R2 HUMAN	ATCCTGCGAATAGGCTTCCG
110	Nebl F	CGGGGGATGTCACAGCG
111	Nebl R	GTAGTGTGCATTGCAATAGGGCT
112	Nes (Nestin) F	GCTACATACAGGACTCTGCTGG
113	Nes (Nestin) R	GGTGCTGGTCCTCTGGTATC
114	NME5 F	ATGAGCTCTGGACCTCTTGTTG
115	NME5 R	CCCTTAAGCTGTCCGGGTG
116	Nxph1-F	CCTGCGGAGTTAAAGGTCATAG
117	Nxph1-R	CAACAAGAGCAGCAAGGTAGA
118	Olfr1174psedo1 FWRD SET1	GGCTGTGTCATGCAATTCTTC
119	Olfr1174psedo1 FWRD SET2	GCTCCACACTCCCATGTATTT
120	Olfr1174psedo1 REV SET1	GGTTGCATACTGCCACAAATC
121	Olfr1174psedo1 REV SET2	AGATCCTTCTGTCTTCCACAATC
122	P1F-EX7-GENOME	TGAAACCAGTGAGAAACGTCCT
123	P1R-EX10-GENOME	GCATGTTGTGATGGCGGAC
124	P2F-EX7-GENOME	GTGCGGCGTGTATCTGGA
125	P2R-EX10-GENOME	TCCGGCAAACCTGATAGGATG
126	P3F-EX7-mRNA	CCGGTCAGCATCTGAAACCA
127	P3R-EX10-mRNA	CTCCTTCCGGCAAACCTGAT
128	P4F-EX7-mRNA	TGCATACCCAGGCTGCAATA
129	P4R-EX10-mRNA	TGTTGTGATGGCGGACCAAT
130	Pax2 (m) qPCR F Ex2	GCTGCACCCACGACAGAAGG
131	Pax2 (m) qPCR R Ex3	GTCTCAATCGGACGGCAGTAG

132	PAX2 F	CCTGTTTCCAGCGCCTCTAA
133	PAX2 R	CAGACACATCTTCCTCGCGT
134	Pax2 set1 F	TCCCAGTGTCTCATCCATCA
135	Pax2 set1 R	GTTAGAGGCGCTGGAAACAG
136	Pax2 set2 F	GCAGGTACTACGAGACTGGC
137	Pax2 set2 R	CAGGCGAACATAGTCGGGTT
138	Pck2 F	TGCGGAGCACAAAGGAAAGA
139	Pck2 R	AACCAGTGTTCCAGGTAGCG
140	Pcp4 F	TGAGTGAGAGACAAAGTGCCG
141	Pcp4 R	TCTCTGGTGCATCCATGTCG
142	Plce1 F	GCTGGTCTCCTATGGCCTTG
143	Plce1 R	GGCACTGTAGATCAGGCACC
144	Prol1 F	AAGCAACAACTGACTGTTCCA
145	Prol1 R	GATGACTTTCACCAGGCATGAA
146	Prp2 FWRD SET1	ATGCTGGTGGTCCTGTTTAC
147	Prp2 FWRD SET2	CCCGTGAAGAACTTCAGAATCA
148	Prp2 REV SET1	GAAGGAGGTGGCCTTTGATT
149	Prp2 REV SET2	CTTGCTGGCTCCCATTAACA
150	Ptpn11 F	GGGGTCATGCGTGTTAGGAA
151	Ptpn11 R	CCTGGAGTAGAGCTTGTCCGA
152	Ptpro F	GGCAGTCTTTGTGGGTGGAT
153	Ptpro R	GGCTGGTTAGGCAGGTAGC
154	Reep1 F	TCATACAAGGCTGTGAAGTCCAA
155	Reep1 R	AGAATGGAAACCAGCAAAGGAAGA
156	RNASE12 F1 HUMAN	GACTCGGGAGCTGATCTTGA
157	RNASE12 F2 HUMAN	GCCAAGGAAACTATCTGGCCT
158	RNASE12 R1 HUMAN	CCCACAGAGGGGTTTGTTCT
159	RNASE12 R2 HUMAN	GCAGGTACCACTATTCCCCC
160	Rnf39 F	TCCCCACGGAGAGGATATGA
161	Rnf39 R	TGTCAGCCTGTGAAGCATGT
162	SALL1 F	AAGCAAGCGAAGCCTCAACA
163	SALL1 R	ACCCTTCTCTGTGTCCCCATC
164	Slc25a18 F	GTACCGAGGGGCTGCAGTAA
165	Slc25a18 R	CATATTCCAGCCCCACACCC

166	Snap91 F	TGGGGAGACCTTTTGGGAGA
167	Snap91 R	AGTAGGAGGGGAAGGCTCTG
168	Sp140 FWRD SET1	CGGAGCAGAAGTTTCAGGAATA
169	Sp140 FWRD SET2	GGAGGCTATGGAAAGTCAAAGA
170	Sp140 REV SET1	CTTTCAGAAGATCCCGGCTAAA
171	Sp140 REV SET2	CGATGTATCCGTGGAGGATTG
172	Stap2 F	GGACCCTGTGACCAGGATTA
173	Stap2 R	GCAGAGCCTCATCTCTGAGC
174	Sulf1-F(Heidet)	CACCTCCCACTCCTCCTTTTG
175	Sulf1-R(Heidet)	GAACTCCCCAGCCAAGTAACCT
176	Tbc1d10a F	CTGGGAAGTTTGATGAGCTGG
177	Tbc1d10a R	CTTCAGCACACGGAACAGGT
178	Tgfb1 F	CTTTGTACAACAGCACCCGC
179	Tgfb1 R	ATAGATGGCGTTGTTGCGGT
180	Tgfbr3 F	AGCTGCCAAAGTGTGTGACT
181	Tgfbr3 R	CCAGGGGCTTGGTGAATGTC
182	tRNA-ala F1 human	GGGCTTAGCTTAATTAAAGTGGCT
183	tRNA-ala F2 human	GGGCTTAGCTTAATTAAAGTGGCTG
184	tRNA-ala F3 human	AGGGCTTAGCTTAATTAAAGTGGCT
185	tRNA-ala NC_005089 FWD	GAGGTCTTAGCTTAATTAAAGC
186	tRNA-ala NC_005089 RVS	TAAGGACTGTAAGACTTCATCC
187	tRNA-ala R1 human	ACCCCACTCTGCATCAACTG
188	tRNA-ala R2 human	AGGACTGCAAAACCCCACTC
189	tRNA-ala R3 human	GCAAAACCCCACTCTGCATC
190	tRNA-arg NC_005089 FWD	TGGTAATTAGTTTAAAAAAAATT
191	tRNA-arg NC_005089 RVS	TTGGTAATTATGAACATCATCA
192	tRNA-his NC_005089 FWD	TGAATATAGTTTACAAAAAACA
193	tRNA-his NC_005089 RVS	GGTGAATAAGGAGGTTTATTTC
194	tRNA-PHE F1 human	GTAGCTTACCTCCTCAAAGCA
195	tRNA-PHE F2 human	TGTAGCTTACCTCCTCAAAGCAA
196	tRNA-phe NC_005089 FWD	GTTAATGTAGCTTAATAACAAAGC
197	tRNA-phe NC_005089 RVS	TGTTTATGGGATACAATTATCC
198	tRNA-PHE R1 human	GTTTATGGGGTGATGTGAGCC
199	tRNA-PHE R2 human	GGTGATGTGAGCCCGTCTAAA

200	tRNA-TYR F1 human	AAAAAGAGGCCTAACCCCTGT
201	tRNA-TYR F2 human	AGAGGCCTAACCCCTGTCTT
202	tRNA-TYR F3 human	AAGAGGCCTAACCCCTGTCT
203	tRNA-tyr NC_005089 FWD	GGTAAAATGGCTGAGTAAGCAT
204	tRNA-tyr NC_005089 RVS	TGGTAAAAAGAGGATTTAAACC
205	tRNA-TYR R1 human	TGGCTGAGTGAAGCATTGGA
206	tRNA-TYR R2 human	GGTAAAATGGCTGAGTGAAGCA
207	tRNA-TYR R3 human	AAATGGCTGAGTGAAGCATTGG
208	Vegfa (m) qPCR F Ex6	GCGTCCTTCCTATCCCGATGTC
209	Vegfa (m) qPCR R Ex7	CTTGACTTCATCAAGCCCAGG
210	VEGFa set1 F	CAGGCTGCTGTAACGATGAA
211	VEGFa set1 R	GCCTTGGCTTGTCACATTTT
212	VEGFa set2 F	ATCTTCAAGCCGTCCTGTGT
213	VEGFa set2 R	GCATTCACATCTGCTGTGCT
214	Vegfa splicing primers F	CACAGCAGATGTGAATGCAG
215	Vegfa splicing primers R	CCTTCCTGCAGCCTGGCTC
216	Wnt10a FWRD SET1	CTCTGCTCCTGTCTTTCACTT
217	Wnt10a FWRD SET2	ACTCCGACCTGGTCTACTTT
218	Wnt10a REV SET1	GTCCCTTAATCAGCCTGTAGAC
219	Wnt10a REV SET2	ACCCGTGCTGCTCTTATTG
220	WNT11 F	GCAACCTCGCAGGCGG
221	WNT11 R	AAGAGCAGAGCCTCGCAGA
222	WNT4 F	GCGAGCAATTGGCTGTACCT
223	WNT4 R	GCCTTTGAGTTTCTCGCACG
224	Wnt5a F	AGCCCTGCTTTGGATTGTCC
225	Wnt5a R	TCCAATGGGCTTCTTCATGGC
226	WT1 F	TTAAAGGGAATGGCTGCTGGG
227	WT1 R	CTCTCATACCCTGTGCCGTG
228	Zbtb20 F	ACTTCCAGGGAGACACCGAT
229	Zbtb20 R	AAGGAAACACCTTCAGCCTTCA
230	zfp507 FRWD SET2	AGCCTTACCAGTGTCCTATCT
231	zfp507 FWRD SET1	CCACCGTCTTCATCTCCTTTAG
232	zfp507 REV SET1	TCCAGCATTTCTTCCTCGTTAG
233	zfp507 REV SET2	GCACTGCTTACATTGGTGTATTC

234	Gapdh F	AACTTTGGCATTGTGGAAGG
235	Gapdh R	ACACATTGGGGGTAGGAACA
236	B-actin F	TGCCGCATCCTCTTCCTC
237	B-actin R	CCACAGGATTCCATACCCAAG
238	Hprt F	TGATTAGCGATGATGAACCAGG
239	Hprt R	CCTTCATGACATCTCGAGCAAG

Appendix for Chapter 3

Length Pole-to-pole (LPP)	longitudinal cross-sectional area	$N_{nephron}$	$N_{glomeruli}$	N_{Comma}	$N_{S\text{-}Shaped}$	Genotype
3205.38	5318570.23	4496	3264	976	256	1 - wt
3333.45	5840747.75	4024	2952	832	240	1
3482.24	6620300.26	4136	2992	824	320	1
3985.87	8407056.84	4768	3504	968	296	1
3620.90	7206341.69	3744	2656	856	232	1
3414.43	6478782.14	4392	3192	1008	192	1
3863.48	7592049.22	4320	2920	1056	344	1
3161.38	5440921.28	3616	2664	824	128	2 - Het
3788.89	7515193.93	3392	2544	752	96	2
3907.12	7062746.49	2740	2120	560	60	2
3201.43	5841391.91	3912	2904	888	120	2
3327.65	5508807.91	3552	2440	944	168	2
3536.84	6445916.81	4192	3248	864	80	2
3585.75	6190513.75	3528	2752	664	112	2

Table A-3.2.1: All values and counts of all variables (as per describe in table headings) involved in calculations.

Case Processing Summary

	Cases					
	Valid		Missing		Total	
	N	Percent	N	Percent	N	Percent
LengthPoleToPole	14	100.0%	0	0.0%	14	100.0%
LongCrossSection	14	100.0%	0	0.0%	14	100.0%
TotalNephronNumber	14	100.0%	0	0.0%	14	100.0%
GlomeruliNumber	14	100.0%	0	0.0%	14	100.0%
CommaBodies	14	100.0%	0	0.0%	14	100.0%
SshapedBodies	14	100.0%	0	0.0%	14	100.0%
Genotypes	14	100.0%	0	0.0%	14	100.0%

Table A-3.2.2: Inclusions of data for testing normality.

Coefficients[a]

Model		Unstandardized Coefficients		Standardized Coefficients	t	Sig.
		B	Std. Error	Beta		
1	(Constant)	2.428	.156		15.546	.000
	SshapedBodies	-.005	.001	-.885	-6.582	.000

a. Dependent Variable: Genotypes

Table A-3.2.3: Beta values for Comma-shaped bodies and glomeruli numbers. The beta coefficients are significant, correlating the two variables, with increment of 0.6 unit of outcome variable per increment of predictor variable.

Model Summary[b]

Model	R	R Square	Adjusted R Square	Std. Error of the Estimate
1	.692[a]	.479	.436	397.88536

a. Predictors: (Constant), Genotypes

b. Dependent Variable: TotalNephronNumber

Model Summary[b]

Model	R	R Square	Adjusted R Square	Std. Error of the Estimate
1	.562[a]	.316	.259	319.06053

a. Predictors: (Constant), Genotypes

b. Dependent Variable: GlomeruliNumber

Coefficients[a]

Model		Unstandardized Coefficients		Standardized Coefficients	t	Sig.	95.0% Confidence Interval for B		Correlations			Collinearity Statistics	
		B	Std. Error	Beta			Lower Bound	Upper Bound	Zero-order	Partial	Part	Tolerance	VIF
1	(Constant)	4975.429	336.275		14.796	.000	4242.749	5708.108					
	Genotypes	-706.857	212.679	-.692	-3.324	.006	-1170.244	-243.470	-.692	-.692	-.692	1.000	1.000

a. Dependent Variable: TotalNephronNumber

Coefficients[a]

Model		Unstandardized Coefficients		Standardized Coefficients	t	Sig.	95.0% Confidence Interval for B		Correlations			Collinearity Statistics	
		B	Std. Error	Beta			Lower Bound	Upper Bound	Zero-order	Partial	Part	Tolerance	VIF
1	(Constant)	3469.714	269.655		12.867	.000	2882.186	4057.243					
	Genotypes	-401.143	170.545	-.562	-2.352	.037	-772.729	-29.557	-.562	-.562	-.562	1.000	1.000

a. Dependent Variable: GlomeruliNumber

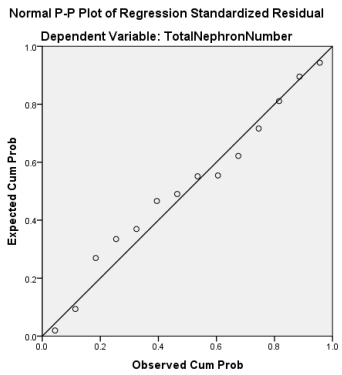

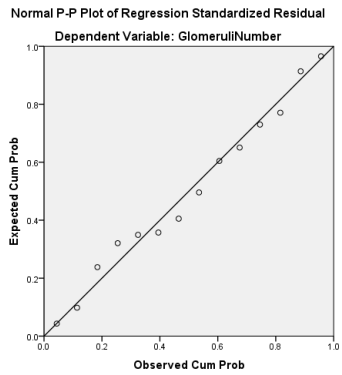

T-test

Group Statistics

	Genotypes	N	Mean	Std. Deviation	Std. Error Mean
LengthPoleToPole	1.00	7	3557.9643	283.27332	107.06725
	2.00	7	3501.2943	286.18605	108.16816
LongCrossSection	1.00	7	6780549.7329	1050611.80473	397093.93711
	2.00	7	6286498.8686	781537.37773	295393.36311
TotalNephronNumber	1.00	7	4268.5714	334.56382	126.45324
	2.00	7	3561.7143	452.42963	171.00233
GlomeruliNumber	1.00	7	3068.5714	275.30762	104.05650
	2.00	7	2667.4286	357.49819	135.12161

CommaBodies	1.00	7	931.4286	92.93521	35.12621
	2.00	7	785.1429	135.40486	51.17823
SshapedBodies	1.00	7	268.5714	53.63723	20.27297
	2.00	7	109.1429	35.07814	13.25829

Robust Tests of Equality of Means

		Statistic[a]	df1	df2	Sig.
LengthPoleToPole	Welch	.139	1	11.999	.716
	Brown-Forsythe	.139	1	11.999	.716
LongCrossSection	Welch	.997	1	11.084	.339
	Brown-Forsythe	.997	1	11.084	.339
TotalNephronNumber	Welch	11.046	1	11.051	.007
	Brown-Forsythe	11.046	1	11.051	.007
GlomeruliNumber	Welch	5.532	1	11.265	.038
	Brown-Forsythe	5.532	1	11.265	.038
CommaBodies	Welch	5.554	1	10.626	.039
	Brown-Forsythe	5.554	1	10.626	.039
SshapedBodies	Welch	43.317	1	10.339	.000
	Brown-Forsythe	43.317	1	10.339	.000

a. Asymptotically F distributed.

Independent Samples Test

		Levene's Test for Equality of Variances		t-test for Equality of Means
		F	Sig.	t
LengthPoleToPole	Equal variances assumed	.004	.949	.372
	Equal variances not assumed			.372
LongCrossSection	Equal variances assumed	.574	.463	.998
	Equal variances not assumed			.998
TotalNephronNumber	Equal variances assumed	.074	.790	3.324
	Equal variances not assumed			3.324
GlomeruliNumber	Equal variances assumed	.173	.685	2.352
	Equal variances not assumed			2.352
CommaBodies	Equal variances assumed	.951	.349	2.357
	Equal variances not assumed			2.357
SshapedBodies	Equal variances assumed	2.162	.167	6.582
	Equal variances not assumed			6.582

Independent Samples Test (continue)

		t-test for Equality of Means		
		df	Sig. (2-tailed)	Mean Difference
LengthPoleToPole	Equal variances assumed	12	.716	56.67000
	Equal variances not assumed	11.999	.716	56.67000
LongCrossSection	Equal variances assumed	12	.338	494050.86429
	Equal variances not assumed	11.084	.339	494050.86429
TotalNephronNumber	Equal variances assumed	12	.006	706.85714
	Equal variances not assumed	11.051	.007	706.85714
GlomeruliNumber	Equal variances assumed	12	.037	401.14286
	Equal variances not assumed	11.265	.038	401.14286
CommaBodies	Equal variances assumed	12	.036	146.28571
	Equal variances not assumed	10.626	.039	146.28571
SshapedBodies	Equal variances assumed	12	.000	159.42857
	Equal variances not assumed	10.339	.000	159.42857

Independent Samples Test

		t-test for Equality of Means		
		Std. Error Difference	95% Confidence Interval of the Difference	
			Lower	Upper
LengthPoleToPole	Equal variances assumed	152.19641	-274.93749	388.27749
	Equal variances not assumed	152.19641	-274.94134	388.28134
LongCrossSection	Equal variances assumed	494914.97639	-584276.23588	1572377.96445
	Equal variances not assumed	494914.97639	-594246.75959	1582348.48817
TotalNephronNumber	Equal variances assumed	212.67867	243.47012	1170.24416
	Equal variances not assumed	212.67867	239.02044	1174.69385
GlomeruliNumber	Equal variances assumed	170.54502	29.55717	772.72854
	Equal variances not assumed	170.54502	26.84984	775.43587
CommaBodies	Equal variances assumed	62.07303	11.04020	281.53123
	Equal variances not assumed	62.07303	9.07539	283.49604
SshapedBodies	Equal variances assumed	24.22345	106.65021	212.20693
	Equal variances not assumed	24.22345	105.69410	213.16304

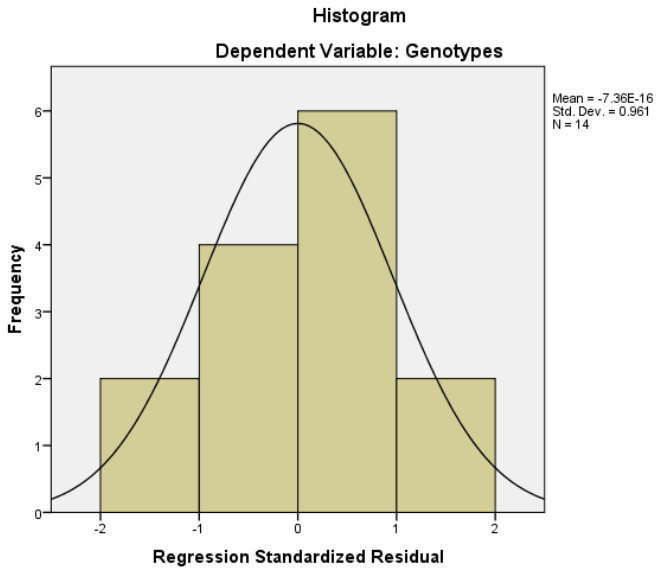

Figure A.3.1: Redual analysis for data normalisation.

Appendix for Chapter 4

4932411E22Rik	**1700041G16Rik**	**1700010H22Rik**	**1700108M19Rik**	**A930002I21Rik**
6530418L21Rik	2310015B20Rik	4430402I18Rik	Abca15	Adam11
Ankrd13c	A930004D18Rik	9830107B12Rik	Akap2	Adamtsl3
Ap1s1	Anxa3	Alpk1	Ankfn1	Adora1
Asb15	Arhgap18	Ano4	Ano6	Afap1l2
B3galt5	Arhgap28	Arhgef3	Anxa2	Agps
C1qtnf6	Arhgef4	Calcrl	Art3	Arhgap25
Ccdc92	Armc4	Cdk15	Atp9b	Ccdc62
Cd34	Ascl1	Clec14a	Cdc20b	Cdc14a
Cd5	Atp2b1	Clic5	Chn2	Cdhr3
Csmd3	Atp2b4	Crip2	Csrp1	Chgb
Daam1	B3galt1	Csdc2	Dhrs7c	Clcn3
Dtd1	Chrdl2	Cxxc4	E230008N13Rik	Creb3
Dtx4	Chst15	Cyp4a12b	Eftud1	D6Ertd474e
Edaradd	E230008N13Rik	Dub1	Enc1	Dnahc7b
Entpd3	E230008N13Rik	Elf4	Esyt2	Dock4
Fabp12	Elmo1	Elovl5	Fat3	Dpp6
Fgf20	Fndc3b	Enox1	Filip1	E330009J07Rik
Gipc1	Grin2a	Fat3	Gm766	Ect2l
Gm973	Hdac5	Gm10637	Greb1l	Fhad1
Gnal	Il15	Gm1110	L1cam	Foxo6
Hmcn1	Kat2b	Grik4	Lhx9	Gas5
Inpp5d	Lamb1	Hs3st3b1	Nebl	Il1rapl1
Klk15	Map4k3	Lrrk1	Net1	Kank4
Magi2	Mast1	Mmrn2	Nlrc5	Lyrm4
Mgat1	Mesdc1	Mylk4	Pcp4	Myof
Ngf	Npr3	Nt5c2	Pcsk6	Nes
Nlrc5	Pknox2	Pde4d	Pld1	Nlrc5
Npas3	Reln	Pex5l	Ptpro	Nmu
Plb1	Scn3a	Pgm2	Rab3il1	Nrxn2
Plce1	Selm	Plekhm3	Rasa4	Pard3b
Rgag4	Sema3f	Ptprr	Rgs8	Parvb
Sat2	Sema6d	Scn4a	Rp1	Pde10a
Sfmbt2	Slc26a7	Slc4a10	S100a10	Prkch
Sh2d4a	Slc35f4	Sqstm1	Senp5	Prss16
Shb	Smoc1	Stac2	Slc12a6	Ptplad2

Slc25a14	Snap91	Tgfbr3	Slc25a40	Rcsd1
Slc9a9	Soat1	Tmprss11f	Slc45a3	Slc4a8
Spats2	Specc1	Tpm4	Spnb1	Susd4
Sulf1	St3gal4	Tspan2	Tchh	Unc13c
Tbc1d10a	Stom	Txndc5	Tgfbr2	Wt1
Tiam2	Tec	Wwc2	Ttc4	Zfp385b
Yipf1	Txnrd2	Zfp353	Zbtb20	

Table A-4.6.2: List of 216 genes that contain WT1 target sequence (intragenic) from my array

Genes	***WT1 Target Domain***	***Descriptions***
Slc25a40	yes	NM_178766 ::: Mus musculus solute carrier family 25, member 40 (Slc25a40), nuclear gene encoding mitochondrial protein, mRNA.
Clic5	yes	NM_172621 ::: Mus musculus chloride intracellular channel 5 (Clic5), nuclear gene encoding mitochondrial protein, mRNA.
Slc25a14	yes	NM_011398 ::: Mus musculus solute carrier family 25 (mitochondrial carrier, brain), member 14 (Slc25a14), nuclear gene encoding mitochondrial protein, transcript variant 2, mRNA.
Txnrd2	yes	NM_013711 ::: Mus musculus thioredoxin reductase 2 (Txnrd2), nuclear gene encoding mitochondrial protein, mRNA.
Dtd1	yes	NM_025314 ::: Mus musculus D-tyrosyl-tRNA deacylase 1 homolog (S. cerevisiae) (Dtd1), nuclear gene encoding mitochondrial protein, mRNA.
Maob	no	NM_172778 ::: Mus musculus monoamine oxidase B (Maob), nuclear gene encoding mitochondrial protein, mRNA.
Reep1	no	NM_178608 ::: Mus musculus receptor accessory protein 1 (Reep1), nuclear gene encoding mitochondrial protein, mRNA.
Tufm	no	NM_001163713 ::: Mus musculus Tu translation elongation factor, mitochondrial (Tufm), nuclear gene encoding mitochondrial protein, transcript variant 2, mRNA.
Opa1	yes	NM_133752 ::: Mus musculus optic atrophy 1 homolog (human) (Opa1), nuclear gene encoding mitochondrial protein, mRNA.
Cps1	no	NM_001080809 ::: Mus musculus carbamoyl-phosphate synthetase 1 (Cps1), nuclear gene encoding mitochondrial protein, mRNA.

Pck2	no	NM_028994 ::: Mus musculus phosphoenolpyruvate carboxykinase 2 (mitochondrial) (Pck2), nuclear gene encoding mitochondrial protein, mRNA.
Slc25a18	no	NM_001081048 ::: Mus musculus solute carrier family 25 (mitochondrial carrier), member 18 (Slc25a18), nuclear gene encoding mitochondrial protein, mRNA.

Table A-4.6.3 : List of mitochondrial related genes (nuclear gene encoding mitochondrial protein, mRNA) (p < 0.05) from my array, excluding the tRNAs.

GENE	REGULATION	WT1 BIND-SEQ
ANGPTL4	DOWN	++
APLNR	DOWN	--
CD55	DOWN	++
CDR2L	UP	+
CLDN12	DOWN	+
CLIC5	DOWN	++
DNAHC7B	DOWN	++
EDNRB	DOWN	--
ELF4	DOWN	++
FILIP1	DOWN	++
FNDC3B	DOWN	++
ITGB4	UP	--
KAT2B	DOWN	++
MAFB	DOWN	++
MSN	DOWN	+
NES	DOWN	++
NPAS3	DOWN	++
PTPRO	DOWN	++
SHB	UP	++
SPHKAP	UP	--
TGFBR3	DOWN	++
THTPA	DOWN	+
TLR1	DOWN	--
TSPAN2	DOWN	++
TUFM	DOWN	--
XIAP	DOWN	+

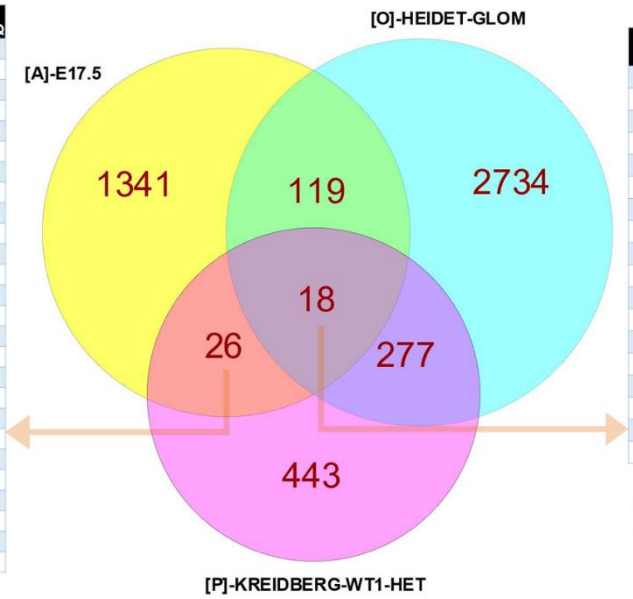

GENE	REGULATION	WT1 BIND-SEQ
B3GALT1	DOWN	++
BMX	DOWN	--
CRTAM	UP	--
CTSK	DOWN	--
DOCK4	DOWN	++
GALC	DOWN	++
GRP	UP	--
NEBL	DOWN	++
NGF	DOWN	++
P2RX1	DOWN	+
PARD3B	DOWN	++
PGM2	DOWN	++
PLCE1	DOWN	++
SEMA6D	DOWN	++
SLC26A7	DOWN	++
SULF1	DOWN	++
WT1	DOWN	++
ZFP385B	DOWN	++

++ Presence of WT1 binding sequence in gene region
+ - Presence of WT1 binding sequence on nearby region
- - No WT1 binding sequence seen
up/down Gene expression from E17.5 microarray kidney

Figure A.4.6.1: A Venn diagram showing overlap of comparison database of 3 microarrays (p<0.05). [A] is E17.5 whole kidney microarray, [O] is DDS/+ heterozygous adult isolated podocyte glomerulus kidney microarray from Ratelade et al., 2010, and [P] is WT1 heterozygous mutant adult isolated glomerulus kidney microarray from Schumacher et al., 2011. Adjacent tables showing the respective overlap list of differentially expressed genes in mutant mice together with regulation status and listed indication for presence of WT1 transcriptional binding.

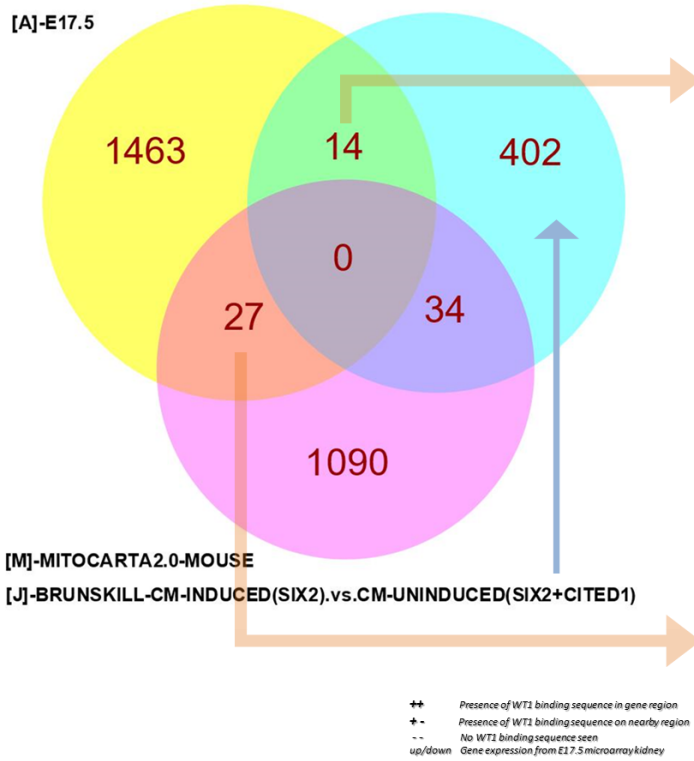

GENE	REGULATION	WT1 BIND-SEQ
1810031K17RIK	DOWN	+
2610204G22RIK	UP	--
ADAM11	UP	++
ANGPTL4	DOWN	++
AP1S1	DOWN	++
CCL27A	UP	--
CREB3	DOWN	++
CRYM	UP	--
KAT2B	DOWN	++
LLPH	DOWN	--
PTPN13	DOWN	++
SULF1	DOWN	++
TGFBR3	DOWN	++
WNT5A	DOWN	--

GENE	REGULATION	WT1 BIND-SEQ
CLPB	DOWN	++
COX17	DOWN	+
CPS1	UP	+
FOXRED1	DOWN	--
LETMD1	DOWN	+
LYRM4	DOWN	--
MAOB	DOWN	--
MTERF4	DOWN	--
OPA1	DOWN	+
OXR1	DOWN	++
PCK2	UP	++
PDHA2	UP	--
RNMTL1	DOWN	--
SEPT4	DOWN	+
SLC25A14	DOWN	++
SLC25A18	UP	++
SLC25A40	DOWN	++
STOM	DOWN	++
TMEM11	UP	++
TUFM	DOWN	--
TXNRD2	DOWN	++
UQCRC1	DOWN	--
MT-T	DOWN	--
MT-T	DOWN	--
MT-T	DOWN	--
MT-T	DOWN	--
MT-T	DOWN	--

Figure A.4.6.2: An extension of previous Venn diagram to include a gene list from MitoMiner website, [M] MitoCarta2.0 that recently updated listing the known genes that directly related to the mitochondrial. Adjacent tables showing the respective overlap list of differentially expressed genes in mutant mice together with regulation status and listed indication for presence of WT1 transcriptional binding.

GENE	REGULATION	WT1 BIND-SEQ
B3GALT1	DOWN	++
BMX	DOWN	--
CRTAM	UP	--
CTSK	DOWN	--
DOCK4	DOWN	++
GALC	DOWN	++
GRP	UP	--
NEBL	DOWN	++
NGF	DOWN	++
P2RX1	DOWN	+
PARD3B	DOWN	++
PGM2	DOWN	++
PLCE1	DOWN	++
SEMA6D	DOWN	++
SLC26A7	DOWN	++
SULF1	DOWN	++
WT1	DOWN	++
ZFP385B	DOWN	++

GENE	REGULATION	WT1 BIND-SEQ
ANGPTL4	DOWN	++
APLNR	DOWN	--
CD55	DOWN	++
CDR2L	UP	+
CLDN12	DOWN	+
CLIC5	DOWN	++
DNAHC7B	DOWN	++
EDNRB	DOWN	--
ELF4	DOWN	++
FILIP1	DOWN	++
FNDC3B	DOWN	++
ITGB4	UP	--
KAT2B	DOWN	++
MAFB	DOWN	++
MSN	DOWN	+
NES	DOWN	++
NPAS3	DOWN	++
PTPRO	DOWN	++
SHB	UP	++
SPHKAP	UP	--
TGFBR3	DOWN	++
THTPA	DOWN	+
TLR1	DOWN	--
TSPAN2	DOWN	++
XIAP	DOWN	+

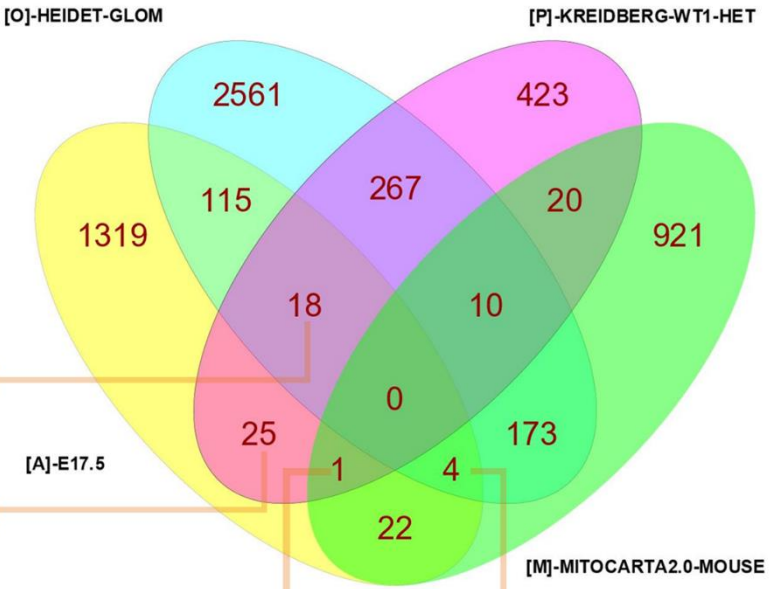

GENE	REGULATION	WT1 BIND-SEQ
TUFM	DOWN	--

GENE	REGULATION	WT1 BIND-SEQ
OPA1	DOWN	+
OXR1	DOWN	++
SEPT4	DOWN	+
TXNRD2	DOWN	++

++ *Presence of WT1 binding sequence in gene region*
+ - *Presence of WT1 binding sequence on nearby region*
- - *No WT1 binding sequence seen*
up/down *Gene expression from E17.5 microarray kidney*

Figure A.4.6.3: A Venn diagram showing overlap of comparison database of 3 microarrays (p<0.05). [A] is E17.5 whole kidney microarray, [O] is DDS/+ heterozygous adult isolated podocyte glomerulus kidney microarray from Ratelade et al., 2010, and [P] is WT1 heterozygous mutant adult isolated glomerulus kidney microarray from Schumacher et al., 2011, and [M] MitoCarta2.0 that listing genes that directly related to the mitochondrial. Adjacent tables showing the respective overlap list of differentially expressed genes in mutant mice together with regulation status and listed indication for presence of WT1 transcriptional binding.

Appendix Chapter 6

Genes	Full name and annotated functions if any
Clpb	ClpB caseinolytic peptidase B; May function as a regulatory ATPase and be related to secretion/protein trafficking process (677 aa)
Ltbp1	latent transforming growth factor beta binding protein 1 (1712 aa)
Tgfb1	transforming growth factor, beta 1; Multifunctional protein that controls proliferation, differentiation and other functions in many cell types. Many cells synthesize TGFB1 and have specific receptors for it. It positively and negatively regulates many other growth factors. It plays an important role in bone remodeling as it is a potent stimulator of osteoblastic bone formation, causing chemotaxis, proliferation and differentiation in committed osteoblasts (390 aa)
Ciao1	cytosolic iron-sulfur protein assembly 1; Key component of the cytosolic iron-sulfur protein assembly (CIA) complex, a multiprotein complex that mediates the incorporation of iron-sulfur cluster into extramitochondrial Fe/S proteins. Seems to specifically modulate the transactivation activity of WT1. As part of the mitotic spindle-associated MMXD complex it may play a role in chromosome segregation (By similarity) (339 aa)
Pdk1	pyruvate dehydrogenase kinase, isoenzyme 1; Serine/threonine kinase that plays a key role in regulation of glucose and fatty acid metabolism and homeostasis via phosphorylation of the pyruvate dehydrogenase subunits PDHA1 and PDHA2. This inhibits pyruvate dehydrogenase activity, and thereby regulates metabolite flux through the tricarboxylic acid cycle, down-regulates aerobic respiration and inhibits the formation of acetyl-coenzyme A from pyruvate. Plays an important role in cellular responses to hypoxia and is important for cell proliferation under hypoxia. Protects cells against apo [...] (434 aa)
Wtap	Wilms' tumour 1-associating protein; Regulates G2/M cell-cycle transition by binding to the 3' UTR of CCNA2, which enhances its stability. Impairs WT1 DNA- binding ability and inhibits expression of WT1 target genes. May be involved in mRNA splicing regulation (By similarity) (396 aa)
Pdk4	pyruvate dehydrogenase kinase, isoenzyme 4; Serine/threonine kinase that plays a key role in regulation of glucose and fatty acid metabolism and homeostasis via phosphorylation of the pyruvate dehydrogenase subunits PDHA1 and PDHA2. This inhibits pyruvate dehydrogenase activity, and thereby regulates metabolite flux through the tricarboxylic acid cycle, down-regulates aerobic respiration and inhibits the formation of acetyl-coenzyme A from pyruvate. Inhibition of pyruvate dehydrogenase decreases glucose utilization and increases fat metabolism in response to prolonged fasting and starv [...] (412 aa)

Tab1	TGF-beta activated kinase 1/MAP3K7 binding protein 1; May be an important signaling intermediate between TGFB receptors and MAP3K7/TAK1. May play an important role in mammalian embryogenesis (502 aa)
Uqcrc1	ubiquinol-cytochrome c reductase core protein 1; This is a component of the ubiquinol-cytochrome c reductase complex (complex III or cytochrome b-c1 complex), which is part of the mitochondrial respiratory chain. This protein may mediate formation of the complex between cytochromes c and c1 (By similarity) (480 aa)
Cps1	carbamoyl-phosphate synthetase 1; Involved in the urea cycle of ureotelic animals where the enzyme plays an important role in removing excess ammonia from the cell (1500 aa)
Mterfd2	MTERF domain containing 2; Required for the targeting of the methyltransferase NSUN4 to mitochondrial large ribosomal subunit and efficient rRNA methylation (346 aa)
Yme1l1	YME1-like 1 (S. cerevisiae); Putative ATP-dependent protease which plays a role in mitochondrial protein metabolism. Ensures cell proliferation, maintains normal cristae morphology and complex I respiration activity, promotes antiapoptotic activity, and protects mitochondria from the accumulation of oxidatively damaged membrane proteins. Requires to control the accumulation of nonassembled respiratory chain subunits (NDUFB6, OX4 and ND1). Seems to act in the processing of OPA1 (By similarity) (715 aa)
Stom	stomatin; Thought to regulate cation conductance. May regulate ASIC2 and ASIC3 gating (284 aa)
Park7	Parkinson disease (autosomal recessive, early onset) 7; Protects cells against oxidative stress and cell death. Plays a role in regulating expression or stability of the mitochondrial uncoupling proteins SLC25A14 and SLC25A27 in dopaminergic neurons of the substantia nigra pars compacta and attenuates the oxidative stress induced by calcium entry into the neurons via L-type channels during pacemaking. Eliminates hydrogen peroxide and protects cells against hydrogen peroxide-induced cell death. May act as an atypical peroxiredoxin-like peroxidase that scavenges hydrogen peroxide. Follow [...] (189 aa)
Pdk3	pyruvate dehydrogenase kinase, isoenzyme 3; Inhibits pyruvate dehydrogenase activity by phosphorylation of the E1 subunit PDHA1, and thereby regulates glucose metabolism and aerobic respiration. Can also phosphorylate PDHA2. Decreases glucose utilization and increases fat metabolism in response to prolonged fasting, and as adaptation to a high-fat diet. Plays a role in glucose homeostasis and in maintaining normal blood glucose levels in function of nutrient levels and under starvation. Plays a role in the generation of reactive oxygen species (By similarity) (415 aa)
Opa1	optic atrophy 1; Dynamin-related GTPase required for mitochondrial fusion and regulation of apoptosis. May form a diffusion barrier for proteins stored in mitochondrial cristae. Proteolytic processing in response to intrinsic apoptotic signals may lead to disassembly

	of OPA1 oligomers and release of the caspase activator cytochrome C (CYCS) into the mitochondrial intermembrane space (978 aa)
Letmd1	LETM1 domain containing 1; Involved in tumorigenesis and may function as a negative regulator of the p53/TP53 (360 aa)
Scube3	signal peptide, CUB domain, EGF-like 3; Binds to TGFBR2 and activates TGFB signaling (By similarity) (993 aa)
Pck2	phosphoenolpyruvate carboxykinase 2 (mitochondrial); Catalyzes the conversion of oxaloacetate (OAA) to phosphoenolpyruvate (PEP), the rate-limiting step in the metabolic pathway that produces glucose from lactate and other precursors derived from the citric acid cycle (By similarity) (667 aa)
Foxred1	FAD-dependent oxidoreductase domain containing 1 (493 aa)
Map3k7	mitogen-activated protein kinase kinase kinase 7; Serine/threonine kinase which acts as an essential component of the MAP kinase signal transduction pathway. Plays an important role in the cascades of cellular responses evoked by changes in the environment. Mediates signal transduction of TRAF6, various cytokines including interleukin-1 (IL-1), transforming growth factor-beta (TGFB), TGFB-related factors like BMP2 and BMP4, toll-like receptors (TLR), tumor necrosis factor receptor CD40 and B-cell receptor (BCR). Ceramides are also able to activate MAP3K7/TAK1. Once activated, acts as a [...] (606 aa)
Maob	monoamine oxidase B; Catalyzes the oxidative deamination of biogenic and xenobiotic amines and has important functions in the metabolism of neuroactive and vasoactive amines in the central nervous system and peripheral tissues. MAOB preferentially degrades benzylamine and phenylethylamine (By similarity) (520 aa)
Chchd4	coiled-coil-helix-coiled-coil-helix domain containing 4; Functions as chaperone and catalyzes the formation of disulfide bonds in substrate proteins, such as COX17. Required for the import and folding of small cysteine-containing proteins (small Tim) in the mitochondrial intermembrane space (IMS). Precursor proteins to be imported into the IMS are translocated in their reduced form into the mitochondria. The oxidized form of CHCHD4/MIA40 forms a transient intermolecular disulfide bridge with the reduced precursor protein, resulting in oxidation of the precursor protein that now contain [...] (139 aa)
Pdk2	pyruvate dehydrogenase kinase, isoenzyme 2; Serine/threonine kinase that plays a key role in the regulation of glucose and fatty acid metabolism and homeostasis via phosphorylation of the pyruvate dehydrogenase subunits PDHA1 and PDHA2. This inhibits pyruvate dehydrogenase activity, and thereby regulates metabolite flux through the tricarboxylic acid cycle, down-regulates aerobic respiration and inhibits the formation of acetyl-coenzyme A from pyruvate. Inhibition of pyruvate dehydrogenase decreases

	glucose utilization and increases fat metabolism. Mediates cellular responses to insuli [...] (407 aa)
Rnmtl1	RNA methyltransferase like 1; Probable RNA methyltransferase (By similarity) (418 aa)
Oma1	OMA1 homolog, zinc metallopeptidase (S. cerevisiae); Metalloprotease that is part of the quality control system in the inner membrane of mitochondria. Following stress conditions that induce loss of mitochondrial membrane potential, mediates cleavage of OPA1 at S1 position, leading to OPA1 inactivation and negative regulation of mitochondrial fusion. Its role in mitochondrial quality control is essential for regulating lipid metabolism as well as to maintain body temperature and energy expenditure under cold-stress conditions (521 aa)
Parl	presenilin associated, rhomboid-like; Required for the control of apoptosis during postnatal growth. Essential for proteolytic processing of an antiapoptotic form of OPA1 which prevents the release of mitochondrial cytochrome c in response to intrinsic apoptoptic signals (By similarity) (377 aa)
Wtip	WT1-interacting protein; Adapter or scaffold protein which participates in the assembly of numerous protein complexes and is involved in several cellular processes such as cell fate determination, cytoskeletal organization, repression of gene transcription, cell-cell adhesion, cell differentiation, proliferation and migration. Positively regulates microRNA (miRNA)-mediated gene silencing. Negatively regulates Hippo signaling pathway and antagonizes phosphorylation of YAP1. Acts as a transcriptional corepressor for SNAI1 and SNAI2/SLUG-dependent repression of E-cadherin transcription. A [...] (398 aa)
Cox17	cytochrome c oxidase, subunit XVII assembly protein homolog (yeast) (63 aa)
Tmem11	transmembrane protein 11; Plays a role in mitochondrial morphogenesis (By similarity) (190 aa)
Pdha2	pyruvate dehydrogenase E1 alpha 2; The pyruvate dehydrogenase complex catalyzes the overall conversion of pyruvate to acetyl-CoA and CO(2), and thereby links the glycolytic pathway to the tricarboxylic cycle (By similarity) (391 aa)
Lyrm4	LYR motif containing 4; Required for nuclear and mitochondrial iron-sulfur protein biosynthesis (By similarity) (91 aa)
Eid2	EP300 interacting inhibitor of differentiation 2; Interacts with EP300 and acts as a repressor of MYOD- dependent transcription and muscle differentiation. Inhibits EP300 histone acetyltransferase activity. Acts as a repressor of TGFB/SMAD transcriptional responses. May act as a repressor of the TGFB/SMAD3-dependent signaling by selectively blocking formation of TGFB-induced SMAD3-SMAD4 complex (By similarity) (236 aa)
Slc25a40	solute carrier family 25, member 40 (337 aa)
Sirt5	sirtuin 5 (silent mating type information regulation 2 homolog) 5 (S. cerevisiae); NAD-dependent lysine demalonylase and desuccinylase that specifically removes malonyl and succinyl groups on target proteins. Activates CPS1 and contributes to the regulation of

	blood ammonia levels during prolonged fasting- acts by mediating desuccinylation of CPS1, thereby increasing CPS1 activity in response to elevated NAD levels during fasting. Has weak NAD- dependent protein deacetylase activity; however this activity may not be physiologically relevant in vivo. Can deacetylate cytochrome c (CYCS) [...] (310 aa)
Tgif2lx2	TGFB-induced factor homeobox 2-like, X-linked 2 (231 aa)
Tgif2lx1	TGFB-induced factor homeobox 2-like, X-linked 1 (231 aa)
mt-Co3	mitochondrially encoded cytochrome c oxidase III; Subunits I, II and III form the functional core of the enzyme complex (By similarity) (261 aa)
mt-Nd3	mitochondrially encoded NADH dehydrogenase 3; Core subunit of the mitochondrial membrane respiratory chain NADH dehydrogenase (Complex I) that is believed to belong to the minimal assembly required for catalysis. Complex I functions in the transfer of electrons from NADH to the respiratory chain. The immediate electron acceptor for the enzyme is believed to be ubiquinone (By similarity) (115 aa)
mt-Nd4	mitochondrially encoded NADH dehydrogenase 4; Core subunit of the mitochondrial membrane respiratory chain NADH dehydrogenase (Complex I) that is believed to belong to the minimal assembly required for catalysis. Complex I functions in the transfer of electrons from NADH to the respiratory chain. The immediate electron acceptor for the enzyme is believed to be ubiquinone (By similarity) (459 aa)
mt-Nd5	mitochondrially encoded NADH dehydrogenase 5; Core subunit of the mitochondrial membrane respiratory chain NADH dehydrogenase (Complex I) that is believed to belong to the minimal assembly required for catalysis. Complex I functions in the transfer of electrons from NADH to the respiratory chain. The immediate electron acceptor for the enzyme is believed to be ubiquinone (By similarity) (607 aa)
mt-Nd4l	mitochondrially encoded NADH dehydrogenase 4L; Core subunit of the mitochondrial membrane respiratory chain NADH dehydrogenase (Complex I) that is believed to belong to the minimal assembly required for catalysis. Complex I functions in the transfer of electrons from NADH to the respiratory chain. The immediate electron acceptor for the enzyme is believed to be ubiquinone (By similarity) (98 aa)
Pawr	PRKC, apoptosis, WT1, regulator; Pro-apoptopic protein capable of selectively inducing apoptosis in cancer cells, sensitizing the cells to diverse apoptotic stimuli and causing regression of tumors in animal models. Induces apoptosis in certain cancer cells by activation of the Fas prodeath pathway and coparallel inhibition of NF-kappa-B transcriptional activity. Inhibits the transcriptional activation and augments the transcriptional repression mediated by WT1. Down- regulates the anti-apoptotic protein BCL2 via its interaction with WT1. Seems also to be a transcriptional repressor by [...] (333 aa)

Tufm	Tu translation elongation factor, mitochondrial; This protein promotes the GTP-dependent binding of aminoacyl-tRNA to the A-site of ribosomes during protein biosynthesis (By similarity) (452 aa)
Thsd4	thrombospondin, type I, domain containing 4; Promotes FBN1 matrix assembly. Attenuates TGFB signaling, possibly by accelerating the sequestration of large latent complexes of TGFB or active TGFB by FBN1 microfibril assembly, thereby negatively regulating the expression of TGFB regulatory targets, such as POSTN (1018 aa)
Tgif2	TGFB-induced factor homeobox 2; Transcriptional repressor, which probably repress transcription by binding directly the 5'-CTGTCAA-3' DNA sequence or by interacting with TGF-beta activated SMAD proteins. Probably represses transcription via the recruitment of histone deacetylase proteins (By similarity) (237 aa)
Oxr1	oxidation resistance 1; May be involved in protection from oxidative damage (866 aa)
Slc25a18	solute carrier family 25 (mitochondrial carrier), member 18; Involved in the transport of glutamate across the inner mitochondrial membrane. Glutamate is cotransported with H(+) (By similarity) (320 aa)
Slc25a14	solute carrier family 25 (mitochondrial carrier, brain), member 14; Participates in the mitochondrial proton leak measured in brain mitochondria (325 aa)
Txnrd2	thioredoxin reductase 2; Maintains thioredoxin in a reduced state. Implicated in the defenses against oxidative stress. May play a role in redox- regulated cell signaling (524 aa)
AI037035	Cytochrome c oxidase copper chaperone ; Copper chaperone for cytochrome c oxidase (COX). Binds two copper ions and deliver them to the Cu(A) site of COX (By similarity) (63 aa)
Wt1	Wilms tumor 1 homolog; Transcription factor that plays an important role in cellular development and cell survival. Regulates the expression of numerous target genes, including EPO. Plays an essential role for development of the urogenital system. Recognizes and binds to the DNA sequence 5'-CGCCCCCGC-3'. It has a tumor suppressor as well as an oncogenic role in tumor formation. Function may be isoform-specific- isoforms lacking the KTS motif may act as transcription factors. Isoforms containing the KTS motif may bind mRNA and play a role in mRNA metabolism or splicing. Isoform 1 has lo [...] (517 aa)
Tgif1	TGFB-induced factor homeobox 1; Binds to a retinoid X receptor (RXR) responsive element from the cellular retinol-binding protein II promoter (CRBPII- RXRE). Inhibits the 9-cis-retinoic acid-dependent RXR alpha transcription activation of the retinoic acid responsive element. May participate in the transmission of nuclear signals during development and in the adult, as illustrated by the down- modulation of the RXR alpha activities (By similarity) (305 aa)

Table A-6.1.3.1: STRING genes list and annotated functions

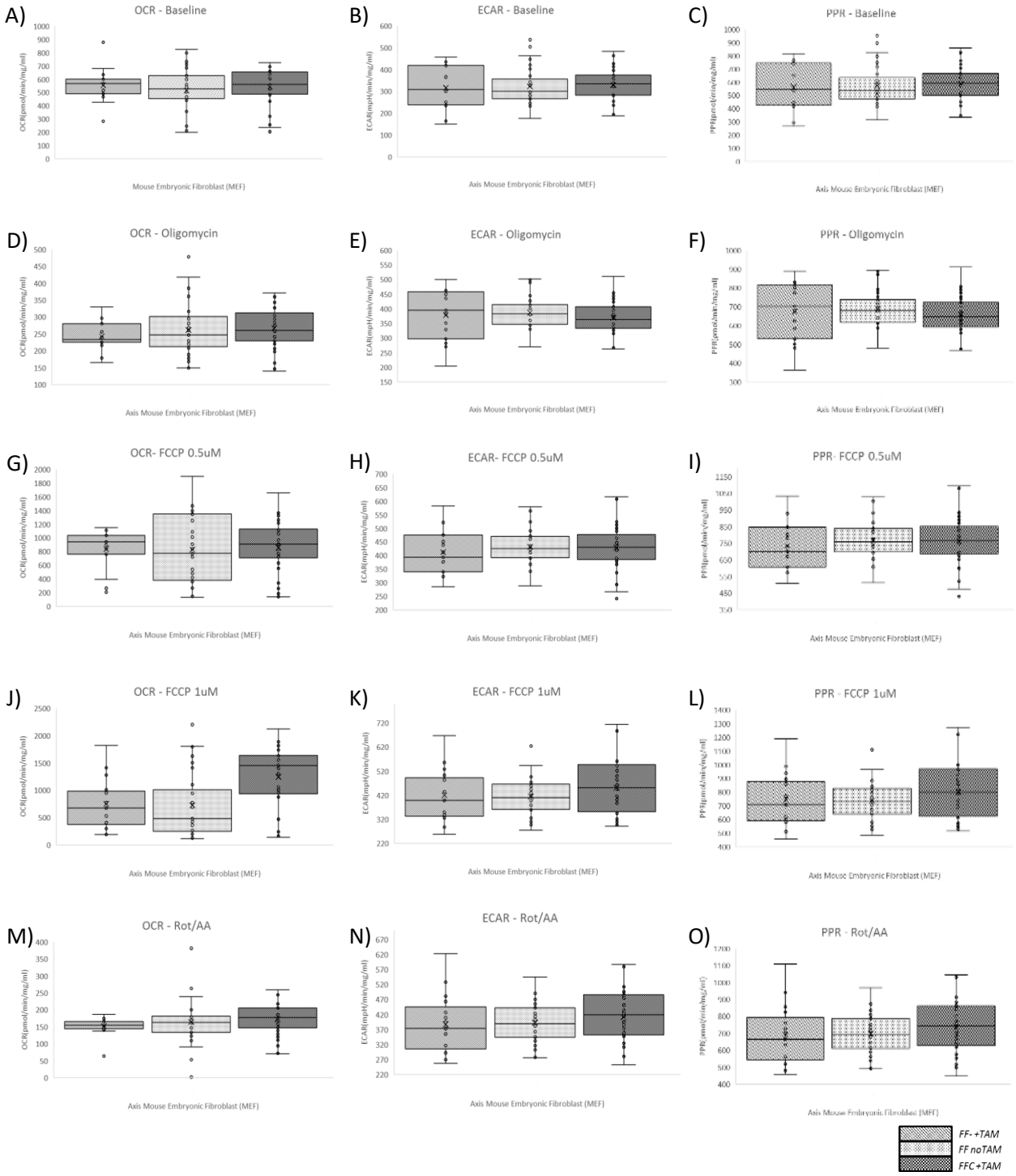

Figure A-6.5.3: Box-plot of individual major time points of XF Cell Mito Stress Test.

REFERENCES

1. Aguer C, Gambarotta D, Mailloux RJ, Moffat C, Dent R, McPherson R, Harper ME. Galactose enhances oxidative metabolism and reveals mitochondrial dysfunction in human primary muscle cells. PLoS One. 2011;6(12):e28536. doi: 10.1371/journal.pone.0028536. Epub 2011 Dec 15.
2. Aguer C, Gambarotta D, Mailloux RJ, Moffat C, Dent R, McPherson R, Harper ME. Galactose enhances oxidative metabolism and reveals mitochondrial dysfunction in human primary muscle cells. PLoS One. 2011;6(12):e28536. doi: 10.1371/journal.pone.0028536. Epub 2011 Dec 15.
3. Ahzad A. Conditional mouse knockout model for Wilms tumor suppressor gene 1 to understand kidney disease/cancer. MSc, 2010.
4. An S. De Vriese, Sanjeev Sethi, Karl A. Nath, Richard J. Glassock and Fernando C. Fervenza. Differentiating Primary, Genetic, and Secondary FSGS in Adults: A Clinicopathologic Approach. JASN March 2018, 29 (3) 759-774; DOI: https://doi.org/10.1681/ASN.2017090958
5. Anderson S, Bankier AT, Barrell BG, et al. Sequence and organization of the human mitochondrial genome. Nature 1981; 290: 457–465.
6. Appel D, Kershaw DB, Smeets B, Yuan G, Fuss A, Frye B, Elger M, Kriz W, Floege J, Moeller MJ. Recruitment of podocytes from glomerular parietal epithelial cells. J Am Soc Nephrol. 20, 333-343 (2009).
7. Appel D, Kershaw DB, Smeets B, Yuan G, Fuss A, Frye B, Elger M, Kriz W, Floege J, Moeller MJ. Recruitment of podocytes from glomerular parietal epithelial cells. J Am Soc Nephrol. 20, 333-343 (2009).
8. Ardissino G, Dacc V, Testa S, Bonaudo R, Claris-Appiani A, Taioli E, Marra G, Edefonti A, Sereni F, ItalKid Project Epidemiology of chronic renal failure in children: data from the ItalKid project. Pediatrics. 2003;111:e382–e387. doi: 10.1542/peds.111.4.e382.
9. Armstrong, J. F., Pritchard Jones, K., Bickmore, W. A., Hastie, N. D. & Bard, J. B. The expression of the Wilms' tumour gene, WT1, in the developing mammalian embryo. Mech. Dev. 40, 85–97 (1993).
10. Arnould, C., Lelièvre-Pégorier, M., Ronco, P., & Lelongt, B. (2009). MMP9 limits apoptosis and stimulates branching morphogenesis during kidney development. Journal of the American Society of Nephrology : JASN, 20(10), 2171-80.
11. Arora P, Rajagopalan S, Patel N, Nainani N, Venuto RC, Lohr JW. The MDRD equation underestimates the prevalence of CKD among blacks and overestimates the prevalence of CKD among whites compared to the CKD-EPI equation: a retrospective cohort study. BMC Nephrol. 2012 Jan 20;13:4. doi: 10.1186/1471-2369-13-4.
12. Ashkenazi A, Dixit VM: Apoptosis control by death and decoy receptors. Curr Opin Cell Biol 11 : 255 –260, 1999
13. Azuma H, Nadeau K, Mackenzie HS, Brenner BM, Tilney NL: Nephron mass modulates the hemodynamic, cellular, and molecular response of the rat renal allograft. Transplantation 63: 519–528, 1997
14. Azuma H, Nadeau K, Mackenzie HS, Brenner BM, Tilney NL: Nephron mass modulates the hemodynamic, cellular, and molecular response of the rat renal allograft. Transplantation 63: 519–528, 1997
15. Bai, Yidong, Rebecca M. Shakeley, and Giuseppe Attardi. Tight Control of Respiration by NADH Dehydrogenase ND5 Subunit Gene Expression in Mouse Mitochondria. Molecular And Cellular Biology, Feb. 2000, p. 805–815
16. Baird, P. N., Santos, A., Groves, N., Jadresic, L., Cowell, J. K. Constitutional mutations in the WT1 gene in patients with Denys-Drash syndrome. Hum. Molec. Genet. 1: 301-305, 1992.
17. Bao L, Haas M, Pippin J, Wang Y, Miwa T, Chang A, Minto AW, Petkova M, Qiao G, Song WC, Alpers CE, Zhang J, Shankland SJ, Quigg RJ. Focal and segmental glomerulosclerosis induced in mice lacking decay-accelerating factor in T cells. J Clin Invest. 2009 May;119(5):1264-74. doi: 10.1172/JCI36000.

18. Bao L, Spiller OB, St John PL, Haas M, Hack BK, Ren G, Cunningham PN, Doshi M, Abrahamson DR, Morgan BP, Quigg RJ. Decay-accelerating factor expression in the rat kidney is restricted to the apical surface of podocytes. Kidney Int. 2002 Dec;62(6):2010-21.
19. Bao L, Spiller OB, St John PL, Haas M, Hack BK, Ren G, Cunningham PN, Doshi M, Abrahamson DR, Morgan BP, Quigg RJ. Decay-accelerating factor expression in the rat kidney is restricted to the apical surface of podocytes. Kidney Int. 2002 Dec;62(6):2010-21.
20. Bao L, Spiller OB, St John PL, Haas M, Hack BK, Ren G, Cunningham PN, Doshi M, Abrahamson DR, Morgan BP, Quigg RJ. Decay-accelerating factor expression in the rat kidney is restricted to the apical surface of podocytes. Kidney Int. 2002 Dec;62(6):2010-21.
21. Barak, H. et al. FGF9 and FGF20 maintain the stemness of nephron progenitors in mice and man. Dev. Cell 22, 1191–1207 (2012).
22. Barua M, Brown EJ, Charoonratana VT, et al. Mutations in the INF2 gene account for a significant proportion of familial but not sporadic focal and segmental glomerulosclerosis. Kidney Int 2013; 83:316.
23. Bauer R, Walter B, Bauer K, Klupsch R, Patt S, Zwiener U: Intrauterine growth restriction reduces nephron number and renal excretory function in newborn piglets. Acta Physiol Scand 176: 83–90, 2002
24. Bauer R, Walter B, Bauer K, Klupsch R, Patt S, Zwiener U: Intrauterine growth restriction reduces nephron number and renal excretory function in newborn piglets. Acta Physiol Scand 176: 83–90, 2002
25. Berger I, Hershkovitz E, Shaag A, Edvardson S, Saada A, Elpeleg O. Mitochondrial complex I deficiency caused by a deleterious NDUFA11 mutation. Ann Neurol 2008; 63: 405–408.
26. Bertram JF, Cullen-McEwen LA, Egan GF, Gretz N, Baldelomar E, Beeman SC, Bennett KM. Why and how we determine nephron number. Pediatr Nephrol. 2014 Apr;29(4):575-80.
27. Bertram, J.F., Douglas-Denton, R.N., Diouf, B., Hughson, M.D., and Hoy, W.E. Human nephron number: implications for health and disease. Pediatr. Nephrol. 2011; 26: 1529–1533
28. Bertram, J.F., Douglas-Denton, R.N., Diouf, B., Hughson, M.D., and Hoy, W.E. Human nephron number: implications for health and disease. Pediatr. Nephrol. 2011; 26: 1529–1533
29. Bourgeron T, Rustin P, Chretien D, et al. Mutation of a nuclear succinate dehydrogenase gene results in mitochondrial respiratory chain deficiency. Nat Genet 1995; 11: 144–149.
30. Boyle, S., Misfeldt, A., Chandler, K.J., Deal, K.K., Southard-Smith, E.M., Mortlock, D.P., Baldwin, H.S., and de Caestecker, M. Fate mapping using Cited1-CreERT2 mice demonstrates that the cap mesenchyme contains self-renewing progenitor cells and gives rise exclusively to nephronic epithelia. Dev. Biol. 2008; 313: 234–245
31. Brand MD, Nicholls DG. Assessing mitochondrial dysfunction in cells. Biochem J. 2011;435:297–312.
32. Brandt U (2006) Energy converting NADH: quinone oxidoreductase (complex I). Annu Rev Biochem 75: 69–92.
33. Brandt U (2006) Energy converting NADH: quinone oxidoreductase (complex I). Annu Rev Biochem 75: 69–92.
34. Brenner B.M., S. Anderson. The interrelationships among filtration surface area, blood pressure, and chronic renal disease. J. Cardiovasc. Pharmacol., 19 (Suppl. 6) (1992), pp. S1–S7
35. Brodsky SV, Nadasdy GM, Pelletier R, Satoskar A, Birmingham DJ, Hadley GA, Obeidat K, Nadasdy T. Expression of the decay-accelerating factor (CD55) in renal transplants--a possible prediction marker of allograft survival. Transplantation. 2009 Aug 27;88(4):457-64. doi: 10.1097/TP.0b013e3181b0517d.
36. Brodsky SV, Nadasdy GM, Pelletier R, Satoskar A, Birmingham DJ, Hadley GA, Obeidat K, Nadasdy T. Expression of the decay-accelerating factor (CD55) in renal transplants--a possible prediction marker of allograft survival. Transplantation. 2009 Aug 27;88(4):457-64. doi: 10.1097/TP.0b013e3181b0517d.
37. Bruening W, Bardeesy N, Silverman BL, Cohn RA, Machin GA, Aronson AJ, Housman D, Pelletier J. Germline intronic and exonic mutations in the Wilms' tumour gene (WT1) affecting urogenital development. Nat Genet. 1992 May; 1(2):144-8.
38. Brunskill E. W., Aronow, B. J., Georgas, K., Rumballe, B., Valerius, M. T., Aronow, J., Kaimal, V., Jegga, A. G., Yu, J., Grimmond, S., et al. (2008). Atlas of gene expression in the developing kidney at microanatomic resolution. Dev. Cell 15, 781-791.

39. Brunskill E.W., H.L. Lai, D.C. Jamison, S.S. Potter, L.T. Patterson. Microarrays and RNA-Seq identify molecular mechanisms driving the end of nephron production. BMC Dev. Biol., 11 (2011), p. 15
40. Brunskill EW, Georgas K, Rumballe B, Little MH, Potter SS. Defining the molecular character of the developing and adult kidney podocyte. PLoS One. 2011;6(9):e24640. doi: 10.1371/journal.pone.0024640. Epub 2011 Sep 8.
41. Brunskill, E.W., Lai, H.L., Jamison, D.C., Potter, S.S., and Patterson, L.T. Microarrays and RNA-Seq identify molecular mechanisms driving the end of nephron production. BMC Dev. Biol. 2011; 11: 15
42. Brunskill, Eric W., Joo-Seop Park, Eunah Chung, Feng Chen, Bliss Magella, and S. Steven Potter. Single cell dissection of early kidney development: multilineage priming. Development. 2014 Aug; 141(15): 3093–3101. doi: 10.1242/dev.110601
43. Buckler AJ, Pelletier J, Haber DA, Glaser T, Housman DE. Isolation, characterization, and expression of the murine Wilms' tumor gene (WT1) during kidney development. Mol Cell Biol. 1991 Mar;11(3):1707-12.
44. Buckler AJ, Pelletier J, Haber DA, Glaser T, Housman DE. Isolation, characterization, and expression of the murine Wilms' tumor gene (WT1) during kidney development. Mol Cell Biol. 1991 Mar;11(3):1707-12.
45. Bustamante E, Pedersen PL (1977) High aerobic glycolysis of rat hepatoma cells in culture: role of mitochondrial hexokinase. Proc Natl Acad Sci U S A 74: 3735–3739.
46. Cain J.E., V. Di Giovanni, J. Smeeton, N.D. Rosenblum Genetics of renal hypoplasia: insights into the mechanisms controlling nephron endowment Pediatr. Res., 68 (2010), pp. 91-98
47. Cain JE, Islam E, Haxho F, Chen L, Bridgewater D, Nieuwenhuis E, Hui CC, Rosenblum ND. GLI3 Repressor Controls Nephron Number via Regulation of Wnt11 and Ret in Ureteric Tip Cells. PLoS One. 2009 Oct 7;4(10):e7313. doi: 10.1371/journal.pone.0007313.
48. Cain, J.E., Di Giovanni, V., Smeeton, J., and Rosenblum, N.D. Genetics of renal hypoplasia: insights into the mechanisms controlling nephron endowment. Pediatr. Res. 2010; 68: 91–98
49. Call KM, Glaser T, Ito CY, Buckler AJ, Pelletier J, Haber DA, Rose EA, Kral A, Yeger H, Lewis WH, et al. Isolation and characterization of a zinc finger polypeptide gene at the human chromosome 11 Wilms' tumor locus. Cell. 1990 Feb 9;60(3):509-20.
50. Call, K. M., Glaser, T., Ito, C. Y., Buckler, A. J., Pelletier, J., Haber, D. A., Rose, E. A., Kral, A., Yeger, H., Lewis, W. H., Jones, C., Housman, D. E. Isolation and characterization of a zinc finger polypeptide gene at the human chromosome 11 Wilms' tumor locus. Cell 60: 509-520, 1990.
51. Calvo SE, Clauser KR, Mootha VK. MitoCarta2.0: an updated inventory of mammalian mitochondrial proteins. Nucleic Acids Res 2016; 44: D1251–D1257.
52. Cantatore, P., P. L. Polosa, F. Fracasso, Z. Flagella, and M. N. Gadalenta. 1986. Quantitation of mitochondrial RNA species during rat liver development: the concentration of cytochrome oxidase subunit I (COI) messenger RNA increases at birth. Cell Differ. 19:125–132.
53. Carbon S, Ireland A, Mungall CJ, Shu S, Marshall B, Lewis S, AmiGO Hub, Web Presence Working Group. "AmiGO: online access to ontology and annotation data." Bioinformatics. Jan 2009;25(2):288-9.
54. Carmona R, J A Guadix, E Cano, A Ruiz-Villalba, V Portillo-Sánchez, J M Pérez-Pomares, and R Muñoz-Chápuli. The embryonic epicardium: an essential element of cardiac development. J Cell Mol Med. 2010 August; 14(8): 2066–2072. Published online 2010 May 14.
55. Caroline Wroe. Investigating the role of the WT1 gene in the development of Murine Denys-Drash syndrome. PhD Thesis, 2009.
56. Chen, W., Chen, W., Wang, H., Dong, X., Liu, Q., Mao, H., Tan, J., Lin, J., Zhou, F., Luo, N., He, H., Johnson, R. J., Zhou, S. F., … Yu, X. (2008). Prevalence and risk factors associated with chronic kidney disease in an adult population from southern China. Nephrology, dialysis, transplantation: official publication of the European Dialysis and Transplant Association - European Renal Association, 24(4), 1205-12.
57. Cheval L, Pierrat F, Rajerison R, Piquemal D, Doucet A (2012) Of Mice and Men: Divergence of Gene Expression Patterns in Kidney. PLoS ONE 7(10): e46876. https://doi.org/10.1371/journal.pone.0046876

58. Clark LC, Jr., Wolf R, Granger D, Taylor Z. Continuous recording of blood oxygen tensions by polarography. J Appl Physiol. 1953;6:189–193.
59. Costantini F., Kopan R. Patterning a complex organ: Branching morphogenesis and nephron segmentation in kidney development. Dev. Cell. 2010;18:698–712. doi: 10.1016/j.devcel.2010.04.008.
60. Costantini F., Kopan R. Patterning a complex organ: Branching morphogenesis and nephron segmentation in kidney development. Dev. Cell. 2010; 18:698–712. doi: 10.1016/j.devcel.2010.04.008.
61. Costantini F., R. Kopan. Patterning a complex organ: branching morphogenesis and nephron segmentation in kidney development. Dev. Cell, 18 (5) (2010), pp. 698–712
62. Cullen-McEwen LA, Armitage JA, Nyengaard JR, Moritz KM, Bertram JF. A design-based method for estimating glomerular number in the developing kidney. Am J Physiol Renal Physiol. 2011 Jun;300(6):F1448-53. doi: 10.1152/ajprenal.00055.2011. Epub 2011 Mar 16.
63. Cullen-McEwen, L.A., Kett, M.M., Dowling, J., Anderson, W.P., and Bertram, J.F. Nephron number, renal function, and arterial pressure in aged GDNF heterozygous mice. Hypertension. 2003; 41: 335–340
64. Cunningham TJ, Palumbo I, Grosso M, Slater N, Miles CG. WT1 regulates murine hematopoiesis via maintenance of VEGF isoform ratio. Blood. 2013 Jul 11;122(2):188-92. doi: 10.1182/blood-2012-11-466086.
65. Cunningham TJ, Palumbo I, Grosso M, Slater N, Miles CG. WT1 regulates murine hematopoiesis via maintenance of VEGF isoform ratio. Blood. 2013 Jul 11;122(2):188-92. doi: 10.1182/blood-2012-11-466086.
66. Darmady EM, Offer J, Woodhouse MA. The parameters of the ageing kidney. J Pathol 1973; 109:195.
67. Davies J.A., Ladomery M., Hohenstein P., Michael L., Shafe A., Spraggon L., Hastie N. Development of an siRNA-based method for repressing specific genes in renal organ culture and its use to show that the Wt1 tumour suppressor is required for nephron differentiation. Hum. Mol. Genet. 2004;13:235-246.
68. Davies R.C., Calvio C., Bratt E., Larsson S.H., Lamond A.I., Hastie N.D. WT1 interacts with the splicing factor U2AF65 in an isoform-dependent manner and can be incorporated into spliceosomes. Genes Dev. 1998;12:3217-3225.
69. Davies, JA., et al. Development of an siRNA-based method for repressing specific genes in renal organ culture and its use to show that the Wt1 tumour suppressor is required for nephron differentiation. Hum Mol Genet. 13, 235-246 (2004).
70. Davies, R. C., Bratt, E., Hastie, N. D. Did nucleotides or amino acids drive evolutionary conservation of the WT1 +/- KTS alternative splice? Hum. Molec. Genet. 9: 1177-1183, 2000.
71. Denic A, Lieske JC, Chakkera HA, et al. The Substantial Loss of Nephrons in Healthy Human Kidneys with Aging. J Am Soc Nephrol 2017; 28:313.
72. Dey, B. R.; Sukhatme, V. P.; Roberts, A. B., et al. Repression of the transforming growth factor β1 gene by the Wilms tumor suppressor WT1 gene product. Mol. Endocrinol. 8:595–602; 1994.
73. Diers AR, Broniowska KA, Chang CF, Hogg N. (2012) Pyruvate fuels mitochondrial respiration and proliferation of breast cancer cells: effect of monocarboxylate transporter inhibition. Biochem J. 2012 Jun 15;444(3):561-71. doi: 10.1042/BJ20120294.
74. Diers AR, Higdon AN, Ricart KC, Johnson MS, Agarwal A, Kalyanaraman B, Landar A, Darley-Usmar VM. Mitochondrial targeting of the electrophilic lipid 15-deoxy-Delta12,14-prostaglandin J2 increases apoptotic efficacy via redox cell signalling mechanisms. Biochem J. 2010;426:31–41.
75. Diya Lahiri, James R. Dutton, Antonio Duarte, Kim Moorwood, Christopher F. Graham, Andrew Ward. Nephropathy and Defective Spermatogenesis in Mice Transgenic for a Single Isoform of the Wilms' Tumour Suppressor Protein, WT1-KTS, Together With One Disrupted Wt1 Allele (2007). MOLECULAR Reproduction And Development 74:300–311 (2007).
76. Dong L, Pietsch S, Tan Z et al. Integration of cistromic and transcriptomic analyses identifies Nphs2, Mafb, and Magi2 as Wilms' Tumor 1 target genes in podocyte differentiation and maintenance. J Am Soc Nephrol 2015.

77. Dov Hershkovitz, Zvi Burbea, Karl Skorecki, and Barry M. Brenner. Fetal Programming of Adult Kidney Disease: Cellular and Molecular Mechanisms. Clin J Am Soc Nephrol 2: 334–342, 2007.
78. Dranka BP, Benavides GA, Diers AR, Giordano S, Zelickson BR, Reily C, Zou L, Chatham JC, Hill BG, Zhang J, Landar A, Darley-Usmar VM. Assessing bioenergetic function in response to oxidative stress by metabolic profiling. Free Radic Biol Med. 2011 Nov 1;51(9):1621-35. doi: 10.1016/j.freeradbiomed.2011.08.005. Epub 2011 Aug 16.
79. Dranka BP, Hill BG, Darley-Usmar VM. Mitochondrial reserve capacity in endothelial cells: The impact of nitric oxide and reactive oxygen species. Free Radic Biol Med. 2010;48:905–914.
80. Dressler G. The cellular basis of kidney development. Annu. Rev. Cell Dev. Biol. 2006; 22:509–529. doi: 10.1146/annurev.cellbio.22.010305.104340.
81. Dressler G. The cellular basis of kidney development. Annu. Rev. Cell Dev. Biol. 2006;22:509–529. doi: 10.1146/annurev.cellbio.22.010305.104340.
82. Drummond, I. A.; Madden, S. L.; Rohives-Nutter, P., et al. Repression of the insulin-like growth factor II gene by the Wilms tumor suppressor WT1. Science 257:674–678; 1992.
83. Duchen MR. Mitochondria and calcium: from cell signalling to cell death. J Physiol 2000; 529: 57–68.
84. Dudley, A. T. and Robertson, E. J. (1997). Overlapping expression domains of bone morphogenetic protein family members potentially account for limited tissue defects in BMP7 deficient embryos. Dev Dyn. 1997 Mar;208(3):349-62.
85. Dudley, A. T., Godin, R. E. & Robertson, E. J. Interaction between FGF and BMP signaling pathways regulates development of metanephric mesenchyme. Genes Dev. 13, 1601–1613 (1999).
86. Dudley, A. T., Lyons, K. M. & Robertson, E. J. A requirement for bone morphogenetic protein-7 during development of the mammalian kidney and eye. Genes Dev. 9, 2795–2807 (1995).
87. Ebert N, Jakob O, Gaedeke J, et al. Prevalence of reduced kidney function and albuminuria in older adults: the Berlin Initiative Study. Nephrol Dial Transplant 2017; 32:997.
88. Fan A.C., M.K. Bhangoo, J.C. Young, Hsp90 functions in the targeting and outer membrane translocation steps of Tom70-mediated mitochondrial import, J. Biol. Chem. 281 (2006) 33313–33324.33
89. Ferri KF, Kroemer G: Organelle-specific initiation of cell death pathways. Nat Cell Biol 3 : E255 – E263, 2001
90. Ferrick DA, Neilson A, Beeson C. Advances in measuring cellular bioenergetics using extracellular flux. Drug Discov Today. 2008;13:268–274.
91. Fivush BA, Jabs K, Neu AM, Sullivan EK, Feld L, Kohaut E, Fine R. Chronic renal insufficiency in children and adolescents: the 1996 annual report of NAPRTCS. North American Pediatric Renal Transplant Cooperative Study. Pediatr Nephrol. 1998;12:328–337. doi: 10.1007/s004670050462.
92. Fogo A. B. (2007). Mechanisms of progression of chronic kidney disease. Pediatric nephrology (Berlin, Germany), 22(12), 2011-22.
93. Francisci S, Montanari A, De Luca C, Frontali L (2011) Peptides from aminoacyl-tRNA synthetases can cure the defects due to mutations in mt tRNA genes. Mitochondrion. 2011 Nov;11(6):919-23. doi: 10.1016/j.mito.2011.08.006. Epub 2011 Aug 31.
94. Fulladosa X, Moreso F, Narváez JA, et al. Estimation of total glomerular number in stable renal transplants. J Am Soc Nephrol 2003; 14:2662.
95. Gao, F., et al. The Wt1+/R394W mouse displays glomerulosclerosis and early-onset renal failure characteristic of human Denys-Drash syndrome. Mol Cell Biol. 24, 9899-9910 (2004).
96. Gbadegesin R, Hinkes B, Vlangos C, Mucha B, Liu J, Hopcian J, Hildebrandt F. Mutational analysis of NPHS2 and WT1 in frequently relapsing and steroid-dependent nephrotic syndrome. Pediatr Nephrol. 2007 Apr;22(4):509-13.
97. Gbadegesin R, Hinkes B, Vlangos C, Mucha B, Liu J, Hopcian J, Hildebrandt F. Mutational analysis of NPHS2 and WT1 in frequently relapsing and steroid-dependent nephrotic syndrome. Pediatr Nephrol. 2007 Apr;22(4):509-13.
98. Gerencser AA, Neilson A, Choi SW, Edman U, Yadava N, Oh RJ, Ferrick DA, Nicholls DG, Brand MD. Quantitative Microplate-Based Respirometry with Correction for Oxygen Diffusion. Anal Chem. 2009

99. Gessler, M., Poustka, A., Cavenee, W., Neve, R. L., Orkin, S. H., Bruns, G. A. P. Homozygous deletion in Wilms tumours of a zinc-finger gene identified by chromosome jumping. Nature 343: 774-778, 1990.
100. Giles RE, Blanc H, Cann HM, Wallace DC. Maternal inheritance of human mitochondrial DNA. Proc Natl Acad Sci USA 1980; 77: 6715–6719.
101. Giovanni, Valeria Di, Adrian Alday, Lijun Chi, Yuji Mishina and Norman D. Rosenblum. Alk3 controls nephron number and androgen production via lineage-specific effects in intermediate mesoderm. Development. 2011 Jul;138(13):2717-27. doi: 10.1242/dev.059030. Epub 2011 May 25.
102. Gorman GS, Schaefer AM, Ng Y, et al. Prevalence of nuclear and mitochondrial DNA mutations related to adult mitochondrial disease. Ann Neurol 2015; 77: 753–759.
103. Granata, Simona, Gianluigi Zaza, Simona Simone, Gaetano Villani, Dominga Latorre, Paola Pontrelli, Massimo Carella, Francesco Paolo Schena, Giuseppe Grandaliano and Giovanni Pertosa. Mitochondrial dysregulation and oxidative stress in patients with chronic kidney disease. BMC Genomics 2009, 10:388.
104. Greaves LC, Nooteboom M, Elson JL, et al. Clonal expansion of early to mid-life mitochondrial DNA point mutations drives mitochondrial dysfunction during human ageing. PLoS Genet 2014; 10: e1004620.
105. Green DR, Kroemer G: Pharmacological manipulation of cell death: Clinical applications in sight? J Clin Invest 115 : 2610 –2617, 2005
106. Guo, J. K. et al. WT1 is a key regulator of podocyte function: reduced expression levels cause crescentic glomerulonephritis and mesangial sclerosis. Hum. Mol. Genet. 11, 651–659 (2002).
107. Haanen C, Vermes I. Apoptosis and inflammation. Mediators Inflamm. 1995;4(1):5-15.
108. Haber, D. A., Sohn, R. L., Buckler, A. J., Pelletier, J., Call, K. M., Housman, D. E. Alternative splicing and genomic structure of the Wilms tumor gene WT1. Proc. Nat. Acad. Sci. 88: 9618-9622, 1991.
109. Hajime Sogabe, Masaomi Nangaku, Yoshitaka Ishibashi, Takehiko Wada, Toshiro Fujita, Xiujun Sun, Takashi Miwa, Michael P. Madaio, and Wen-Chao Song. Increased Susceptibility of Decay-Accelerating Factor Deficient Mice to Anti-Glomerular Basement Membrane Glomerulonephritis. J Immunol 2001; 167:2791-2797.
110. Hales CN. Suicide of the nephron. Lancet. 2001 Jan 13;357(9250):136-7.
111. Halestrap A P and R M Denton. The specificity and metabolic implications of the inhibition of pyruvate transport in isolated mitochondria and intact tissue preparations by alpha-Cyano-4-hydroxycinnamate and related compounds. Biochem J. 1975 Apr; 148(1): 97–106.
112. Halestrap AP, Price NT. The proton-linked monocarboxylate transporter (MCT) family: structure, function and regulation. Biochem J. 1999 Oct 15;343 Pt 2:281-99.
113. Hamilton TB, Barilla KC, Romaniuk PJ. High affinity binding sites for the Wilms' tumour suppressor protein WT1. Nucleic Acids Res. 1995 Jan 25;23(2):277-84.
114. Hammes A, Guo JK, Lutsch G, Leheste JR, Landrock D, Ziegler U, Gubler MC, Schedl A. Two splice variants of the Wilms' tumor 1 gene have distinct functions during sex determination and nephron formation. Cell. 2001 Aug 10;106(3):319-29. PubMed PMID: 11509181.
115. Hammes, A., Guo, J. K., Lutsch, G., Leheste, J. R., Landrock, D., Ziegler, U., Gubler, M. C. and Schedl, A. (2001). Two splice variants of the Wilms' tumor 1 gene have distinct functions during sex determination and nephron formation. Cell 106,319 -329.
116. Harambat, J., van Stralen, K. J., Kim, J. J., & Tizard, E. J. (2011). Epidemiology of chronic kidney disease in children. Pediatric nephrology (Berlin, Germany), 27(3), 363-73.
117. Hartman, H.A., Lai, H.L., and Patterson, L.T. Cessation of renal morphogenesis in mice. Dev. Biol. 2007; 310: 379–387
118. Hartwig S, Ho J, Pandey P, Macisaac K, Taglienti M, Xiang M, Alterovitz G, Ramoni M, Fraenkel E, Kreidberg JA. (2010) Genomic characterization of Wilms' tumor suppressor 1 targets in nephron progenitor cells during kidney development. Development. 2010 Apr;137(7):1189-203. doi: 10.1242/dev.045732.

119. Hartwig, S., Hu, M. C., Cella, C., Piscione, T., Filmus, J. and Rosenblum, N. D. (2005). Glypican-3 modulates inhibitory Bmp2-Smad signaling to control renal development in vivo. Mech Dev. 2005 Jul;122(7-8):928-38.
120. Hashimoto H, Olanrewaju YO, Zheng Y, Wilson GG, Zhang X, Cheng X. Wilms tumor protein recognizes 5-carboxylcytosine within a specific DNA sequence. Genes Dev. 2014 Oct 15;28(20):2304-13. doi: 10.1101/gad.250746.114. Epub 2014 Sep 25.
121. Hastie, N. D. Dominant negative mutations in the Wilms tumour (WT1) gene cause Denys-Drash syndrome--proof that a tumour-suppressor gene plays a crucial role in normal genitourinary development. Hum. Molec. Genet. 1: 293-295, 1992.
122. Heemann UW, Azuma H, Tullius SG, Mackenzie H, Brenner BM, Tilney NL: The contribution of reduced functioning mass to chronic kidney allograft dysfunction in rats. Transplantation 58: 1317–1322, 1994
123. Heemann UW, Azuma H, Tullius SG, Mackenzie H, Brenner BM, Tilney NL: The contribution of reduced functioning mass to chronic kidney allograft dysfunction in rats. Transplantation 58: 1317–1322, 1994
124. Hendry C., B.A. Rumballe, K. Moritz, M.H. Little. Defining and redefining the nephron progenitor population. Pediatr. Nephrol., 26 (9) (2011), pp. 1395–1406
125. Hershkovitz, Dov, Zvi Burbea, Karl Skorecki, and Barry M. Brenner. Fetal Programming of Adult Kidney Disease: Cellular and Molecular Mechanisms. Clin J Am Soc Nephrol 2: 334–342, 2007.
126. Hill BG, Dranka BP, Bailey SM, Lancaster JR, Jr., Darley-Usmar VM. What part of NO don't you understand? Some answers to the cardinal questions in nitric oxide biology. J Biol Chem. 2010;285:19699–19704.
127. Hill BG, Dranka BP, Zou L, Chatham JC, Darley-Usmar VM. Importance of the bioenergetic reserve capacity in response to cardiomyocyte stress induced by 4-hydroxynonenal. Biochem J. 2009;424:99–107.
128. Hill BG, Higdon AN, Dranka BP, Darley-Usmar VM. Regulation of vascular smooth muscle cell bioenergetic function by protein glutathiolation. Biochim Biophys Acta. 2010;1797:285–295.
129. Hinchliffe S.A., P.H. Sargent, C.V. Howard, Y.F. Chan, D. van Velzen. Human intrauterine renal growth expressed in absolute number of glomeruli assessed by the disector method and Cavalieri principle. Lab. Invest., 64 (6) (1991), pp. 777–784 Jun
130. Hinkes BG, Mucha B, Vlangos CN, et al. Nephrotic syndrome in the first year of life: two thirds of cases are caused by mutations in 4 genes (NPHS1, NPHS2, WT1, and LAMB2). Pediatrics 2007; 119:e907.
131. Hinkes BG, Mucha B, Vlangos CN, Gbadegesin R, Liu J, Hasselbacher K, Hangan D, Ozaltin F, Zenker M, Hildebrandt F. Nephrotic syndrome in the first year of life: two thirds of cases are caused by mutations in 4 genes (NPHS1, NPHS2, WT1, and LAMB2). Pediatrics. 2007 Apr;119(4):e907-19.
132. Hinkes BG, Mucha B, Vlangos CN, Gbadegesin R, Liu J, Hasselbacher K, Hangan D, Ozaltin F, Zenker M, Hildebrandt F. Nephrotic syndrome in the first year of life: two thirds of cases are caused by mutations in 4 genes (NPHS1, NPHS2, WT1, and LAMB2). Pediatrics. 2007 Apr;119(4):e907-19.
133. Hinkes, BG., et al. Nephrotic syndrome in the first year of life; two thirds of cases are caused by mutations in 4 genes (NPHS1, NPHS2, WT1 and LAMB2). Pediatrics 119, e907-919 (2007).
134. Ho J. The regulation of apoptosis in kidney development: implications for nephron number and pattern? Front Pediatr. 2014 Nov 18;2:128. doi: 10.3389/fped.2014.00128. eCollection 2014.
135. Ho, Theodore T., Matthew R. Warr, Emmalee R. Adelman, Olivia M. Lansinger, Johanna Flach, Evgenia V. Verovskaya, Maria E. Figueroa & Emmanuelle Passegué. Autophagy maintains the metabolism and function of young and old stem cells. Nature volume 543, pages 205–210 (09 March 2017).
136. Hodgin JB, Bitzer M, Wickman L, et al. Glomerular Aging and Focal Global Glomerulosclerosis: A Podometric Perspective. J Am Soc Nephrol 2015; 26:3162.
137. Hommos MS, Zeng C, Liu Z, et al. Global glomerulosclerosis with nephrotic syndrome; the clinical importance of age adjustment. Kidney Int 2018; 93:1175.

138. Hooi LS, Wong HS, Morad Z. Prevention of renal failure: the Malaysian experience. Send to Kidney Int Suppl. 2005 Apr;(94):S70-4.
139. Hossain, A., Saunders, G. F. The human sex-determining gene SRY is a direct target of WT1. J. Biol. Chem. 276: 16817-16823, 2001.
140. Hossain, A., Saunders, G. F. The human sex-determining gene SRY is a direct target of WT1. J. Biol. Chem. 276: 16817-16823, 2001.
141. Hoy WE, Douglas-Denton RN, Hughson MD, et al. A stereological study of glomerular number and volume: preliminary findings in a multiracial study of kidneys at autopsy. Kidney Int Suppl 2003; :S31.
142. Hoy WE, Hughson MD, Singh GR, Douglas-Denton R, Bertram JF. Reduced nephron number and glomerulomegaly in Australian Aborigines: a group at high risk for renal disease and hypertension. Kidney Int. 2006 Jul;70(1):104-10. Epub 2006 May 24.
143. Hughes J, Savill JS: Apoptosis in glomerulonephritis. Curr Opin Nephrol Hypertens 14 : 389 –395, 2005
144. Hughson M., A.B. Farris III, R. Douglas-Denton, W.E. Hoy, J.F. Bertram. Glomerular number and size in autopsy kidneys: the relationship to birth weight. Kidney Int., 63 (2003), pp. 2113–2122
145. Humphreys B.D.. Kidney structures differentiated from stem cells. Nat Cell Biol, 16 (2014), pp. 19–21
146. Humphreys, B.D., Valerius, M.T., Kobayashi, A., Mugford, J.W., Soeung, S., Duffield, J.S., McMahon, A.P., and Bonventre, J.V. (2008). Intrinsic epithelial cells repair the kidney after injury. Cell Stem Cell 2, 284–291.
147. Ikeya, Makoto, Kumi Fukushima, Masako Kawada, Sachiko Onishi, Yasuhide Furuta , Shigenobu Yonemura, Toshio Kitamura, Tetsuya Nosaka, Yoshiki Sasai. Cv2, functioning as a pro-BMP factor via twisted gastrulation, is required for early development of nephron precursors. Dev Biol. 2010 Jan 15;337(2):405-14. doi: 10.1016/j.ydbio.2009.11.013. Epub 2009 Nov 13.
148. Indra AK, Warot X, Brocard J, Bornert JM, Xiao JH, Chambon P, Metzger D. Temporally-controlled site-specific mutagenesis in the basal layer of the epidermis: comparison of the recombinase activity of the tamoxifen-inducible Cre-ER(T) and Cre-ER(T2) recombinases. Nucleic Acids Res. 1999 Nov 15;27(22):4324-7.
149. Ingsathit A, Thakkinstian A, Chaiprasert A, Sangthawan P, Gojaseni P, Kiattisunthorn K, Ongaiyooth L, Vanavanan S, Sirivongs D, Thirakhupt P, Mittal B, Singh AK; Thai-SEEK Group. Prevalence and risk factors of chronic kidney disease in the Thai adult population: Thai SEEK study. Nephrol Dial Transplant. 2010 May;25(5):1567-75. doi: 10.1093/ndt/gfp669. Epub 2009 Dec 27.
150. Jekabsons MB, Nicholls DG. In situ respiration and bioenergetic status of mitochondria in primary cerebellar granule neuronal cultures exposed continuously to glutamate. J Biol Chem. 2004;279:32989–33000.
151. Jennings BJ, Ozanne SE, Dorling MW, and Hales CN: Early growth determines longevity in male rats and may be related to telomere shortening in the kidney. FEBS Lett 448: 4–8, 1999
152. Jennings BJ, Ozanne SE, Dorling MW, and Hales CN: Early growth determines longevity in male rats and may be related to telomere shortening in the kidney. FEBS Lett 448: 4–8, 1999
153. Jensflorian, https://commons.wikimedia.org/wiki/File:Cox-deficient_fibers_in_mitochondrial_myopathy.jpg. Creative Commons Attribution-Share Alike 4.0 International.
154. Jing Chen, Scott Boyle, Min Zhao, Wei Su, Keiko Takahashi, Linda Davis,Mark DeCaestecker, Takamune Takahashi, Matthew D. Breyer, and Chuan-Ming Hao. Differential Expression of the Intermediate Filament Protein Nestin during Renal Development and Its Localization in Adult Podocytes. J Am Soc Nephrol 17: 1283–1291, 2006.
155. Jinno, Y., Yun, K., Nishiwaki, K., Kubota, T., Ogawa, O., Reeve, A. E., Niikawa, N. Mosaic and polymorphic imprinting of the WT1 gene in humans. Nature Genet. 6: 305-309, 1994.
156. Jones CH. Serum albumin – a marker of fluid overload in dialysis patients? Journal of Renal Nutrition 2001;11:59–56
157. Kambiz Zandi-Nejad, Valerie A. Luyckx and Barry M. Brenner. Adult Hypertension and Kidney Disease : The Role of Fetal Programming. Hypertension. 2006; 47:502-508.

158. Kaplan C, Pasternack B, Shah H, Gallo G. Age-related incidence of sclerotic glomeruli in human kidneys. Am J Pathol 1975; 80:227.
159. Kappel B, Olsen S. Cortical interstitial tissue and sclerosed glomeruli in the normal human kidney, related to age and sex. A quantitative study. Virchows Arch A Pathol Anat Histol 1980; 387:271.
160. Karner C.M., A. Das, Z. Ma, M. Self, C. Chen, L. Lum, G. Oliver, T.J. Carroll. Canonical Wnt9b signaling balances progenitor cell expansion and differentiation during kidney development. Development, 138 (7) (2011), pp. 1247–1257
161. KDIGO 2012 Clinical Practice Guideline for the Evaluation and Management of Chronic Kidney Disease. Kidney Int Suppl 2013; 3:1.
162. Kidney Disease: Improving Global Outcomes (KDIGO) CKD Work Group. KDIGO 2012 clinical practice guideline for the evaluation and management of chronic kidney disease. Kidney Int Suppl 2013; 3: 1–150.
163. Kim I, Lemasters JJ. Mitophagy selectively degrades individual damaged mitochondria after photoirradiation. Antioxid Redox Signal. 2011 May 15;14(10):1919-28. doi: 10.1089/ars.2010.3768. Epub 2011 Mar 6.
164. Kinzfogl, J., Hangoc, G., & Broxmeyer, H. E. (2011). Neurexophilin 1 suppresses the proliferation of hematopoietic progenitor cells. Blood, 118(3), 565-75.
165. Kobayashi, A., Valerius, M.T., Mugford, J.W., Carroll, T.J., Self, M., Oliver, G., and McMahon, A.P. Six2 defines and regulates a multipotent self-renewing nephron progenitor population throughout mammalian kidney development. Cell Stem Cell. 2008; 3: 169–181
166. Koseki C, Herzlinger D, al-Awqati Q: Apoptosis in metanephric development. J Cell Biol 119 : 1327 –1333, 1992
167. Kreidberg J.A., Sariola H., Loring J.M., Maeda M., Pelletier J., Housman D., Jaenisch R. WT-1 is required for early kidney development. Cell 1993;74:679-691.
168. Kreidberg, JA., et al. Coordinate action of Wt1 and a modifier gene supports embryonic survival in the oviduct. Mol Reprod Dev. 52, 366-375 (1999).
169. Kreidberg, JA., et al. WT-1 is required for early kidney development. Cell 74, 679-691 (1993).
170. Kremers WK, Denic A, Lieske JC, et al. Distinguishing age-related from disease-related glomerulosclerosis on kidney biopsy: the Aging Kidney Anatomy study. Nephrol Dial Transplant 2015; 30:2034.
171. Kroemer G, El-Deiry WS, Golstein P, Peter ME, Vaux D, Vandenabeele P, Zhivotovsky B, Blagosklonny MV, Malorni W, Knight RA, Piacentini M, Nagata S, Melino G: Classification of cell death: recommendations of the Nomenclature Committee on Cell Death. Cell Death Differ 12 [Suppl 2]: 1463 –1467, 2005
172. Kubo M, Kiyohara Y, Kato I, et al. Risk factors for renal glomerular and vascular changes in an autopsy-based population survey: the Hisayama study. Kidney Int 2003; 63:1508.
173. Lahiri D, Dutton JR, Duarte A, Moorwood K, Graham CF, Ward A. Nephropathy and defective spermatogenesis in mice transgenic for a single isoform of the Wilms' tumour suppressor protein, WT1-KTS, together with one disrupted Wt1 allele. Mol Reprod Dev. 2007 Mar;74(3):300-11.
174. Laity, J. H., Chung, J., Dyson, H. J., Wright, P. E. Alternative splicing of Wilms' tumor suppressor protein modulates DNA binding activity through isoform-specific DNA-induced conformational changes. Biochemistry 39: 5341-5348, 2000.
175. Larsson SH, Charlieu JP, Miyagawa K, Engelkamp D, Rassoulzadegan M, Ross A, Cuzin F, van Heyningen V, Hastie ND. Subnuclear localization of WT1 in splicing or transcription factor domains is regulated by alternative splicing. Cell. 1995 May 5; 81(3):391-401.
176. Larsson SH, Charlieu JP, Miyagawa K, Engelkamp D, Rassoulzadegan M, Ross A, Cuzin F, van Heyningen V, Hastie ND. Subnuclear localization of WT1 in splicing or transcription factor domains is regulated by alternative splicing. Cell. 1995 May 5; 81(3):391-401.
177. Lightowlers RN, Taylor RW, Turnbull DM. Mutations causing mitochondrial disease: what is new and what challenges remain? Science (New York, NY) 2015; 349: 1494–1499.

178. Lihua Bao, Mark Haas, Jeffrey Pippin, Ying Wang, Takashi Miwa,Anthony Chang, Andrew W. Minto, Miglena Petkova, Guilin Qiao, Wen-Chao Song,Charles E. Alpers, Jian Zhang, Stuart J. Shankland, and Richard J. Quigg. Focal and segmental glomerulosclerosis induced in mice lacking decay-accelerating factor in T cells.J. Clin. Invest. 119:1264–1274 (2009). doi:10.1172/JCI36000
179. Lihua Dong, Stefan Pietsch, and Christoph Englert. Towards an understanding of kidney diseases associated with WT1 mutations. Kidney Int. 2015 Oct; 88(4): 684–690.
180. Lim YN, Ghazali A, Tan CC, Lee DG. Kuala Lumpur: Malaysia: Malaysian Society of Nephrology; 2011. Dialysis in Malaysia: 18th Report of The Malaysian Dilaysis and Transplant Registry 2010.
181. Little MH, McMahon AP. Mammalian kidney development: principles, progress, and projections. Cold Spring Harb Perspect Biol. 2012 May 1;4(5). pii: a008300. doi: 10.1101/cshperspect.a008300.
182. Little, M.H. and McMahon, A.P. Mammalian kidney development: principles, progress, and projections. Cold Spring Harb. Perspect. Biol. 2012; 4: a008300
183. Lopardo T, Lo Iacono N, Marinari B, Giustizieri ML, Cyr DG, et al. (2008) Claudin-1 Is a p63 Target Gene with a Crucial Role in Epithelial Development. PLoS ONE 3(7): e2715. doi:10.1371/journal.pone.0002715
184. Lorz C, Benito-Martin A, Justo P, Sanz AB, Sanchez Niño MD, Egido J, Ortiz A: Modulation of renal tubular cell survival: where is the evidence? Curr Med Chem 13 : 763 –771, 2006
185. Luyckx V.A., B.M. Brenner. The clinical importance of nephron mass. J. Am. Soc. Nephrol., 21 (6) (2010), pp. 898–910
186. Luyckx VA, Bertram JF, Brenner BM, et al. Effect of fetal and child health on kidney development and long-term risk of hypertension and kidney disease. Lancet 2013; 382:273.
187. Mackenzie HS, Azuma H, Rennke HG, Tilney NL, and Brenner BM: Renal mass as a determinant of late allograft outcome: Insights from experimental studies in rats. Kidney Int Suppl 52: S38–S42, 1995
188. Mackenzie HS, Azuma H, Troy JL, Rennke HG, Tilney NL, and Brenner BM: Augmenting kidney mass at transplantation abrogates chronic renal allograft injury in rats. Proc Assoc Am Physicians 108: 127–133, 1996
189. Mackenzie HS, Azuma H, Troy JL, Rennke HG, Tilney NL, and Brenner BM: Augmenting kidney mass at transplantation abrogates chronic renal allograft injury in rats. Proc Assoc Am Physicians 108: 127–133, 1996
190. Mackenzie HS, Tullius SG, Heemann UW, Azuma H, Rennke HG, Brenner BM, Tilney NL: Nephron supply is a major determinant of long-term renal allograft outcome in rats. J Clin Invest 94: 2148–2152, 1994
191. Madden, S. L.; Cook, D. M.; Morris, J. F., et al. Transcriptional repression mediated by the WT1 Wilms tumor gene product. Science 253:1550–1553; 1991.
192. Madden, S. L.; Cook, D. M.; Rauscher, F. J. A structure-function analysis of transcriptional repression mediated by WT1, Wilms' tumor suppressor protein. Oncogene 8:1713–1720; 1993.
193. Manalich R, Reyes L, Herrera M, Melendi C, Fundora I: Relationship between weight at birth and the number and size of renal glomeruli in humans: A histomorphometric study. Kidney Int 58: 770–773, 2000
194. Manalich R, Reyes L, Herrera M, Melendi C, Fundora I: Relationship between weight at birth and the number and size of renal glomeruli in humans: A histomorphometric study. Kidney Int 58: 770–773, 2000
195. Mancilla E, Avila-Casado C, Uribe-Uribe N, et al. Time-zero renal biopsy in living kidney transplantation: a valuable opportunity to correlate predonation clinical data with histological abnormalities. Transplantation 2008; 86:1684.
196. Maria Teresa Discenza and Jerry Pelletier. Insights into the physiological role of WT1 from studies of genetically modified mice, (2004). Physiol Genomics 16:287-300, 2004. doi:10.1152/physiolgenomics.00164.2003.
197. Markus MA, Heinrich B, Raitskin O, Adams DJ, Mangs H, Goy C, Ladomery M, Sperling R, Stamm S, Morris BJ. WT1 interacts with the splicing protein RBM4 and regulates its ability to

modulate alternative splicing in vivo. Exp Cell Res. 2006 Oct 15;312(17):3379-88. Epub 2006 Jul 25.
198. Marroquin LD, Hynes J, Dykens JA, Jamieson JD, Will Y (2007) Circumventing the Crabtree effect: replacing media glucose with galactose increases susceptibility of HepG2 cells to mitochondrial toxicants. Toxicol Sci 97: 539–547.
199. Martin JE, Sheaff MT. Renal ageing. J Pathol 2007; 211:198.
200. McNamara BJ, Diouf B, Douglas-Denton RN, Hughson MD, Hoy WE, Bertram JF. A comparison of nephron number, glomerular volume and kidney weight in Senegalese Africans and African Americans. Nephrol Dial Transplant. 2010 May;25(5):1514-20. doi: 10.1093/ndt/gfq030. Epub 2010 Feb 11.
201. Meier P, Finch A, Evan G. Apoptosis in development. Nature (2000) 407(6805):796–80110.1038/35037734
202. Merlet-Bénichou, C., Gilbert, T., Vilar, J., Moreau, E., Freund, N., and Lelièvre-Pégorier, M. Nephron number: variability is the rule. Causes and consequences. Lab. Invest. 1999; 79: 515–527
203. Miguel N. Rivera and Daniel A. Haber. Wilms' tumour: Connecting tumorigenesis and organ development in the kidney, (2005) Nature Publishing Group. Volume 5 September 2005 pg699-712.
204. Miguel N. Rivera and Daniel A. Haber. Wilms' tumour: Connecting tumorigenesis and organ development in the kidney, (2005) Nature Publishing Group. Volume 5 September 2005 pg699-712.
205. Mishmar D, Ruiz-Pesini E, Brandon M, Wallace DC. Mitochondrial DNA-like sequences in the nucleus (NUMTs): insights into our African origins and the mechanism of foreign DNA integration. Hum Mutat. 2004 Feb; 23(2):125-33.
206. Mishmar D, Ruiz-Pesini E, Brandon M, Wallace DC. Mitochondrial DNA-like sequences in the nucleus (NUMTs): insights into our African origins and the mechanism of foreign DNA integration. Hum Mutat. 2004 Feb; 23(2):125-33.
207. Mitochondria. Edited by Leslie Wilson Paul T. Matsudaira Eric A. Schon Liza A. Pon. (Optical Imaging Techniques (Histochemical, Immunohistochemical, and In Situ Hybridization Staining Methods) to Visualize Mitochondrial by Kurenai Tanji and Eduardo Bonilla) Academic Press- Publisher - May 23, 2001.
208. MITOMAP: A Human Mitochondrial Genome Database. http://www.mitomap.org, Access on 25th July 2013.
209. Mitsuya, K., Sui, H., Meguro, M., Kugoh, H., Jinno, Y., Niikawa, N., Oshimura, M. Paternal expression of WT1 in human fibroblasts and lymphocytes. Hum. Molec. Genet. 6: 2243-2246, 1997.
210. Mong Hiep TT, Ismaili K, Collart F, Damme-Lombaerts R, Godefroid N, Ghuysen MS, Hoeck K, Raes A, Janssen F, Robert A. Clinical characteristics and outcomes of children with stage 3–5 chronic kidney disease. Pediatr Nephrol. 2010;25:935–940. doi: 10.1007/s00467-009-1424-2.
211. Moreno-Loshuertos R, Ferrín G, Acín-Pérez R, Gallardo M, Viscomi C, et al. (2011) Evolution meets disease: penetrance and functional epistasis of mitochondrial tRNA mutations. PLoS Genet. 2011 Apr;7(4):e1001379. doi: 10.1371/journal.pgen.1001379. Epub 2011 Apr 21.
212. Morrison AA, Viney RL, Ladomery MR. The post-transcriptional roles of WT1, a multifunctional zinc-finger protein. Biochim Biophys Acta. 2008 Jan;1785(1):55-62. Epub 2007 Oct 14.
213. Morrison AA, Viney RL, Ladomery MR. The post-transcriptional roles of WT1, a multifunctional zinc-finger protein. Biochim Biophys Acta. 2008 Jan;1785(1):55-62. Epub 2007 Oct 14.
214. Mundlos, S., et al. Nuclear localization of the protein encoded by the Wilms' tumor gene WT1 in embryonic and adult tissues. Development 119, 1329-1341 (1993).
215. Mundlos, S., et al. Nuclear localization of the protein encoded by the Wilms' tumor gene WT1 in embryonic and adult tissues. Development 119, 1329-1341 (1993).
216. Munnich A, Rustin P: Clinical spectrum and diagnosis of mitochondrial disorders. Am J Med Genet 106: 4–17, 2001

217. Murawski IJ, Maina RW, Gupta IR. The relationship between nephron number, kidney size and body weight in two inbred mouse strains. Organogenesis. 2010 Jul-Sep;6(3):189-94.
218. Nachtigal, M. W., Hirokawa, Y., Enyeart-VanHouten, D. L., Flanagan, J. N., Hammer, G. D., Ingraham, H. A. Wilms' tumor 1 and Dax-1 modulate the orphan nuclear receptor SF-1 in sex-specific gene expression. Cell 93: 445-454, 1998.
219. NAPRTCS 2008 Annual report. Rockville, MD: The EMMES Corporation; 2008.
220. Naryzhny, Stanislav N., Lee, Hoyun. Proliferating cell nuclear antigen in the cytoplasm interacts with components of glycolysis and cancer. FEBS Letters 584 (2010) Volume 584, Issue 20.
221. National Kidney Foundation. K/DOQI Clinical Practice Guidelines for Chronic Kidney Disease: Evaluation, Classification and Stratification. Am J Kidney Dis 39:S1-S266, 2002
222. National Kidney Foundation. K/DOQI clinical practice guidelines for chronic kidney disease: evaluation, classification, and stratification. Am J Kidney Dis 2002; 39:S1.
223. Newsholme E.A., B. Crabtree, M.S. Ardawi. The role of high rates of glycolysis and glutamine utilization in rapidly dividing cells. Biosci. Rep., 5 (1985), pp. 393-400
224. Niksic, M., Slight, J., Sanford, J. R., Caceres, J. F., Hastie, N. D. The Wilms' tumour protein (WT1) shuttles between nucleus and cytoplasm and is present in functional polysomes. Hum. Molec. Genet. 13: 463-471, 2004.
225. Nourbakhsh M, Douglas DN, Pu CH, Lewis JT, Kawahara T, Lisboa LF, Wei E, Asthana S, Quiroga AD, Law LM, Chen C, Addison WR, Nelson R, Houghton M, Lehner R, Kneteman NM. Arylacetamide deacetylase: a novel host factor with important roles in the lipolysis of cellular triacylglycerol stores, VLDL assembly and HCV production. J Hepatol. 2013 Aug;59(2):336-43. doi: 10.1016/j.jhep.2013.03.022. Epub 2013 Mar 28.
226. Nyengaard JR, Bendtsen TF. Glomerular number and size in relation to age, kidney weight, and body surface in normal man. Anat Rec 1992; 232:194.
227. Olsen TS, Olsen HS, Hansen HE: Tubular ultrastructure in acute renal failure in man: Epithelial necrosis and regeneration. Virchows Arch A Pathol Anat Histopathol 406 : 75 –89, 1985
228. Olson JL, Heptinstall RH (1988) Nonimmunologic mechanisms of glomerular injury. Lab Invest 59:564–578
229. Ostronoff, L. K., J. M. Izquierdo, and J. M. Cuezva. 1995. mt-mRNA stability regulates the expression of the mitochondrial genome during liver development. Biochem. Biophys. Res. Commun. 217:1094–1098.
230. Page A.B., Page A.M., Noel C. A new fluorimetric assay for cytotoxicity measurements *in vitro*. Int. J. Oncol. 1993;3:473–476.
231. Page A.B., Page A.M., Noel C. A new fluorimetric assay for cytotoxicity measurements in vitro. Int. J. Oncol. 1993;3:473–476.
232. Patek C.E., Fleming S., Miles C.G., Bellamy C.O., Ladomery M., Spraggon L., Mullins J., Hastie N.D., Hooper M.L. Murine Denys-Drash syndrome: evidence of podocyte de-differentiation and systemic mediation of glomerulosclerosis. Hum. Mol. Genet. 2003;12:2379-2394.
233. Patek CE, Brownstein DG, Fleming S, Wroe C, Rose L, Webb A, Berry RL, Devenney PS, Walker M, Maddocks OD, Lawrence NJ, Harrison DJ, Wood KM, Miles CG, Hooper ML. Effects on kidney disease, fertility and development in mice inheriting a protein-truncating Denys-Drash syndrome allele (Wt1tmT396). Transgenic Res. 2008 Jun; 17(3):459-75. Epub 2007 Nov 27.
234. Patek CE, Brownstein DG, Fleming S, Wroe C, Rose L, Webb A, Berry RL, Devenney PS, Walker M, Maddocks OD, Lawrence NJ, Harrison DJ, Wood KM, Miles CG, Hooper ML. Effects on kidney disease, fertility and development in mice inheriting a protein-truncating Denys-Drash syndrome allele (Wt1tmT396). Transgenic Res. 2008 Jun; 17(3):459-75. Epub 2007 Nov 27.
235. Patek CE, Brownstein DG, Fleming S, Wroe C, Rose L, Webb A, Berry RL, Devenney PS, Walker M, Maddocks OD, Lawrence NJ, Harrison DJ, Wood KM, Miles CG, Hooper ML. Effects on kidney disease, fertility and development in mice inheriting a protein-truncating Denys-Drash syndrome allele (Wt1tmT396). Transgenic Res. 2008 Jun; 17(3):459-75. Epub 2007 Nov 27.
236. Patek CE, Fleming SF, Miles CG, Bellamy CO, Ladomery M,Spraggon L, Mullins J, Hastie ND, Hooper ML (2003)Murine Denys-Drash syndrome: evidence of podocyte de-differentiation and systemic mediation of glomeruloscle-rosis. Hum Mol Genet 12:2379–2394

237. Patek, C. E., Little, M. H., Fleming, S., Miles, C., Charlieu, J. P., Clarke, A. R., Miyagawa, K., Christie, S., Doig, J., Harrison, D. J., Porteous, D. J., Brookes, A. J., Hooper, M. L., … Hastie, N. D. (1999). A zinc finger truncation of murine WT1 results in the characteristic urogenital abnormalities of Denys-Drash syndrome. Proceedings of the National Academy of Sciences of the United States of America, 96(6), 2931-6.
238. Patek, CE., et al. Murine Denys-Drash syndrome: evidence of podocyte dedifferentiation and systemic mediation of glomerulosclerosis. Hum Mol Genet. 12, 2379-2394 (2003). 6
239. Paulien Smits, Sandy Mattijssen, Eva Morava, Marie¨l van den Brand, Frans van den Brandt, Frits Wijburg, Ger Pruijn, Jan Smeitink, Leo Nijtmans, Richard Rodenburg and Lambert van den Heuvel. Functional consequences of mitochondrial tRNATrp and tRNA-Arg mutations causing combined OXPHOS defects. European Journal of Human Genetics (2010) 18, 324–329.
240. Pelletier, J., Bruening, W., Kashtan, C. E., Mauer, S. M., Manivel, J. C., Striegel, J. E., Houghton, D. C., Junien, C., Habib, R., Fouser, L., Fine, R. N., Silverman, B. L., Haber, D. A., Housman, D. Germline mutations in the Wilms' tumor suppressor gene are associated with abnormal urogenital development in Denys-Drash syndrome. Cell 67: 437-447, 1991.
241. Pelletier, J., et al. Germline mutations in the Wilms' tumor suppressor gene are associated with abnormal urogenital development in Denys-Drash syndrome. Cell 67, 437-447 (1991).
242. Perez J, Hill BG, Benavides GA, Dranka BP, Darley-Usmar VM. Role of cellular bioenergetics in smooth muscle cell proliferation induced by platelet-derived growth factor. Biochem J. 2010;428:255–267.
243. Perli E, Giordano C, Tuppen HA, Montopoli M, Montanari A, et al. (2012) Isoleucyl-tRNA synthetase levels modulate the penetrance of a homoplasmic m.4277T>C mitochondrial tRNA(Ile) mutation causing hypertrophic cardiomyopathy. Hum Mol Genet. 2012 Jan 1;21(1):85-100. doi: 10.1093/hmg/ddr440. Epub 2011 Sep 26.
244. Pinheiro C, Longatto-Filho A, Simoes K, Jacob CE, Bresciani CJ, Zilberstein B, Cecconello I, Alves VA, Schmitt F, Baltazar F. The prognostic value of CD147/EMMPRIN is associated with monocarboxylate transporter 1 co-expression in gastric cancer. Eur.J.Cancer. 2009;45:2418–2424.
245. Pritchard-Jones K., Fleming, S., Davidson, D., Bickmore, W., Porteous, D., Gosden, C., Bard, J., Buckler, A., Pelletier, J., Housman, D., et al. (1990). The candidate Wilms' tumour gene is involved in genitourinary development. Nature 346, 194-197.
246. Rackley, R. R.; Flenniken, A. M.; Kuriyan, N. P., et al. Expression of the Wilms' tumor suppressor gene WT1 during mouse embryogenesis. Cell Growth Differ. 4:1–9; 1993.
247. Rampersad S. N. (2012). Multiple applications of Alamar Blue as an indicator of metabolic function and cellular health in cell viability bioassays. Sensors (Basel, Switzerland), 12(9), 12347-60.
248. Rampersad, Sephra N. (2012) Multiple Applications of Alamar Blue as an Indicator of Metabolic Function and Cellular Health in Cell Viability Bioassays. Sensors (Basel). 2012; 12(9): 12347–12360. doi: 10.3390/s120912347
249. Ratelade J, Arrondel C, Hamard G, Garbay S, Harvey S, Biebuyck N, Schulz H, Hastie N, Pontoglio M, Gubler MC, Antignac C, Heidet L. A murine model of Denys-Drash syndrome reveals novel transcriptional targets of WT1 in podocytes. Hum Mol Genet. 2010 Jan 1; 19(1):1-15. doi: 10.1093/hmg/ddp462.
250. Ratelade J, Arrondel C, Hamard G, Garbay S, Harvey S, Biebuyck N, Schulz H, Hastie N, Pontoglio M, Gubler MC, Antignac C, Heidet L. A murine model of Denys-Drash syndrome reveals novel transcriptional targets of WT1 in podocytes. Hum Mol Genet. 2010 Jan 1; 19(1):1-15. doi: 10.1093/hmg/ddp462.
251. Ravagnan L, Roumier T, Kroemer G: Mitochondria, the killer organelles and their weapons. J Cell Physiol 192 : 131 –137, 2002
252. Reyes L, Mañalich R. Long-term consequences of low birth weight. Kidney Int Suppl 2005; :S107.
253. Riedl SJ, Salvesen GS: The apoptosome: Signalling platform of cell death. Nat Rev Mol Cell Biol 8 : 405 –413, 2007

254. Robinson BH, Petrova-Benedict R, Buncic JR, Wallace DC (1992) Nonviability of cells with oxidative defects in galactose medium: a screening test for affected patient fibroblasts. Biochem Med Metab Biol 48: 122–126.
255. Robinson BH, Petrova-Benedict R, Buncic JR, Wallace DC. (1992). Nonviability of cells with oxidative defects in galactose medium: a screening test for affected patient fibroblasts. Biochem Med Metab Biol. 1992 Oct;48(2):122-6.
256. Rossignol R, Gilkerson R, Aggeler R, Yamagata K, Remington SJ, et al. (2004) Energy substrate modulates mitochondrial structure and oxidative capacity in cancer cells. Cancer Res 64: 985–993.
257. Ruf RG, Schultheiss M, Lichtenberger A, Karle SM, Zalewski I, Mucha B, Everding AS, Neuhaus T, Patzer L, Plank C, Haas JP, Ozaltin F, Imm A, Fuchshuber A, Bakkaloglu A, Prevalence of WT1 mutations in a large cohort of patients with steroid-resistant and steroid-sensitive nephrotic syndrome. Kidney Int. 2004 Aug;66(2):564-70.
258. Ruf RG, Schultheiss M, Lichtenberger A, Karle SM, Zalewski I, Mucha B, Everding AS, Neuhaus T, Patzer L, Plank C, Haas JP, Ozaltin F, Imm A, Fuchshuber A, Bakkaloglu A, Prevalence of WT1 mutations in a large cohort of patients with steroid-resistant and steroid-sensitive nephrotic syndrome. Kidney Int. 2004 Aug;66(2):564-70.
259. Rugiu C, Oldrizzi L, Lupo A, Valvo E, Loschiavo C, Tessitore N, Gammaro L, Ortalda V, Fabris A, Panzetta G, et al.: Clinical features of patients with solitary kidneys. Nephron 43: 10–15, 1986
260. Rugiu C, Oldrizzi L, Lupo A, Valvo E, Loschiavo C, Tessitore N, Gammaro L, Ortalda V, Fabris A, Panzetta G, et al.: Clinical features of patients with solitary kidneys. Nephron 43: 10–15, 1986
261. Rule AD, Amer H, Cornell LD, et al. The association between age and nephrosclerosis on renal biopsy among healthy adults. Ann Intern Med 2010; 152:561.
262. Rumballe B., K. Georgas, M.H. Little. High-throughput paraffin section in situ hybridization and dual immunohistochemistry on mouse tissues. CSH Protoc., 1 (2008) 2008:pdb.prot5030. doi:http://dx.doi.org/10.1101/pdb.prot5030
263. Rumballe Bree A., Kylie M. Georgas, Alexander N. Combes, Adler L. Ju, Thierry Gilbert, Melissa H. Little. Nephron formation adopts a novel spatial topology at cessation of nephrogenesis. Developmental Biology. Volume 360, Issue 1, 1 December 2011, Pages 110–122
264. Rumballe, B.A., Georgas, K.M., Combes, A.N., Ju, A.L., Gilbert, T., and Little, M.H. Nephron formation adopts a novel spatial topology at cessation of nephrogenesis. Dev. Biol. 2011; 360: 110–122
265. Rumballe, B.A., Georgas, K.M., Combes, A.N., Ju, A.L., Gilbert, T., and Little, M.H. Nephron formation adopts a novel spatial topology at cessation of nephrogenesis. Dev. Biol. 2011; 360: 110–122
266. Saifudeen Z, Dipp S, El-Dahr SS (2002) A role for p53 in terminal epithelial cell differentiation. J Clin Invest. 2002 Apr;109(8):1021-30.
267. Sainio, K., Suvanto, P., Davies, J. A., Wartiovaara, J., Wartiovaara, K., Saarma, M., Arumäe, U., Meng, X., Lindahl, M., Pachnis, V., Sariola, H. (1997). Glial cell-line derived neurotrophic factor is required for bud initiation from ureteric epithelium. Development 124, 4077-4087
268. Saleem MA, O'Hare MJ, Reiser J, Coward RJ, Inward CD, Farren T, Xing CY, Ni L, Mathieson PW, Mundel P. A conditionally immortalized human podocyte cell line demonstrating nephrin and podocin expression. J Am Soc Nephrol. 2002 Mar;13(3):630-8.
269. Santín S, Bullich G, Tazón-Vega B, et al. Clinical utility of genetic testing in children and adults with steroid-resistant nephrotic syndrome. Clin J Am Soc Nephrol 2011; 6:1139.
270. Sanz AB, Santamaría B, Ruiz-Ortega M, Egido J, Ortiz A. Mechanisms of renal apoptosis in health and disease. J Am Soc Nephrol. 2008 Sep;19(9):1634-42. doi: 10.1681/ASN.2007121336. Epub 2008 Jul 16.
271. Saxén L, Sariola H. Early organogenesis of the kidney. Pediatr Nephrol. 1987 Jul;1(3):385-92.

272. Saxén L., Sariola H. Early organogenesis of the kidney. Pediatr. Nephrol. 1987; 1:385–392. doi: 10.1007/BF00849241.
273. Saxen, L. Organogenesis of the kidney. Cambridge University Press, Cambridge, (U.K.); 1987.
274. Scharnhorst, V., Dekker, P., van der Eb, A. J., Jochemsen, A. G. Internal translation initiation generates novel WT1 protein isoforms with distinct biological properties. J. Biol. Chem. 274: 23456-23462, 1999.
275. Schreuder M.F., J. Nauta, Prenatal programming of nephron number and blood pressure, Kidney International,Volume 72, Issue 3,2007,Pages 265-268,ISSN 0085-2538, https://doi.org/10.1038/sj.ki.5002307.
276. Schumacher VA, Schlötzer-Schrehardt U, Karumanchi SA, Shi X, Zaia J, Jeruschke S, Zhang D, Pavenstädt H, Drenckhan A, Amann K, Ng C, Hartwig S, Ng KH, Ho J, Kreidberg JA, Taglienti M, Royer-Pokora B, Ai X. WT1-dependent sulfatase expression maintains the normal glomerular filtration barrier. J Am Soc Nephrol. 2011 Jul; 22(7):1286-96. doi: 10.1681/ASN.2010080860. Epub 2011 Jun 30.
277. Schumacher VA, Schlötzer-Schrehardt U, Karumanchi SA, Shi X, Zaia J, Jeruschke S, Zhang D, Pavenstädt H, Drenckhan A, Amann K, Ng C, Hartwig S, Ng KH, Ho J, Kreidberg JA, Taglienti M, Royer-Pokora B, Ai X. WT1-dependent sulfatase expression maintains the normal glomerular filtration barrier. J Am Soc Nephrol. 2011 Jul; 22(7):1286-96. doi: 10.1681/ASN.2010080860. Epub 2011 Jun 30.
278. Scott Lozanoff, Jayne Johnston, Wenbin Ma and Claude Jourdan-Le Saux . Immunohistochemical Localization of Pax2 and Associated Proteins in the Developing Kidney of Mice with Renal Hypoplasia. J Histochem Cytochem 2001 49: 1081 DOI: 10.1177/002215540104900903
279. Shankland SJ: The podocyte's response to injury: Role in proteinuria and glomerulosclerosis. Kidney Int 69 : 2131 –2147, 2006
280. Short, K., Hodson, M., and Smyth, I. Spatial mapping and quantification of developmental branching morphogenesis. Development. 2013; 140: 471–478
281. Short, K.M., Hodson, M.J., and Smyth, I.M. Tomographic quantification of branching morphogenesis and renal development. Kidney Int. 2010; 77: 1132–1139
282. Shulga N, Wilson-Smith R, Pastorino JG (2010) Sirtuin-3 deacetylation of cyclophilin D induces dissociation of hexokinase II from the mitochondria. J Cell Sci 123: 894–902.
283. Simona Granata, Gianluigi Zaza, Simona Simone, Gaetano Villani, Dominga Latorre, Paola Pontrelli, Massimo Carella, Francesco Paolo Schena, Giuseppe Grandaliano and Giovanni Pertosa. Mitochondrial dysregulation and oxidative stress in patients with chronic kidney disease. BMC Genomics 2009, 10:388.
284. Skladal D, Halliday J, Thorburn DR. Minimum birth prevalence of mitochondrial respiratory chain disorders in children. Brain 2003; 126: 1905–1912.
285. Smith DH, Gullion CM, Nichols G, Keith DS, Brown JB. Cost of medical care for chronic kidney disease and comorbidity among enrollees in a large HMO population. J Am Soc Nephrol. 2004 May;15(5):1300-6.
286. Smolen GA, Vassileva MT, Wells J, Matunis MJ, Haber DA. SUMO-1 modification of the Wilms' tumor suppressor WT1. Cancer Res. 2004 Nov 1;64(21):7846-51.
287. Sogabe, Hajime, Masaomi Nangaku, Yoshitaka Ishibashi, Takehiko Wada, Toshiro Fujita, Xiujun Sun, Takashi Miwa, Michael P. Madaio, and Wen-Chao Song. Increased Susceptibility of Decay-Accelerating Factor Deficient Mice to Anti-Glomerular Basement Membrane Glomerulonephritis. J Immunol 2001; 167:2791-2797.
288. Sonveaux P, Vegran F, Schroeder T, Wergin MC, Verrax J, Rabbani ZN, De Saedeleer CJ, Kennedy KM, Diepart C, Jordan BF, Kelley MJ, Gallez B, Wahl ML, Feron O, Dewhirst MW. Targeting lactate-fueled respiration selectively kills hypoxic tumor cells in mice. J.Clin.Invest. 2008;118:3930–3942.
289. Sperl W, Fleuren L, Freisinger P, et al. The spectrum of pyruvate oxidation defects in the diagnosis of mitochondrial disorders. J Inherit Metab Dis 2015; 38: 391–403.
290. Spinazzola A, Zeviani M: Disorders from perturbations of nuclear-mitochondrial intergenomic cross-talk. J Intern Med 2009; 265: 174–192.

291. Spitz DR, Malcolm RR, Roberts RJ. Cytotoxicity and metabolism of 4-hydroxy-2-nonenal and 2-nonenal in H2O2-resistant cell lines. Do aldehydic by-products of lipid peroxidation contribute to oxidative stress? Biochem.J. 1990;267:453–459.
292. Srivastava A, Palsson R, Kaze AD, et al. The Prognostic Value of Histopathologic Lesions in Native Kidney Biopsy Specimens: Results from the Boston Kidney Biopsy Cohort Study. J Am Soc Nephrol 2018; 29:2213.
293. Stehling O, Lill R. The role of mitochondria in cellular iron–sulfur protein biogenesis: mechanisms, connected processes, and diseases. Cold Spring Harbor Perspect Biol 2013; 5: a011312.
294. Stepien, K. M., Heaton, R., Rankin, S., Murphy, A., Bentley, J., Sexton, D., & Hargreaves, I. P. (2017). Evidence of Oxidative Stress and Secondary Mitochondrial Dysfunction in Metabolic and Non-Metabolic Disorders. Journal of clinical medicine, 6(7), 71. doi:10.3390/jcm6070071
295. Stewart JB, Chinnery PF. The dynamics of mitochondrial DNA heteroplasmy: implications for human health and disease. Nat Rev Genet 2015; 16: 530–542.
296. Stoll R, Lee BM, Debler EW, Laity JH, Wilson IA, Dyson HJ, Wright PE. Structure of the Wilms tumor suppressor protein zinc finger domain bound to DNA. J Mol Biol. 2007 Oct 5;372(5):1227-45. Epub 2007 Jul 21.
297. Suzuki T, Nagao A, Suzuki T. Human mitochondrial tRNAs: biogenesis, function, structural aspects, and diseases. Annu Rev Genet. 2011;45:299-329. doi: 10.1146/annurev-genet-110410-132531. Epub 2011 Sep 6.
298. Szczech L. A. and Lazar I. L., “Projecting the United States ESRD population: issues regarding treatment of patients with ESRD,” Kidney International, Supplement, vol. 66, no. 90, pp. S3–S7, 2004.
299. Taanman, Jan-Willem. The mitochondrial genome: structure, transcription, translation and replication. Biochimica et Biophysica Acta (BBA) – Bioenergetics Volume 1410, Issue 2, 9 February 1999, Pages 103–123
300. Tait SW, Green DR.. Mitochondria and cell death: outer membrane permeabilization and beyond. Nat Rev Mol Cell Biol (2010) 11(9):621–32.10.1038/nrm2952
301. Tan JC, Busque S, Workeneh B, et al. Effects of aging on glomerular function and number in living kidney donors. Kidney Int 2010; 78:686.
302. Tan JC, Workeneh B, Busque S, et al. Glomerular function, structure, and number in renal allografts from older deceased donors. J Am Soc Nephrol 2009; 20:181.
303. Tang S, Wang J, Lee NC, et al. Mitochondrial DNA polymerase gamma mutations: an ever expanding molecular and clinical spectrum. J Med Genet 2011; 48: 669–681.
304. Tanji, Kurenai and Bonilla, Eduardo. Mitochondria. Edited by Leslie Wilson Paul T. Matsudaira Eric A. Schon Liza A. Pon. (Optical Imaging Techniques (Histochemical, Immunohistochemical, and In Situ Hybridization Staining Methods) to Visualize Mitochondrial by Kurenai Tanji and Eduardo Bonilla) Academic Press- Publisher - May 23, 2001.
305. Taylor RC, Cullen SP, Martin SJ.. Apoptosis: controlled demolition at the cellular level. Nat Rev Mol Cell Biol (2008) 9(3):231–41.10.1038/nrm2312
306. Taylor RW, Taylor GA, Durham SE, and Turnbull DM: The determination of complete human mitochondrial DNA sequences in single cells: implications for the study of somatic mitochondrial DNA point mutations. Nucleic Acids Res 2001; 29: E74.
307. Terasaki PI, Koyama H, Cecka JM, Gjertson DW: The hyperfiltration hypothesis in human renal transplantation. Transplantation 57: 1450–1454, 1994
308. Terasaki PI, Koyama H, Cecka JM, Gjertson DW: The hyperfiltration hypothesis in human renal transplantation. Transplantation 57: 1450–1454, 1994
309. Theodore T. Ho, Matthew R. Warr, Emmalee R. Adelman, Olivia M. Lansinger, Johanna Flach1, Evgenia V. Verovskaya1, Maria E. Figueroa & Emmanuelle Passegué. Autophagy maintains the metabolism and function of young and old stem cells. Nature 543, 205–210 (09 March 2017) doi:10.1038/nature21388.
310. Thompson K, Majd H, Dallabona C, et al. Recurrent de novo dominant mutations in SLC25A4 cause severe early-onset mitochondrial disease and loss of mitochondrial DNA copy number. Am J Hum Genet 2016; 99: 860–876.
311. Thorburn A: Death receptor-induced cell killing. Cell Signal 16 : 139 –144, 2004

312. Thorner PS, Arbus GS, Celermajer DS, Baumal R: Focal segmental glomerulosclerosis and progressive renal failure associated with a unilateral kidney. Pediatrics 73: 806–810, 1984
313. Thorner PS, Arbus GS, Celermajer DS, Baumal R: Focal segmental glomerulosclerosis and progressive renal failure associated with a unilateral kidney. Pediatrics 73: 806–810, 1984
314. Vazquez Martul E, Veiga Barreiro A. Importance of kidney biopsy in graft selection. Transplant Proc 2003; 35:1658.
315. Vikse BE, Irgens LM, Leivestad T, et al. Low birth weight increases risk for end-stage renal disease. J Am Soc Nephrol 2008; 19:151.
316. Vogetseder, A., Karadeniz, A., Kaissling, B., and Le Hir, M. (2005). Tubular cell proliferation in the healthy rat kidney. Histochem. Cell Biol. 124, 97–104.
317. Vooijs M, Jonkers J, Berns A (2001). A highly efficient ligand-regulated Cre recombinase mouse line shows that LoxP recombination is position dependent. EMBO Rep. 2001 Apr;2(4):292-7.
318. Wai T, García-Prieto J, Baker MJ, Merkwirth C, Benit P, Rustin P, Rupérez FJ, Barbas C, Ibañez B, Langer T. Imbalanced OPA1 processing and mitochondrial fragmentation cause heart failure in mice. Science. 2015 Dec 4;350(6265):aad0116. doi: 10.1126/science.aad0116.
319. Walker JE (1992) The NADH: ubiquinone oxidoreductase (complex I) of respiratory chains. Q Rev Biophys 25: 253–324.
320. Walker JE (1992) The NADH: ubiquinone oxidoreductase (complex I) of respiratory chains. Q Rev Biophys 25: 253–324.
321. Walker, R., Marshall, M. R., Polaschek, N. (2013). Improving self-management in chronic kidney disease: A pilot study. Renal Society of Australasia Journal, 9, 116-125.
322. Wallace DC, Fan W, Procaccio V. Mitochondrial energetics and therapeutics. Annu Rev Pathol.2010;5:297–348.
323. Wang, Z.-Y.; Madden, S. L.; Deuel, T. F., et al. The Wilms' tumor gene product, WT1, represses transcription of the platelet-derived growth factor A-chain gene. J. Biol. Chem. 267:21999–22002; 1992.
324. Wang, Z.-Y.; Qui, Q.-Q.; Enger, K. T., et al. A second transcriptionally active DNA-binding site for the Wilms tumor gene product, WT1. Proc. Natl. Acad. Sci. USA 90:8896–8900; 1993.
325. Weinberg F, Hamanaka R, Wheaton WW, Weinberg S, Joseph J, Lopez M, Kalyanaraman B, Mutlu GM, Budinger GR, Chandel NS. Mitochondrial metabolism and ROS generation are essential for Kras-mediated tumorigenicity. Proc Natl Acad Sci U S A. 2010 May 11;107(19):8788-93. doi: 10.1073/pnas.1003428107. Epub 2010 Apr 26.
326. Welham SJ, Wade A, and Woolf AS: Protein restriction in pregnancy is associated with increased apoptosis of mesenchymal cells at the start of rat metanephrogenesis. Kidney Int 61: 1231–1242, 2002
327. Welham SJ, Wade A, and Woolf AS: Protein restriction in pregnancy is associated with increased apoptosis of mesenchymal cells at the start of rat metanephrogenesis. Kidney Int 61: 1231–1242, 2002
328. White SL, Perkovic V, Cass A, et al. Is low birth weight an antecedent of CKD in later life? A systematic review of observational studies. Am J Kidney Dis 2009; 54:248.
329. Wiggins JE, Goyal M, Sanden SK, et al. Podocyte hypertrophy, "adaptation," and "decompensation" associated with glomerular enlargement and glomerulosclerosis in the aging rat: prevention by calorie restriction. J Am Soc Nephrol 2005; 16:2953.
330. Will Y, Hynes J, Ogurtsov VI, Papkovsky DB. Analysis of mitochondrial function using phosphorescent oxygen-sensitive probes. Nat Protoc. 2006;1:2563–2572.
331. Williams, R. S. 1986. Mitochondrial gene expression in mammalian striated muscle: evidence that variation in gene dosage is the major regulatory event. J. Biol. Chem. 261:12390–12394.
332. Williams, R. S., S. Salmons, E. A. Newsholme, R. E. Kaufman, and J. Mellor. 1986. Regulation of nuclear and mitochondrial gene expression by contractile activity in skeletal muscle. J. Biol. Chem. 261:376–380.
333. Wojtek Steffen, Anja C. Gemperli, Nevena Cvetesic & Julia Steuber. Organelle-speci¢c expression of subunitND5of human complex I (NADHdehydrogenase) alters cation homeostasis inSaccharomyces cerevisiae. FEMS Yeast Res 10 (2010) 648–659

334. Woods LL, Weeks DA, Rasch R: Programming of adult blood pressure by maternal protein restriction: Role of nephrogenesis. Kidney Int 65: 1339–1348, 2004.
335. Woods LL, Weeks DA, Rasch R: Programming of adult blood pressure by maternal protein restriction: Role of nephrogenesis. Kidney Int 65: 1339–1348, 2004.
336. Wroe, Caroline. Investigating the role of the WT1 gene in the development of Murine Denys-Drash syndrome. PhD Thesis, 2009.
337. Wroe, Caroline. Investigating the role of the WT1 gene in the development of Murine Denys-Drash syndrome. PhD Thesis, 2009.
338. Wu M, Neilson A, Swift AL, Moran R, Tamagnine J, Parslow D, Armistead S, Lemire K, Orrell J, Teich J, Chomicz S, Ferrick DA. Multiparameter metabolic analysis reveals a close link between attenuated mitochondrial bioenergetic function and enhanced glycolysis dependency in human tumor cells. Am J Physiol Cell Physiol. 2007;292:C125–136.
339. Wu Y, Song P, Xu J, Zhang M, Zou MH. Activation of protein phosphatase 2A by palmitate inhibits AMP-activated protein kinase. J Biol Chem. 2007;282:9777–9788.
340. Yagi T, Matsuno-Yagi A. The proton-translocating NADH-quinone oxidoreductase in the respiratory chain: the secret unlocked. Biochemistry. 2003 Mar 4;42(8):2266-74.
341. Yee C, Yang W, Hekimi S. The intrinsic apoptosis pathway mediates the pro-longevity response to mitochondrial ROS in C. elegans. Cell. 2014 May 8;157(4):897-909. doi: 10.1016/j.cell.2014.02.055.
342. Yeger H, Forget D, Alami J, Williams BR. Analysis of WT1 gene expression during mouse nephrogenesis in organ culture. In Vitro Cell Dev Biol Anim. 1996 Sep;32(8):496-504
343. Yeger H, Forget D, Alami J, Williams BR. Analysis of WT1 gene expression during mouse nephrogenesis in organ culture. In Vitro Cell Dev Biol Anim. 1996 Sep;32(8):496-504
344. Yeger, H.; Baumal, R.; Pawlin, G., et al. Phenotypic and molecular characterization of inducible human neuroblastoma cell lines. Differentiation 39:216–227; 1988.
345. Yeger, H.; Cullinane, C.; Flenniken, A., et al. Coordinate expression of Wilms tumor genes correlates with Wilms tumor phenotypes. Cell Growth Differ. 3:855–865; 1992.
346. Yeger, H.; Cullinane, C.; Flenniken, A., et al. Coordinate expression of Wilms tumor genes correlates with Wilms tumor phenotypes. Cell Growth Differ. 3:855–865; 1992.
347. Yidong Bai, Rebecca M. Shakeley, and Giuseppe Attardi. Tight Control of Respiration by NADH Dehydrogenase ND5 Subunit Gene Expression in Mouse Mitochondria. Molecular And Cellular Biology, Feb. 2000, p. 805–815
348. Zhou X, Zoltona G, Silva F. Anatomical Changes in the Aging Kidney. In: The Aging Kidney in Health and Disease, Macias Nunez J, JS C, Oreopoulos D (Eds), Springer Science+Business Media, LLC, New York 2008. p.39.
349. Zickermann V., Kerscher S., Zwicker K., Tocilescu M.A., Radermacher M., Brandt U. (2009). Architecture of complex I and its implications for electron transfer and proton pumping. Biochim. Biophys. Acta 1787: 574–583
350. Zucchelli P, Cagnoli L: Proteinuria and hypertension after unilateral nephrectomy. Lancet 2: 212, 1985
351. Zucchelli P, Cagnoli L: Proteinuria and hypertension after unilateral nephrectomy. Lancet 2: 212, 1985